UNIVERSITÉ DE LIÈGE
Faculté des Sciences Appliquées

High order hybrid finite element schemes for Maxwell's equations taking thin structures and global quantities into account

Christophe GEUZAINE
Ingénieur civil électricien (électronique)

Thèse présentée en vue de l'obtention
du grade de Docteur en Sciences Appliquées

Octobre 2001

Acknowledgment

First of all, I wish to thank both Professor W. Legros for the opportunity he gave me to do research in excellent conditions and with great freedom in the Department of Electrical Engineering of the University of Liège, and the Belgian Industry and Agriculture Research Training Fund (FRIA) for funding my research during four years. I also thank Professor R. Belmans (Katholieke Universiteit Leuven), Professor J. Destiné (University of Liège), P. Dular (University of Liège), Professor A. Genon (University of Liège), Professor L. Kettunen (Technical University of Tampere), Professor A. Razek (University of Paris VI and Paris XI, Supélec), Professor M. Van Droogenbroeck (University of Liège) and Professor B. Vanderheyden (University of Liège) for accepting to be members of the examining board of this thesis.

In addition I want to warmly thank all the members of the Department of Electrical Engineering I worked with for the last five years. In particular, I am much indebted to P. Dular, F. Henrotte, B. Meys and J.-F. Remacle for their involvement in our common works. I am very grateful to them for introducing me to the world of scientific research, each with their personal approach. In the same way, I want to express my gratitude to Professor L. Kettunen and T. Tarhasaari, from the Technical University of Tampere, as well as to Professor A. Nicolet, from the University of Aix-Marseille, for the chance they gave me to co-operate on exciting research topics. Credit goes to J. Gyselinck and to my mother for their careful proofreading of the manuscript.

Finally, I want to thank my family and friends who shared my daily life during the realization of this thesis and who made that period so enriching for me.

Liège, October 2001 Christophe Geuzaine

List of Symbols

Alphanumeric symbols

$\mathbb{E}^3$	: Three-dimensional oriented Euclidean space
$\boldsymbol{x} = (x, y, z)$	: Point of $\mathbb{E}^3$
t	: Time instant
$C^p(\Omega)$, $\boldsymbol{C}^p(\Omega)$	: Spaces of p times continuously differentiable scalar and vector fields over Ω
$L^2(\Omega)$, $\boldsymbol{L}^2(\Omega)$	: Spaces of square integrable scalar and vector fields over Ω
$H^p(\Omega)$, $\boldsymbol{H}^p(\Omega)$	: pth order Sobolev spaces of scalar and vector fields over Ω
$\boldsymbol{H}(\mathbf{curl}; \Omega)$	: Stream function space $\{\boldsymbol{v} \in \boldsymbol{L}^2(\Omega) : \mathbf{curl}\, \boldsymbol{v} \in \boldsymbol{L}^2(\Omega)\}$
$\boldsymbol{H}(\mathrm{div}; \Omega)$	: Flux space $\{\boldsymbol{v} \in \boldsymbol{L}^2(\Omega) : \mathrm{div}\, \boldsymbol{v} \in L^2(\Omega)\}$
$W_p^i(\Omega)$	: Discrete subspace of incomplete pth polynomial order of $H^1(\Omega)$, $\boldsymbol{H}(\mathbf{curl}; \Omega)$, $\boldsymbol{H}(\mathrm{div}; \Omega)$ and $L^2(\Omega)$ for $i = 0, \ldots, 3$ respectively
$V_p^i(\Omega)$	: Discrete subspace of complete pth polynomial order of $H^1(\Omega)$, $\boldsymbol{H}(\mathbf{curl}; \Omega)$, $\boldsymbol{H}(\mathrm{div}; \Omega)$ and $L^2(\Omega)$ for $i = 0, \ldots, 3$ respectively
$\mathcal{NS}_p^i(\Omega, \Omega_c^{\mathrm{C}})$	: Discrete reduced nullspace of the **grad**, **curl** and div operator for $i = 0, \ldots, 2$ respectively
$\mathcal{S}_p^i(\Omega, \Omega_c^{\mathrm{C}})$	: Discrete reduced orthogonal complement to the nullspace of the **grad**, **curl** and div operator for $i = 0, \ldots, 2$ respectively
$\mathcal{R}_p^i(\Omega)$	: Discrete range of the **grad**, **curl** and div operator for $i = 0, \ldots, 2$ respectively
$\boldsymbol{h}$	: Magnetic field (A/m)
$\boldsymbol{b}$	: Magnetic flux density (T)
$\boldsymbol{e}$	: Electric field (V/m)
$\boldsymbol{d}$	: Electric flux density (C/m^2)
$\boldsymbol{j}$	: Current density (A/m^2)
q	: Electric charge density (C/m^3)
$\boldsymbol{m}$	: Magnetization (A/m)
$\boldsymbol{p}$	: Electric polarization (C/m^2)
$\boldsymbol{a}$	: Magnetic vector potential (Wb/m)
v	: Electric scalar potential (V)
c	: Speed of light in vacuum ($= 1/\sqrt{\epsilon_0 \mu_0} = 2.99792458\, 10^8$ m/s)
T, H, P	: Reference tetrahedron, hexahedron and prism
$\mathcal{M}$	: Finite element mesh
$\mathcal{N}$, $\mathcal{E}$, $\mathcal{F}$, $\mathcal{V}$	: Sets of nodes, edges, faces and elements

Greek symbols

Ω	: Bounded open set of $\mathbb{E}^3$
Γ	: Boundary of Ω $(= \partial\Omega)$
ϕ	: Magnetic scalar potential (A)
σ	: Electric conductivity (S/m)
μ	: Magnetic permeability (H/m)
μ_0	: Magnetic permeability of vacuum $(= 4\pi\, 10^{-7}\,\mathrm{H/m})$
μ_r	: Relative magnetic permeability $(= \mu/\mu_0)$
ϵ	: Electric permittivity (F/m)
ϵ_0	: Electric permittivity of vacuum $(\simeq 8.854187817\, 10^{-17}\,\mathrm{F/m})$
ϵ_r	: Relative electric permittivity $(= \epsilon/\epsilon_0)$
χ_m	: Magnetic susceptibility
χ_e	: Electric susceptibility (F/m)

Abbreviations

FEM	: Finite element method
BEM	: Boundary element method
IEM	: Integral equation method

Operators

∂	: Boundary operator
$^{\mathrm{C}}$	: Complement
$\bar{}$	: Closure
∂_x, ∂_y, ∂_z	: Space derivatives
∂_t	: Time derivative
grad	: Gradient
curl	: Curl
div	: Divergence
supp	: Support
dim	: Dimension
$\mathcal{NS}$	: Nullspace (kernel)
$\mathcal{D}$	: Domain
$\mathcal{R}$	: Range (codomain)
$\times$	: Vector product
$\cdot$	: Scalar product
$\| \, \|_K$	: Norm on the domain K
$\oplus$, $\ominus$	: Direct sum and subtraction
re, im	: Real and imaginary parts

Introduction

Computational electromagnetism deals with the mathematical modeling of electromagnetic systems. Its purpose is not to establish physical theories, but to use these theories to translate questions about a physical situation into a mathematical problem—a set of equations that will be solved with a computer in order to answer these questions.

An interesting class of such physical situations is the one dealing with the electromagnetic interaction between several equipments or between these equipments and their natural environment—problems often gathered under the generic denomination of electromagnetic compatibility (EMC) problems. An important question in EMC problems is to find how to design new components or how to add systems to existing components to limit the electromagnetic interactions to an admissible level (which can be dictated by purely technical considerations or by various norms and regulations). If the source of the electromagnetic perturbations cannot be modified, a frequent solution is to design shields, with the aim to reduce the electromagnetic fields in some parts of space.

Passive electromagnetic shields can be classified according to the operating frequency of the shielded components. At low frequencies (more precisely when the characteristic length of the structure is much smaller than the wavelength) the electric and magnetic fields can be considered as uncoupled. Whereas grounded plates or conducting nettings are generally sufficient to attenuate the electric field, two physical mechanisms (often acting in a joint way) can contribute to the magnetic shielding. On the one hand, one may use ferromagnetic materials of high permeability, which, by attracting and shunting the magnetic flux, prevent it from polluting the shielded area. This method remains effective even for static fields. On the other hand, one may use conducting materials, where, if the disturbing field is alternating, the induced currents produce a field which is opposed to the applied field. As soon as the frequency increases, the electric and magnetic fields are strongly coupled in the form of electromagnetic waves (the threshold frequency depending on the dimension of the structure to be shielded and on the considered materials). One has then to use other types of screens, such as metal nettings whose mesh size is comparable with the field wavelength, honeycomb structures, or absorbing materials.

Until the last decade, the analysis of this class of electromagnetic problems was limited to measurements or to the use of approximate analytical developments and equivalent electrical diagrams. Recently, numerical models have increasingly been used to answer certain questions arising in EMC problems with greater precision.

However, the analysis of such problems by means of a computer still faces several challenges, as has recently been highlighted in e.g. [62, 117]:

1. due to the complexity of the devices as well as to their level of optimization (with regard to cost, volume and weight), the geometries to consider can usually not be approximated by one or two-dimensional models, and thus require a fully three-dimensional treatment. Moreover, due to advanced computer-aided manufacturing, most modern devices exhibit complex, curved shapes;

2. the sensitivity of the components is sometimes very high and the norms regulating the interactions between equipments and between equipments and their environment become stricter and stricter;

3. the dimensions of some parts of the structures are often very small compared to the overall size of the devices, as for example the thickness of shielding plates or the size of the slits and openings in these shields;

4. the electromagnetic fields naturally extend to infinity, and the interactions between distant devices have to be considered;

5. the systems are driven by complex electric or electronic circuits;

6. the electromagnetic phenomena often cannot be considered as isolated from other physical phenomena, such as heat transfer or mechanical stress and vibrations.

Scope and objectives of this work

This work contributes to the modeling of electromagnetic phenomena in three-dimensional structures by finite element-type techniques. In particular, it is focused on the computation of local and global electromagnetic quantities characterizing open systems involving electromagnetic shields. Although most developments are focused on low frequency phenomena, many of the results can be extended to the propagation of electromagnetic fields in a rather straightforward way.

The following strategy is followed to address the six aforementioned challenges, point-by-point:

1. use a finite element-type discretization scheme on unstructured three-dimensional meshes, which permits to handle complex geometries and to respect prescribed characteristic length fields;

2. develop all formulations in a dual way so that error estimation techniques based on the non-fulfillment of the constitutive laws can straightforwardly be applied. Combine the error estimation with adaptive mesh refinement and high order mixed finite elements in order to meet the accuracy constraints;

3. introduce one-dimensional approximations to avoid the discretization of thin structures, where classical treatments would lead to prohibitive computational costs or ill-conditioned problems;

4. couple the partial differential equation approach with integral schemes to take the extension of the fields toward infinity into account (the resulting hybrid finite element formulations should preserve some sparseness in the discrete linear operator, while suppressing the need for a mesh in some parts of space);

5. introduce the coupling between the local electromagnetic fields and the global electrical variables directly in the mathematical formulations of the problems;

6. implement the numerical methods inside a general software environment making use of a limited number of tools directly accessible through a dedicated language, allowing a coupling between various physical problems.

Hereafter the main aspects of the present work are outlined in greater detail.

Dual hybrid finite element formulations

The finite element method (FEM), contrary to the method of finite differences (FDM), is very appealing for solving partial differential equations on complex geometries due to its natural use of unstructured meshes [120, 228]. Moreover, automatic mesh adaptation in regions where the error is important is relatively straightforward [7, 138]. Though, constraints arising in the treatment of electromagnetic shielding problems (i.e. important aspect ratios and the obligation to take into account the extension toward infinity of the computed fields) make it interesting to couple the finite element method, which is well adapted to the solving of nonlinear problems, with others—such as integral equation methods (IEM) and boundary element methods (BEM). The latter methods are less suited for nonlinear analyzes, but permit the computation of long range interactions without requiring a mesh [118,28].

Hybrid formulations are thus a natural choice, either in the form of coupled finite element and boundary equation methods (FEM-BEM) [227] or in the form of finite element and integral equation methods (FEM-IEM) [71]. In this work we develop two families of dual hybrid FEM-BEM formulations for the magnetostatic and magnetodynamic case. By dual, we mean that both families lead to a solution of the same problem, in a deliberately redundant way, but adding valuable benefits: a posteriori error bounds and appropriate error estimators for mesh refinement procedures.

One-dimensional approximations

The direct application of the developed formulations for the resolution of electromagnetic problems involving thin shells is often not appropriate or even not possible (highly stretched meshes are often difficult to generate and lead to ill-conditioned matrices, while isotropic meshes are either impossible to generate or result in a

prohibitive number of unknowns). While the literature on the subject is abundant [196, 136, 152, 11, 99, 185], we present in this work a dual approach for the construction of such formulations, based on an appropriate treatment of the surface terms arising in the weak formulations. Contrary to the commonly encountered approaches, the thin structure approximation is introduced at the continuous level, while the discretization step is kept as general as possible.

Coupling between local and global physical quantities

The solution of Maxwell's equations provides the local physical quantities such as the electric and magnetic fields, the current density or various potentials throughout the three-dimensional space. However, global quantities like the voltage drop or the current intensity, coupling the electromagnetic device with an external electronic circuit, are often those which permit to describe the overall functioning of the system. Indeed, such global quantities can often be easily measured, which is not always the case for local quantities, especially inside materials. One benefit of the proposed formulations is that they provide, as a natural result of the computation, both these local and global quantities. An important application of the coupling of local and global quantities is the modeling of inductors (consisting of a massive conductor, or of stranded or foil windings), where either the current or more frequently the voltage can be imposed or, in a more general way, both of them must be taken into account when a coupling with circuit equations is considered [146,168]. A rigorous treatment of such devices is proposed, together with a natural method for the computation of the various source fields required by the formulations.

Unstructured mesh approach with high order mixed finite elements

A complete sequence of mixed finite elements, constructed on tetrahedra, hexahedra and prisms, is consistently used for all spatial discretizations (for both finite element and integral equation schemes). Special attention is paid to the discretization of the sources of integral operators, for which two discretization strategies are presented: the Galerkin method and the de Rham (or generalized collocation) method. An optimization procedure is applied to the function spaces resulting from the discretization procedure in order to constrain the global error to a given value. Among the methods to perform this optimization, we classically combine the modification of the order of the local polynomial interpolation and the modification of the size of the geometrical elements in the mesh [8].

Outline

This work is divided into four chapters. The chapter following this introduction presents the hypotheses on which all developments are based. After a short reminder of the equations governing electromagnetic phenomena, three physical models are defined, as well as the supplementary hypotheses needed for the modeling of source

regions and thin structures. The continuous function spaces to which the unknown fields and potentials belong are briefly presented, as well as the complexes they form.

In Chapter 2, a sequence of mixed high order finite elements built on tetrahedra, hexahedra and prisms is constructed. Global finite element spaces, approximating the continuous spaces presented in Chapter 1, are then presented, and an optimization procedure of these spaces is proposed.

Chapter 3 deals with the establishment of the hybrid formulations. Two sets of weak formulations, well adapted for discretization by the Galerkin technique, are first presented. Particular attention is paid to the expression of discontinuities introduced by the thin region approximations, the coupling between local and global quantities, and the construction of source fields. A second discretization technique, called the de Rham map, is elaborated for the discretization of the sources of the integral operators.

The solutions obtained for two test problems are presented in Chapter 4. The choice of these problems is dictated by the availability of reference results, which permit a detailed analysis of the precision of the solution obtained by the different numerical schemes. These problems also permit to illustrate some of the possibilities of the developed software tools and can lead to their validation.

Finally, general conclusions are formulated. The methods presented throughout the different chapters are summarized and suggestions for future work are given.

Original contributions

Here is the list, with references to papers published in the frame of this thesis and section numbers in the manuscript, of the contributions that we believe to be (at least partly) original:

1. a generalized summary of the construction of mixed hierarchical finite element spaces built on a collection of tetrahedra, hexahedra and prisms, conforming in $H^1(\Omega)$, $\boldsymbol{H}(\mathbf{curl};\Omega)$, $\boldsymbol{H}(\mathrm{div};\Omega)$ and $L^2(\Omega)$. See Sections 2.3, 2.4 and 2.5. This is connected with publications [87, 84];

2. the explicit definition of the reduced discrete nullspace and of the reduced discrete orthogonal complement to the nullspace of the **curl** operator with high order curl-conforming finite elements. See Sections 2.6.4.1 and 2.6.4.2. This is connected with publications [105, 106];

3. the application of an error estimator based on the error in the constitutive relations to the *h*-, *p* and *hp*-optimization of global finite element spaces built with hierarchical tetrahedral, hexahedral and prismatic finite elements conforming in $H^1(\Omega)$, $\boldsymbol{H}(\mathbf{curl};\Omega)$, $\boldsymbol{H}(\mathrm{div};\Omega)$ and $L^2(\Omega)$. See Section 2.7. This has led to publication [178] and is connected with publication [180];

4. the treatment of thin shell structures in dual magnetostatic and magnetodynamic formulations. See Sections 3.2.1.2, 3.2.2, 3.3.1.2 and 3.3.2. This has led to publications [82, 83];

5. the coupling between local and global electromagnetic quantities in three-dimensional magnetodynamic formulations for massive, stranded and foil winding inductors, both in the continuous and in the discrete case. See Sections 3.2.1.3, 3.2.1.4, 3.2.3, 3.3.1.3, 3.3.1.4 and 3.3.3. This has led to publications [52, 57, 49];

6. the computation of discrete source fields of minimal geometrical support in the magnetic field conforming formulations. See Section 3.2.4. This has led to publication [86] and is connected with publications [105, 106];

7. the application of the de Rham map on primal and dual meshes for the discretization of the sources of integral operators. See Section C.4.2. This has led to publications [88, 209].

We shall not finish this introduction without underlining that this work is, although presenting some relatively abstract topics, an electrical engineering thesis, thus quite different from what would have been achieved by a mathematician dealing with the same subject. And as such, an important part of the time devoted to the realization of the thesis has been spent on implementing and testing the proposed methods, and on making them usable by researchers in other teams. Appendix D gives a short overview of the two computer codes that have resulted from these implementation efforts. These codes are freely available for further tests and collaborations over the Internet at the address `http://www.geuz.org`. We believe that sharing the developed software tools with the rest of the computational electromagnetics community is also an original aspect of this work. Publications related to the software tools include [51, 81, 53, 50, 78].

Chapter 1

Electromagnetic models

1.1 Introduction

Our aim is to solve numerically Maxwell's equations for macroscopic media, which can be written in the three-dimensional Euclidean space $\mathbb{E}^3$ as[1]

$$\mathbf{curl}\, \boldsymbol{h} - \partial_t \boldsymbol{d} = \boldsymbol{j}, \tag{1.1}$$
$$\mathbf{curl}\, \boldsymbol{e} + \partial_t \boldsymbol{b} = 0, \tag{1.2}$$
$$\operatorname{div} \boldsymbol{b} = 0, \tag{1.3}$$
$$\operatorname{div} \boldsymbol{d} = q, \tag{1.4}$$
$$\boldsymbol{b} = \mu_0(\boldsymbol{h} + \boldsymbol{m}), \tag{1.5}$$
$$\boldsymbol{d} = \epsilon_0 \boldsymbol{e} + \boldsymbol{p}. \tag{1.6}$$

Equations (1.1), (1.2), (1.3) and (1.4) are respectively the generalized Ampère law, Faraday's law, the magnetic Gauss law and the electric Gauss law. The four vector fields $\boldsymbol{h}$, $\boldsymbol{e}$, $\boldsymbol{b}$, $\boldsymbol{d}$ are called the magnetic field, the electric field, the magnetic flux density and the electric flux density. Taken together, they form a mathematical representation of the same physical phenomenon: the electromagnetic field [205,101].

The electric charge density q, the current density $\boldsymbol{j}$, the magnetization $\boldsymbol{m}$ and the electric polarization $\boldsymbol{p}$ are the source terms in these equations. Given q, $\boldsymbol{j}$, $\boldsymbol{m}$, $\boldsymbol{p}$ and proper initial values for $\boldsymbol{e}$ and $\boldsymbol{h}$ at the initial time instant $t = t_0$, the system (1.1)–(1.6) determines $\boldsymbol{h}$, $\boldsymbol{e}$, $\boldsymbol{b}$, $\boldsymbol{d}$ for any other time instant t [40, 18].

Note that (1.4) implies, by (1.1), the equation of conservation of charge

$$\operatorname{div} \boldsymbol{j} + \partial_t q = 0, \tag{1.7}$$

so that, if $\boldsymbol{j}$ is given from the origin of time to the present, the charge can be obtained by integrating (1.7) with respect to time. In the same way, Gauss's law (1.3) can be deduced from (1.2) if a zero divergence of the magnetic induction is initially assumed[2].

[1] See page i for the definition of symbols and Section A.1 for a note about the formalism.

[2] See [108] for a discussion of the non-redundancy of the divergence equations for boundary-initial value problems.

All the preceding equations are general, and have never been invalidated since their completion by Maxwell in the late 19th century [151]. In vacuum, and, more generally, in systems that do not react with the electromagnetic field, we have $\boldsymbol{m} = 0$ and $\boldsymbol{p} = 0$. These systems are thus described by the two constants ϵ_0 and μ_0. In the MKSA system, $\mu_0 = 4\pi\,10^{-7}\,\mathrm{H/m}$ and $\epsilon_0 = 1/(\mu_0 c^2)\,\mathrm{F/m}$, where c is the speed of light in vacuum.

In all other situations, when field-matter interaction occurs, $\boldsymbol{j}$, $\boldsymbol{m}$ and $\boldsymbol{p}$ are obtained by solving the equations describing the physical phenomena (mechanical, thermal, chemical, etc.) related to the dynamics of the charges involved in the interaction. Rigorously, one should then deal with the resolution of complex coupled systems. But constitutive laws [115] give us the means to bypass the explicit solving of these problems, by summarizing the complex interaction between the physical compartment of main interest (electromagnetism in this work) and those of secondary importance, the detailed modeling of which can be avoided. It is important to note that, even if all the constitutive relations are (sometimes rough) approximations of the physical behavior of the considered coupled systems, they often permit to describe very accurately the macroscopic behavior of the considered systems.

The first constitutive law we adopt is Ohm's law, valid for conductors (where the current density is considered to be proportional to the electric field) and generators (where the source current density $\boldsymbol{j}_s$ can be considered as imposed, independently of the local electromagnetic field):

$$\boldsymbol{j} = \sigma \boldsymbol{e} + \boldsymbol{j}_s. \tag{1.8}$$

The conductivity σ is always positive (or equal to zero for insulators), and can be a tensor, in order to take an anisotropic behavior into account. Note that this relation is only valid for non-moving conductors: for a conductor moving at speed $\boldsymbol{v}$, (1.8) becomes $\boldsymbol{j} = \sigma(\boldsymbol{e} + \boldsymbol{v} \times \boldsymbol{b}) + \boldsymbol{j}_s$.

The second constitutive law describes the behavior of dielectric materials, stating a proportionality between the polarization and the electric field, as it would be if the charges were elastically bound, with a restoring force proportional to the electric field:

$$\boldsymbol{p} = \chi_e \boldsymbol{e} + \boldsymbol{p}_e. \tag{1.9}$$

Again, the electric susceptibility χ_e can be a tensor to describe an anisotropic behavior. A permanent polarization $\boldsymbol{p}_e$ is considered for materials exhibiting a permanent polarization independent of the electric field, such as electrets. Introducing (1.9) in (1.6), we get

$$\begin{aligned} \boldsymbol{d} &= \epsilon_0 \boldsymbol{e} + \chi_e \boldsymbol{e} + \boldsymbol{p}_e \\ &= (\epsilon_0 + \chi_e)\boldsymbol{e} + \boldsymbol{p}_e \\ &= \epsilon_0 \epsilon_r \boldsymbol{e} + \boldsymbol{p}_e \\ &= \epsilon \boldsymbol{e} + \boldsymbol{p}_e, \end{aligned} \tag{1.10}$$

where ϵ and $\epsilon_r = 1 + \chi_e/\epsilon_0$ are the electric permittivity and the relative electric permittivity of the material respectively. We always have $\epsilon \geq \epsilon_0$.

The third constitutive law expresses an approximate relation between the magnetization and the magnetic field in magnetic materials [74, 119]:

$$\boldsymbol{m} = \chi_m \boldsymbol{h} + \boldsymbol{h}_m. \tag{1.11}$$

For paramagnetic and ferromagnetic materials, the magnetic susceptibility χ_m is always positive. For diamagnetic materials the magnetic susceptibility is negative. Again, it can be a tensor to describe an anisotropic behavior. For permanent magnets [137], one considers a non-zero permanent magnetic field $\boldsymbol{h}_m$ supported by the magnet, and independent of the local magnetic field. Introducing (1.11) in (1.5), we get

$$\begin{aligned} \boldsymbol{b} &= \mu_0(\boldsymbol{h} + \chi_m \boldsymbol{h} + \boldsymbol{h}_m) \\ &= \mu_0(1 + \chi_m)\boldsymbol{h} + \mu_0 \boldsymbol{h}_m \\ &= \mu_0 \mu_r \boldsymbol{h} + \mu_0 \boldsymbol{h}_m \\ &= \mu \boldsymbol{h} + \mu_0 \boldsymbol{h}_m, \end{aligned} \tag{1.12}$$

where μ and $\mu_r = 1 + \chi_m$ are the magnetic permeability and the relative magnetic permeability of the material respectively. We always have $\mu > 0$.

In the simplest modeling option, the material characteristics σ, ϵ and μ involved in (1.8), (1.10) and (1.12) are considered as constants. This situation is the linear case without memory. All the test problems solved in Chapter 4 belong to this class.

Constitutive laws in the form of convolution products, as it occurs for example for constitutive laws expressed in the Fourier space when the material characteristics are frequency dependent, or simple hysteresis models [41], lead to linear problems with memory. In this case, the value of one field in the constitutive law at the time instant t depends not only on the other field at the same instant, but also on past values of the latter. When the dependences in the constitutive equations cannot be considered as linear (as for example in ferromagnetic materials), or when it is necessary to consider other physical parameters influencing the physical characteristics (as in the resolution of coupled electromagnetic problems, taking for example thermal and mechanical effects into account [103,104]), one should consider σ, ϵ and μ as functions of the fields, which leads to the resolution of a nonlinear problem, with or without memory. Section D.1 shows how such interactions can be tackled in the practical implementation of the studied numerical methods.

We deliberately do not present any further details about the constitutive relations and their dependence regarding other compartments of physics: all classical electromagnetic textbooks propose a fairly good introduction to these topics: see for example [115], [173, chapter 13], [73], [160] or [212] (and, for the topic of magnetic materials, which play an important role in the problems we are interested in, see [119], as well as [23, 41, 145] for the particular case of hysteresis modeling). From now on, we will simply consider all the physical characteristics as mathematical functions to introduce in Maxwell's equations (1.1)–(1.4) via the constitutive relations (1.8), (1.10) and (1.12).

Two strategies for the time integration of the equations can be used. For a classical time domain analysis, appropriate initial conditions must be provided. But

if the system is fed by a sinusoidal excitation and if its response is linear (which is the case if all operators and the material characteristics are linear), the problem can also be solved in the frequency domain [173, 155]. For a sinusoidal variation of angular frequency ω, any field can then be described as

$$f(\boldsymbol{x},t) = f_m(\boldsymbol{x})\cos(\omega t + \varphi(\boldsymbol{x})), \tag{1.13}$$

where $\varphi(\boldsymbol{x})$ is a phase angle (expressed in radians) which can depend on the position. The harmonic approach then consists in defining this physical field as the real part of a complex field, i.e.:

$$f(\boldsymbol{x},t) = \mathrm{re}(f_m(\boldsymbol{x})e^{i(\omega t+\varphi(\boldsymbol{x}))}) = \mathrm{re}(f_p(\boldsymbol{x})e^{i\omega t}), \tag{1.14}$$

where $i = \sqrt{-1}$ denotes the imaginary unit. The complex field

$$f_p(\boldsymbol{x}) = f_m(\boldsymbol{x})e^{i\varphi(\boldsymbol{x})} = f_r(\boldsymbol{x}) + if_i(\boldsymbol{x}) \tag{1.15}$$

appearing in (1.14) is called a phasor, $f_r(\boldsymbol{x})$ and $f_i(\boldsymbol{x})$ being its real and imaginary parts respectively. If all physical fields are expressed as in (1.14), their substitution in the equations of the system leads to complex equations, the unknowns of which are phasors. Through (1.14), the time derivative operator becomes a product by the factor $i\omega$. In particular, Maxwell's equations (1.1)–(1.4) in harmonic regime become

$$\mathbf{curl}\,\boldsymbol{h} - i\omega\boldsymbol{d} = \boldsymbol{j}, \tag{1.16}$$
$$\mathbf{curl}\,\boldsymbol{e} + i\omega\boldsymbol{b} = 0, \tag{1.17}$$
$$\mathrm{div}\,\boldsymbol{b} = 0, \tag{1.18}$$
$$\mathrm{div}\,\boldsymbol{d} = q, \tag{1.19}$$

where all the fields are now phasors.

It is interesting to notice that the harmonic approach can be extended to non-sinusoidal excitations or to nonlinear systems thanks to the harmonic balance technique, where a finite number of harmonics in the spectral decomposition of the signal is considered [100]. It is also important to notice that when using harmonic approaches, the function spaces to which the fields belong (see Section 1.3) are different from those in a time domain analysis (see e.g. [19, chapter 9]).

1.2 Assumptions and definitions

In this section we put forward the basic hypotheses on which all developments in Chapters 2 and 3 are based: the assumptions made about the geometric and electromagnetic properties of the system are first given; the electromagnetic fields and potentials are then introduced in a complex formed by two sequences of function spaces put in duality.

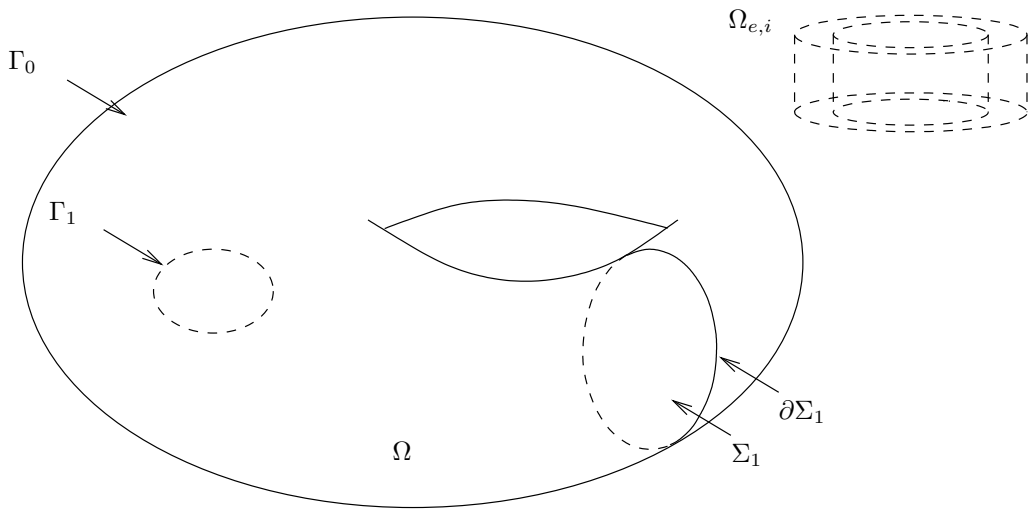

Figure 1.1: Bounded open set Ω of $\mathbb{E}^3$, with $l = c = 1$, and external inductor $\Omega_{e,i}$.

1.2.1 Bounded region Ω

We want to solve (1.1), (1.2), (1.3) and (1.4) together with (1.8), (1.10) and (1.12), with $\sigma \geq 0$, $\epsilon \geq \epsilon_0$ and $\mu > 0$, in a bounded open set Ω of the oriented Euclidean space $\mathbb{E}^3$. The boundary $\partial\Omega$ of Ω is denoted by Γ. The field of outward directed normal unit vectors on Γ is denoted by $\boldsymbol{n}$. An example of such a domain is shown in Figure 1.1.

The boundary Γ may consist of $c + 1$ closed surfaces Γ_i, $i = 0, \ldots, c$, which means that there are c cavities in Ω. The region Ω may also contain l loops, if there exists l cutting surfaces Σ_i (called cuts), $i = 1, \ldots, l$, inside Ω that make Ω homologically simple [132, 13]. It should be noted that a homologically simple domain is not necessarily simply connected (for example in the case of the complement of a knotted torus [27]). A general algorithm to construct such cutting surfaces when Ω is discretized by a tetrahedral mesh is proposed by Kotiuga in [133]. It is important to note that the preceding characterization of Ω also applies to any of its subsets (e.g. its non-conducting parts: see Section 1.2.2).

Even if the domain of resolution is limited to Ω, sources of electromagnetic fields can be located outside Ω. Ω_e denotes the set of all inductor domains $\Omega_{e,i}$, $i = 1, \ldots, e$, outside Ω. The field produced by these external inductors is completely determined a priori (this is for example the case when we assume that we put the domain of study inside a source field of uniform direction). There can, of course, also be sources inside Ω: this is explained in the next section.

1.2.2 Subsets of Ω

Having defined the general characteristics of the domain in which we will solve Maxwell's equations, we now take a closer look at some of its subregions.

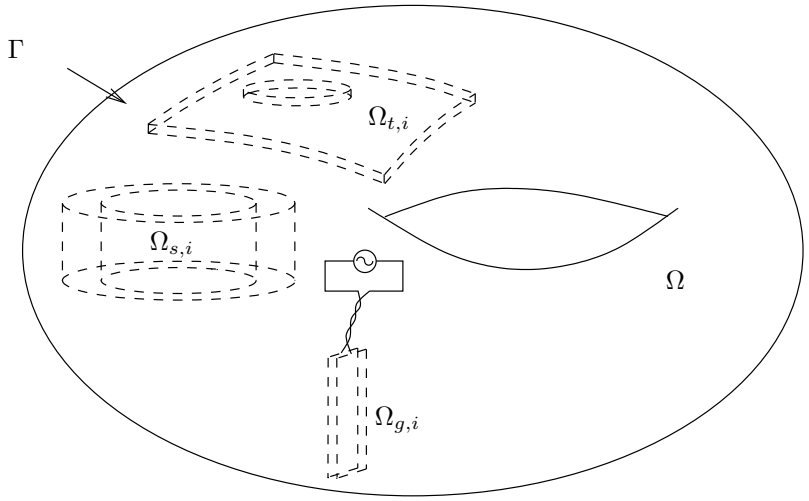

Figure 1.2: Bounded domain Ω and subregions $\Omega_{t,i}$, $\Omega_{s,i}$ and $\Omega_{g,i}$.

First the distinction is made between the conducting (i.e. where $\sigma > 0$) and non-conducting parts of Ω: the conducting part is denoted by Ω_c and the non-conducting one by Ω_c^{C}, with $\Omega_c^{\mathrm{C}} = \Omega - \Omega_c$.

We then define the three following generic subsets of Ω (see Figure 1.2):

1. Ω_t is composed of all thin regions $\Omega_{t,i}$, $i = 1, \ldots, t$, i.e. regions for which one dimension is much smaller than the two others. Each thin region $\Omega_{t,i}$ is either a subset of Ω_c or of Ω_c^{C}. The thickness (or depth) of the thin region $\Omega_{t,i}$, denoted d_i, is defined as a function giving the smallest dimension of the thin region for each point of $\Omega_{t,i}$;

2. Ω_s is composed of all inductor domains $\Omega_{s,i}$, $i = 1, \ldots, s$, carrying an imposed source current density $\boldsymbol{j}_{s,i}$. In order to simplify further developments, we assume that $\Omega_s \subset \Omega_c^{\mathrm{C}}$;

3. Ω_g is composed of all source domains $\Omega_{g,i}$ (also called generators of electromotive force, or, more simply, generators), $i = 1, \ldots, g$, where either a global voltage V_i or a global current I_i is imposed (or, in a more general way, where both V_i and I_i are a priori unknown when a coupling with circuit equations is considered). Each generator $\Omega_{g,i}$ is either a subset of Ω_c or of Ω_c^{C}.

Let us examine these three categories in greater detail.

1.2.2.1 Set of thin regions Ω_t

A typical thin region $\Omega_{t,i} \subset \Omega_t$ is shown in Figure 1.3. The field of outward directed normal unit vectors on the boundary $\partial\Omega_{t,i}$ of $\Omega_{t,i}$ is denoted by $\boldsymbol{n}_{t,i}$. The boundary $\partial\Omega_{t,i}$ is decomposed into three subsets, corresponding to the upper side $\Gamma_{t,i}^{+}$, the lower side $\Gamma_{t,i}^{-}$ and the borders $\Gamma_{t,i}^{=}$ of the region:

$$\partial\Omega_{t,i} = \Gamma_{t,i}^{+} \cup \Gamma_{t,i}^{-} \cup \Gamma_{t,i}^{=}.$$

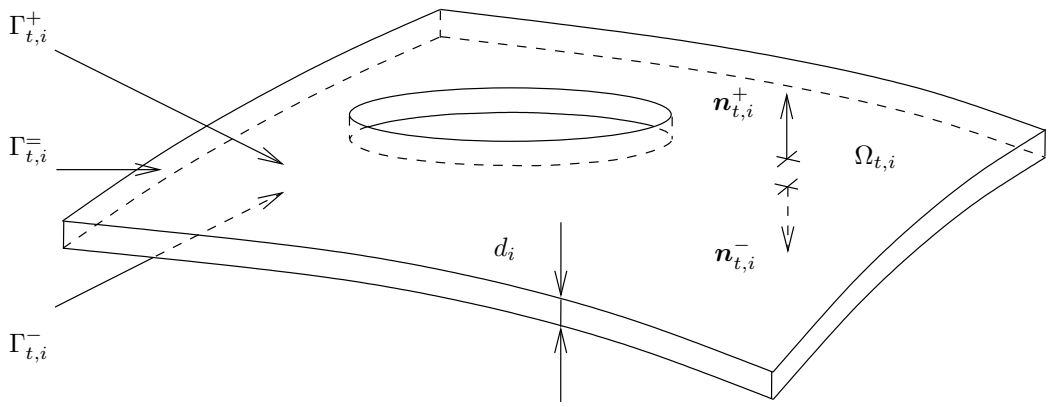

Figure 1.3: Thin region $\Omega_{t,i}$.

In the case of a closed shell, we have $\Gamma^=_{t,i} = \emptyset$. Note that a thin structure can consist of several layers, all exhibiting different physical characteristics σ, ϵ and μ.

The hypothesis that the region Ω_t is thin means that it can be locally assumed that, inside the thin region, the electromagnetic fields $\boldsymbol{e}$ and $\boldsymbol{h}$ have no component perpendicular to its main directions. The criterion for a region Ω_t to be considered as thin is thus that all corner and extremity effects can be neglected, and that the electromagnetic problem amounts to a one-dimensional one [136]. For such problems impedance-type boundary conditions (IBC) can be established [152, 11, 114]. If we denote the tangential component $\boldsymbol{n} \times (\boldsymbol{f} \times \boldsymbol{n})$ of a field $\boldsymbol{f}$ on a surface of normal $\boldsymbol{n}$ by $\boldsymbol{f}_t$, and if we keep the symbolic time derivative notation even in the Fourier space (where ∂_t should be read $i\omega$), these conditions can be written as (see Section B.1)

$$\boldsymbol{n}_t \times \boldsymbol{h}\,\big|_{\Gamma_t^+} - \boldsymbol{n}_t \times \boldsymbol{h}\,\big|_{\Gamma_t^-} = \sigma\beta\,(\boldsymbol{e}_t\big|_{\Gamma_t^+} + \boldsymbol{e}_t\big|_{\Gamma_t^-}), \tag{1.20}$$

$$\boldsymbol{n}_t \times \boldsymbol{e}\,\big|_{\Gamma_t^+} - \boldsymbol{n}_t \times \boldsymbol{e}\,\big|_{\Gamma_t^-} = -\partial_t\big[\mu\beta\,(\boldsymbol{h}_t\big|_{\Gamma_t^+} + \boldsymbol{h}_t\big|_{\Gamma_t^-})\big]. \tag{1.21}$$

When the skin depth $\delta = \sqrt{2/(\omega\mu\sigma)}$ (ω is the pulsation) is large in comparison with the thickness d_i of the shell $\Omega_{t,i}$, we have $\beta = d_i/2$. Otherwise, we have (using the complex formalism) $\beta = \gamma^{-1}\tanh(\gamma d_i/2)$, with $\gamma = (1+i)/\delta$.

1.2.2.2 Set of inductors Ω_s

This first kind of source region, which is a subset of Ω_c^{C}, is composed of idealized inductors $\Omega_{s,i}$, $i = 1, \ldots, s$, where the source current density $\boldsymbol{j}_s$ is imposed, and assumed to be independent of the local electromagnetic fields. This is the case for stranded inductors, which consist of a winding of N_i turns of a conducting wire having a diameter smaller than the skin depth, with one input and one output of

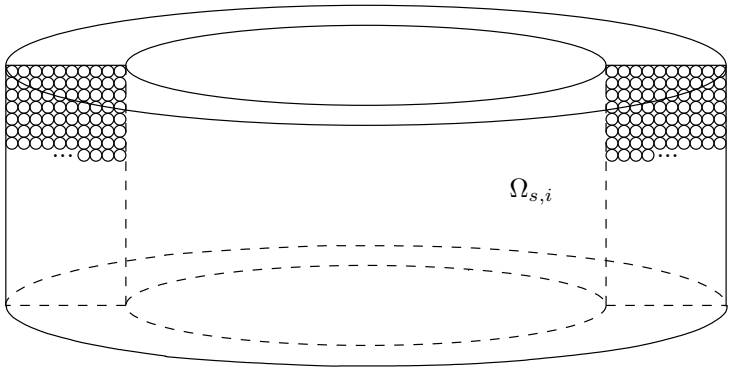

Figure 1.4: Stranded inductor $\Omega_{s,i}$.

current. Such inductors can be modeled by the definition of a field $\boldsymbol{h}_s$, called source magnetic field, verifying

$$\begin{cases} \mathbf{curl}\, \boldsymbol{h}_s = \boldsymbol{j}_s & \text{in } \Omega_s \\ \mathbf{curl}\, \boldsymbol{h}_s = 0 & \text{in } \Omega_s^{\mathrm{C}} \end{cases}. \tag{1.22}$$

Since this field is not unique, we have some freedom for its computation (see Section 1.4.1).

When the actual current density $\boldsymbol{j}_s$ is not known in advance and the stranded inductor is connected to a generator imposing a global current or voltage (see the next section), we have to define independent source fields $\boldsymbol{h}_{s,i}$ associated with each inductor $\Omega_{s,i}$, i.e. satisfying

$$\begin{cases} \mathbf{curl}\, \boldsymbol{h}_{s,i} = \boldsymbol{j}_{s,i} & \text{in } \Omega_{s,i} \\ \mathbf{curl}\, \boldsymbol{h}_{s,i} = 0 & \text{in } \Omega_{s,i}^{\mathrm{C}} \end{cases}, \tag{1.23}$$

where $\boldsymbol{j}_{s,i}$ is the equivalent current density of a unit current flowing in the N_i turns of the ith inductor in Ω_s.

1.2.2.3 Set of generators Ω_g

The second kind of source region is an idealization of a source of electromotive force located between two sections (being two electrodes very close to each other) of an inductor domain, and is either a subset of Ω_c or Ω_c^{C}. We consider three different sets of inductors to be connected to these generators (see Figures 1.4 and 1.5):

1. Ω_s is composed of all the stranded inductors $\Omega_{s,i}$, $i = 1, \ldots, s$ (see Section 1.2.2.2);

2. Ω_m is composed of all massive inductors $\Omega_{m,i}$, $i = 1, \ldots, m$. Massive inductors are a subset of the conducting domain where induced currents take place ($\Omega_m \subset \Omega_c$). As their name suggests, massive inductors are made of one piece of a conducting material, where the currents may be non-uniformly distributed if the skin depth is smaller than some of its dimensions;

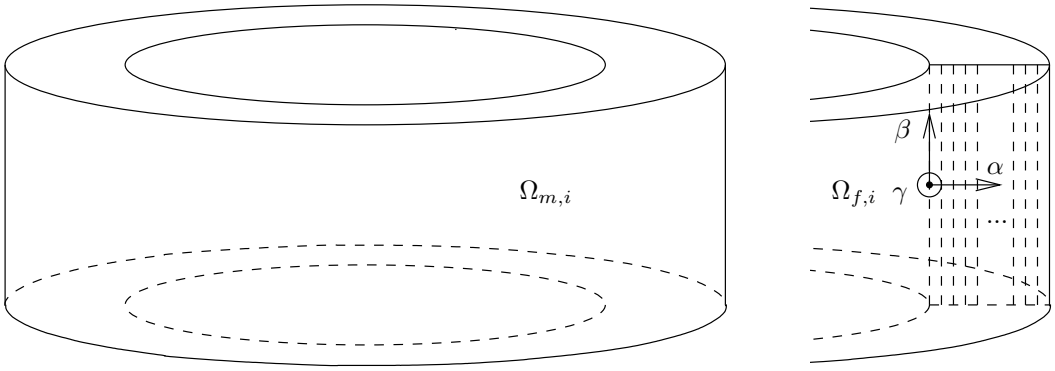

Figure 1.5: Massive inductor $\Omega_{m,i}$ and foil winding $\Omega_{f,i}$.

3. Ω_f is composed of all foil windings $\Omega_{f,i}$, $i = 1, \ldots, f$ ($\Omega_m \subset \Omega_c$). Foil windings are halfway between massive and stranded inductors: they are composed of N_i turns of conducting sheets (or foils), whose thickness is smaller than the skin depth, so that no skin effect appears along the thickness of the foils. Special treatments will be elaborated so that the foils themselves do not have to be separately modeled.

Regardless of the actual type of inductor, each generator $\Omega_{g,i}$ has an associated voltage V_i and current I_i flowing through the surface $\Gamma^+_{g,i}$ (i.e. one of the electrodes, considered as a cross-section of the inductor: see Figure 1.6). For massive inductors, the electric field $\boldsymbol{e}$ in $\Omega_{g,i}$ can be considered as being known (as a conservative electric field) and its circulation along any path from one electrode to the other in $\Omega_{g,i}$ is actually the applied voltage V_i. One thus has

$$\int_{\gamma_{g,i}} \boldsymbol{e} \cdot d\boldsymbol{l} = V_i \quad \text{and} \quad \int_{\Gamma^+_{g,i}} \boldsymbol{n} \cdot \boldsymbol{j}\, ds = I_i, \tag{1.24a,b}$$

where $\gamma_{g,i}$ is a path in $\Omega_{g,i}$ connecting its two electrodes. The convention used gives the same direction to I_i and V_i. For stranded inductors or foil windings, condition (1.24a) has to be expressed as the sum of the circulations of $\boldsymbol{e}$ for all the wires or foils, and (1.24) becomes

$$\sum_{j=1}^{N_i} \int_{\gamma_{g,i,j}} \boldsymbol{e} \cdot d\boldsymbol{l} = V_i \quad \text{and} \quad \int_{\Gamma^+_{g,i}} \boldsymbol{n} \cdot \boldsymbol{j}\, ds = N_i I_i, \tag{1.25a,b}$$

where $\gamma_{g,i,j}$ is a path in $\Omega_{g,i}$ connecting the jth wire on its two electrodes. Moreover, for all kinds of inductors, one must satisfy the local conditions

$$\boldsymbol{n} \times \boldsymbol{e}\big|_{\partial\Omega_{g,i}} = 0 \quad \text{and} \quad \boldsymbol{n} \cdot \boldsymbol{j}\big|_{\partial\Omega \left\{ \begin{smallmatrix} m,i \\ w,i \\ f,i \end{smallmatrix} \right.} = 0.$$

An assumption has also to be made on the connection of the external circuit: this external circuit is considered to be far enough from the main structure and connected to it through twisted pairs (see Figure 1.6).

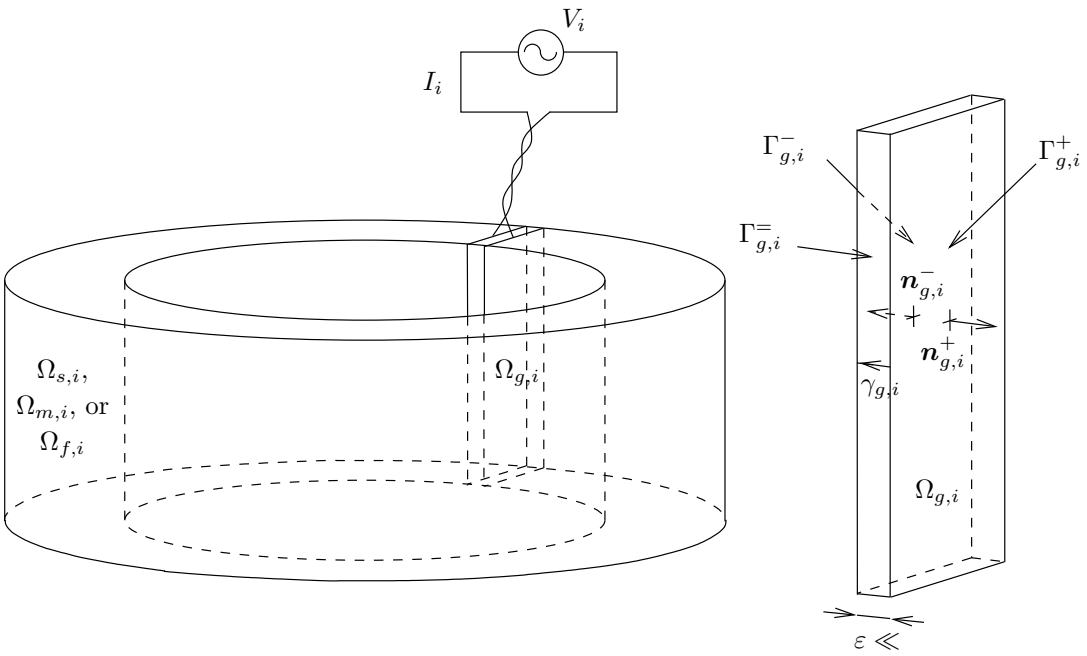

Figure 1.6: Generator $\Omega_{g,i}$ with associated global voltage V_i and current I_i.

1.2.2.4 Abstraction of Ω_t and Ω_g from Ω

The subregions $\Omega_{t,i}$ and $\Omega_{g,i}$ have a common characteristic: their behavior can be described by the values of the electromagnetic fields on their boundaries. Each case has nevertheless its own particularities:

1. thin regions $\Omega_{t,i}$ are passive (they contain no source of electromagnetic fields). If the region is sufficiently thin (see Section 1.2.2.1), the electromagnetic fields inside the region locally obey a one-dimensional equation, whose analytical solution provides the relation between the values of the field on both sides of the region;

2. generators $\Omega_{g,i}$ are active regions, which contain sources of electromagnetic fields. We are not interested in the distribution of the electromagnetic fields inside these regions: the important relations we want to obtain are between global values associated with the generator such as the voltage and the current.

These observations suggest the following procedure for the abstraction of Ω_t and Ω_g from Ω:

1. the domain Ω is replaced by a domain in which the subregions Ω_t and Ω_g are removed;

2. the equations are written for $\Omega - \Omega_t - \Omega_g$, whose boundary contains the boundaries of Ω_t and Ω_g;

3. in these equations the limit is taken for thicknesses of the subregions Ω_t and Ω_g tending to zero. We then denote by Γ_t the set of all abstracted thin regions $\Gamma_{t,i}$ and by Γ_g the set of all abstracted generators $\Gamma_{g,i}$.

At the discrete level, we will see that this procedure results in a treatment similar to the treatment of the cutting surfaces defined in Section 1.2.1. The subregions Ω_t and Ω_g will be reduced to the surfaces Γ_t and Γ_g (discretized by two-dimensional geometrical elements), and a transition layer (discretized by three-dimensional elements) will be considered in order to impose the discontinuity of the fields. This is important in practice because of the characteristics of the finite element meshes of these subregions: highly stretched meshes are often difficult to generate and lead to ill-conditioned matrices, while isotropic meshes usually result in a prohibitive number of unknowns.

We already mentioned that the boundary of $\Omega - \Omega_t - \Omega_g$ contains the boundary of the removed subregions. It is important to note that the field of unit normals on this boundary is pointing inside each subregion $\Omega_{t,i}$ and $\Omega_{g,i}$:

$$\boldsymbol{n} = -\boldsymbol{n}_{t,i} \quad \text{and} \quad \boldsymbol{n} = -\boldsymbol{n}_{g,i}. \tag{1.26}$$

As a consequence of (1.26), the following relations hold for the fields of normals on the upper and lower sides of $\Omega_{t,i}$ and $\Omega_{g,i}$:

$$\begin{aligned} \boldsymbol{n}^+_{t,i} &= \boldsymbol{n}_{t,i} \quad \text{and} \quad \boldsymbol{n}^-_{t,i} = -\boldsymbol{n}_{t,i}, \\ \boldsymbol{n}^+_{g,i} &= \boldsymbol{n}_{g,i} \quad \text{and} \quad \boldsymbol{n}^-_{g,i} = -\boldsymbol{n}_{g,i}. \end{aligned}$$

1.3 Continuous mathematical structure

1.3.1 Helmholtz decomposition

The spaces of square integrable scalar and vector fields $L^2(\Omega)$ and $\boldsymbol{L}^2(\Omega)$ (see Appendix A for related definitions) are the spaces in which we seek for the solutions of (1.1)–(1.4).

In order to construct formulations for topologically non-trivial domains, the Helmholtz decomposition of $\boldsymbol{L}^2(\Omega)$ into a direct sum of five mutually orthogonal subspaces is of great importance. This decomposition is widely covered in the literature: see e.g. [38] for a general overview or [13,125] for an analysis of the implications in the case of electromagnetic formulations.

The subspaces that will be abundantly used in the establishment of the continuous formulations and in the discretization process are schematically represented on the second and third level of Figure 1.7. This figure depicts the domain, nullspace and range of the three differential operators appearing in (1.1)–(1.4): **grad**, **curl** and div (see Section A.2.5). The spaces $L^2(\Omega)$ and $\boldsymbol{L}^2(\Omega)$ are represented by the horizontal axes on four levels (0, 1, 2 and 3 for $L^2(\Omega)$, $\boldsymbol{L}^2(\Omega)$, $\boldsymbol{L}^2(\Omega)$ and $L^2(\Omega)$ respectively), and some of their subspaces are represented by subdivisions of these axes (the axis on level 2 should be read from right to left). The arrows correspond

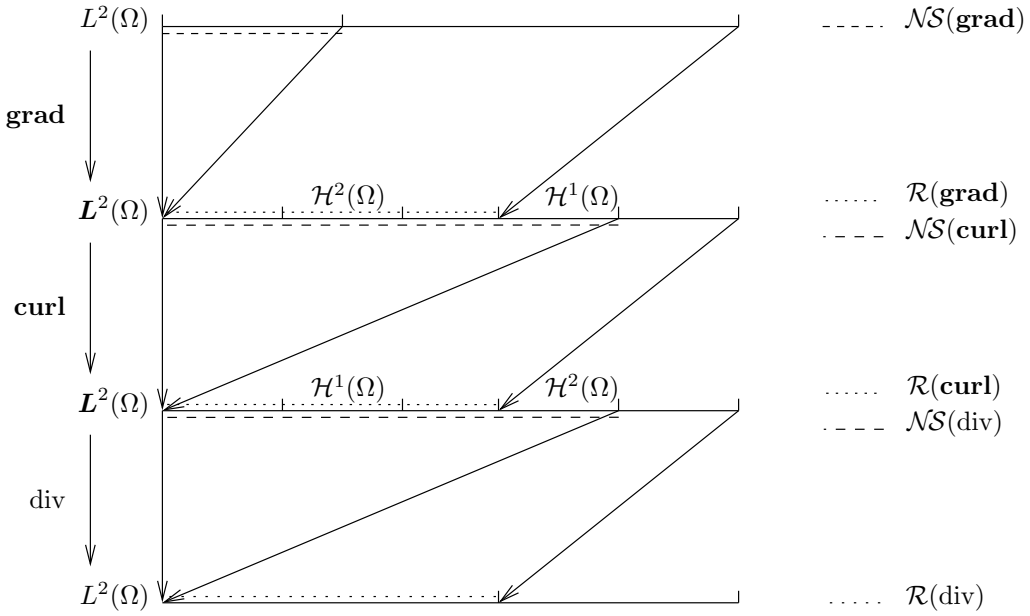

Figure 1.7: de Rham complex for the continuous case.

to the application of the operators **grad**, **curl** and div, depending on the level (i.e. a subspace located between two arrow origins has for image, by the associated operator, the subspace located between the tips of these arrows).

The two exceptional subspaces appearing in Figure 1.7 are

$$\mathcal{H}^1(\Omega) = \left\{\boldsymbol{u} \in \boldsymbol{L}^2(\Omega) : \mathbf{curl}\,\boldsymbol{u} = 0, \mathrm{div}\,\boldsymbol{u} = 0, \boldsymbol{n}\cdot\boldsymbol{u}\big|_\Gamma = 0\right\}, \tag{1.27}$$

$$\mathcal{H}^2(\Omega) = \left\{\boldsymbol{u} \in \boldsymbol{L}^2(\Omega) : \mathbf{curl}\,\boldsymbol{u} = 0, \mathrm{div}\,\boldsymbol{u} = 0, \boldsymbol{n}\times\boldsymbol{u}\big|_\Gamma = 0\right\}. \tag{1.28}$$

$\mathcal{H}^1(\Omega)$ is the set of elements having a zero curl, but which are not gradients. The dimension of $\mathcal{H}^1(\Omega)$ equals l, the number of loops in Ω (see Section 1.2.1). This number is finite, and equal to the number of cuts Σ_i, $i = 1, \ldots, l$ in Ω. $\mathcal{H}^2(\Omega)$ is the set of elements having a zero divergence, but which are not curls. The dimension of $\mathcal{H}^2(\Omega)$ equals c, the number of cavities in Ω.

The subspace $\mathcal{H}^1(\Omega)$ will be very important in the construction of the hybrid formulations in Chapter 3. We thus briefly recall the following classical results characterizing $\mathcal{H}^1(\Omega)$ [38]. Since $\mathrm{div}\,\boldsymbol{u} = 0$ in Ω, $\boldsymbol{u}$ is locally the gradient of a harmonic function q. If l cutting surfaces Σ_i are defined, we have by analytic prolongation $\boldsymbol{u} = \mathbf{grad}\,q$ in Ω, and thus

$$\mathrm{div}\,\mathbf{grad}\,q = 0 \quad \text{in } \Omega. \tag{1.29}$$

The condition $\boldsymbol{n}\cdot\boldsymbol{u}\big|_\Gamma = 0$ becomes

$$\partial_{\boldsymbol{n}} q\big|_\Gamma = 0, \tag{1.30}$$

and since $\boldsymbol{u}\big|_{\Sigma_i^+} - \boldsymbol{u}\big|_{\Sigma_i^-} = 0$, $i = 1, \ldots, l$, we have

$$q\big|_{\Sigma_i^+} - q\big|_{\Sigma_i^-} = c_i, \quad i = 1, \ldots, l, \tag{1.31}$$

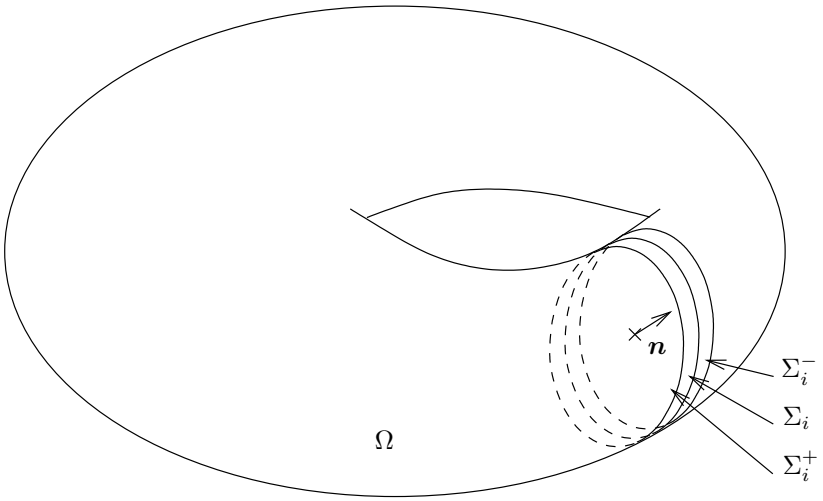

Figure 1.8: Both sides of a cut Σ_i and the associated normal.

where c_i is a constant associated with the cut Σ_i. Using Green's formula (A.25), one can then show that

$$\partial_{\boldsymbol{n}} q\big|_{\Sigma_i^+} - \partial_{\boldsymbol{n}} q\big|_{\Sigma_i^-} = 0, \quad i = 1, \dots, l. \tag{1.32}$$

The solutions of the problem defined by (1.29)–(1.32) depend linearly on the l constant jumps c_i of the function q across the cuts Σ_i. A basis of the space $\mathcal{H}^1(\Omega)$ can therefore be defined by the l functions q_j, solutions of (1.29), (1.30), (1.32) and

$$q_j\big|_{\Sigma_i^+} - q_j\big|_{\Sigma_i^-} = \delta_{ij}, \quad i = 1, \dots, l, \tag{1.33}$$

for $j = 1, \dots, l$ (δ_{ij} denotes the Kronecker symbol). The basis function q_j of $\mathcal{H}^1(\Omega)$ is thus a function defined in Ω which presents a unit discontinuity across the cut Σ_j. One should note that the field q_j only depends on the topology of Ω: the way q_j varies does not matter. In order to simplify further developments, we will always assume that the field q_j varies from 1 on one side of the cut (Σ_j^+) to 0 on the other side (Σ_j^-) (see Figure 1.8).

1.3.2 Maxwell's house

The basic continuous structure is formed by two de Rham complexes (see Section A.2.6), put into correspondence in the following Tonti diagram [14]:

$$\begin{array}{ccccccc}
H_h^1(\Omega) & \xrightarrow{\mathbf{grad}_h} & \boldsymbol{H}_h(\mathbf{curl};\Omega) & \xrightarrow{\mathbf{curl}_h} & \boldsymbol{H}_h(\mathrm{div};\Omega) & \xrightarrow{\mathrm{div}_h} & L^2(\Omega) \\
\updownarrow & & \updownarrow & & \updownarrow & & \updownarrow \\
L^2(\Omega) & \xleftarrow{\mathrm{div}_e} & \boldsymbol{H}_e(\mathrm{div};\Omega) & \xleftarrow{\mathbf{curl}_e} & \boldsymbol{H}_e(\mathbf{curl};\Omega) & \xleftarrow{\mathbf{grad}_e} & H_e^1(\Omega)
\end{array} \tag{1.34}$$

The domains of the differential operators are defined in a restrictive way, in the sense that they are defined as subspaces of $L^2(\Omega)$ and $\boldsymbol{L}^2(\Omega)$ for which appropriate boundary conditions have to be satisfied [16]. Let Γ_h and Γ_e represent two complementary parts of the boundary Γ of Ω, so that

$$\Gamma = \Gamma_h \cup \Gamma_e \quad \text{and} \quad \Gamma_h \cap \Gamma_e = \emptyset, \tag{1.35}$$

where scalar fields u_h or u_e, or the trace of vector fields $\boldsymbol{u}_h$ or $\boldsymbol{u}_e$, are imposed. The domains of the operators $\mathbf{grad}_h$, $\mathbf{curl}_h$ and div_h are then defined by

$$H_h^{10}(\Omega) = \{u \in L^2(\Omega) : \mathbf{grad}\, u \in \boldsymbol{L}^2(\Omega), u|_{\Gamma_h} = 0\}, \tag{1.36}$$
$$\boldsymbol{H}_h^0(\mathbf{curl};\Omega) = \{\boldsymbol{u} \in \boldsymbol{L}^2(\Omega) : \mathbf{curl}\, \boldsymbol{u} \in \boldsymbol{L}^2(\Omega), \boldsymbol{n} \times \boldsymbol{u}|_{\Gamma_h} = 0\}, \tag{1.37}$$
$$\boldsymbol{H}_h^0(\mathrm{div};\Omega) = \{\boldsymbol{u} \in \boldsymbol{L}^2(\Omega) : \mathrm{div}\, \boldsymbol{u} \in L^2(\Omega), \boldsymbol{n} \cdot \boldsymbol{u}|_{\Gamma_h} = 0\}, \tag{1.38}$$

and the domains of the operators $\mathbf{grad}_e$, $\mathbf{curl}_e$ and div_e by

$$H_e^{10}(\Omega) = \{u \in L^2(\Omega) : \mathbf{grad}\, u \in \boldsymbol{L}^2(\Omega), u|_{\Gamma_e} = 0\}, \tag{1.39}$$
$$\boldsymbol{H}_e^0(\mathbf{curl};\Omega) = \{\boldsymbol{u} \in \boldsymbol{L}^2(\Omega) : \mathbf{curl}\, \boldsymbol{u} \in \boldsymbol{L}^2(\Omega), \boldsymbol{n} \times \boldsymbol{u}|_{\Gamma_e} = 0\}, \tag{1.40}$$
$$\boldsymbol{H}_e^0(\mathrm{div};\Omega) = \{\boldsymbol{u} \in \boldsymbol{L}^2(\Omega) : \mathrm{div}\, \boldsymbol{u} \in L^2(\Omega), \boldsymbol{n} \cdot \boldsymbol{u}|_{\Gamma_e} = 0\}. \tag{1.41}$$

The meaning of the subscripts h and e will become clear in the next section: Γ_h and Γ_e represent the parts of the boundary where the trace of the magnetic field and the trace of the electric field are imposed respectively. In the following, the two complexes (upper and lower) in (1.34) will be referred to as the primal and dual de Rham complexes when dealing with magnetic field conforming formulations, and inversely when dealing with magnetic flux density (and electric field) conforming formulations. It can be easily shown by using Green's formulas (see Section A.3) that the operators $\mathbf{grad}_e$, $\mathbf{curl}_e$ and div_e are the adjoint operators of $-\mathrm{div}_h$, $\mathbf{curl}_h$ and $-\mathbf{grad}_h$ respectively.

By a little abuse of notation, we then denote by $H_h^1(\Omega)$, $\boldsymbol{H}_h(\mathbf{curl};\Omega)$, $\boldsymbol{H}_h(\mathrm{div};\Omega)$, $H_e^1(\Omega)$, $\boldsymbol{H}_e(\mathbf{curl};\Omega)$ and $\boldsymbol{H}_e(\mathrm{div};\Omega)$ the affine spaces corresponding ("parallel") to the vector spaces defined above, for which non-homogeneous boundary conditions are imposed (i.e. for which the traces $u|_{\Gamma_h}$, $\boldsymbol{n} \times \boldsymbol{u}|_{\Gamma_h}$, $\boldsymbol{n} \cdot \boldsymbol{u}|_{\Gamma_h}$, $u_e|_{\Gamma_e}$, $\boldsymbol{n} \times \boldsymbol{u}|_{\Gamma_e}$ or $\boldsymbol{n} \cdot \boldsymbol{u}|_{\Gamma_e}$ do not vanish on Γ_h and Γ_e respectively).

Maxwell's equations (1.1)–(1.4) and the constitutive relations (1.8), (1.10) and (1.12) fit naturally in (1.34). Indeed, the affine spaces that are appropriate to the fields $\boldsymbol{h}$, $\boldsymbol{d}$, $\boldsymbol{j}$, $\boldsymbol{e}$ and $\boldsymbol{b}$ are (see Section A.1):

$$\boldsymbol{h} \in \boldsymbol{H}_h(\mathbf{curl};\Omega), \quad \boldsymbol{d}, \boldsymbol{j} \in \boldsymbol{H}_h(\mathrm{div};\Omega),$$
$$\boldsymbol{e} \in \boldsymbol{H}_e(\mathbf{curl};\Omega), \quad \text{and} \quad \boldsymbol{b} \in \boldsymbol{H}_e(\mathrm{div};\Omega),$$

and they constitute the domains of definition of the differential operators that can be applied to these fields. It is important to remark that these domains of definition take the boundary conditions into account, and that the physical constraint of finite

energy is also met. The equations, the constitutive relations and the boundary conditions can thus be summarized in the following diagram (where the time derivative has been abstracted: one may as well consider two copies of (1.34), bound by the time derivative operator):

$$\begin{array}{ccccccc} & \xrightarrow{\mathbf{grad}_h} & \boldsymbol{h} & \xrightarrow{\mathbf{curl}_h} & \boldsymbol{j},\boldsymbol{d} & \xrightarrow{\mathrm{div}_h} & q \\ & & \uparrow\downarrow \mu & & \uparrow\downarrow \sigma,\epsilon & & \\ 0 & \xleftarrow{\mathrm{div}_e} & \boldsymbol{b} & \xleftarrow{\mathbf{curl}_e} & \boldsymbol{e} & \xleftarrow{\mathbf{grad}_e} & \end{array} \tag{1.42}$$

Tonti diagrams like (1.34) can welcome a great variety of partial differential equation models [16,103,104,154]. The magnetostatic and magnetodynamic models presented in the next section will fit very naturally in this structure. In all cases, we shall see that the constitutive laws appear vertically, whereas the differential operators appear horizontally. As for the boundary conditions, they are directly taken into account in the domains of definition of the differential operators.

1.4 Two model problems

We can now define two special cases of what has been presented in Section 1.3.2: the case where all time dependences are dropped, and the case where the wavelength of the electromagnetic phenomena is much greater than the dimensions of the domain.

1.4.1 Magnetostatics

We first consider electromagnetic phenomena independent of time (i.e. direct currents at the terminals, or currents with variations that are slow enough to lead to a skin depth much greater than the characteristic size of the domain), i.e. with $\partial_t \boldsymbol{d} = 0$ and $\partial_t \boldsymbol{b} = 0$. The Maxwell system (1.1)–(1.6) can then be uncoupled into two independent systems[3]:

$$\mathbf{curl}\,\boldsymbol{e} = 0, \quad \mathrm{div}\,\boldsymbol{d} = q \quad \text{and} \quad \boldsymbol{d} = \epsilon_0 \boldsymbol{e} + \boldsymbol{p}, \tag{1.43a–c}$$

and

$$\mathbf{curl}\,\boldsymbol{h} = \boldsymbol{j}, \quad \mathrm{div}\,\boldsymbol{b} = 0 \quad \text{and} \quad \boldsymbol{b} = \mu_0(\boldsymbol{h} + \boldsymbol{m}). \tag{1.44a–c}$$

These two systems model what is usually called electrostatic and magnetostatic phenomena respectively. Since we are only interested in magnetic phenomena, let us examine (1.44) in greater detail (the treatment of (1.43) is analogous). In magnetostatics, the current density $\boldsymbol{j}$ is given ($\boldsymbol{j} = \boldsymbol{j}_s$, cf. Section 1.2.2.2) and constitutes the source of the magnetic field. Permanent magnets can be considered as another source if the magnetic constitutive relation $\boldsymbol{b} = \mu_0(\boldsymbol{h} + \boldsymbol{m})$ is rewritten so as to highlight the remanent magnetism of these materials, i.e. as (1.12).

[3]Note that a third static problem can be defined if one considers Ohm's law and a stationary charge density ($\partial_t q = 0$), which leads to the so-called electrokinetic model: $\mathbf{curl}\,\boldsymbol{e} = 0$, $\mathrm{div}\,\boldsymbol{j} = 0$ and $\boldsymbol{j} = \sigma \boldsymbol{e} + \boldsymbol{j}_s$.

If the definition of the magnetic field $\boldsymbol{h}$ and the magnetic flux density $\boldsymbol{b}$ is sufficient to characterize a magnetic state in space, magnetic potentials can be precious auxiliaries for the reduction of the computational cost associated with the resolution of the formulations presented in Chapter 3. Indeed, the definition of potentials can enforce the strong verification (see Section A.3) of the equation associated with the nullspace of an operator (**curl** for the scalar electric and magnetic potentials and div for the electric and magnetic vector potentials).

If we can decompose the magnetic field $\boldsymbol{h}$ into two components $\boldsymbol{h}_s$ and $\boldsymbol{h}_r$, so that

$$\boldsymbol{h} = \boldsymbol{h}_s + \boldsymbol{h}_r, \quad \text{with} \quad \mathbf{curl}\, \boldsymbol{h}_s = \boldsymbol{j} \quad \text{and} \quad \mathbf{curl}\, \boldsymbol{h}_r = 0, \tag{1.45}$$

we can derive the field $\boldsymbol{h}_r$ from a scalar potential ϕ, i.e.:

$$\boldsymbol{h}_r = -\mathbf{grad}\, \phi. \tag{1.46}$$

This scalar potential is defined up to a constant term, and is often called the reduced scalar potential. One should notice that, by the extension of the Poincaré lemma, (1.46) is only valid if l cuts Σ_i, $i = 1, \ldots, l$ are defined in Ω [132, 135, 38, 13] (see Section 1.2.1).

The source magnetic field obeying $\mathbf{curl}\, \boldsymbol{h}_s = \boldsymbol{j}$ is not unique, and we have some freedom for its computation. It can, for example, be chosen as the field created by the current when all magnetic materials are removed from the domain (i.e. by assuming $\mu = \mu_0$ everywhere in Ω). In this case, $\boldsymbol{h}_s$ is given, at any point $\boldsymbol{x}$ of Ω, by the Biot-Savart law [61]

$$\boldsymbol{h}_s(\boldsymbol{x}) = \frac{1}{4\pi} \int_{\mathbb{E}^3} \frac{\boldsymbol{j}(\boldsymbol{y}) \times (\boldsymbol{x} - \boldsymbol{y})}{|\boldsymbol{x} - \boldsymbol{y}|^3}\, d\boldsymbol{y}. \tag{1.47}$$

The field $\boldsymbol{h}_r$ is then caused by the magnetization of the magnetic materials and is called the reaction field (and ϕ is called the reaction potential).

But the zero divergence insured by (1.47) is not mandatory, and there exists a whole family of fields satisfying $\mathbf{curl}\, \boldsymbol{h}_s = \boldsymbol{j}$ lacking a precise physical interpretation. We will, in general, choose the field $\boldsymbol{h}_s$ (then called generalized source field) equal to zero almost everywhere outside conductors, except in the vicinity of their associated cuts [159, 55] (see Section 3.2.4). One should note that in this case a global scalar potential (i.e. satisfying $\boldsymbol{h} = -\mathbf{grad}\, \phi$) is defined almost everywhere in Ω and that an implicit coupling with the reduced scalar potential is achieved.

Since $\mathrm{div}\, \boldsymbol{b} = 0$, we can also always derive the magnetic flux density $\boldsymbol{b}$ from a vector potential $\boldsymbol{a}$ such that

$$\boldsymbol{b} = \mathbf{curl}\, \boldsymbol{a}. \tag{1.48}$$

This potential is not unique ($\boldsymbol{a}$ is defined up to the gradient of an arbitrary scalar function). As for the source magnetic field, this gives us some freedom for its computation: introducing a gauge [4] will select one of its representatives (see Section 2.6.4.2).

We can now set up our framework for the magnetostatic model. We look for the fields $\boldsymbol{h} \in \boldsymbol{H}_h(\mathbf{curl}; \Omega)$, $\boldsymbol{j} \in \boldsymbol{H}_h(\mathrm{div}; \Omega)$ and $\boldsymbol{b} \in \boldsymbol{H}_e(\mathrm{div}; \Omega)$, solutions of (1.44)

with the constitutive law (1.12). For this purpose, the potentials $\phi \in H^1_h(\Omega)$ and $\boldsymbol{a} \in \boldsymbol{H}_e(\mathbf{curl};\Omega)$ can be introduced, which verify (1.46) and (1.48) respectively. The spaces $H^1_h(\Omega)$, $\boldsymbol{H}_h(\mathbf{curl};\Omega)$, $\boldsymbol{H}_e(\mathbf{curl};\Omega)$ and $\boldsymbol{H}_e(\mathrm{div};\Omega)$ have been defined in Section 1.3.2 and contain the boundary conditions applicable to the fields on the complementary parts Γ_h and Γ_e of the domain Ω (defined in Section 1.2.1).

The magnetostatic problem can thus be fitted in the following Tonti diagram, which is a particular case of the diagram presented in Section 1.3.2 for the whole Maxwell system:

$$\begin{array}{ccccccc} \phi & \xrightarrow{\mathbf{grad}_h} & \boldsymbol{h} & \xrightarrow{\mathbf{curl}_h} & \boldsymbol{j} & \xrightarrow{\mathrm{div}_h} & 0 \\ & & \updownarrow \mu & & & & \\ 0 & \xleftarrow{\mathrm{div}_e} & \boldsymbol{b} & \xleftarrow{\mathbf{curl}_e} & \boldsymbol{a} & & \end{array} \tag{1.49}$$

As will be seen in Chapter 3, at the discrete level, it is impossible to satisfy exactly both levels of the Tonti diagram and the constitutive relations inside the same formulation. Formulations which respect the upper level of the Tonti diagram will be called magnetic field conforming or simply "$\boldsymbol{h}$-conforming" (the upper de Rham complex will be strongly verified), while formulations which respect the lower level of the Tonti diagram will be called magnetic flux density conforming or simply "$\boldsymbol{b}$-conforming" (the lower de Rham complex will be strongly verified). Both kind of formulations will be developed and will be joined to evaluate the error committed on the connection between the primal and dual complexes: the error in the constitutive relation (see Section 2.7.4).

1.4.2 Magnetodynamics

The magnetodynamic model consists in studying electromagnetic phenomena in dynamic regime, whereby the displacement currents (the $\partial_t \boldsymbol{d}$ term in (1.1)) are neglected. This approximation is justifiable when the wavelength is much greater than the characteristic size of the domain of study Ω. Maxwell's equations (1.1)–(1.6) can thus be particularized to

$$\mathbf{curl}\,\boldsymbol{e} = -\partial_t \boldsymbol{b}, \quad \mathbf{curl}\,\boldsymbol{h} = \boldsymbol{j}, \quad \mathrm{div}\,\boldsymbol{b} = 0 \quad \text{and} \quad \boldsymbol{b} = \mu_0(\boldsymbol{h} + \boldsymbol{m}), \tag{1.50a–d}$$

to which we add the two constitutive relations (1.12) and (1.8) to close the system. As in the magnetostatic case, even if the knowledge of the magnetic field $\boldsymbol{h}$, the current density $\boldsymbol{j}$, the electric field $\boldsymbol{e}$ and the magnetic flux density $\boldsymbol{b}$ is then sufficient to characterize an electromagnetic state (provided that appropriate initial and boundary conditions are given), potentials can be precious auxiliaries for the reduction of the computational cost associated with the resolution of the magnetodynamic formulations.

In non-conducting regions Ω_c^{C}, we can decompose the magnetic field $\boldsymbol{h}$ exactly in the same way as in magnetostatics (since $\boldsymbol{j} = 0$ in Ω_c^{C}):

$$\boldsymbol{h} = \boldsymbol{h}_s + \boldsymbol{h}_r, \quad \text{with} \quad \mathbf{curl}\,\boldsymbol{h}_s = \boldsymbol{j}_s \quad \text{and} \quad \mathbf{curl}\,\boldsymbol{h}_r = 0. \tag{1.51}$$

We can then derive the field $\boldsymbol{h}_r$ from a scalar potential ϕ, i.e.:

$$\boldsymbol{h}_r = -\mathbf{grad}\,\phi. \tag{1.52}$$

The treatment of a topologically non-trivial non-conducting domain Ω_c^{C} is made in exactly the same way as the treatment of the global domain Ω in the magnetostatic case. An alternative method could of course also be considered, which consists in filling the "holes" inside the loops with a weakly conducting material (see e.g. [196]). It should also be pointed out that a somewhat more general (and more common) approach is to define an electric vector potential $\boldsymbol{t}$ by $\mathbf{curl}\,\boldsymbol{t} = \boldsymbol{j}$ [171,159,105]. This then leads to the definition of a scalar magnetic potential ω so that $\boldsymbol{h} = \boldsymbol{t} - \mathbf{grad}\,\omega$. The approach we follow is a particular case which leads to smaller problems to be solved (i.e. fewer unknowns at the discrete level): taking $\omega = 0$ gives $\boldsymbol{h} = \boldsymbol{t}$, and a scalar potential ϕ can be redefined in non-conducting regions.

Since $\mathrm{div}\,\boldsymbol{b} = 0$, we can also, as in magnetostatics, derive the magnetic flux density $\boldsymbol{b}$ from a vector potential $\boldsymbol{a}$ so that

$$\boldsymbol{b} = \mathbf{curl}\,\boldsymbol{a}. \tag{1.53}$$

Equation (1.2) then implies that $\mathbf{curl}\,(\boldsymbol{e} + \partial_t \boldsymbol{a}) = 0$, which leads to the definition of a scalar electric potential v such that

$$\boldsymbol{e} = -\partial_t \boldsymbol{a} - \mathbf{grad}\,v. \tag{1.54}$$

As in the magnetostatic case, a gauge condition has to be defined in order to select one of the possible vector potentials. We will see that setting the electric scalar potential to zero (almost everywhere) in the conducting regions will provide an implicit gauge in Ω_c, leading to a generalization of the so-called modified magnetic vector potential formulation [63,121].

We can now set up our framework for the magnetodynamic model. We look for the fields $\boldsymbol{h} \in \boldsymbol{H}_h(\mathbf{curl};\Omega)$, $\boldsymbol{j} \in \boldsymbol{H}_h(\mathrm{div};\Omega)$, $\boldsymbol{b} \in \boldsymbol{H}_e(\mathrm{div};\Omega)$ and $\boldsymbol{e} \in \boldsymbol{H}_e(\mathbf{curl};\Omega)$, solutions of (1.50) with the constitutive laws (1.12) and (1.8). For this purpose, the potentials $\phi \in H_h^1(\Omega)$, $\boldsymbol{a} \in \boldsymbol{H}_e(\mathbf{curl};\Omega)$ and $v \in H_e^1(\Omega)$ can be introduced, which verify (1.52), (1.53) and (1.54) respectively. The spaces $H_h^1(\Omega)$, $\boldsymbol{H}_h(\mathbf{curl};\Omega)$, $H_e^1(\Omega)$, $\boldsymbol{H}_e(\mathbf{curl};\Omega)$ and $\boldsymbol{H}_e(\mathrm{div};\Omega)$ have been defined in Section 1.3.2 and contain the boundary conditions applicable to the fields on the complementary parts Γ_h and Γ_e of the domain Ω.

The magnetodynamic problem can thus be fitted in the following Tonti diagram, which is a particular case of the diagram presented in Section 1.3.2 for the whole Maxwell system:

$$\begin{array}{ccccccc}
\phi & \xrightarrow{\mathbf{grad}_h} & \boldsymbol{h} & \xrightarrow{\mathbf{curl}_h} & \boldsymbol{j} & \xrightarrow{\mathrm{div}_h} & 0 \\
 & & \updownarrow{\scriptstyle \mu} & & \updownarrow{\scriptstyle \sigma} & & \\
0 & \xleftarrow{\mathrm{div}_e} & \boldsymbol{b} & \xleftarrow{\mathbf{curl}_e} & \boldsymbol{e},\boldsymbol{a} & \xleftarrow{\mathbf{grad}_e} & v
\end{array} \tag{1.55}$$

Chapter 2

Mixed finite elements

2.1 Introduction

The purpose of a discretization procedure is to "replace" the infinite dimensional (or continuous) spaces $H^1(\Omega)$, $\boldsymbol{H}(\mathbf{curl};\Omega)$, $\boldsymbol{H}(\mathrm{div};\Omega)$ and $L^2(\Omega)$ by some finite dimensional (or discrete) subspaces. The main challenge of the discretization is to preserve the structure of the complexes in (1.34), even if it is agreed that both complexes and the constitutive law isomorphisms all together cannot be preserved with finite dimensional subspaces [21, 16]. If the domains on which these subspaces are defined are themselves discretized (i.e. if they are defined as the union of elementary geometrical elements of simple shapes), and if the finite dimensional subspaces are built in such a way that their elements are piece-wise defined, then the discretization method is called a finite element method (FEM) [39, 44, 120].

The theory of curl- and div-conforming finite elements (so-called mixed finite elements) was introduced in the late 70's and in the 80's by Raviart and Thomas [175] for finite dimensional subspaces of $\boldsymbol{H}(\mathrm{div};\Omega)$ and by Nédélec [161, 162] for finite dimensional subspaces of $\boldsymbol{H}(\mathbf{curl};\Omega)$. Since then, the topic has been extensively covered in the literature, both in the world of computational electromagnetics (with an emphasis on tetrahedral curl-conforming elements [157, 141, 218, 1, 223]) and in many other fields of application [175, 29, 163, 89]. However, a recurrent problem with mixed finite elements has always been the actual expression of the vector basis functions (which were seldom explicitly written) and the construction of a complete sequence of finite element spaces. The introduction of Whitney elements by Bossavit in 1988 [14] was a major step forward in the solving of these two problems: Whitney elements reinterpreted Nédélec's lowest order tetrahedral curl- and div-conforming elements and the classical continuous and piece-wise continuous tetrahedral elements in terms of discrete differential forms (the Whitney forms [222]), in order to build a complete sequence of finite elements for three-dimensional computations.

The closeness of Whitney elements to the nature of the interpolated fields (the degrees of freedom all have a clear physical interpretation) has made them the natural choice for the discretization of electromagnetic fields for the last decade. They have since then been proved to provide the sound discretization basis for

electromagnetic field problems in any configuration, and in particular for gauging, for making cuts, and for building global discrete shape functions (source fields) for the non-exact part of the fields in the presence of holes and loops. Indeed, the Whitney nodal element, based on the Whitney differential form of degree zero, is the classical first order scalar Lagrange finite element [228], well suited for the discretization of scalar fields like a scalar potential, a temperature field, etc. The degrees of freedom of Whitney nodal elements are associated with the nodes of the finite element mesh and consist of the punctual evaluation of the field at these nodes. The edge and face elements (derived from the Whitney differential forms of degree one and two respectively, which are polynomials on tetrahedra whose tangential or normal components match on the faces and which are uniquely determined by their integrals on the edges or the faces) span an incomplete first order polynomial basis. They are well suited for the discretization of vector fields whose tangential or normal components are continuous across material interfaces, like the electric and magnetic fields or the magnetic flux density and the current density. Their degrees of freedom are the circulation along the edges of the mesh for edge elements and the fluxes across the faces of the mesh for face elements. The volume element (derived from the Whitney differential form of degree three) is the classical piece-wise continuous scalar element of order zero (i.e. with constant interpolation), whose unique degree of freedom is the integration over its volume. This makes it, for example, suitable for the discretization of densities like the electric charge or a heat source density.

But Whitney elements still lack some important features: they are only defined on tetrahedra, and span at most the space of first order polynomials. The two main objectives should thus be:

1. to define a sequence of finite elements not limited to tetrahedra, but to a collection of tetrahedra, hexahedra and prisms. This is interesting for models of greater geometrical complexity, as well as for a more efficient use of both structured and unstructured meshes;

2. to increase the accuracy of interpolation, which means introducing higher order polynomial spaces. Although this may seem a step backward in terms of intuitive physical interpretation (the degrees of freedom will loose the simplicity that make Whitney elements so appealing), it is mandatory for the implementation of modern adaptation techniques. Moreover, it would be interesting for these high order finite elements to fulfill the hierarchy property, which means that the basis functions for a given interpolation order would be a subset of the basis functions used for the interpolation at any higher order. This would allow to combine elements of different orders in the same mesh and would also be useful for the development of adaptive multigrid solvers (see e.g. [109, 211]).

In this chapter we present a complete sequence of high order hierarchical finite elements built on tetrahedra, hexahedra and prisms. (Note that mixed elements have also been recently designed for pyramids [95, 226, 35].) This sequence is based on the work done by Nédélec in [161] for tetrahedra and hexahedra and in [162] for prisms,

and extends the work by Dular [47,56,58]. Our aim is not to build new finite element bases, but rather to present the general framework required for the construction of the hierarchical elements used for the discretization of the formulations established in Chapter 3. The actual basis functions for tetrahedra that fit in this framework have for example been presented by Bossavit [21] for the lowest order and by Webb and Forghani [218] (later generalized by Ren [190]) for higher orders. Hexahedral basis functions have been presented by van Welij [221], Kameari [121] and Dular [56] and many others, while prismatic basis functions have been presented by Dular in [56]. Other useful references include Cendes [32], Demcowicz [43], Lee [141], Yioultsis and Tsiboukis [223, 224], Wang [213] and Hiptmair [110].

2.2 Definitions

2.2.1 Finite element (K, Σ, S)

A finite element is defined by the triplet (K, Σ, S), where [120, 162, 163]:

1. K is a geometrical element of $\mathbb{E}^3$;
2. Σ is a set of N degrees of freedom (or connectors) consisting of linear forms (functionals) on the space of scalar or vector-valued functions defined on K;
3. S is a function space of finite dimension N, of the space of scalar or vector valued functions.

We restrict our study to three-dimensional finite elements built on tetrahedra, hexahedra and prisms. We denote by T, H and P the reference tetrahedron, hexahedron and prism defined in a local coordinate system (u, v, w) (see Figures 2.2, 2.3 and 2.4 on pages 38, 39 and 40 respectively):

$$\mathrm{T} = \{(u, v, w) \in \mathbb{E}^3 : 0 < u < 1 - v - w, v > 0, w > 0\}, \tag{2.1}$$
$$\mathrm{H} = \{(u, v, w) \in \mathbb{E}^3 : -1 < u < 1, -1 < v < 1, -1 < w < 1\}, \tag{2.2}$$
$$\mathrm{P} = \{(u, v, w) \in \mathbb{E}^3 : 0 < u < 1 - v, v > 0, -1 < w < 1\}. \tag{2.3}$$

The geometrical element K is then obtained by affine transformation of the reference elements T, H or P (see Section 2.6.2). The sets of nodes, edges and faces of the element K are denoted by $\mathcal{N}(K)$ (with $\dim(\mathcal{N}(K)) = 4$, 8 or 6 for tetrahedra, hexahedra or prims respectively), $\mathcal{E}(K)$ (with $\dim(\mathcal{E}(K)) = 6$, 12 or 9) and $\mathcal{F}(K)$ (with $\dim(\mathcal{F}(K)) = 4$, 6 or 5). Note that the restriction of all the following developments to the two-dimensional case (with triangular and quadrangular geometrical elements) is straightforward.

The N functionals $\sigma_i \in \Sigma$ $(i = 1, \ldots, N)$ are called the degrees of freedom of the finite element (K, Σ, S). Basis functions of (K, Σ, S) can be defined as N linearly independent functions $s_j \in S$ $(j = 1, \ldots, N)$ chosen such that

$$\forall \sigma_i \in \Sigma : \sigma_i(s_j) = \delta_{ij}, \quad i = 1, \ldots, N, \tag{2.4}$$

where δ_{ij} denotes the Kronecker symbol.

The unisolvence of the finite element (K, Σ, S) is assured if any function of S can be uniquely determined thanks to the degrees of freedom σ_i of Σ [120, 163]. Equivalently, the finite element is unisolvent if, for any set of real numbers $\alpha_1, \alpha_2, \ldots, \alpha_N$, there exists only one element s of S such that

$$\forall \sigma_i \in \Sigma : \sigma_i(s) = \alpha_i, \quad i = 1, \ldots, N.$$

If (K, Σ, S) is unisolvent, one can associate one interpolant πs with each s on K such that

$$\sigma_j(s) = \sigma_j(\pi s), \quad \forall \sigma_j \in \Sigma.$$

Note that the choice of the basis functions of S is not unique: (2.4) is generally chosen so that the coefficients of the basis functions in the interpolant πs of the function s are the degrees of freedom.

2.2.2 Conformity

From now on we only consider either scalar polynomial basis functions or vector basis functions whose components are polynomials. The three following lemmas [161] give the main properties of finite elements in $H^1(\Omega)$, $\boldsymbol{H}(\mathbf{curl}; \Omega)$ and $\boldsymbol{H}(\mathrm{div}; \Omega)$. If Ω is the union of two geometrical elements K_1 et K_2 with a common face f of normal $\boldsymbol{n}$:

1. a function u of $H^1(K_1) \cup H^1(K_2)$ belongs to $H^1(\Omega)$ if and only if the function u is the same on both sides of the face f. Such a function is called "conform";

2. a vector field $\boldsymbol{u}$ of $\boldsymbol{H}^1(K_1) \cup \boldsymbol{H}^1(K_2)$ belongs to $\boldsymbol{H}(\mathbf{curl}; \Omega)$ if and only if its trace $\boldsymbol{u} \times \boldsymbol{n}$ is the same on both sides of the face f. Such a vector field is called "curl-conform";

3. a vector field $\boldsymbol{u}$ of $\boldsymbol{H}^1(K_1) \cup \boldsymbol{H}^1(K_2)$ belongs to $\boldsymbol{H}(\mathrm{div}; \Omega)$ if and only if its trace $\boldsymbol{u} \cdot \boldsymbol{n}$ is the same on both sides of the face f. Such a vector field is called "div-conform".

A family of finite elements is said to be of class $V(\Omega)$, or conforming in $V(\Omega)$, when the function defined by $\pi_1 s$ in K_1 and by $\pi_2 s$ in K_2 belongs to the function space $V(\Omega)$ [161, 163]. We can thus define four types of mixed elements, depending on their class: $H^1(\Omega)$, $\boldsymbol{H}(\mathbf{curl}; \Omega)$, $\boldsymbol{H}(\mathrm{div}; \Omega)$ or $L^2(\Omega)$.

1. Finite elements of class $H^1(\Omega)$, i.e. conforming finite elements, interpolate scalar fields that are continuous across any interface. These elements are sometimes referred to as "nodal elements", due to the fact that their degrees of freedom are associated with the nodes of the element for the lowest interpolation order. This is no longer appropriate for high order elements, where the degrees of freedom are associated with the nodes, edges, faces and the element itself (see Section 2.4). These kinds of elements will for example be used to discretize the scalar magnetic potential ϕ and the scalar electric potential v.

2. Finite elements of class $\boldsymbol{H}(\mathbf{curl};\Omega)$, i.e. curl-conforming finite elements, only ensure the continuity of the tangential part of the interpolated field. These elements are sometimes referred to as "edge elements", since their degrees of freedom are associated with the edges in the case of the lowest order elements. As for nodal elements, this is no longer appropriate for high order cases, where the degrees of freedom are associated with the edges, the faces and the volume of the element. Curl-conforming elements will be used to discretize the magnetic field $\boldsymbol{h}$, the magnetic vector potential $\boldsymbol{a}$ and the electric field $\boldsymbol{e}$.

3. Finite elements of class $\boldsymbol{H}(\mathrm{div};\Omega)$, i.e. div-conforming finite elements, only ensure the continuity of the normal component of the interpolated field. These elements are sometimes referred to as "face elements", since their degrees of freedom are associated with the faces in the case of the lowest interpolation order. This is no longer appropriate for high order cases, where the degrees of freedom are then associated with the faces and the volume of the element. Div-conforming elements may be used to discretize the magnetic flux density $\boldsymbol{b}$, the current density $\boldsymbol{j}$ or the electric displacement $\boldsymbol{d}$

4. Finite elements of class $L^2(\Omega)$ do not impose any inter-element continuity requirement on the interpolated field. These elements are sometimes called "volume elements", since their degrees of freedom are always associated with the volume of the element. They may for example be used to interpolate the electric charge density ρ.

These concepts are in fact tightly related to the geometrical nature of electromagnetic phenomena (see Section A.1).

2.3 Local spaces $W_p^i(K)$

2.3.1 Introduction

We have to define the local function spaces S of order p for the four kinds of mixed elements (K, Σ, S) built on tetrahedra, hexahedra and prisms. We denote these function spaces by

$$W_p^0(K) \subset H^1(K), \tag{2.5}$$
$$W_p^1(K) \subset \boldsymbol{H}(\mathbf{curl}; K), \tag{2.6}$$
$$W_p^2(K) \subset \boldsymbol{H}(\mathrm{div}; K), \tag{2.7}$$
$$W_p^3(K) \subset L^2(K), \tag{2.8}$$

for $p > 0$ and $K \in \{\mathrm{T}, \mathrm{H}, \mathrm{P}\}$.

Each function space can be decomposed into the nullspace (or kernel) of the associated differential operator (**grad**, **curl** and div respectively) and its orthogonal complement, i.e.:

$$W_p^i(K) = \mathcal{NS}_p^i(K) \oplus \mathcal{S}_p^i(K), \quad i = 0, \ldots, 2.$$

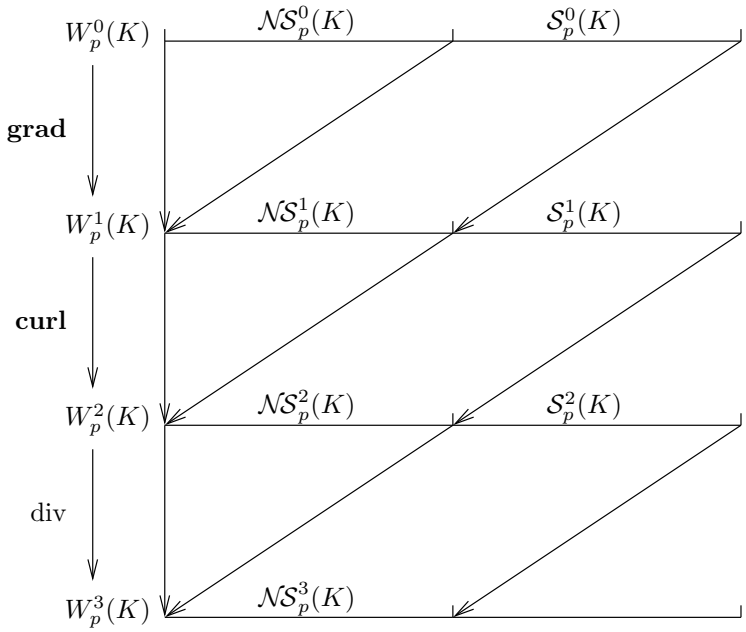

Figure 2.1: Local de Rham complex for the discrete case.

By the Poincaré lemma [38], since the geometric elements K are topologically trivial, the differential operators **grad**, **curl** and div are isomorphisms of $\mathcal{S}_p^0(K)$ onto $\mathcal{NS}_p^1(K)$, $\mathcal{S}_p^1(K)$ onto $\mathcal{NS}_p^2(K)$ and $\mathcal{S}_p^2(K)$ onto $\mathcal{NS}_p^3(K)$ respectively, and thus

$$\dim(\mathcal{S}_p^i(K)) = \dim(\mathcal{R}_p^i(K)) = \dim(\mathcal{NS}_p^{i+1}(K)), \quad i = 0, \ldots, 2.$$

In other words, the fields whose curl or divergence vanishes in K can be expressed as the gradient or the curl of some other fields. The sequence

$$W_p^0(K) \xrightarrow{\textbf{grad}} W_p^1(K) \xrightarrow{\textbf{curl}} W_p^2(K) \xrightarrow{\text{div}} W_p^3(K)$$

formed by the local spaces is thus exact (see Section A.2.6). The decomposition is summed up on the de Rham complex shown in Figure 2.1, which should be compared with Figure 1.7, where, due to the loops and cavities in Ω, the sequence is not exact (the "defects" being described by the spaces $\mathcal{H}^1$ and $\mathcal{H}^2$).

In addition to the properties stated in Section 2.2, the element of order p should:

1. correctly model the nullspace of the differential operator **grad**, **curl** or div;
2. be complete to the polynomial order $p-1$ in the range of the differential operator **grad**, **curl** or div.

It is important to note that such elements, conforming in $\boldsymbol{H}(\textbf{curl};\Omega)$, $\boldsymbol{H}(\text{div};\Omega)$ and $L^2(\Omega)$, will only present incomplete polynomial bases in the domain of the considered operator [87, 190]. This is what happens with Whitney elements: they are complete to the first polynomial order for nodal elements, but are of incomplete first order for the edge and face elements, and of order zero for volume elements.

It is of course also possible to design elements of complete polynomial bases (as, for example, in [162]). Complete elements do not improve the modeling of the range of the differential operator (they only increase the size of the space discretizing the nullspace of the operator). For example, the use of complete $\boldsymbol{H}(\mathbf{curl};\Omega)$ and $\boldsymbol{H}(\mathrm{div};\Omega)$ elements to model rotational and divergent fields, respectively, is redundant. But even if they do not affect the accuracy of the curl or divergence, these complete elements still allow a better approximation of the vector field itself. Thus, complete $\boldsymbol{H}(\mathbf{curl};\Omega)$ elements may for example be better at modeling the curl-free fields appearing in magnetodynamic or high frequency problems. Anyway, by building hierarchical bases for the whole family of mixed elements, we will see that each complete element appears, when increasing the order p, as a natural intermediate between two incomplete elements. In correspondence with the incomplete local spaces $W_p^i(K)$, $i = 0,\ldots,3$, we will denote the complete local spaces by $V_p^i(K)$, $i = 0,\ldots,3$.

2.3.2 Tetrahedra

In order to construct the local spaces $W_p^i(\mathrm{T})$ ($i = 0,\ldots,3$, $p > 0$), we need to introduce the following spaces of polynomials [161, 190]:

1. P_p, the space of polynomials of order p of three variables u, v and w. We have $\dim(P_p) = (p+1)(p+2)(p+3)/6$;
2. $\widetilde{P}_p$, the space of homogeneous polynomials of order p of three variables u, v and w. We have $\dim(\widetilde{P}_p) = (p+1)(p+2)/2$;
3. $\widetilde{S}_p = \{\boldsymbol{u} \in (\widetilde{P}_p)^3 : \boldsymbol{u}\cdot\boldsymbol{r} = 0\}$, where $\boldsymbol{r}$ is the vector (u,v,w), the space of homogeneous polynomial vectors of order p having a non-zero curl. We thus have $\dim(\widetilde{S}_p) = \dim((\widetilde{P}_p)^3) - \dim(\widetilde{P}_{p+1}) = p(p+2)$;
4. $\widetilde{T}_p = \{\boldsymbol{u} \in (\widetilde{P}_p)^3 : \boldsymbol{u}\times\boldsymbol{r} = 0\}$, where $\boldsymbol{r}$ is the vector (u,v,w), the space of homogeneous polynomial vectors of order p having a non-zero divergence. We thus have $\dim(\widetilde{T}_p) = \dim(\widetilde{P}_{p-1}) = p(p+1)/2$.

The local function spaces for the tetrahedral elements conforming in $H^1(\Omega)$, $\boldsymbol{H}(\mathbf{curl};\Omega)$, $\boldsymbol{H}(\mathrm{div};\Omega)$ and $L^2(\Omega)$ are [161]

$$W_p^0(\mathrm{T}) = P_p, \tag{2.9}$$
$$W_p^1(\mathrm{T}) = (P_{p-1})^3 \oplus \widetilde{S}_p, \tag{2.10}$$
$$W_p^2(\mathrm{T}) = (P_{p-1})^3 \oplus \widetilde{T}_p, \tag{2.11}$$
$$W_p^3(\mathrm{T}) = P_{p-1}. \tag{2.12}$$

The lowest order function spaces (for $p = 1$) are those spanned by the Whitney elements [21]. The dimension of the spaces (2.9)–(2.12) is summed up in Table 2.1, together with the dimension of the nullspace of the associated differential operator and its orthogonal complement.

It is interesting to analyze (2.9)–(2.12) in the light of the remark made at the end of Section 2.3.1 about mixed elements of complete and incomplete polynomial bases. For this purpose, we introduce the following spaces:

1. $\widetilde{G}_p = \{\boldsymbol{u} \in (\widetilde{P}_p)^3 : \boldsymbol{u} = \mathbf{grad}\, v, v \in \widetilde{P}_{p+1}\}$, the space of homogeneous polynomial vectors of order p which are the gradients of a homogeneous polynomial of order $p+1$. We have $\dim(\widetilde{G}_p) = \dim(\widetilde{P}_{p+1}) = (p+2)(p+3)/2$, and the following Helmholtz decomposition holds: $(\widetilde{P}_p)^3 = \widetilde{G}_p \oplus \widetilde{S}_p$;

2. $\widetilde{C}_p = \{\boldsymbol{u} \in (\widetilde{P}_p)^3 : \boldsymbol{u} = \mathbf{curl}\, \boldsymbol{v}, \boldsymbol{v} \in \widetilde{S}_{p+1}\}$, the space of homogeneous polynomial vectors of order p which are the curls of a homogeneous polynomial of order $p+1$. We have $\dim(\widetilde{C}_p) = \dim(\widetilde{S}_{p+1}) = (p+1)(p+3)$, and the following Helmholtz decomposition holds: $(\widetilde{P}_p)^3 = \widetilde{C}_p \oplus \widetilde{T}_p$.

We can now explicitly express the function spaces $W_p^i(\mathrm{T})$ in terms of the nullspace and the orthogonal complement to the nullspace of the operators **grad**, **curl**, and div:

$$
\begin{aligned}
W_1^0(\mathrm{T}) &= \underbrace{\widetilde{P}_0}_{\mathcal{NS}_1^0(\mathrm{T})} \oplus \underbrace{\widetilde{P}_1}_{\mathcal{S}_1^0(\mathrm{T})} = P_1, & W_p^0(\mathrm{T}) &= \underbrace{W_{p-1}^0(\mathrm{T}) \oplus \widetilde{P}_p}_{V_p^0(\mathrm{T})} = P_p,\\
W_1^1(\mathrm{T}) &= \underbrace{\widetilde{G}_0}_{\mathcal{NS}_1^1(\mathrm{T})} \oplus \underbrace{\widetilde{S}_1}_{\mathcal{S}_1^1(\mathrm{T})}, & W_p^1(\mathrm{T}) &= \underbrace{W_{p-1}^1(\mathrm{T}) \oplus \widetilde{G}_{p-1}}_{V_{p-1}^1(\mathrm{T})} \oplus \widetilde{S}_p = \underbrace{G_{p-1}}_{\mathcal{NS}_p^1(\mathrm{T})} \oplus \underbrace{S_p}_{\mathcal{S}_p^1(\mathrm{T})},\\
W_1^2(\mathrm{T}) &= \underbrace{\widetilde{C}_0}_{\mathcal{NS}_1^2(\mathrm{T})} \oplus \underbrace{\widetilde{T}_1}_{\mathcal{S}_1^2(\mathrm{T})}, & W_p^2(\mathrm{T}) &= \underbrace{W_{p-1}^2(\mathrm{T}) \oplus \widetilde{C}_{p-1}}_{V_{p-1}^2(\mathrm{T})} \oplus \widetilde{T}_p = \underbrace{C_{p-1}}_{\mathcal{NS}_p^2(\mathrm{T})} \oplus \underbrace{T_p}_{\mathcal{S}_p^2(\mathrm{T})},\\
W_1^3(\mathrm{T}) &= \underbrace{\widetilde{P}_0}_{\mathcal{NS}_1^3(\mathrm{T})} = P_0, & W_p^3(\mathrm{T}) &= \underbrace{W_{p-1}^3(\mathrm{T}) \oplus \widetilde{P}_{p-1}}_{V_{p-1}^3(\mathrm{T})} = P_{p-1}.
\end{aligned}
$$

In the preceding expressions, we posed $G_p = \widetilde{G}_0 \oplus \cdots \oplus \widetilde{G}_p$, $S_p = \widetilde{S}_0 \oplus \cdots \oplus \widetilde{S}_p$, $C_p = \widetilde{C}_0 \oplus \cdots \oplus \widetilde{C}_p$ and $T_p = \widetilde{T}_0 \oplus \cdots \oplus \widetilde{T}_p$. The complete local spaces $V_p^i(\mathrm{T})$ $(i = 0, \ldots, 3)$ can then be simply expressed as

$$
\begin{aligned}
V_p^0(\mathrm{T}) &= W_p^0(\mathrm{T}) = P_p,\\
V_p^1(\mathrm{T}) &= W_p^1(\mathrm{T}) \oplus \widetilde{G}_p = (P_p)^3,\\
V_p^2(\mathrm{T}) &= W_p^2(\mathrm{T}) \oplus \widetilde{C}_p = (P_p)^3,\\
V_p^3(\mathrm{T}) &= W_p^3(\mathrm{T}) \oplus \widetilde{P}_p = P_p,
\end{aligned}
$$

and we can see, for example, that to build a curl-conforming element complete to the pth polynomial order in the domain of the **curl** operator, we can only complete the nullspace of the incomplete element by the missing gradient fields (since, by the Helmholtz decomposition, $(\widetilde{P}_p)^3 = \widetilde{S}_p \oplus \widetilde{G}_p$). For this element, we can thus only expect an improvement of the field representation and not of its curl.

Table 2.1: Dimension of function spaces for the tetrahedral element.

i	$\mathcal{NS}_p^i(\mathrm{T})$	$\mathcal{S}_p^i(\mathrm{T})$	$W_p^i(\mathrm{T})$
0	1	$(p+1)(p+2)(p+3)/6-1$	$(p+1)(p+2)(p+3)/6$
1	$(p+1)(p+2)(p+3)/6-1$	$p(p+1)(2p+7)/6$	$p(p+2)(p+3)/2$
2	$p(p+1)(2p+7)/6$	$p(p+1)(p+2)/6$	$p(p+1)(p+3)/2$
3	$p(p+1)(p+2)/6$	–	$p(p+1)(p+2)/6$

2.3.3 Hexahedra

The case of hexahedral elements is simpler. In order to construct the local spaces $W_p^i(\mathrm{H})$ $(i=0,\ldots,3,\ p>0)$, we need to introduce $Q_{p,q,r}$, the space of polynomials of order p, q and r in u, v and w respectively, with $\dim(Q_{p,q,r})=(p+1)(q+1)(r+1)$. We have [161]

$$W_p^0(\mathrm{H}) = Q_{p,p,p}, \tag{2.13}$$
$$W_p^1(\mathrm{H}) = Q_{p,p,p-1}\times Q_{p,p-1,p}\times Q_{p-1,p,p}, \tag{2.14}$$
$$W_p^2(\mathrm{H}) = Q_{p-1,p-1,p}\times Q_{p-1,p,p-1}\times Q_{p,p-1,p-1}, \tag{2.15}$$
$$W_p^3(\mathrm{H}) = Q_{p-1,p-1,p-1}. \tag{2.16}$$

For $p=1$, the preceding expressions correspond to the function spaces spanned by the generalization of Whitney elements to cubes [161, 56, 95]. The dimension of the spaces (2.13)–(2.16) is summed up in Table 2.2. In the same way as for tetrahedra, complete polynomial spaces can also be constructed by completing the nullspace of the differential operators, which leads to: $V_p^0(\mathrm{H})=V_p^3(\mathrm{H})=Q_{p,p,p}$ and $V_p^1(\mathrm{H})=V_p^2(\mathrm{H})=(Q_{p,p,p})^3$.

Table 2.2: Dimension of function spaces for the hexahedral element.

i	$\mathcal{NS}_p^i(\mathrm{H})$	$\mathcal{S}_p^i(\mathrm{H})$	$W_p^i(\mathrm{H})$
0	1	$(p+1)^3-1$	$(p+1)^3$
1	$(p+1)^3-1$	$p^2(2p+3)$	$3p(p+1)^2$
2	$p^2(2p+3)$	p^3	$3p^2(p+1)$
3	p^3	–	p^3

2.3.4 Prisms

Prismatic elements can be seen as a combination of tetrahedral and hexahedral elements. In order to construct the local spaces $W_p^i(\mathrm{P})$ $(i=0,\ldots,3,\ p>0)$ we introduce the following spaces, based on the definition of the spaces P_p, $\widetilde{S}_p$ and $\widetilde{T}_p$ introduced in Section 2.3.2:

1. $P_{p,q}$, the space of polynomials of order p in the two variables u and v, and of order q in the variable w. We have $\dim(P_{p,q}) = (q+1)(p+1)(p+2)/2$;

2. $R_{p,q}$, the space of polynomials of order q in w and which are in $P^3_{p-1} \oplus \widetilde{S}_p$ for w fixed;

3. $D_{p,q}$, the space of polynomials of order q in w and which are in $P^3_{p-1} \oplus \widetilde{T}_p$ for w fixed.

We have [162]

$$W^0_p(\mathrm{P}) = P_{p,p}, \tag{2.17}$$
$$W^1_p(\mathrm{P}) = R_{k,k} \times P_{p,p-1}, \tag{2.18}$$
$$W^2_p(\mathrm{P}) = D_{k,k} \times P_{p-1,p}, \tag{2.19}$$
$$W^3_p(\mathrm{P}) = P_{p-1,p-1}. \tag{2.20}$$

For $p = 1$, the preceding expressions correspond to the function spaces spanned by the generalization of Whitney elements to prims [56]. The dimension of the spaces (2.17)–(2.20) is summed up in Table 2.3. In the same way as for tetrahedra and hexahedra, complete polynomial spaces can also be constructed by completing the nullspace of the differential operators: $V^0_p(\mathrm{P}) = V^3_p(\mathrm{P}) = P_{p,p}$ and $V^1_p(\mathrm{P}) = V^2_p(\mathrm{P}) = (P_{p,p})^3$.

Table 2.3: Dimension of function spaces for the prismatic element.

i	$\mathcal{NS}^i_p(\mathrm{P})$	$\mathcal{S}^i_p(\mathrm{P})$	$W^i_p(\mathrm{P})$
0	1	$(p+1)^2(p+2)/2 - 1$	$(p+1)^2(p+2)/2$
1	$(p+1)^2(p+2)/2 - 1$	$p(2p^2+5p+1)/2$	$3p(p+1)(p+2)/2$
2	$p(2p^2+5p+1)/2$	$p^2(p+1)/2$	$p^2(p+2) + p(p+1)^2/2$
3	$p^2(p+1)/2$	–	$p^2(p+1)/2$

2.3.5 Local trace spaces

We will sometimes have to consider the restriction of a field on the boundary of the geometrical element K as an unknown. For this purpose, we have to define the traces of the local spaces on two-dimensional geometrical elements, i.e. on triangular and quadrangular elements mapped on the faces of the three-dimensional elements T, H and P. It is easy to show that ($\boldsymbol{n}$ denotes the exterior normal on ∂K):

1. for $u \in W^0_p(K)$, the trace $u\big|_{\partial K}$ belongs to $W^0_p(\partial K)$;

2. for $\boldsymbol{u} \in W^1_p(K)$, the trace $\boldsymbol{n} \times \boldsymbol{u}\big|_{\partial K}$ belongs to $W^2_p(\partial K)$;

3. for $\boldsymbol{u} \in W^2_p(K)$, the trace $\boldsymbol{n} \cdot \boldsymbol{u}\big|_{\partial K}$ belongs to $W^3_p(\partial K)$.

2.4 Degrees of freedom

2.4.1 General expressions

The degrees of freedom $\sigma \in \Sigma$ are momenta of appropriate polynomials $q(u,v,w)$ or $\boldsymbol{q}(u,v,w)$ over the nodes $n \in \mathcal{N}(K)$, the edges $e \in \mathcal{E}(K)$, the faces $f \in \mathcal{F}(K)$ and the volume K of the element. In order to keep the notations as generic as possible, all the degrees of freedom will be from now on denoted by the general expression

$$\sigma = \sigma_p^{i,x}, \tag{2.21}$$

where i corresponds to the type of the discrete space $W_p^i(K)$ (i.e. 0 for conforming elements, 1 for curl-conforming elements, 2 for div-conforming elements and 3 for piece-wise continuous elements), where x stands either for n, e, f or K, and where p is the order of the corresponding discrete space. When a subscript or a superscript is omitted, the whole range of values is implicitly assumed. For an element $(K, \Sigma, W_p^0(K))$ conforming in $H^1(\Omega)$, we have, with $s \in W_p^0(K)$:

$$\sigma_p^{0,n} = s\big|_n, \quad \forall n \in \mathcal{N}(K), \tag{2.22}$$

$$\sigma_p^{0,e} = \int_e q\, s\, dl, \quad \forall q \in X_p^{0,e}, \quad \forall e \in \mathcal{E}(K), \tag{2.23}$$

$$\sigma_p^{0,f} = \int_f q\, s\, ds, \quad \forall q \in X_p^{0,f}, \quad \forall f \in \mathcal{F}(K), \tag{2.24}$$

$$\sigma_p^{0,K} = \int_K q\, s\, dv, \quad \forall q \in X_p^{0,K}, \tag{2.25}$$

where the spaces X_p will have to be defined for each kind of geometrical element K. For an element conforming in $\boldsymbol{H}(\mathbf{curl};\Omega)$, the momenta are, with $\boldsymbol{s} \in W_p^1(K)$:

$$\sigma_p^{1,e} = \int_e q\, \boldsymbol{s} \cdot d\boldsymbol{l}, \quad \forall q \in X_p^{1,e}, \quad \forall e \in \mathcal{E}(K), \tag{2.26}$$

$$\sigma_p^{1,f} = \int_f \boldsymbol{q} \cdot \boldsymbol{s} \times \boldsymbol{n}\, ds, \quad \forall \boldsymbol{q} \in X_p^{1,f}, \quad \forall f \in \mathcal{F}(K), \tag{2.27}$$

$$\sigma_p^{1,K} = \int_K \boldsymbol{q} \cdot \boldsymbol{s}\, dv, \quad \forall \boldsymbol{q} \in X_p^{1,K}. \tag{2.28}$$

And, in a similar way, for elements conforming in $\boldsymbol{H}(\mathrm{div};\Omega)$ and $L^2(\Omega)$, we have, with $\boldsymbol{s} \in W_p^2(K)$ and $s \in W_p^3(K)$ respectively:

$$\sigma_p^{2,f} = \int_f q\, \boldsymbol{s} \cdot \boldsymbol{n}\, ds, \quad \forall q \in X_p^{2,f}, \quad \forall f \in \mathcal{F}(K), \tag{2.29}$$

$$\sigma_p^{2,K} = \int_K \boldsymbol{q} \cdot \boldsymbol{s}\, dv, \quad \forall \boldsymbol{q} \in X_p^{2,K}, \tag{2.30}$$

and

$$\sigma_p^{3,K} = \int_K q\, s\, dv, \quad \forall q \in X_p^{3,K}. \tag{2.31}$$

The spaces of polynomials $X_p^{i,j}$ depend, of course, on the type of the geometrical element K. For tetrahedra, we have (see [161, 89] for X_p^1 and [161, 29] for X_p^2)

$$X_p^{0,e} = P_{p-2}(e), \qquad X_p^{0,f} = P_{p-3}(f), \qquad X_p^{0,K} = P_{p-4}, \tag{2.32}$$
$$X_p^{1,e} = P_{p-1}(e), \qquad X_p^{1,f} = (P_{p-2}(f))^2, \qquad X_p^{1,K} = (P_{p-3})^3, \tag{2.33}$$
$$X_p^{2,f} = P_{p-1}(f), \qquad X_p^{2,K} = (P_{p-2})^3, \tag{2.34}$$
$$X_p^{3,K} = P_{p-1}. \tag{2.35}$$

For hexahedra, we have (see [161] for X_p^1 and X_p^2)

$$X_p^{0,e} = P_{p-2}(e), \tag{2.36}$$
$$X_p^{0,f} = Q_{p-3,p-2}(f) \times Q_{p-2,p-3}(f), \tag{2.37}$$
$$X_p^{0,K} = Q_{p-2,p-3,p-3} \times Q_{p-3,p-2,p-3} \times Q_{p-3,p-3,p-2}, \tag{2.38}$$
$$X_p^{1,e} = P_{p-1}(e), \tag{2.39}$$
$$X_p^{1,f} = Q_{p-2,p-1}(f) \times Q_{p-1,p-2}(f), \tag{2.40}$$
$$X_p^{1,K} = Q_{p-1,p-2,p-2} \times Q_{p-2,p-1,p-2} \times Q_{p-2,p-2,p-1}, \tag{2.41}$$
$$X_p^{2,f} = Q_{p-1,p-1}(f), \tag{2.42}$$
$$X_p^{2,K} = Q_{p-2,p-1,p-1} \times Q_{p-1,p-2,p-1} \times Q_{p-1,p-1,p-2}, \tag{2.43}$$
$$X_p^{3,K} = Q_{p-1,p-1,p-1}. \tag{2.44}$$

The degrees of freedom associated with the edges of the prismatic element are identical to the degrees of freedom of the tetrahedral and hexahedral element (i.e. (2.32a) or (2.36), and (2.33a) or (2.39)). The degrees of freedom associated with the two triangular faces are identical to the degrees of freedom of the tetrahedral element (i.e. (2.32b), (2.33b) and (2.34a)), while the degrees of freedom associated with the three quadrangular faces are identical to the degrees of freedom of the hexahedral element (i.e. (2.37), (2.40) and (2.42)).

2.4.2 Discussion

As can be deduced from the expressions presented in the preceding section, the degrees of freedom for the first order tetrahedra, hexahedra and prisms conforming in $H^1(\Omega)$, $\boldsymbol{H}(\mathbf{curl};\Omega)$, $\boldsymbol{H}(\mathrm{div};\Omega)$ and $L^2(\Omega)$ are the punctual evaluation at the vertices, the circulation on the edges, the flux across the faces and the integral over the volume (the constant coefficients have all been chosen equal to 1):

$$\sigma_1^{0,n} = s\big|_n, \quad \forall n \in \mathcal{N}(K), \tag{2.45}$$
$$\sigma_1^{1,e} = \int_e \boldsymbol{s} \cdot d\boldsymbol{l}, \quad \forall e \in \mathcal{E}(K), \tag{2.46}$$
$$\sigma_1^{2,f} = \int_f \boldsymbol{s} \cdot \boldsymbol{n}\, ds, \quad \forall f \in \mathcal{F}(K), \tag{2.47}$$
$$\sigma_1^{3,K} = \int_K s\, dv. \tag{2.48}$$

These degrees of freedom are those of the classical Whitney elements [14] (see also Section 2.1).

Except for the lowest order case, the selection of the individual polynomial weighting functions is a matter of convenience. However, once the actual expression of the degrees of freedom is fixed, the same is true for the set of the basis functions of the finite element space. And since a crucial topic in the practical construction of the finite element spaces is the resulting conditioning number of the discretized operator [188], the freedom left in the determination of the coefficients of the polynomial weighting functions (and thus the coefficients of the basis function expressions given in Section 2.5) could then be used to obtain an optimal matrix conditioning. It is interesting to note that, since a good matrix conditioning requires the matrix to be diagonally dominant, the ideal would be to have mutually orthogonal basis functions, which is however usually impossible in practice. It should also be pointed out that the orthogonality is problem dependent, i.e. dependent on the shape of the elements and on the material properties, which makes it difficult to find a general rule [207]. An example of the explicit expression of the degrees of freedom for actual expressions of the basis functions of two-dimensional elements in $H^1(\Omega)$ and $\boldsymbol{H}(\mathbf{curl};\Omega)$ can, for example, be found in [87, 79].

2.5 Basis functions

2.5.1 Generalities

Although high order $H^1(\Omega)$ finite elements have been widespread since the 70's in many applications of finite element methods, their basis functions are still usually associated with nodes located in the same way as those used for geometrical transformations (see for example [44, 228]). This approach is not well adapted when going for higher polynomial orders. In fact, even the connection of $H^1(\Omega)$ tetrahedral elements of order two and three poses the problem of the value to attribute to the two degrees of freedom associated with the two mid-nodes of an edge shared by the two elements. A more general approach is to associate the basis functions with all the geometrical entities of the element, following the definition of the degrees of freedom presented in the previous section [161, 141, 218, 223, 213, 110, 190]. This avoids any reordering of the nodes or cumbersome reinterpolation, and, in the case of hierarchical bases (see Section 2.5.2), allows an easy connection of elements of different orders.

In order to define the basis functions for the tetrahedral, hexahedral and prismatic elements whose local spaces and degrees of freedom were defined in the preceding sections, we introduce the function λ_n, defined as the lowest order scalar function of the space coordinates associated with the node n of the element K, taking the value 1 at this node, continuously varying in all elements sharing the node, and having the value 0 in all other elements without presenting any discontinuity. The functions λ_n will serve as the lowest order $H^1(\Omega)$ basis functions for the element K.

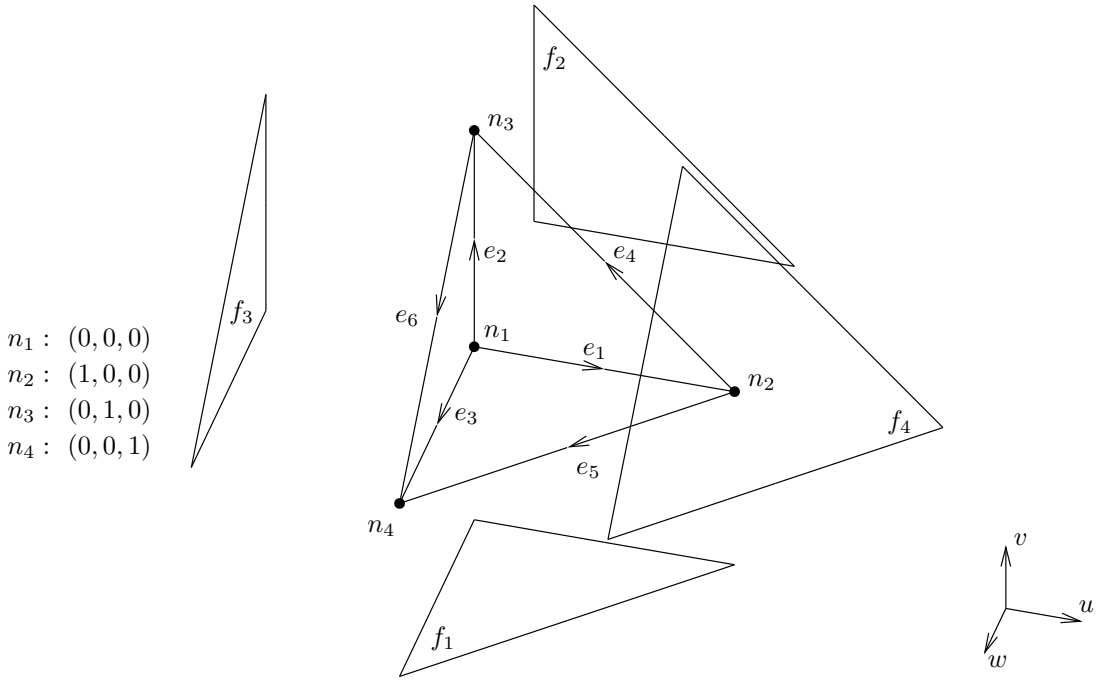

Figure 2.2: Reference tetrahedron T.

For the reference tetrahedron T defined by (2.1) and presented in Figure 2.2, the functions λ_n are the four barycentric coordinates [44]

$$\lambda_1 = 1 - u - v - w, \qquad \lambda_2 = u, \qquad \lambda_3 = v, \qquad \lambda_4 = w. \tag{2.49}$$

For the reference hexahedron H presented in Figure 2.3, these functions λ_n are [44]

$$\begin{aligned}
\lambda_1 &= 1/8\,(1-u)(1-v)(1-w), & \lambda_2 &= 1/8\,(1+u)(1-v)(1-w),\\
\lambda_3 &= 1/8\,(1+u)(1+v)(1-w), & \lambda_4 &= 1/8\,(1-u)(1+v)(1-w),\\
\lambda_5 &= 1/8\,(1-u)(1-v)(1+w), & \lambda_6 &= 1/8\,(1+u)(1-v)(1+w),\\
\lambda_7 &= 1/8\,(1+u)(1+v)(1+w), & \lambda_8 &= 1/8\,(1-u)(1+v)(1+w).
\end{aligned} \tag{2.50}$$

Finally, for the reference prism P presented in Figure 2.4, the functions λ_n are [44]

$$\begin{aligned}
\lambda_1 &= 1/2\,(1-u-v)(1-w), & \lambda_2 &= 1/2\,u\,(1-w),\\
\lambda_3 &= 1/2\,v\,(1-w), & \lambda_4 &= 1/2\,(1-u-v)(1+w),\\
\lambda_5 &= 1/2\,u\,(1+w), & \lambda_6 &= 1/2\,v\,(1+w).
\end{aligned} \tag{2.51}$$

We are now able to build the bases of the discrete spaces $W_p^i(K)$ (i.e. construct the basis functions of the various mixed finite elements). Adopting the same notation as for the expression of the degrees of freedom in Section 2.4, each basis function is characterized by its type i (corresponding to the type of the function space $W_p^i(K)$), by an associated geometrical entity (being either a node n, an edge e, a face f or the element K itself, i.e. $x \in \{n, e, f, K\}$), and by the interpolation order p:

$$s = s_p^{i,x}. \tag{2.52}$$

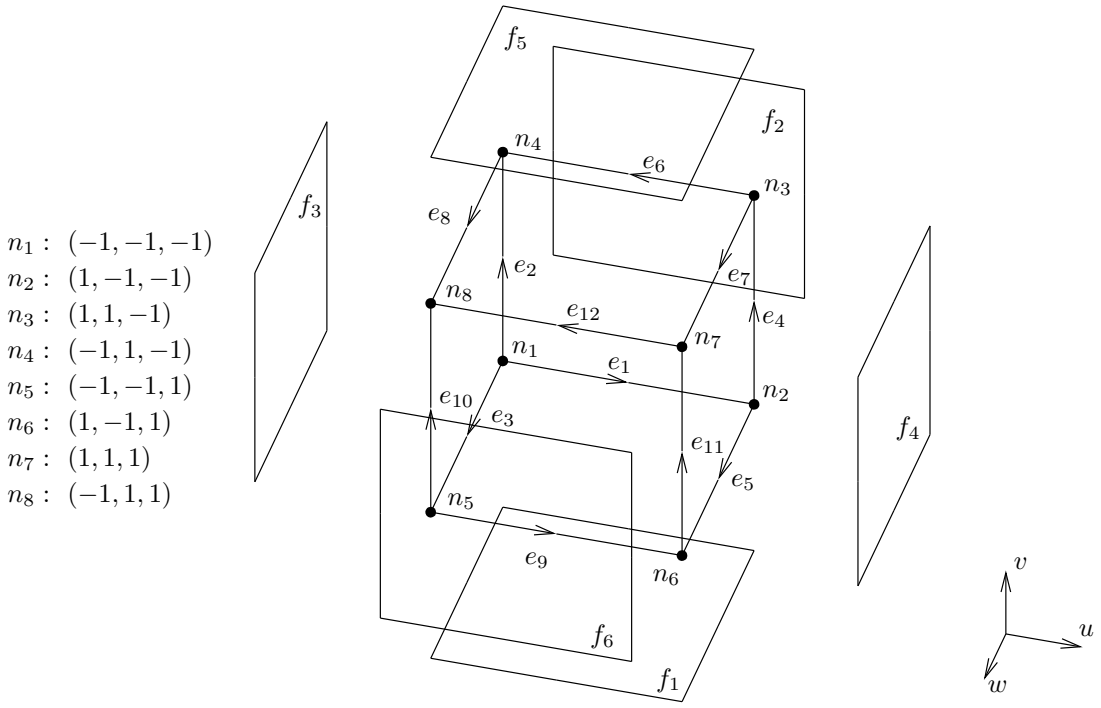

Figure 2.3: Reference Hexahedron H.

2.5.2 Hierarchical bases

2.5.2.1 Definition

In order to permit an easy combination of elements of different orders in the same mesh (mandatory for p-adaptation, see Section 2.7.5.3), the following conditions should be fulfilled:

1. no geometrical entity different from the nodes, the edges, the faces and the volume of the element should be created when increasing the interpolation order. This means that no special geometrical treatment for connecting two elements of different order has to be effected;

2. the bases of the local function spaces should be hierarchical, so that the connection of two elements of different orders can be done by locally setting the value of some degrees of freedom to zero.

The first condition is met thanks to the definition of the degrees of freedom (see Section 2.4). The second condition is made possible thanks to the incremental definition of the function spaces (see Sections 2.3.2, 2.3.3 and 2.3.4), but adds constraints on the actual choice of the basis functions (and on the expression of their associated degrees of freedom, i.e. the value of the polynomials $q(u,v,w)$ and $\boldsymbol{q}(u,v,w)$ in Section 2.4).

Let us now examine the hierarchical property in greater detail. Finite elements are said to be hierarchical if the basis functions of one element are a subset of

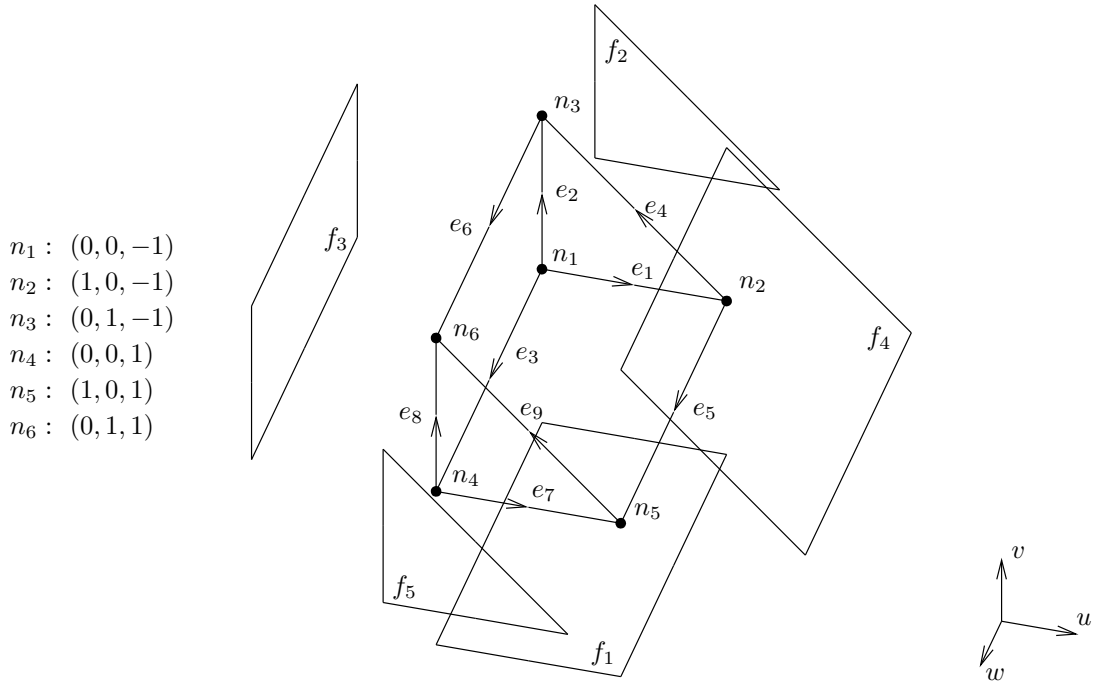

Figure 2.4: Reference Prism P.

the basis functions of any element of higher order [228]. For example, classical Lagrange elements [44] do not possess this property, since the set of basis functions is completely renewed when the interpolation order goes from order $p-1$ to order p. Since the basis functions of the function space S of the finite element (K, Σ, S) are linearly independent (by definition), the finite elements have to be constructed according to the principle of bases completion, which implies the following property: if S_{p-1} and S_p are the local function spaces of two finite elements $(K, \Sigma_{p-1}, S_{p-1})$ and (K, Σ_p, S_p), of order $p-1$ and p respectively, and if the basis functions of (K, Σ_p, S_p) are constructed by completion of the basis functions of those of $(K, \Sigma_{p-1}, S_{p-1})$, the degrees of freedom σ_i added to Σ_{p-1} to form Σ_p have to be such that

$$\sigma_i(s) = 0, \quad \forall s \in S_{p-1}. \tag{2.53}$$

Increasing the order of the elements in a given mesh will thus amount to adding, to the degrees of freedom already present, another set of degrees of freedom. It should be noted that (2.53) is mandatory to determine the actual expression of the degrees of freedom [87, 79].

As stated above, a choice of basis functions (and degrees of freedom) that respect the preceding properties makes it easy to combine elements of different orders in the same mesh. Let us for example consider an element (K_1, Σ_1, S_1) of class $H^1(\Omega)$ and of order one sharing a face with an element (K_2, Σ_2, S_2), also of class $H^1(\Omega)$ but of order two. If the basis of S_1 is not a subset of the basis of S_2 (i.e., if the elements are not hierarchical), the basis functions of (K_1, Σ_1, S_1) and (K_2, Σ_2, S_2) do not match on the common face, and the continuity is lost. On the other hand, if the elements are hierarchical, the basis functions of (K_1, Σ_1, S_1) constitute a subset of

the basis functions of (K_2, Σ_2, S_2), and, to maintain continuity, it is sufficient to set the coefficients of the basis functions associated with the common face to zero (i.e., thanks to the choice of the basis functions, setting to zero the value of all degrees of freedom associated with the face, and not existing in (K_1, Σ_1, S_1)).

The method to connect two adjacent elements of different orders is thus straightforward and can be summarized as follows: set to zero the value of all degrees of freedom that are common to the two elements and that are associated with basis functions whose order is higher than the order of the lowest order element. This connection method is exploited in the *p*- and *hp*-refinement schemes presented in Section 2.7.

The next section gives a general algorithm to generate hierarchical basis functions of elements conforming in $H^1(\Omega)$, $\boldsymbol{H}(\mathbf{curl};\Omega)$, $\boldsymbol{H}(\mathrm{div};\Omega)$ and $L^2(\Omega)$. The actual basis functions used in the practical implementation (see the references listed at the end of the introduction of this chapter, page 26) are all special cases of these general expressions, for polynomial orders up to 3. It is worth noticing that the two-dimensional basis functions for the trace spaces defined in Section 2.3.5 can be easily deduced from the same expressions.

2.5.2.2 Construction

Hierarchical bases for $W_p^i(K)$, $i = 0, \ldots, 3$, can be constructed in a recursive manner, given the following first order bases [47]:

1. $W_1^0(K) = \mathrm{span}(s_1^{0,n}), \forall n \in \mathcal{N}(K)$, with

$$s_1^{0,n} = \lambda_n. \tag{2.54}$$

   The basis functions $s_1^{0,n}$ are the nodal basis functions of Lagrange elements;

2. $W_1^1(K) = \mathrm{span}(s_1^{1,e}), \forall e \in \mathcal{E}(K)$, with (if the edge e joins the nodes i and j, i.e. $e = \{i, j\}$):

$$s_1^{1,e} = \lambda_j \,\mathbf{grad} \sum_{r \in \mathcal{N}(j,\overline{i})} \lambda_r - \lambda_i \,\mathbf{grad} \sum_{r \in \mathcal{N}(i,\overline{j})} \lambda_r. \tag{2.55}$$

   In this expression, $\mathcal{N}(m, \overline{n})$ stands for the set of nodes of the face f which contains the node m, but not the node n (such a face is uniquely defined for elements which have three edges incident to each node). The basis functions $s_1^{1,e}$ are the edge basis functions of the lowest order curl-conforming element. If K is a tetrahedron, (2.55) comes down to the classical Whitney edge basis function, i.e. $\lambda_i \,\mathbf{grad}\, \lambda_j + \lambda_j \,\mathbf{grad}\, \lambda_i$;

3. $W_1^2(K) = \mathrm{span}(s_1^{2,f}), \forall f \in \mathcal{F}(K)$, with (if the face f contains the nodes i, j and k or i, j, k and l, i.e. $f = \{i, j, k\}$ or $f = \{i, j, k, l\}$):

$$s_1^{2,f} = a \sum_{q \in \mathcal{N}(f)} \lambda_q \left(\mathbf{grad} \sum_{r \in \mathcal{N}(q,\overline{q+1})} \lambda_r \right) \times \left(\mathbf{grad} \sum_{r \in \mathcal{N}(q,\overline{q-1})} \lambda_r \right), \tag{2.56}$$

where $a = 2$ if $\dim(\mathcal{N}(f)) = 3$ and $a = 1$ if $\dim(\mathcal{N}(f)) = 4$, and where $\mathcal{N}(m, \overline{n})$ has the same signification as above, agreeing that $n + 1$ denotes the node following n in the set $\mathcal{N}(f)$ considered as a circular list. If K is a tetrahedron, (2.56) comes down to the classical Whitney face basis function, i.e. $2(\lambda_i \, \mathbf{grad}\, \lambda_j \times \mathbf{grad}\, \lambda_k + \lambda_j \, \mathbf{grad}\, \lambda_k \times \mathbf{grad}\, \lambda_i + \lambda_k \, \mathbf{grad}\, \lambda_i \times \mathbf{grad}\, \lambda_j)$;

4. $W_1^3(K) = \mathrm{span}(s_1^{3,K})$, with

$$s_1^{3,K} = \frac{1}{\mathrm{vol}(K)}, \tag{2.57}$$

where $\mathrm{vol}(K)$ represents the volume of the geometrical element K.

Extending (in a hierarchical way) $W_{p-1}^0(K)$ to $W_p^0(K)$ is commonplace [228, 31]. Let us then denote by $\widetilde{E}_p^0$, $\widetilde{F}_p^0$ and $\widetilde{V}_p^0$ the sets of hierarchical basis functions of these conforming elements associated with the edges, faces and the volume when the order is upgraded from $p-1$ to p. A general procedure to generate a hierarchical basis for $W_p^1(K)$, $p > 1$, is:

1. take $a = \dim(X_p^{1,e}) - \dim(X_{p-1}^{1,e})$ functions which are a gradient of $\widetilde{E}_p^0$ on each edge;
2. take $b = \dim(X_p^{2,f}) - \dim(X_{p-1}^{2,f})$ functions which are a gradient of $\widetilde{F}_p^0$ on each face;
3. add $c = \dim(X_p^{1,f}) - \dim(X_{p-1}^{1,f}) - b$ functions of non-zero curl on each face;
4. take $d = \dim(X_p^{2,v}) - \dim(X_{p-1}^{2,v})$ functions which are a gradient of $\widetilde{V}_p^0$ on the volume;
5. add $e = \dim(X_p^{1,K}) - \dim(X_{p-1}^{1,K}) - d$ functions of non-zero curl on the volume.

This procedure clearly highlights the decomposition of the basis into the nullspace and the orthogonal complement to the nullspace of the **curl** operator, since $a+b+d = \dim(\mathcal{NS}_p^1(K) \ominus \mathcal{NS}_{p-1}^1(K))$, and $d + e = \dim(\mathcal{S}_p^1(K) \ominus \mathcal{S}_{p-1}^1(K))$. In the same way, if $\widetilde{F}_p^1$ and $\widetilde{V}_p^1$ denote the sets of hierarchical basis functions of the curl-conforming elements associated with the faces and the volume when the order is upgraded from $p-1$ to p, a general procedure to generate a hierarchical basis for $W_p^2(K)$, $p > 1$, is:

1. take $a = \dim(X_p^{2,f}) - \dim(X_{p-1}^{2,f})$ functions which are the curl of $\widetilde{F}_p^1$ on each face;
2. take $b = \dim(X_p^{3,K}) - \dim(X_{p-1}^{3,K})$ functions which are the curl of $\widetilde{V}_p^1$ in the volume;
3. add $c = \dim(X_p^{2,K}) - \dim(X_{p-1}^{2,K}) - b$ functions of non-zero divergence in the volume.

The generation of the bases of $W_p^3(K)$ is straightforward.

It is important to notice that, during the construction of curl-conforming finite elements, the bases of the nullspace are built by using the gradient of basis functions of the conforming elements. This will permit the easy connection of vector and scalar fields when discretizing the reduced nullspace of the **curl** operator (see Section 2.6.4.1). In the same way, for the construction of div-conforming elements, the bases of the nullspace are built by using the curl of basis functions of the curl-conforming elements. As an example, the Table 2.4 summarizes the conforming and curl-conforming basis functions of the tetrahedral element built up to the order 3 using the aforementioned algorithm. These elements were first proposed by Webb and Forghani in [218], and extended (with a slight modification of $s_2^{1,f}$ and $s_3^{1,e}$) by Ren in [189].

Table 2.4: Example of hierarchical basis functions for the conforming and curl-conforming tetrahedral element [218, 189].

Order (p)	Entity	Conforming ($W_p^0(\mathrm{T})$)	Curl-conforming ($W_p^1(\mathrm{T})$)
1	n	λ_n	
	$e=\{i,j\}$		$\lambda_i\,\mathbf{grad}\,\lambda_j-\lambda_j\,\mathbf{grad}\,\lambda_i$
2	$e=\{i,j\}$	$\lambda_i\lambda_j$	$\mathbf{grad}\,(\lambda_i\lambda_j)$
	$f=\{i,j,k\}$		$\lambda_k\lambda_j\,\mathbf{grad}\,\lambda_i,\ \lambda_k\lambda_i\,\mathbf{grad}\,\lambda_j$
3	$e=\{i,j\}$	$\lambda_i\lambda_j(\lambda_i-\lambda_j)$	$\mathbf{grad}\,(\lambda_i\lambda_j(\lambda_i-\lambda_j))$
	$f=\{i,j,k\}$	$\lambda_i\lambda_j\lambda_k$	$\mathbf{grad}\,(\lambda_i\lambda_j\lambda_k)),$
			$\lambda_i^2(\lambda_j\,\mathbf{grad}\,\lambda_k-\lambda_k\,\mathbf{grad}\,\lambda_j),$
			$\lambda_j^2(\lambda_k\,\mathbf{grad}\,\lambda_i-\lambda_i\,\mathbf{grad}\,\lambda_k),$
			$\lambda_k^2(\lambda_i\,\mathbf{grad}\,\lambda_j-\lambda_j\,\mathbf{grad}\,\lambda_i)$
	$\mathrm{T}=\{i,j,k,l\}$		$\lambda_i\lambda_j(\lambda_k\,\mathbf{grad}\,\lambda_l-\lambda_k\,\mathbf{grad}\,\lambda_l),$
			$\lambda_j\lambda_k(\lambda_l\,\mathbf{grad}\,\lambda_i-\lambda_l\,\mathbf{grad}\,\lambda_i),$
			$\lambda_k\lambda_l(\lambda_i\,\mathbf{grad}\,\lambda_j-\lambda_i\,\mathbf{grad}\,\lambda_j)$

2.5.3 Conformity

To prove that the proposed finite elements are of class $H^1(\Omega)$, $\boldsymbol{H}(\mathbf{curl};\Omega)$, $\boldsymbol{H}(\mathrm{div};\Omega)$ or $L^2(\Omega)$, it is sufficient, according to the three lemmas given in Section 2.2.2, to verify that their basis functions, or the tangential or normal components of their basis functions, are continuous across the faces of two adjacent elements. First, by construction, when a degree of freedom is associated with a given geometrical entity x (node, edge, face or volume), the support $\mathrm{supp}(x)$ of the associated basis function is limited to the elements sharing this geometrical entity. We then have the following properties for all the basis functions presented in the previous section:

1. for a basis function associated with a node n, the property is well-known (and is usually called a patching condition [44]) and can be easily verified;

2. for a basis function associated with an edge e, the value of the function, its tangential or normal component (depending on the class of the element: $H^1(\Omega)$, $\boldsymbol{H}(\mathbf{curl};\Omega)$ or $\boldsymbol{H}(\mathrm{div};\Omega)$) on a face f'

   (a) is equal to zero if $e \notin \mathrm{supp}(f')$;

   (b) depends only, if $e \in \mathrm{supp}(f')$, on the coordinates of the nodes of f'.

   This can be easily shown by examining the individual expressions of the basis functions or, in a more general way, by considering the expression of the degrees of freedom (see e.g. [161, 163]);

3. for a basis function associated with a face f, the value of the function, its tangential or normal component on a face f'

   (a) is equal to zero if $f \neq f'$;

   (b) depends only, if $f = f'$, on the coordinates of the nodes of f'.

   This can be verified in the same way as for the basis functions associated with the edges;

4. for a basis function associated with the volume v, the property is straightforward, since the support of the function is limited to the element itself (the function being equal to zero everywhere outside the element).

2.6 Global spaces $W_p^i(\Omega)$

2.6.1 Introduction

A finite element mesh $\mathcal{M}(\Omega)$ of Ω is a tessellation of Ω by volumes of various shapes (in our case tetrahedra, prisms and hexahedra: see Section D.2), arranged in such a way that if two of them intersect, they do so along a common face, edge or node, and never otherwise. We consider all finite element meshes as unstructured, even if they are generated in a structured way [116]. This implies that the elementary volumes are defined only by the ordered list of their vertices (which allows the orientation of all their other geometrical entities) but no predefined ordering is assumed between any two elementary volumes.

Once a finite element mesh is constructed in Ω, global finite element spaces $W_p^i(\mathcal{M}(\Omega))$ can be constructed, based on the elementary finite elements $(K, \Sigma, W_p^i(K))$ associated with each $K \in \mathcal{M}(\Omega)$. Given a function u defined in Ω, its interpolant $u_{\mathcal{M}(\Omega)} \in W_p^i(\mathcal{M}(\Omega))$ is uniquely defined: the restriction $u_{\mathcal{M}(\Omega)}\big|_K$ belongs to $W_p^i(K)$, and, since the finite element is unisolvent, $u_{\mathcal{M}(\Omega)}\big|_K$ is completely determined by the values $\sigma_j(u)$ $(\forall \sigma_j \in \Sigma)$ of the degrees of freedom of the function u.

To be concise, we will from now on omit the explicit reference to the mesh whenever this dependence is obvious. We thus simply define the sets of nodes, edges, faces and elements (volumes) of the mesh $\mathcal{M}(\Omega)$ as $\mathcal{N}(\Omega)$, $\mathcal{E}(\Omega)$, $\mathcal{F}(\Omega)$ and $\mathcal{V}(\Omega)$ (instead of $\mathcal{N}(\mathcal{M}(\Omega))$, $\mathcal{E}(\mathcal{M}(\Omega))$, $\mathcal{F}(\mathcal{M}(\Omega))$ and $\mathcal{V}(\mathcal{M}(\Omega))$). In the same way, we simply write $W_p^i(\Omega)$ instead of $W_p^i(\mathcal{M}(\Omega))$. It should nevertheless be reminded that it is always the discretized domain which is considered.

2.6.2 Canonical transformations

All finite elements presented in Section 2.3 were defined locally (i.e. on the reference elements T, H and P from Figures 2.2, 2.3 and 2.4). In order to construct the global finite element spaces, we need to assemble the transformed reference elements into the actual finite element mesh $\mathcal{M}(\Omega)$.

Let K and K' be two domains of respective dimensions $\dim(K)$ and $\dim(K')$. The system of coordinates defined on K and K' is respectively $\{u^i : i = 1, \ldots, \dim(K)\}$ and $\{x^j : j = 1, \ldots, \dim(K')\}$. We then consider the differentiable application $\phi : K \mapsto K'$, mapping K onto K' [104, chapter 5]. The definition of this application amounts to defining a set of $\dim(K')$ relations

$$x^j = x^j(u^1, \ldots, u^{\dim(K)}), \quad j = 1, \ldots, \dim(K').$$

The Jacobian matrix of the transformation, of dimension $\dim(K) \times \dim(K')$ is defined as

$$\mathbf{J}(i,j) = \frac{\partial x^j}{\partial u^i} \quad \text{i.e.} \quad \mathbf{J} = \begin{pmatrix} \frac{\partial x^1}{\partial u^1} & \cdots & \frac{\partial x^{\dim(K')}}{\partial u^1} \\ \vdots & \ddots & \vdots \\ \frac{\partial x^1}{\partial u^{\dim(K)}} & \cdots & \frac{\partial x^{\dim(K')}}{\partial u^{\dim(K)}} \end{pmatrix}. \tag{2.58}$$

In the case of a regular change of coordinates mapping a reference element K onto the actual element K' in the finite element mesh, the dimension of K and that of K' are identical, e.g. $\dim(K) = \dim(K') = 3$. The geometrical transformation ϕ must fulfill the following conditions:

1. ϕ is bijective: to each point $\boldsymbol{u}$ in K corresponds one point $\boldsymbol{x}$ of K', and conversely;
2. the nodes of K correspond to the nodes of K';
3. each part of ∂K, defined by the nodes on the boundary of K, corresponds to the part of $\partial K'$ defined by the corresponding nodes.

The evaluation of the Jacobian matrix is done numerically, by using the barycentric functions λ_k ($k = 1, \ldots, \mathcal{N}(K)$) introduced in Section 2.5.1. Indeed, if x_k^j denotes the jth coordinate of the kth node of the element, we have

$$x^j = \sum_{k=1}^{\mathcal{N}(K)} x_k^j \lambda_k,$$

and thus

$$\frac{\partial x^j}{\partial u^i} = \sum_{k=1}^{\mathcal{N}(K)} x_k^j \frac{\partial \lambda_k}{\partial u^i}.$$

Since ϕ is bijective, the Jacobian matrix $\mathbf{J}$ is non-singular: its inverse $\mathbf{J}^{-1}$ exists and corresponds to the application ϕ^* mapping K' onto K, equivalently defined by $\dim(K)$ relations:

$$u^i = u^i(x^1, \ldots, x^{\dim(K')}), \quad i = 1, \ldots, \dim(K).$$

The expression of this inverse is actually never constructed analytically, but obtained by numerical inversion of (2.58).

It can be shown (see e.g. [109, chapter 2] or [104, chapter 8]) that functions f^0 in $H^1(K)$, $\boldsymbol{f}^1$ in $\boldsymbol{H}(\mathbf{curl}; K)$, $\boldsymbol{f}^2$ in $\boldsymbol{H}(\mathrm{div}; K)$ and f^3 in $L^2(K)$ are transformed into functions $f^{0'}$, $\boldsymbol{f}^{1'}$, $\boldsymbol{f}^{2'}$ and $f^{3'}$ respectively, such that

$$f^{0'} = f^0, \quad \boldsymbol{f}^{1'} = \mathbf{J}^{-1}\boldsymbol{f}^1, \quad \boldsymbol{f}^{2'} = \frac{\mathbf{J}^T}{\det \mathbf{J}}\boldsymbol{f}^2 \quad \text{and} \quad f^{3'} = \frac{1}{\det \mathbf{J}} f^3.$$

These four rules give the generic relations necessary to transform any function belonging to $H^1(K)$, $\boldsymbol{H}(\mathbf{curl}; K)$, $\boldsymbol{H}(\mathrm{div}; K)$ and $L^2(K)$, and in particular the basis functions presented in Section 2.5.

Now, let us consider the case of the trace spaces mentioned in Section 2.3.5. The tessellation $\mathcal{M}(\Omega)$ of Ω generates a surface mesh $\mathcal{M}(\Gamma)$ on Γ, onto which the reference (triangular and quadrangular) two-dimensional elements have to be mapped. This process is called the parametrization, and its associated non-square Jacobian matrix (with $\dim(K) < \dim(K')$) is built exactly in the same way as for the regular transformations. To "invert" the mapping, we now have to project a space of dimension $\dim(K')$ onto a space of dimension $\dim(K) = \dim(K') - 1$. To achieve this, a singular value decomposition (SVD) [36, 204] is used, which permits to build a left inverse of the singular parametrization Jacobian matrix.

2.6.3 Discrete mathematical structure

Thanks to the properties of the local spaces defined in Section 2.3, one can show that the following inclusions also hold for the global spaces defined on the mesh $\mathcal{M}(\Omega)$ of Ω:

$$\mathbf{grad}\, W_p^0(\Omega) \subset W_p^1(\Omega), \tag{2.59}$$

$$\mathbf{curl}\, W_p^1(\Omega) \subset W_p^2(\Omega), \tag{2.60}$$

$$\mathrm{div}\, W_p^2(\Omega) \subset W_p^3(\Omega). \tag{2.61}$$

The global spaces $W_p^i(\Omega)$ $(i = 0, \ldots, 3)$ thus constitute a de Rham complex (see Section A.2.6) and form a discrete counterpart of the continuous mathematical structure presented in Section 1.3.1:

$$W_p^0(\Omega) \xrightarrow{\mathbf{grad}} W_p^1(\Omega) \xrightarrow{\mathbf{curl}} W_p^2(\Omega) \xrightarrow{\mathrm{div}} W_p^3(\Omega)\ .$$

Let us study in greater detail two important subspaces of the curl-conforming discrete space $W_p^1(\Omega)$.

2.6.4 Subspaces of $W_p^1(\Omega)$

A field $\boldsymbol{u}$ belonging to $W_p^1(\Omega)$ can be written as

$$\boldsymbol{u} = \sum_{i=1}^{\dim(W_p^1(\Omega))} u_i s_p^{1,x_i}, \tag{2.62}$$

where x_i represents an edge $e \in \mathcal{E}(\Omega)$, a face $f \in \mathcal{F}(\Omega)$ or an element $K \in \mathcal{V}(\Omega)$. The basis functions s_p^{1,x_i} are linearly independent if they cover the whole space $W_p^1(\Omega)$. However, these functions are too rich to cover only a subspace of $W_p^1(\Omega)$, of lower dimension. In this case they are linearly dependent, and a new basis has to be constructed. In this section, we consider two important subsets of $W_p^1(\Omega)$ which will be used in Chapter 3: the discrete reduced nullspace and the discrete reduced complement to the nullspace of the **curl** operator.

2.6.4.1 Nullspace and reduced nullspace of the curl operator

The discrete reduced nullspace of the **curl** operator relative to a subdomain Ω_c^{C} of Ω is defined as

$$\mathcal{NS}_p^1(\Omega, \Omega_c^{\mathrm{C}}) = \{\boldsymbol{u} \in W_p^1(\Omega) : \mathbf{curl}\,\boldsymbol{u} = 0 \text{ in } \Omega_c^{\mathrm{C}}\}. \tag{2.63}$$

Let us first construct a basis of $\mathcal{NS}_1^1(\Omega, \Omega_c^{\mathrm{C}})$, i.e. the reduced nullspace for first order elements. A field $\boldsymbol{u}$ belonging to $W_1^1(\Omega)$ can be expressed as

$$\boldsymbol{u} = \sum_{e \in \mathcal{E}(\Omega)} u_e s_1^{1,e}, \tag{2.64}$$

since all the degrees of freedom for first order curl-conforming elements are associated with the edges of the mesh (see Section 2.4). Splitting the edges of the mesh into the two complementary sets $\mathcal{E}(\Omega_c) - \mathcal{E}(\partial\Omega_c)$ (which contains all the interior edges of the mesh of Ω_c) and $\mathcal{E}(\Omega_c^{\mathrm{C}})$ (which contains all the edges of the mesh of Ω_c^{C}, including the edges on its boundary), (2.64) can be rewritten as

$$\boldsymbol{u} = \sum_{e \in \mathcal{E}(\Omega_c) - \mathcal{E}(\partial\Omega_c)} u_e s_1^{1,e} + \sum_{e \in \mathcal{E}(\Omega_c^{\mathrm{C}})} u_e s_1^{1,e}. \tag{2.65}$$

But if $\boldsymbol{u}$ belongs to $\mathcal{NS}_p^1(\Omega, \Omega_c^{\mathrm{C}})$, $\mathbf{curl}\,\boldsymbol{u} = 0$ in Ω_c^{C}, and $\boldsymbol{u}$ can thus be derived from a scalar potential v in Ω_c^{C} such that $\boldsymbol{u} = -\mathbf{grad}\, v$. Thanks to the definition (2.46) of the degrees of freedom for first order curl-conforming elements, it follows that

$$u_e = \int_e \boldsymbol{u} \cdot d\boldsymbol{l} = \int_e -\mathbf{grad}\, v \cdot d\boldsymbol{l} = v\big|_i - v\big|_j, \tag{2.66}$$

where $e = \{i, j\}$ is the edge joining the nodes i and j. The expression (2.65) then becomes

$$\boldsymbol{u} = \sum_{e \in \mathcal{E}(\Omega_c) - \mathcal{E}(\partial\Omega_c)} u_e s_1^{1,e} + \sum_{n \in \mathcal{N}\Omega_c^{\mathrm{C}}} v_n \Big(\sum_{\{n,k\} \in \mathcal{E}(\Omega_c^{\mathrm{C}})} s_1^{1,\{n,k\}} \Big). \tag{2.67}$$

In the second term of this expression, a summation is performed for all the curl-conforming basis functions associated with the edges incident to the node n. It can be shown that for the interior nodes of Ω_c^{C} one has

$$\sum_{\{n,k\} \in \mathcal{E}(\Omega_c^{\mathrm{C}})} s_1^{1,\{n,k\}} = -\mathbf{grad}\, s_1^{0,n}, \tag{2.68}$$

so that the discrete field is simply expressed inside Ω_c^{C} through the gradient of the conforming basis functions associated with the nodes, i.e. $s_1^{0,n}$ [19, 217]. Two problems however remain:

1. if Ω_c^{C} is topologically non-trivial, the expression (2.67) lacks the explicit definition of the discontinuities of the field v across the l cutting surfaces. We have seen in Section 1.3.1 that a basis for the subspace $\mathcal{H}^1(\Omega_c^{\mathrm{C}})$ (whose dimension is equal to the number of cutting surfaces Σ_i, $i = 1, \ldots, l$) consists of l basis functions q_i, $i = 1, \ldots, l$, which present a unit discontinuity across the cuts Σ_i (with $q_i\big|_{\Sigma_i^+} = 1$ and $q_i\big|_{\Sigma_i^-} = 0$);

2. (2.67) also lacks the definition of the discontinuities of the potential that may result from the abstraction of thin regions from Ω.

For this purpose, let us split the potential v as follows:

$$v = v_c + v_l + v_d = v_c + \sum_{i=1}^{l} v_{l,i} + \sum_{i=1}^{t} v_{d,i}, \tag{2.69}$$

where v_c is continuous in Ω_c^{C}, $v_{l,i}$ is discontinuous across the cutting surface Σ_i, and $v_{d,i}$ is discontinuous across the surface $\Gamma_{t,i}$. The discrete form of the discontinuous fields $v_{l,i}$ or $v_{d,i}$ is constructed by restricting their support to layers of elements adjacent to the "+" side of the surfaces Σ_i or $\Gamma_{t,i}$, to which are added the elements of Ω_c which touch this layer by at least one edge e such that $e \in \mathcal{E}(\Omega_c^{\mathrm{C}})$ and $e \notin \mathcal{E}(\Sigma_i)$ or $e \notin \mathcal{E}(\Gamma_{t,i})$. These layers are called transition layers and are denoted by $\mathrm{supp}(v_{l,i})$ and $\mathrm{supp}(v_{d,i})$ respectively. In the general case, (2.67) can thus be expressed as

$$\boldsymbol{u} = \sum_{e \in \mathcal{E}(\Omega_c) - \mathcal{E}(\partial\Omega_c)} u_e s_1^{1,e} + \sum_{n \in \mathcal{N}(\Omega_c^{\mathrm{C}})} v_{c,n}\, f_{c,n} + \sum_{i=1}^{l} \Big(I_i \sum_{n \in \mathcal{N}(\Sigma_i)} f_{l,n} \Big) + \sum_{i=1}^{t} \Big(\sum_{n \in \mathcal{N}(\Gamma_{t,i})} v_{d,i}\, f_{d,n} \Big), \tag{2.70}$$

with

$$f_{c,n} = \sum_{\{n,k\} \in \mathcal{E}(\Omega_c^{\mathrm{C}})} s_1^{1,\{n,k\}}, \qquad f_{l,n} = \begin{cases} \displaystyle\sum_{\{n,k\} \in \mathcal{E}(\Omega_c^{\mathrm{C}}), k \notin \mathcal{N}(\Sigma_i)} s_1^{1,\{n,k\}} & \text{in } \mathrm{supp}(v_{l,i}) \\ 0 & \text{otherwise} \end{cases},$$

and

$$f_{d,n} = \begin{cases} \displaystyle\sum_{\{n,k\}\in\mathcal{E}(\Omega_c^{\mathrm{C}})} s_1^{1,\{n,k\}} & \text{in supp}(v_{d,i}) \\ 0 & \text{otherwise} \end{cases}.$$

The apparent complexity of this decomposition should not mask its meaning: the last three terms of (2.70) simply represent the gradients of the three components of the potential v and can thus be rewritten, in Ω_c^{C}, in terms of gradients of conforming (nodal) basis functions.

If $\Omega_c^{\mathrm{C}} = \Omega$, the reduced nullspace $\mathcal{NS}_1^1(\Omega, \Omega_c^{\mathrm{C}})$ comes down to the nullspace $\mathcal{NS}_1^1(\Omega)$ of the **curl** operator. The field $\boldsymbol{u}$ can then be derived from a scalar potential v everywhere in Ω, and this potential can simply be discretized (with the same notations and under the same hypotheses as above) as

$$v = \sum_{n\in\mathcal{N}(\Omega)} v_{c,i}\, s_1^{0,n} + \sum_{i=1}^{l} \Big(I_i \sum_{n\in\mathcal{N}(\Sigma_i)} g_{l,n} \Big) + \sum_{i=1}^{t} \Big(\sum_{n\in\mathcal{N}(\Gamma_{t,i})} v_{d,i}\, g_{d,n} \Big), \tag{2.71}$$

with

$$g_{l,n} = \begin{cases} s_1^{0,n} & \text{in supp}(v_{l,i}) \\ 0 & \text{otherwise} \end{cases} \quad \text{and} \quad g_{d,n} = \begin{cases} s_1^{0,n} & \text{in supp}(v_{d,i}) \\ 0 & \text{otherwise} \end{cases}.$$

Thanks to the hierarchical bases defined in Section 2.5, the generalization of the previous developments to finite elements of order $p > 1$ is relatively straightforward. For each high order conforming basis function there is a corresponding curl-conforming basis function which is its gradient. Therefore, it is only necessary to set the coefficient $v_{c,i}$ of the conforming basis function equal to the negative (since $\boldsymbol{u} = -\mathbf{grad}\, v$) of the corresponding curl-conforming basis function. In addition, on each face $f \in \mathcal{F}(\partial\Omega_c)$, each basis function which is not a gradient of a conforming basis function is eliminated by setting its associated coefficient to zero.

2.6.4.2 Orthogonal complement and reduced orthogonal complement to the nullspace of the curl operator

Let us assume that a field $\boldsymbol{w} \in W_p^2(\Omega)$ is derived from the potential $\boldsymbol{u} \in W_p^1(\Omega)$ through the relation

$$\boldsymbol{w} = \mathbf{curl}\, \boldsymbol{u}. \tag{2.72}$$

Since $\operatorname{div} \boldsymbol{w} = 0$, $\boldsymbol{w}$ belongs to $\mathcal{NS}_p^2(\Omega)$, the nullspace of the divergence operator. If the dimension of the discrete nullspace of the **curl** operator is different from zero, a whole class of fields $\boldsymbol{u}$ verifying (2.72) exist, and the system matrix resulting from the discretization of the **curl-curl** operator is singular [5].

In the case of a topologically simple domain, the de Rham diagram in Figure 2.1 suggests that the selection of a unique representative of the field $\boldsymbol{u}$ (a procedure that is usually called gauging [126]) may be done by restricting the space $W_p^1(\Omega)$ to the discrete orthogonal complement $\mathcal{S}_p^1(\Omega)$ to the nullspace $\mathcal{NS}_p^1(\Omega)$. When this restriction is only applied in a subdomain Ω_c^{C} of Ω (i.e. when other conditions permit to ensure the unicity of $\boldsymbol{u}$ in $\Omega_c = \Omega - \Omega_c^{\mathrm{C}}$), the gauging process amounts to finding

$\boldsymbol{u} \in \mathcal{S}_p^1(\Omega, \Omega_c^{\mathrm{C}})$, where $\mathcal{S}_p^1(\Omega, \Omega_c^{\mathrm{C}})$ is called the reduced orthogonal complement to the nullspace of the **curl** operator relative to the subdomain Ω_c^{C} of Ω. Let us first construct $\mathcal{S}_1^1(\Omega, \Omega_c^{\mathrm{C}})$, i.e. the reduced orthogonal complement to the nullspace for first order curl-conforming elements. It was first demonstrated in [4] that in this case the singularity of the system matrix is intimately related to the graph structure of the finite element mesh. Specifically, a tree co-tree decomposition of the edges of the finite element mesh was shown to sort edge variables into dependent and independent degrees of freedom. The tree (or, more accurately, the spanning tree) involved in this decomposition is defined as a connected subset of the edges in the mesh that visit every node, but contains no closed loops. The co-tree is defined as the complement of the tree. It can be shown [4, 215] that the basis functions associated with the edges of the tree span the nullspace of the **curl** operator, while the basis functions of the co-tree span its orthogonal complement (i.e. its range after application of the **curl** operator). If $\widetilde{\mathcal{E}}(\Omega_c^{\mathrm{C}})$ represents the set of edges of a tree constructed in Ω_c^{C}, the reduced orthogonal complement to the nullspace of first order curl-conforming elements can thus be characterized as

$$\mathcal{S}_1^1(\Omega, \Omega_c^{\mathrm{C}}) = \{\boldsymbol{u} \in W_1^1(\Omega) : u_e = 0, \forall e \in \widetilde{\mathcal{E}}(\Omega_c^{\mathrm{C}})\}, \tag{2.73}$$

where u_e is the coefficient of the basis function associated with the edge e. It is important to point out that the tree should be constrained on the boundary of Ω_c^{C} [58]:

1. on a surface where an essential boundary condition is applied (i.e. $n \times u\big|_{\Gamma_e} = 0$ or $n \times u\big|_{\Gamma_h} = 0$), the basis functions have to be linearly independent, which can be achieved if the tree is complete on the surface. In practice, the tree thus has to be first generated on such a surface before being extended into the volume Ω_c^{C}. If the surface is topologically trivial, the essential boundary condition then comes down to setting to zero all the coefficients of the basis functions associated with the edges of the surface;

2. the tree should not contain any edge of the surface mesh of the boundary between Ω_c and Ω_c^{C} (but one edge of the tree has contain one node of the surface mesh). Indeed, if $\boldsymbol{u}$ is uniquely defined in Ω_c, it is also uniquely defined on its boundary by continuity (only its tangential component is continuous across $\partial\Omega_c$) and no condition should be imposed on the coefficients of the basis functions associated with the edges of $\partial\Omega_c$.

An algorithm for the construction of such a tree can be found in e.g. [105]. Let us now explicitly write the discrete expression of a field $\boldsymbol{u}$ belonging to the reduced orthogonal complement to the nullspace of the **curl** operator relative to a subdomain Ω_c^{C} of Ω. For the sake of generality, we consider, as in the previous section, that the tangential component of the field $\boldsymbol{u}$ may be discontinuous across the surfaces $\Gamma_{t,i}$, $i = 1, \ldots, t$. It is thus convenient to decompose $\boldsymbol{u}$ as

$$\boldsymbol{u} = \boldsymbol{u}_c + \boldsymbol{u}_d = \boldsymbol{u}_c + \sum_{i=1}^{t} \boldsymbol{u}_{d,i}, \tag{2.74}$$

where $\boldsymbol{u}_c$ is curl-conforming in Ω_c^{C} and the tangential component of $\boldsymbol{u}_{d,i}$ is discontinuous across the surface $\Gamma_{t,i}$, and we can write:

$$\boldsymbol{u} = \sum_{e\in\mathcal{E}(\Omega_c)} u_{c,e}\, s_1^{1,e} + \sum_{e\in\mathcal{E}(\Omega_c^{\mathrm{C}})-\mathcal{E}(\partial\Omega_c)-\widetilde{\mathcal{E}}(\Omega_c^{\mathrm{C}})} u_{c,e}\, s_1^{1,e} + \sum_{i=1}^{t}\Big(\sum_{e\in\mathcal{E}(\Gamma_{t,i})} u_{d,e}\, f_{d,e}\Big), \tag{2.75}$$

with

$$f_{d,e} = \begin{cases} s_1^{1,e} & \text{in } \mathrm{supp}(\boldsymbol{u}_{d,i}) \\ 0 & \text{otherwise} \end{cases}, \tag{2.76}$$

where $\mathrm{supp}(\boldsymbol{u}_{d,i})$ is the layer of elements of Ω_c^{C} adjacent to $\Gamma_{t,i}^{+}$.

When $\Omega_c = \emptyset$ (i.e. $\Omega_c^{\mathrm{C}} = \Omega$), $\mathcal{S}_p^1(\Omega, \Omega_c^{\mathrm{C}})$ comes down to $\mathcal{S}_p^1(\Omega)$. The field $\boldsymbol{u}$ can simply be expressed as

$$\boldsymbol{u} = \sum_{e\in\mathcal{E}(\Omega)-\widetilde{\mathcal{E}}(\Omega)} u_{c,e}\, s_1^{1,e} + \sum_{i=1}^{t}\Big(\sum_{e\in\mathcal{E}(\Gamma_{t,i})} u_{d,e}\, f_{d,e}\Big). \tag{2.77}$$

Contrary to the basis functions of $W_1^1(\Omega)$, the basis functions added hierarchically to span the spaces $W_p^1(\Omega)$, $p>1$, can be separated into basis functions of $\mathcal{NS}_p^1(\Omega) \ominus \mathcal{NS}_1^1(\Omega)$ and $\mathcal{S}_p^1(\Omega) \ominus \mathcal{S}_1^1(\Omega)$ (see Section 2.5.2.2). The generalization of the tree co-tree gauging procedure to finite elements of order $p>1$ is thus straightforward: it amounts to setting to zero the coefficients of all the basis functions spanning $\mathcal{NS}_p^1(\Omega) \ominus \mathcal{NS}_1^1(\Omega)$, $p>1$, i.e. the coefficients of all the basis functions which are the gradient of a corresponding conforming basis function. This process is notably simpler than with other (non-hierarchical) high order curl-conforming elements (see e.g. [147]).

When the domain on which the gauge condition has to be applied is not topologically simple, the simple spanning tree technique mentioned above will not work satisfactorily, since there are curl-free fields which are not gradients (see e.g. Figure 1.7). Results from the theory of homology (which largely exceed the scope of this work) can then show that, if l loops exist in the domain, one should add to the tree l edges of the co-tree, for which the circuits they close surround the loops. The augmented tree constructed in this way is sometimes called a belted tree [19, 126].

It should finally be noted that, if a conjugate gradient-like algorithm is used for solving the system of equations, it is possible to leave the space $W_p^1(\Omega)$ non-gauged under certain conditions. The selection of one field $\boldsymbol{u}$ among all its representatives is then implicitly achieved by the iterative algorithm [182, 183].

2.7 Optimization of the global spaces

In the previous sections we presented a method to generate discrete approximation spaces for $H^1(\Omega)$, $\boldsymbol{H}(\mathbf{curl};\Omega)$, $\boldsymbol{H}(\mathrm{div};\Omega)$ and $L^2(\Omega)$. The question is now: how should these spaces be actually constructed, or modified, in order to fulfill some prescribed quality constraints for the discretized fields? In this section we apply three classical optimization schemes to the discrete spaces $W_p^i(\Omega)$ so as to meet these requirements.

2.7.1 Generalities

The error committed on the solutions of the formulations that will be presented in Chapter 3 can be split into:

1. the error in the continuous models, resulting from the hypotheses under which the integro-differential equations describing the models are valid, and in particular the hypotheses which lead to the construction of the constitutive equations (see Section 1.1);

2. the error in the discretization of the continuous model, resulting from the finite dimension of the finite element spaces used to approximate the continuous function spaces (of infinite dimension) to which the solutions of the continuous models belong. This discretization error can be split up into:

   (a) the error made in discretizing the geometry (the problem is solved on an idealized geometry, meshed with a finite number of elementary elements);

   (b) the error made in discretizing the fields (the fields are locally approximated by polynomials of finite order).

The adaptation process aims at foreseeing and controlling the second type of error (the discretization error). This process is only possible if [165]:

1. the asymptotic error convergence is known;

2. an approximation of the discretization error is available.

Eventually, the goal of the adaptation process is to generate the best possible discrete function space, with either the dimension of the function space or the discretization error constrained to a certain value. Among the methods to perform adaptation, we combine the modification of the order of the polynomial interpolation (p-refinement) and the modification of the size of the geometrical elements paving the domain (h-refinement). Both modifications can be either global or local, the latter case leading to a so-called adaptive refinement. These techniques have been widespread in the domain of finite element computations for more than twenty years (see for example [7, 8]) and are applied here to the whole range of mixed finite elements built on tetrahedra, hexahedra and prisms.

Note that the computation of lower and upper bounds for the convergence of p- and hp-methods in three dimensions is still an ongoing work [6]. Notably, while we are only concerned with the estimation of the global error (in some energy norm) committed on the solution of our discretization schemes, local error estimates can also be obtained, at least for static problems [97, 2, 3].

2.7.2 Local and global errors

Let u and u' be the exact and the approximate solutions on Ω of a given problem. The elementary error e_i in the geometrical element $K_i \subset \Omega$ of the mesh and the global

error e are defined as $L^2(\Omega)$-norms (cf. Section A.2.3) of the differences between the computed and the exact fields:

$$e_i^2 = (u' - u, u' - u)_{K_i} \quad \text{and} \quad e^2 = (u' - u, u' - u)_\Omega.$$

Introducing

$$n^2 = (u' + u, u' + u)_\Omega,$$

we define the relative elementary error contribution ε_i and the global relative error ε as

$$\varepsilon_i^2 = e_i^2/n^2 \quad \text{and} \quad \varepsilon^2 = e^2/n^2 = \sum_{i=1}^{N_\mathcal{V}} \varepsilon_i^2, \tag{2.78}$$

where $N_\mathcal{V} = \dim(\mathcal{V}(\Omega))$ is the number of elements in the mesh $\mathcal{M}(\Omega)$ of Ω. (These definitions can be easily generalized when the problem leads to the computation of several independent fields, for example by considering the elementary error as the maximum of all elementary errors on the different solutions [176].)

2.7.3 Error convergence

If we define the size h_i of the geometrical element K_i as the length of its longest edge (this is an upper bound for all other measures of the size of an element, e.g. the radius of the circumsphere, and thus well suited for adaptation), the asymptotic convergence rate (in the $L^2(\Omega)$-norm) of the elementary error in an elliptic problem is [165]

$$\varepsilon_i = \mathcal{O}\Big(\frac{1}{p_i} h_i^{\min(p_i,\gamma)}\Big), \tag{2.79}$$

where p_i is the order of the local function space and γ depends on the smoothness of the solution. When the solution exhibits no singularities (neither geometrical nor in the source fields), or when the mesh is constructed so that the elementary error is uniformly distributed on all elements, the convergence rate becomes independent of the singularities:

$$\varepsilon_i = \mathcal{O}\Big(\frac{1}{p_i} h_i^{p_i}\Big). \tag{2.80}$$

2.7.4 Error estimates

The common denominator of all a posteriori error estimators is the extrapolation of the exact solution of the problem from the computed solution (we do not use a priori error estimates, which are based on the nature and the physical behavior of the problem, to guess before any computation where the error will be important). The way to approximate this exact solution differentiates the various error estimators.

The development of the dual formulations that will be presented in Chapter 3 permits to take advantage of the conformity of the solution of each formulation on either side of the Tonti diagram to estimate the error through the non-fulfillment of the constitutive relation by the couple formed by the primal and dual solution [193,

194, 138, 179, 177]. For the three constitutive relations (1.8), (1.10) and (1.12), the error in the constitutive relations is defined as

$$e_i^\sigma = \frac{1}{2}\|\boldsymbol{j} - \sigma\boldsymbol{e}\|_{K_i}, \quad e_i^\epsilon = \frac{1}{2}\|\boldsymbol{d} - \epsilon\boldsymbol{e}\|_{K_i} \quad \text{and} \quad e_i^\mu = \frac{1}{2}\|\boldsymbol{b} - \mu\boldsymbol{h}\|_{K_i}.$$

Taking $\frac{1}{2}(\boldsymbol{j}+\sigma\boldsymbol{e})$, $\frac{1}{2}(\boldsymbol{d}+\epsilon\boldsymbol{e})$ and $\frac{1}{2}(\boldsymbol{b}+\mu\boldsymbol{h})$ respectively as the approximation of the exact solutions, the elementary errors coincide with the errors in the constitutive relations, and, from (2.78), the relative errors can be written as

$$\varepsilon_i^\sigma = \frac{\|\boldsymbol{j} - \sigma\boldsymbol{e}\|_{K_i}}{\|\boldsymbol{j} + \sigma\boldsymbol{e}\|_\Omega}, \quad \varepsilon_i^\epsilon = \frac{\|\boldsymbol{d} - \epsilon\boldsymbol{e}\|_{K_i}}{\|\boldsymbol{d} + \epsilon\boldsymbol{e}\|_\Omega} \quad \text{and} \quad \varepsilon_i^\mu = \frac{\|\boldsymbol{b} - \mu\boldsymbol{h}\|_{K_i}}{\|\boldsymbol{b} + \mu\boldsymbol{h}\|_\Omega}.$$

The major advantage of this technique is that, thanks to the hypercircle theorem, upper bounds to the exact error can be derived provided that the error functional is separable [194, 193, 176, 93][1]. The main disadvantage is the computational cost, since both dual formulations have to be solved. We developed a projection-reconstruction technique in [180] to avoid the resolution of both formulations: the main idea is to reconstruct, from the finite element solution of a primal formulation, a field belonging to the space of the dual finite element formulation (this technique thus combines the estimation of the error due to a lack of fulfillment of the constitutive relation and the evaluation of numerical discontinuities at interfaces). Similar approaches can be found in [148, 19].

In order to focus on the properties of the dual formulations (without introducing additional approximations due to the projection-reconstruction operator), we will stick to the complete resolution of the dual formulations in all the applications of Chapter 4. It should nevertheless be noticed that the adaptation procedures described in the next section can also be used with any error estimator (as for example, error estimators based on the lack of fulfillment of the weakly solved equation [172, 92, 144, 7, 165], where the error is computed thanks to the evaluation of numerical discontinuities at interfaces, or error estimators based on solution smoothing, which consider the smoothed field as a better approximation of the exact solution [228]).

2.7.5 Adaptation schemes

2.7.5.1 Optimality

Let $\mathcal{M}(\Omega)$ and $\mathcal{M}'(\Omega)$ be the initial and the adapted mesh of Ω. If h_i and p_i are the size and order of the element (K_i, Σ, S) of $\mathcal{M}(\Omega)$, we define h_i' and p_i' as the target size and order of all elements of $\mathcal{M}'(\Omega)$ whose barycenters belong to K_i. If $N_\mathcal{V}$ represents the number of elements of the initial mesh $\mathcal{M}(\Omega)$, the number of elements

[1] Even if the error functional is not separable (e.g. for dissipative systems), the method appears to be nevertheless asymptotically valid, i.e. valid as soon as the mesh size is sufficiently small. In practice, the framing of the exact solution by the solutions of the dual formulations is thus experimentally verified as soon as the mesh size is compatible with the skin depth and the wavelength of the problem.

$N_{\mathcal{V}}{}'$ of the adapted mesh $\mathcal{M}'(\Omega)$ is thus approximatively given by (we consider only the three-dimensional case)

$$N_{\mathcal{V}}{}' = \sum_{i=1}^{N_{\mathcal{V}}} (h_i/h_i')^3. \tag{2.81}$$

From Tables 2.1, 2.2 and 2.3, we know that the size of the local function spaces behave like $\mathcal{O}(p^3)$ for $W_p^0(K)$, $W_p^1(K)$, $W_p^2(K)$ and $W_p^3(K)$. We can thus estimate the worst asymptotic behavior of the number of unknowns in the adapted mesh as

$$I' = \mathcal{O}\Big(\sum_{i=1}^{N_{\mathcal{V}}} p_i'^3 N_{\mathcal{V}}{}'\Big) = \mathcal{O}\Big(\sum_{i=1}^{N_{\mathcal{V}}} p_i'^3 (h_i/h_i')^3\Big).$$

Using (2.80), the modification of the elementary error between the initial and adapted mesh can be written as

$$\frac{\varepsilon_i}{\varepsilon_i'} = \frac{p_i'\, h_i{}^{p_i}}{p_i\, h_i'^{p_i'}},$$

which leads by (2.78) to the following expression for the global error in the adapted mesh:

$$\varepsilon'^2 = \sum_{i=1}^{N_{\mathcal{V}}} \varepsilon_i^2 \frac{p_i^2\, h_i'^{2p_i'}}{p_i'^2\, h_i^{2p_i}}.$$

We then define the optimality property as the minimization of the number of unknowns, while respecting a prescribed global error ε_0:

$$\min_{h_i', p_i'} \sum_{i=1}^{N_{\mathcal{V}}} p_i'^3 (h_i/h_i')^3 \quad \text{with} \quad \varepsilon_0^2 = \sum_{i=1}^{N_{\mathcal{V}}} \varepsilon_i^2 \frac{p_i^2\, h_i'^{2p_i'}}{p_i'^2\, h_i^{2p_i}}. \tag{2.82}$$

Note that the optimality property could also be stated the other way around, i.e. minimizing the global error while the number of unknowns is limited to an imposed value [176].

Three mesh adaptation strategies are considered: h-, p- and hp-refinement, where the sizes of the elements, their orders, or both their sizes and orders are locally modified in order to produce adapted meshes.

2.7.5.2 h-adaptation

Since only the elementary sizes are modified (hence, $p_i' = p_i$, $i = 1, \ldots, N_{\mathcal{V}}$), the introduction of a Lagrange multiplier λ permits to reformulate the constraint optimization problem (2.82) into the minimization of the functional

$$L_h = \sum_{i=1}^{N_{\mathcal{V}}} q_i + \lambda \Big(\sum_{i=1}^{N_{\mathcal{V}}} \varepsilon_i^2\, q_i^{2p_i/3} - \varepsilon_0^2 \Big), \tag{2.83}$$

where we posed $q_i = (h_i/h'_i)^3$. The extremality condition $\partial_{q_i} L_h = 0$ then leads to

$$q_i = (2\lambda p_i \varepsilon_i^2/3)^{3/(3+2p_i)}, \tag{2.84}$$

and the value of the Lagrange multiplier is obtained by solving (for example by means of the golden section technique [170]) the nonlinear equation in λ obtained by introducing (2.84) into (2.83). It can be easily verified that this optimum corresponds to a uniform distribution of the error across the elements, thus making (2.80) hold. Once the Lagrange multiplier is determined, the elementary sizes in the adapted mesh can be deduced from (2.84) (with $q_i = (h_i/h'_i)^3$) and be used to provide the characteristic length field [33, 179] in the form of a background mesh to an automatic mesh generator. The mesh generator can either perform a (partial or complete) remeshing (see Section D.2), which is the technique we use in Chapter 4, or simply subdivide the elements of the initial mesh into smaller elements. If this second technique is the faster, it however exhibits some disadvantages when used with unstructured meshes:

1. the size of an element in the initial mesh is at least twice the size of an element in the adapted mesh if no relocalization of the nodes is performed (the remeshing technique allows greater smoothness of the adapted mesh);

2. the derefinement (i.e. local augmentation of the size) is cumbersome to implement, since the meshes have to fulfill the conditions for finite element meshes given in Section 2.6.1;

3. simple subdivision algorithms (which are not coupled with the geometrical model) do not enhance the geometrical description (e.g. the respect of the curved boundaries) when the mesh is refined, and introduce artificial anisotropy in the mesh.

2.7.5.3 p-adaptation

In the case of a p-adaptation, only the elementary orders are modified (hence, $h'_i = h_i$, $i = 1, \ldots, N_{\mathcal{V}}$). The introduction of a Lagrange multiplier λ permits to reformulate a simplified version of the constraint optimization problem (2.82) into the minimization of the functional

$$L_p = \sum_{i=1}^{N_{\mathcal{V}}} q_i - \lambda \Big(\sum_{i=1}^{N_{\mathcal{V}}} \varepsilon_i^2 \, h_i^{-2q_i/3} - \varepsilon_0^2 \Big), \tag{2.85}$$

where we posed $q_i = (p'_i - p_i)^3$. The extremality condition $\partial_{q_i} L_h = 0$ then leads to

$$q_i = -3 \log(2\lambda \log h_i \varepsilon_i^2)/(2 \log h_i), \tag{2.86}$$

and the value of the Lagrange multiplier is obtained by solving the nonlinear equation in λ obtained by introducing (2.86) into (2.85). Once the Lagrange multiplier is determined, the elementary orders in the adapted mesh can be computed through

(2.86) (with $q_i = (h_i/h'_i)^3$). The advantage of the p-refinement is of course that the geometrical elements do not need to be modified. Three main disadvantages should be pointed out:

1. the convergence of the p-refinement dramatically depends on the smoothness of the solution (see (2.79)). Thus, the solution we advocate is to combine h- and p-refinements, as explained in the next section;

2. the elementary orders cannot vary continuously, so the actual values of p'_i are chosen as the integer values directly superior to the computed ones;

3. high interpolation orders lead to elevated bandwidths in the system matrix.

2.7.5.4 *hp*-adaptation

The combination of h- and p-adaptations leads to the so-called hp-method. The strategy we consider is uncoupled [165, 178]:

1. the problem is first solved on the initial mesh $\mathcal{M}(\Omega)$;

2. an h-adapted mesh $\mathcal{M}'(\Omega)$ is created with a global error constraint $\varepsilon' = \alpha\varepsilon''$, where $\alpha > 1$ and ε'' is the desired final global error;

3. the problem is solved on $\mathcal{M}'(\Omega)$;

4. a p-adapted mesh $\mathcal{M}''(\Omega)$ is created with the error constraint ε''. Since the error is uniformly distributed on $\mathcal{M}'(\Omega)$, the p-adaptation should lead to the ideal convergence rate (2.80);

5. the final solution is then computed on $\mathcal{M}''(\Omega)$.

The main disadvantage lies of course in the additional computation in comparison with one step adaptation techniques (for example presented in [228], where the h-refinement is followed by a uniform augmentation of the interpolation order).

Chapter 3

Hybrid Formulations

3.1 Introduction

In Chapter 1, we fitted the continuous electromagnetic field problems (magnetostatics, magnetodynamics and electromagnetic propagation problems) inside Maxwell's house: a diagram made of two dual de Rham complexes, put into relation by the constitutive laws. In Chapter 2, a way to approximate each de Rham complex by discrete subspaces was proposed. The resulting spaces were called $W_p^i(\Omega)$, $i = 0, \ldots, 3$, and were piece-wise defined on a finite element mesh $\mathcal{M}(\Omega)$ of the domain Ω, thus deserving the name of finite element spaces. It is now time to express the continuous electromagnetic problems in forms (called the continuous formulations) suitable for their discretization thanks to these finite element spaces.

Two approaches will be considered to build these continuous formulations, which can both be interpreted as particular cases of the general weighted residual method. The first approach rests on the use of the adjoints of the differential operators to build weak formulations (see Section A.3). This approach leads in a natural way to the Galerkin method [120], which we will use as our favorite discretization scheme. As an immediate consequence of the use of the adjoint operators, the Galerkin approach is dependent on inner products. The second approach is based on the definition of left inverses for the considered operators. It leads to what will be called the de Rham (or collocation) method. When dealing with purely differential equations, the de Rham method directly maps the first order equations of the physical models to systems of algebraic equations. Disguised as a finite volume scheme, this is the gist of the finite integration technique (FIT) [219] and constitutes a generalization of finite difference techniques to non-orthogonal meshes [24, 150]. One advantage of the de Rham method is that the inner product dependent and purely topological operations are clearly uncoupled. Starting directly in integral form with global quantities like circulations or fluxes, a variant of the de Rham method expressing the equations directly at the discrete level (without any notion of partial differential equations or function spaces) is favored by Tonti [210].

Indeed, the Galerkin and the de Rham approaches are tightly related to each other. It has been shown in [208, 111] that, in the case of partial differential equa-

tions, the Galerkin and de Rham methods lead to identical mass matrices at the discrete level, provided that Whitney forms are used for the discretization and that a suitable discretization of the Hodge operator (see Section A.1) is selected. It should nevertheless be noted that, while the formal connection with the de Rham map is rather new, the reinterpretation of the finite element methods by circuit-like relations has already been at the heart of the rediscovery of the Whitney forms for finite element computations (see [14] and the historical comments in the introduction of [19]). Many other authors have also worked on such interpretations [210, 208, 42].

Since the use of both Galerkin and de Rham methods is widespread in the case of purely differential equations, we will not go into too many details while establishing the weak formulations (i.e. suitable for the Galerkin method) of the model problems defined in Chapter 1, and we will only give references on how to achieve comparable results with the de Rham method. More interesting is the case of the integral parts of the models: if Galerkin approaches are also widely used in this case, de Rham methods are most of the time reduced to their simplest expression—nodal collocation (see e.g. [28, 187]). Though, when dealing with integral operators, there is no reason why the benefits of mixed finite elements should not be exploited as well. Appendix C presents the general background of the hybrid formulations established in this chapter as well as the different discretization alternatives. The results outlined in this chapter permit to justify the expression of the integral operators in terms of equivalent sources and the choice of the discretization strategies of these sources (in particular the necessity to rely on a dual mesh when using the de Rham method). To the best of our knowledge, no work has been carried out in this direction, although some fundamental ideas have already been alluded to by Bossavit in [18, p. 77].

In this chapter, two sets of dual formulations are constructed. First, the classical weak formulations are re-established, conforming either in the magnetic field ($\boldsymbol{h}$-conforming) or in the magnetic flux density ($\boldsymbol{b}$-conforming). New formulations adapted to the discretization of thin conducting and magnetic structures are then derived. While the literature dealing with this kind of approximation is abundant (see e.g. [196, 197, 136, 99, 152, 185, 11]), we present a fully dual approach for the construction of the continuous formulations based on an appropriate treatment of the surface terms arising in the weak formulations. Contrary to the approach presented for example in [185], all approximations are thus introduced at the continuous level, before any discretization. And contrary to the approaches favored for example in [134, 196, 197], no stream function for the current has to be introduced, since we directly work with the traces of the electromagnetic fields or potentials on the boundary of the thin structures. The coupling between the local electromagnetic quantities and the global current and voltages is then presented for each set of formulations, and particular attention is given to an original treatment of massive, stranded and foil winding inductors. A method to compute the source fields involved in the magnetic field conforming formulations is introduced as well. The coupling of the continuous formulations with integral equations is eventually presented.

The developments made in this chapter are mainly based on the work by Bossavit and Vérité for the $\boldsymbol{h}$-conforming formulations [25, 26] and on the work by Ren and

coauthors for the $\boldsymbol{b}$-conforming formulations [186, 191, 192]. Most original contributions of this chapter have been published separately in [82, 83, 52, 57, 49, 86].

3.2 Magnetic field conforming formulations

3.2.1 Magnetodynamics

3.2.1.1 Generalities

Let us first consider the magnetodynamic problem defined in Section 1.4.2 (the magnetostatic case will be treated as a particularization of the results presented in this section). We thus want to solve (1.50) together with the constitutive relations (1.12) and (1.8). We start by writing a weak form (see Section A.3) of Faraday's law (1.50a), i.e.

$$\partial_t(\boldsymbol{b}, \boldsymbol{h}')_\Omega + (\boldsymbol{e}, \mathbf{curl}\, \boldsymbol{h}')_\Omega + \langle \boldsymbol{n} \times \boldsymbol{e}, \boldsymbol{h}' \rangle_{\Gamma_e} = 0, \quad \forall \boldsymbol{h}' \in \boldsymbol{H}^0_h(\mathbf{curl}; \Omega), \tag{3.1}$$

where the field $\boldsymbol{h}' \in \boldsymbol{H}^0_h(\mathbf{curl}; \Omega)$ is a field of test functions independent of time (see Section 1.3.2 for the definition of the function spaces). In order to satisfy the upper part of the Tonti diagram (1.55) (i.e. Ampère's law) in a strong sense, we first introduce the magnetic constitutive relation (1.12) in the weak form (3.1) to obtain

$$\partial_t(\mu \boldsymbol{h}, \boldsymbol{h}')_\Omega + (\boldsymbol{e}, \mathbf{curl}\, \boldsymbol{h}')_\Omega + \langle \boldsymbol{n} \times \boldsymbol{e}, \boldsymbol{h}' \rangle_{\Gamma_e} = 0, \quad \forall \boldsymbol{h}' \in \boldsymbol{H}^0_h(\mathbf{curl}; \Omega). \tag{3.2}$$

Combining the electric constitutive relation (1.8) with Ampère's law (1.50b), we have $\mathbf{curl}\, \boldsymbol{h} = \boldsymbol{j} = \sigma^{-1}\boldsymbol{e}$ in Ω_c, and thus

$$\partial_t(\mu \boldsymbol{h}, \boldsymbol{h}')_\Omega + (\sigma^{-1}\mathbf{curl}\, \boldsymbol{h}, \mathbf{curl}\, \boldsymbol{h}')_{\Omega_c} + (\boldsymbol{e}, \mathbf{curl}\, \boldsymbol{h}')_{\Omega_c^{\mathrm{C}}} + \langle \boldsymbol{n} \times \boldsymbol{e}, \boldsymbol{h}' \rangle_{\Gamma_e} = 0, \quad \forall \boldsymbol{h}' \in \boldsymbol{H}^0_h(\mathbf{curl}; \Omega). \tag{3.3}$$

As has been seen in Section 1.2.2.2, the constraint $\boldsymbol{j} = \boldsymbol{j}_s$ on the current density in the (stranded) inductors Ω_s leads to the definition of a source magnetic field $\boldsymbol{h}_s$ that fulfills (1.22). Let us explicitly introduce $\boldsymbol{h}_s$ in the expression of the magnetic field $\boldsymbol{h}$ thanks to (1.51), i.e.:

$$\boldsymbol{h} = \boldsymbol{h}_s + \boldsymbol{h}_r. \tag{3.4}$$

Since

$$\mathbf{curl}\, \boldsymbol{h} = \boldsymbol{j}_s \quad \text{in } \Omega_s \quad \text{and} \quad \mathbf{curl}\, \boldsymbol{h} = 0 \quad \text{in } \Omega_c^{\mathrm{C}} - \Omega_s, \tag{3.5}$$

we have

$$\mathbf{curl}\, \boldsymbol{h}_r = 0 \quad \text{in } \Omega_c^{\mathrm{C}}. \tag{3.6}$$

The field $\boldsymbol{h}_r$, called the reaction magnetic field, is the unknown of our problem. The test field $\boldsymbol{h}'$ appearing in the weak form (3.2) may thus be chosen in a subspace of $\boldsymbol{H}^0_h(\mathbf{curl}; \Omega)$ for which $\mathbf{curl}\, \boldsymbol{h}'_r = 0$ in Ω_c^{C}, with $\boldsymbol{h}' = \boldsymbol{h}'_s + \boldsymbol{h}'_r$. This causes the cancellation of the third term of (3.3), and the weak form (3.3) can thus be rewritten as

$$\partial_t(\mu \boldsymbol{h}, \boldsymbol{h}')_\Omega + (\sigma^{-1}\mathbf{curl}\, \boldsymbol{h}, \mathbf{curl}\, \boldsymbol{h}')_{\Omega_c} + (\sigma^{-1}\boldsymbol{j}_s, \mathbf{curl}\, \boldsymbol{h}')_{\Omega_s} + \langle \boldsymbol{n} \times \boldsymbol{e}, \boldsymbol{h}' \rangle_{\Gamma_e} = 0,$$

$$\forall \boldsymbol{h}' \in \boldsymbol{H}^0_h(\mathbf{curl};\Omega) \quad \text{with} \quad \mathbf{curl}\,\boldsymbol{h}'_r = 0 \text{ in } \Omega_c^{\mathrm{C}} \quad \text{and} \quad \boldsymbol{h}' = \boldsymbol{h}'_s + \boldsymbol{h}'_r. \tag{3.7}$$

It should be noticed that this formulation of the magnetodynamic problem does not permit to determine the electric field $\boldsymbol{e}$ in the non-conducting regions Ω_c^{C}. The trace of the electric field $\boldsymbol{n} \times \boldsymbol{e}$ is subject to a natural boundary condition on the boundaries Γ_e of the domain Ω (more precisely, of the domain obtained after the removal of the thin regions; cf. Section 1.2.2.4). This condition can take various forms:

1. the trace of the electric field can be locally specified. In particular, this is the case for a homogeneous Neumann boundary condition imposing a symmetry condition of "perpendicular current" or "zero magnetic flux" (since $\boldsymbol{n}\times\boldsymbol{e}\big|_{\Gamma_e} = 0$ implies $\boldsymbol{n}\cdot\boldsymbol{b}\big|_{\Gamma_e} = 0$);

2. the trace of the electric field can appear in local implicit boundary conditions, such as the conditions established for the treatment of thin structures. This is developed in Section 3.2.1.2;

3. the trace can be a field for which only associated global quantities are known (i.e. functional of $\boldsymbol{n} \times \boldsymbol{e}$). This is developed in Sections 3.2.1.3 and 3.2.1.4 for the treatment of massive, stranded and foil winding inductors;

4. the traces can appear in the definition of an integral operator. In that case they constitute local unknowns of the problem. This is developed in Section 3.2.1.5.

3.2.1.2 Thin conducting and magnetic structures

Across conducting and/or magnetic thin structures, the tangential magnetic field is discontinuous (see Section 1.2.2.1). We thus decompose $\boldsymbol{h}$ as follows:

$$\boldsymbol{h} = \boldsymbol{h}_c + \boldsymbol{h}_d, \tag{3.8}$$

where the tangential components $\boldsymbol{h}_{c,t}$ and $\boldsymbol{h}_{d,t}$ of $\boldsymbol{h}_c$ and $\boldsymbol{h}_d$ are continuous and discontinuous across the thin structures Ω_t respectively. To simplify further developments, we assume that $\boldsymbol{h}_d$ is equal to zero on the side Γ_t^- of the thin structure. Performing the cross product of $\boldsymbol{n}_t$ by (1.20) and developing (1.21), we obtain

$$\boldsymbol{n}_t \times \boldsymbol{e}\,\big|_{\Gamma_t^+} + \boldsymbol{n}_t \times \boldsymbol{e}\,\big|_{\Gamma_t^-} = -(\sigma\beta)^{-1}\,\boldsymbol{h}_{d,t}\,, \tag{3.9}$$

$$\boldsymbol{n}_t \times \boldsymbol{e}\,\big|_{\Gamma_t^+} - \boldsymbol{n}_t \times \boldsymbol{e}\,\big|_{\Gamma_t^-} = -\partial_t\big(\mu\beta\,(2\boldsymbol{h}_{c,t} + \boldsymbol{h}_{d,t})\big), \tag{3.10}$$

which can be solved for $\boldsymbol{n}_t \times \boldsymbol{e}\,\big|_{\Gamma_t^+}$ and $\boldsymbol{n}_t \times \boldsymbol{e}\,\big|_{\Gamma_t^-}$ to give

$$\boldsymbol{n}_t \times \boldsymbol{e}\,\big|_{\Gamma_t^+} = \frac{1}{2}\Big[-\partial_t\big(\mu\beta\,(2\boldsymbol{h}_{c,t} + \boldsymbol{h}_{d,t})\big) - \frac{1}{\sigma\beta}\,\boldsymbol{h}_{d,t}\Big], \tag{3.11}$$

$$\boldsymbol{n}_t \times \boldsymbol{e}\,\big|_{\Gamma_t^-} = \frac{1}{2}\Big[\partial_t\big(\mu\beta\,(2\boldsymbol{h}_{c,t} + \boldsymbol{h}_{d,t})\big) - \frac{1}{\sigma\beta}\,\boldsymbol{h}_{d,t}\Big]. \tag{3.12}$$

As explained in Section 1.2.2.4, the thin regions Ω_t can then be removed from the domain Ω. If we rewrite the formulation (3.7) for the resulting transformed domain, the boundary Γ_e now contains the boundary of the thin regions Ω_t, i.e. $\Gamma_t^+ \cup \Gamma_t^- \cup \Gamma_t^=$ (see Figure 1.3). Thanks to the hypothesis made in Section 1.2.2.1, $\Gamma_t^+ \cup \Gamma_t^- \cup \Gamma_t^=$ can then be replaced by a single thin region Γ_t, and the corresponding part of the surface term in (3.7) successively becomes, using (3.11) and (3.12):

$$\begin{aligned}
\langle \boldsymbol{n} \times \boldsymbol{e}, \boldsymbol{h}' \rangle_{\Gamma_t^+ \cup \Gamma_t^- \cup \Gamma_t^=} &= -\langle \boldsymbol{n}_t \times \boldsymbol{e}, \boldsymbol{h}' \rangle_{\Gamma_t^+} + \langle \boldsymbol{n}_t \times \boldsymbol{e}, \boldsymbol{h}' \rangle_{\Gamma_t^-} \\
&= -\langle \frac{1}{2} \big[-\partial_t \big(\mu\beta \, (2\boldsymbol{h}_{c,t} + \boldsymbol{h}_{d,t}) \big) - \frac{1}{\sigma\beta} \, \boldsymbol{h}_{d,t} \big], \boldsymbol{h}'_c + \boldsymbol{h}'_d \rangle_{\Gamma_t} \\
&\quad + \langle \frac{1}{2} \big[\partial_t \big(\mu\beta \, (2\boldsymbol{h}_{c,t} + \boldsymbol{h}_{d,t}) \big) - \frac{1}{\sigma\beta} \, \boldsymbol{h}_{d,t} \big], \boldsymbol{h}'_c \rangle_{\Gamma_t}.
\end{aligned} \tag{3.13}$$

The magnetic field conforming magnetodynamic formulation (3.7) then becomes

$$\begin{aligned}
&\partial_t (\mu \boldsymbol{h}, \boldsymbol{h}')_\Omega + (\sigma^{-1} \mathbf{curl}\, \boldsymbol{h}, \mathbf{curl}\, \boldsymbol{h}')_{\Omega_c} + (\sigma^{-1} \boldsymbol{j}_s, \mathbf{curl}\, \boldsymbol{h}')_{\Omega_s} + \langle \boldsymbol{n} \times \boldsymbol{e}, \boldsymbol{h}' \rangle_{\Gamma_e - \Gamma_t} \\
&\quad + 2\, \partial_t \langle \mu\beta \, \boldsymbol{h}_{c,t}, \boldsymbol{h}'_c \rangle_{\Gamma_t} + \partial_t \langle \mu\beta \, \boldsymbol{h}_{d,t}, \boldsymbol{h}'_c \rangle_{\Gamma_t} + \partial_t \langle \mu\beta \, \boldsymbol{h}_{c,t}, \boldsymbol{h}'_d \rangle_{\Gamma_t} \\
&\quad + \frac{1}{2} \partial_t \langle \mu\beta \, \boldsymbol{h}_{d,t}, \boldsymbol{h}'_d \rangle_{\Gamma_t} + \frac{1}{2} \langle \frac{1}{\sigma\beta} \, \boldsymbol{h}_{d,t}, \boldsymbol{h}'_d \rangle_{\Gamma_t} = 0, \\
&\forall \boldsymbol{h}' \in \boldsymbol{H}_h^0(\mathbf{curl}; \Omega) \quad \text{with} \quad \mathbf{curl}\, \boldsymbol{h}'_r = 0 \text{ in } \Omega_c^{\mathrm{C}} \quad \text{and} \quad \boldsymbol{h}' = \boldsymbol{h}'_s + \boldsymbol{h}'_r.
\end{aligned} \tag{3.14}$$

The magnetic field $\boldsymbol{h}$ has been decomposed in (3.4) into a reaction field $\boldsymbol{h}_r$ and a source field $\boldsymbol{h}_s$. In the non-conducting regions Ω_c^{C}, the reaction field $\boldsymbol{h}_r$ can be derived from a scalar potential ϕ such that $\boldsymbol{h}_r = -\mathbf{grad}\, \phi$ (see also Section 1.4.2). This derivation is only valid if l cutting surfaces Σ_i, $i = 1, \ldots, l$ are defined in Ω_c^{C} (see Section 1.2.1). In order to express the constraints associated with these cuts (as seen in Section 1.3.1) and the discontinuity of the tangential component of the magnetic field across the thin structures (cf. (3.8)), we decompose the magnetic scalar potential ϕ into three parts:

$$\phi = \phi_c + \phi_l + \phi_d, \tag{3.15}$$

where ϕ_c is continuous in Ω_c^{C}, where ϕ_l is discontinuous across the cutting surfaces Σ_i, and where ϕ_d is discontinuous across the set of thin structures Γ_t. The introduction of this potential ϕ in the non-conducting regions and its coupling with the magnetic field $\boldsymbol{h}$ in the conducting regions is made in the discrete form of the formulation (see Section 3.2.3). At the continuous level, it is already interesting to note that, as seen in Section 1.3.1, the discontinuities of ϕ_l are constant on each cut and can be written as

$$\phi_l = \sum_{i=1}^{l} I_i q_i, \tag{3.16}$$

where I_i is the value associated with the cut Σ_i and where q_i is the ith basis function of $\mathcal{H}^1(\Omega_c^{\mathrm{C}})$, exhibiting a unit discontinuity across Σ_i.

One should also remark that the formulation (3.14) does not make any use of current stream functions [196, 197]. The treatment of topologically non-trivial domains

is handled in a natural way by considering the cuts on Γ_t as the traces of the cuts in Ω (this technique was already favored in [134]). As mentioned in the introduction of this chapter, the preceding developments were carried out while building a weak formulation suitable for a Galerkin-type discretization. They could of course also be expressed without the use of adjoint operators (see e.g. [208] or [34] for directions on how to do this in the case of magnetostatic or magnetodynamic problems respectively).

3.2.1.3 Currents as strong global quantities

In weak $\boldsymbol{h}$-conforming formulations, the total electric current flowing in a conductor is a global quantity directly obtained from the magnetic field $\boldsymbol{h}$, with (1.50b) and (1.24b) or (1.25b). The current is said to be expressed in a strong sense in contrast with the associated voltage being only defined in a weak sense, i.e. through an integration procedure in close relation with the considered weak formulation (the definition of the voltage is indeed contained in Faraday's law expressed in a weak form).

Current driven massive inductors can be directly considered through the expression of the reaction magnetic field in (3.4) and so the circulation of $\boldsymbol{h}_r$ along any closed path C_i around each massive inductor $\Omega_{m,i}$ has to be equal to its current I_i:

$$\int_{C_i} \boldsymbol{h}_r \cdot d\boldsymbol{l} = I_i. \tag{3.17}$$

This relation implies that for each inductor there exists one basis function of $\boldsymbol{h}$ (called the current basis function and denoted $\boldsymbol{c}_i$) associated with its current, with the property of having a unit circulation along any closed path C_i around the inductor. This function $\boldsymbol{c}_i$, associated with the cut Σ_i, is precisely the gradient of the scalar potential q_i appearing in (3.16), i.e. $\boldsymbol{c}_i = -\mathbf{grad}\, q_i$, the potential being defined in the domain Ω_c^{C} made topologically simple.

Foil winding inductors can be first considered as a set of massive subregions, treated in the same way as classical massive inductors. The constraints on the current in each foil of the inductor $\Omega_{f,i}$ are then fixed through global current basis functions $\boldsymbol{c}_{i,j}$, $j = 1, \ldots, N_i$, where N_i is the total number of foils (Figure 3.1). Because the current I_i is the same in each foil, a global cut function $\boldsymbol{c}_i$ can be defined in the whole inductor by

$$\boldsymbol{c}_i = \sum_{j=1}^{N_i} (N_i - j + 1)\boldsymbol{c}_{i,j}. \tag{3.18}$$

This method can further be simplified if the space to which the magnetic field belongs is decomposed into orthogonal subspaces, uncoupling the components of the field along the height of the foils as well as the component along the foil thickness. This method will be elaborated in the discrete form of the formulation (see Section 3.2.3.2).

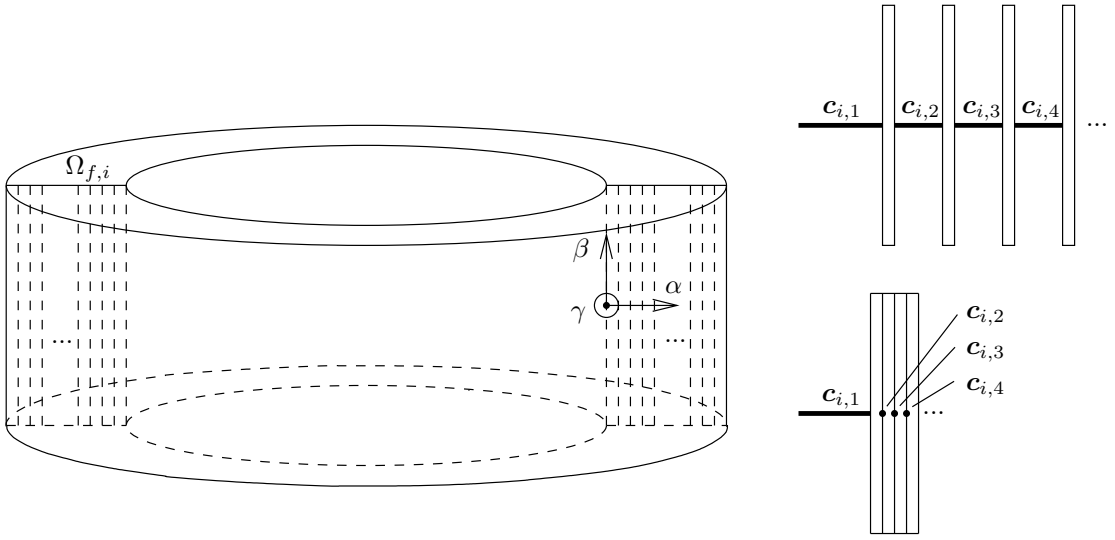

Figure 3.1: Foil winding inductor $\Omega_{f,i}$. Cuts for magnetic scalar potential discontinuities between massive subregions.

For stranded inductors, the constraint of uniformity of the current density is automatically satisfied through source magnetic fields $\boldsymbol{h}_{s,i}$, each one being associated with an inductor $\Omega_{s,i}$ with a unit current, i.e. satisfying $\mathbf{curl}\,\boldsymbol{h}_{s,i} = \boldsymbol{j}_{s,i}$ (see Section 1.2.2.2). Then the total source magnetic field $\boldsymbol{h}_s$ can be expressed as

$$\boldsymbol{h}_s = \sum_i I_{s,i}\boldsymbol{h}_{s,i}, \tag{3.19}$$

where $I_{s,i}$ is the current flowing in the ith stranded inductor. The actual source current density in the ith inductor is $\boldsymbol{j}_s = I_{s,i}\boldsymbol{j}_{s,i}$. Therefore, source magnetic fields given by (3.19) make it possible to directly take current driven stranded inductors into account in the formulation (3.7).

3.2.1.4 Voltages as weak global quantities and circuit relations

Voltages are expressed in a weak sense in accordance with the considered weak formulation (3.7). Let us examine the inductor in Figure 3.2 (initially defined in Figure 1.6) with its source of electromotive force located between two sections. The electric field $\boldsymbol{e}$ in the ith generator $\Omega_{g,i}$ can be considered as being known (as a conservative electric field) and its circulation along any path from one electrode to the other in $\Omega_{g,i}$ is actually the applied voltage V_i.

For massive inductors, in a treatment similar to the one applied to thin structures in Section 3.2.1.2, the generator $\Omega_{g,i}$ can be removed from the domain Ω. The formulation (3.7), rewritten for the resulting transformed domain, then involves a boundary integral on Γ_e which now contains the boundary of the generators, i.e. Γ_g (see Figure 1.6). For a test magnetic field $\boldsymbol{h}'$ equal to the current basis function $\boldsymbol{c}_i$ (see Section 3.2.1.3), the part of this integral on $\Gamma_{g,i}$ becomes successively ($\boldsymbol{n}\times\boldsymbol{e} = 0$

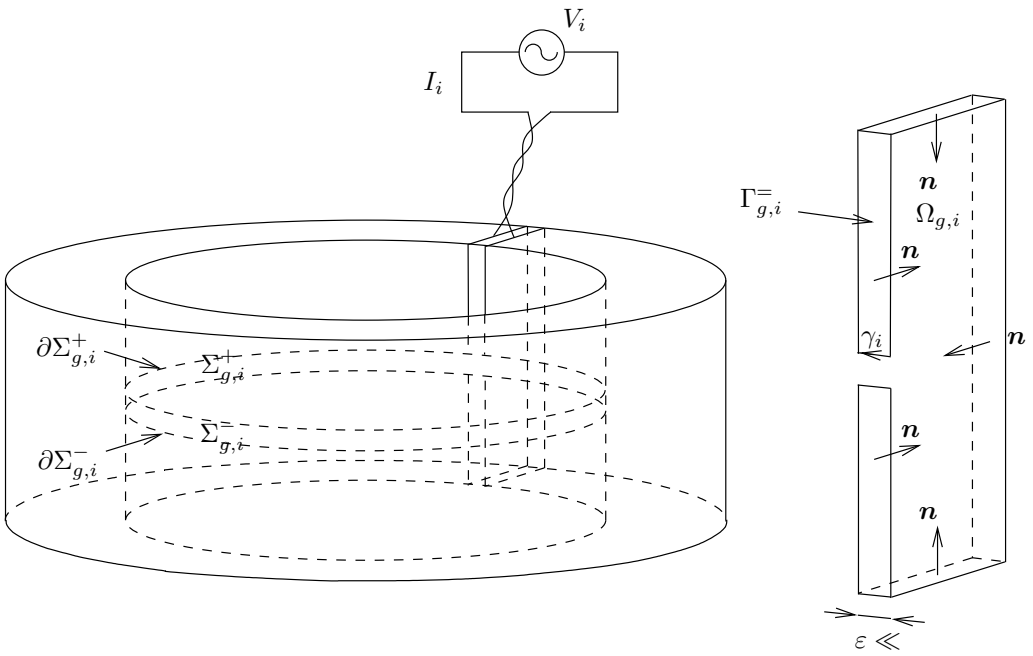

Figure 3.2: Inductor with a source of electromotive force $\Omega_{g,i}$ and its cut.

on each electrode):

$$\begin{aligned}\langle \boldsymbol{n}\times\boldsymbol{e},\boldsymbol{c}_i\rangle_{\Gamma_{g,i}} &= \langle \boldsymbol{n}\times\boldsymbol{e},\boldsymbol{c}_i\rangle_{\Gamma^{=}_{g,i}} = \langle \boldsymbol{n}\times\boldsymbol{e},-\mathbf{grad}\,q_i\rangle_{\Gamma^{=}_{g,i}} = \langle \mathbf{grad}\,q_i\times\boldsymbol{e},\boldsymbol{n}\rangle_{\Gamma^{=}_{g,i}}\\ &= \langle \mathbf{curl}\,(q_i\,\boldsymbol{e}),\boldsymbol{n}\rangle_{\Gamma^{=}_{g,i}} - \langle q_i\,\mathbf{curl}\,\boldsymbol{e},\boldsymbol{n}\rangle_{\Gamma^{=}_{g,i}}. \end{aligned} \tag{3.20}$$

Using the Stokes formula for the first integral and observing that the second vanishes, we obtain

$$\langle \boldsymbol{n}\times\boldsymbol{e},\boldsymbol{c}_i\rangle_{\Gamma_{g,i}} = \int_{\partial\Gamma^{=}_{g,i}} q_i\boldsymbol{e}\cdot d\boldsymbol{l} = \int_{\gamma_i}\boldsymbol{e}\cdot d\boldsymbol{l} = V_i, \tag{3.21}$$

because only the part γ_i of the oriented contour $\partial\Gamma^{=}_{g,i}$ in contact with $\partial\Sigma^{+}_{g,i}$ gives a non-zero contribution (see Figure 3.2). Consequently, for the test function $\boldsymbol{h}' = \boldsymbol{c}_i$ and with (3.21), (3.7) becomes

$$\partial_t(\mu\boldsymbol{h},\boldsymbol{c}_i)_\Omega + (\sigma^{-1}\mathbf{curl}\,\boldsymbol{h},\mathbf{curl}\,\boldsymbol{c}_i)_{\Omega_c} = -V_i. \tag{3.22}$$

This relation is the weak circuit relation for the ith inductor and can be physically interpreted as "∂_t(magnetic flux) + resistance × current = voltage".

Foil winding inductors, when treated as a set of massive subregions, can be handled by (3.22) if the current basis function $\boldsymbol{c}_i$ is taken as (3.18). The same kind of relation could also be written for each separate foil using associated functions $\boldsymbol{c}_j$, $j = 1,\ldots,N_i$. The simplified case, when the foil winding inductor is considered as a continuous region, will be treated at the discrete level (see Section 3.2.3.2).

The treatment of stranded inductors is similar to the treatment of massive inductors, except that the basis functions of the source magnetic field $\boldsymbol{h}_s$ defined in

(3.19) (i.e. the unit source magnetic fields $\boldsymbol{h}_{s,i}$) are used as test functions $\boldsymbol{h}'$. The very same treatment of the surface term arising in (3.7) then leads to

$$\partial_t(\mu \boldsymbol{h}, \boldsymbol{h}_{s,i})_\Omega + I_i(\sigma^{-1}\boldsymbol{j}_{s,i}, \mathbf{curl}\, \boldsymbol{h}_{s,i})_{\Omega_{s,i}} = -V_i, \tag{3.23}$$

which is the weak circuit relation for the ith stranded inductor. This relation allows a natural computation of the total magnetic flux linked with all the turns of the inductor in perfect accordance with the weak formulation, without the need for any supplementary integral formula.

3.2.1.5 Integral operators

For open boundary problems (i.e. when the domain of study is not bounded), the surface term $\langle \boldsymbol{n} \times \boldsymbol{e}, \boldsymbol{h}' \rangle_{\Gamma_e}$ in (3.7), which can be reduced to $\partial_t \langle \boldsymbol{n} \cdot \boldsymbol{b}, \phi' \rangle_{\Gamma_e}$, is not fixed a priori and constitutes an unknown of the problem. Using the exterior hybrid approach presented in Appendix C, we introduce a boundary operator relating the trace of the magnetic flux density on the boundary Γ_e and a magnetic scalar potential ϕ in the exterior domain $\mathbb{E}^3 - \Omega$, which leads in a natural way to a classical magnetic field conforming hybrid finite element and boundary element method [25, 26].

If a source current $\boldsymbol{j}_e$ exists in the exterior inductor domain Ω_e (see Section 1.2.1), the magnetic field in $\mathbb{E}^3 - \Omega$ can be decomposed in the same way as in (1.45), i.e. into a source magnetic field $\boldsymbol{h}_e$ generated by the source current (determined by the Biot-Savart law (1.47)) and a reduced magnetic field deriving from the scalar potential ϕ:

$$\boldsymbol{h} = \boldsymbol{h}_e + \boldsymbol{h}_r = \boldsymbol{h}_e - \mathbf{grad}\, \phi. \tag{3.24}$$

If the exterior domain $\mathbb{E}^3 - \Omega$ contains l loops, l cuts have to be introduced in $\mathbb{E}^3 - \Omega$ in order to make the scalar potential ϕ single valued. To avoid the definition of these cuts, one may rewrite the coupling directly in terms of the magnetic field, as proposed in [191]. Nevertheless, in order to minimize the number of unknowns in the discrete formulation, the boundary of Ω is usually extended so that Ω exhibits the simplest possible and most regular shape. As a consequence, $\mathbb{E}^3 - \Omega$ is in general of very simple topology.

Let us define the integral operator $\mathcal{P}^e(0, \sigma)$ by the following Fredholm integral of the first kind:

$$\mathcal{P}^e(0, \sigma) = \boldsymbol{x} \mapsto \frac{1}{4\pi} \int_{\Gamma_e} \frac{\sigma(\boldsymbol{y})}{|\boldsymbol{x} - \boldsymbol{y}|}\, d\boldsymbol{y}. \tag{3.25}$$

Its normal derivative at a point $\boldsymbol{x}$ on Γ_e is given by (beware that $\boldsymbol{n}$ represents the exterior normal to the exterior domain $\mathbb{E}^3 - \Omega$, and thus the interior normal to Ω: see Section C.3):

$$\boldsymbol{n} \cdot \mathbf{grad}\, \mathcal{P}^e(0, \sigma) = \boldsymbol{x} \mapsto \frac{1}{2}\sigma(\boldsymbol{x}) + \frac{1}{4\pi} \int_{\Gamma_e} \frac{\boldsymbol{n}(\boldsymbol{x}) \cdot (\boldsymbol{y} - \boldsymbol{x})\, \sigma(\boldsymbol{y})}{|\boldsymbol{x} - \boldsymbol{y}|^3}\, d\boldsymbol{y}. \tag{3.26}$$

Thanks to the properties of $\mathcal{P}^e(0, \sigma)$ (similar to those presented in Appendix C for the two-dimensional case), at any point $\boldsymbol{x}$ in the exterior domain $\mathbb{E}^3 - \Omega$, the

scalar potential can then be expressed as

$$\phi(\boldsymbol{x}) = \mu^{-1}\mathcal{P}^e(0,\sigma), \tag{3.27}$$

and its derivative at a point $\boldsymbol{x}$ on Γ_e as

$$\boldsymbol{n}\cdot\mathbf{grad}\,\phi(\boldsymbol{x}) = \mu^{-1}\boldsymbol{n}\cdot\mathbf{grad}\,\mathcal{P}^e(0,\sigma). \tag{3.28}$$

It is interesting to notice that the sources σ of the integral operator can in this case be interpreted as virtual magnetic charges [139]. The goal of the hybrid formulation is then to establish a relation between $\boldsymbol{n}\cdot\boldsymbol{b}$ and ϕ on Γ_e, which can be obtained in various ways depending on the scheme chosen to discretize (3.27)–(3.28). Among these schemes [187], the most widespread are the collocation method [28], the Treffz method [227] and the variational method [25]. Following the strategy presented in Appendix C for the discretization of the sources σ, the variational formulation becomes (beware that the normal $\boldsymbol{n}$ now points outward Ω): find $\sigma \in H_h^{10}(\Gamma_e)$ and $\phi \in H_h^{10}(\Gamma_e)$ such that

$$\langle\phi,\sigma'\rangle_{\Gamma_e} = \langle\mu^{-1}\mathcal{P}^e(0,\sigma),\sigma'\rangle_{\Gamma_e}, \quad \forall\sigma' \in H_h^{10}(\Gamma_e), \tag{3.29}$$

and

$$\langle\boldsymbol{n}\cdot\boldsymbol{b},\phi'\rangle_{\Gamma_e} = -\langle\boldsymbol{n}\cdot\mathbf{grad}\,\mathcal{P}^e(0,\sigma),\phi'\rangle_{\Gamma_e} + \langle\mu\,\boldsymbol{n}\cdot\boldsymbol{h}_e,\phi'\rangle_{\Gamma_e}, \quad \forall\phi' \in H_h^{10}(\Gamma_e). \tag{3.30}$$

The generalized collocation technique can be applied in exactly the same way as in Section C.4.2.

3.2.2 Magnetostatics

Keeping in mind the developments that were made for the magnetodynamic problem in the previous section, we now consider the simplified case of magnetostatics, where all time dependent phenomena are neglected (see Section 1.4.1).

Let us start by writing a weak form of (1.44b), i.e.

$$(\boldsymbol{b},-\mathbf{grad}\,\phi')_\Omega + \langle\boldsymbol{n}\cdot\boldsymbol{b},\phi'\rangle_{\Gamma_e} = 0, \quad \forall\phi' \in H_h^{10}(\Omega). \tag{3.31}$$

In order to satisfy in a strong sense the upper part of the Tonti diagram (1.49), we first introduce (1.12) into (3.31) to obtain

$$(\mu\boldsymbol{h},-\mathbf{grad}\,\phi')_\Omega + \langle\boldsymbol{n}\cdot\boldsymbol{b},\phi'\rangle_{\Gamma_e} = 0, \quad \forall\phi' \in H_h^{10}(\Omega). \tag{3.32}$$

Then, decomposing $\boldsymbol{h} \in \boldsymbol{H}(\mathbf{curl};\Omega)$ by (3.4) in the same way as in Section 3.2.1, we can derive the reaction field $\boldsymbol{h}_r$ from a scalar potential ϕ such that $\boldsymbol{h}_r = -\mathbf{grad}\,\phi$ everywhere in Ω. Of course, this derivation is only valid if the l cuts Σ_i, $i = 1,\ldots,l$ are introduced in Ω. The weak form (3.32) can then be written as

$$(\mu\,(\boldsymbol{h}_s - \mathbf{grad}\,\phi),-\mathbf{grad}\,\phi')_\Omega + \langle\boldsymbol{n}\cdot\boldsymbol{b},\phi'\rangle_{\Gamma_e} = 0, \quad \forall\phi' \in H_h^{10}(\Omega). \tag{3.33}$$

The treatment of thin magnetic structures is similar to the treatment of thin magnetic and conducting structures presented in Section 3.2.1.2. On account of

$$\langle \boldsymbol{n} \times \boldsymbol{e}, \boldsymbol{h} \rangle = -\langle \boldsymbol{n} \times \boldsymbol{e}, \mathbf{grad}\, \phi \rangle = -\langle \boldsymbol{n}, \phi\, \mathbf{curl}\, \boldsymbol{e} \rangle + \langle \boldsymbol{n}, \mathbf{curl}\, (\phi \boldsymbol{e}) \rangle = \langle \partial_t (\boldsymbol{n} \cdot \boldsymbol{b}), \phi \rangle, \tag{3.34}$$

and since $\boldsymbol{h}_d = 0$ as no current flows in the shell, we can rewrite a time primitive of (3.13) as

$$\langle \boldsymbol{n} \cdot \boldsymbol{b}, \phi' \rangle_{\Gamma_t^+ \cup \Gamma_t^- \cup \Gamma_{\bar{t}}^=} = \langle \mu d\, \boldsymbol{h}_{c,t}, \boldsymbol{h}'_c \rangle_{\Gamma_t}. \tag{3.35}$$

The scalar potential ϕ is now continuous across the thin structures Γ_t and the $\boldsymbol{h}$-conforming magnetostatic formulation becomes

$$(\mu\, (\boldsymbol{h}_s - \mathbf{grad}\, \phi), -\mathbf{grad}\, \phi')_\Omega + \langle \boldsymbol{n} \cdot \boldsymbol{b}, \phi' \rangle_{\Gamma_e - \Gamma_t} \tag{3.36}$$

$$+\langle \mu d\, (\boldsymbol{h}_{s,t} - \mathbf{grad}_s \phi), -\mathbf{grad}_s \phi' \rangle_{\Gamma_t} = 0, \quad \forall \phi' \in H_h^{10}(\Omega), \tag{3.37}$$

where grad_s represents the surface gradient on Γ_t. This formulation has been known for many years and is widely used [30]. Taking (3.34) into account, the treatment of global electrical quantities, as well as the introduction of integral operators for the treatment of unbounded domains, is the same as what has been presented for the magnetodynamic formulation in Sections 3.2.1.3, 3.2.1.4 and 3.2.1.5.

3.2.3 Discretization

3.2.3.1 Local quantities

Discrete counterparts of the spaces $H^1(\Omega)$ and $\boldsymbol{H}(\mathbf{curl}; \Omega)$ have been constructed in Chapter 2, namely $W_p^0(\Omega)$ and $W_p^1(\Omega)$. Since the reaction magnetic field $\boldsymbol{h}_r$ appearing in the magnetodynamic formulations established above fulfills $\mathbf{curl}\, \boldsymbol{h}_r = 0$ in Ω_c^{C}, it belongs to the reduced nullspace $\mathcal{NS}_p^1(\Omega, \Omega_c^{\mathrm{C}})$ of the **curl** operator defined in Section 2.6.4.1. Its discrete expression is thus given by (2.70), with $\boldsymbol{u} = \boldsymbol{h}_r$, $\boldsymbol{v} = \phi$, $\boldsymbol{v}_c = \phi_c$, $\boldsymbol{v}_l = \phi_l$ and $\boldsymbol{v}_d = \phi_d$. The scalar potential ϕ involved in the magnetostatic formulation belongs to the nullspace $\mathcal{NS}_p^1(\Omega)$ and its discrete expression is thus given by (2.71), with $v = \phi$, $v_c = \phi_c$, $v_l = \phi_l$ and $v_d = 0$.

Several ways of defining the source magnetic field $\boldsymbol{h}_s$ can be considered. These methods differ in the way the source field is approximated as well as in the extent of its domain of definition [159, 216, 128, 169, 55, 52, 153]. Indeed, as has been pointed out in Section 1.4.1, there exists a whole class of source fields $\boldsymbol{h}_s$ verifying $\mathbf{curl}\, \boldsymbol{h}_s = \boldsymbol{j}_s$, the one calculated by the Biot-Savart law being one of those for which the gauge condition $\mathrm{div}\, \boldsymbol{h}_s = 0$ is implicitly satisfied. But at the discrete level it is computationally more interesting to choose other fields (without physical meaning) thanks to other gauges, e.g. similar to the gauges presented in Section 2.6.4.2. The Section 3.2.4 presents a method to actually compute the discrete source field $\boldsymbol{h}_s$.

The last local quantity to be discretized is the source σ of the integral operator $\mathcal{P}(0, \sigma)$, which belongs to $W_p^0(\Gamma_e)$ (see Section C.4).

3.2.3.2 Global quantities

Each source magnetic field $\boldsymbol{h}_{s,i}$ is discretized exactly in the same way as the source field $\boldsymbol{h}_s$ (see Section 3.2.4), by considering the domain $\Omega_{s,i}$ instead of the full inductor domain Ω_s, and by considering the source current density $\boldsymbol{j}_{s,i}$ (whose magnetomotive force is equal to the number of turns N_i of the inductor) instead of $\boldsymbol{j}_s$.

In the case of foil windings, the continuous potential can be continuously extended in the foil region, which makes the explicit definition of multiple foil interfaces superfluous. The discrete space of the magnetic field adapted to such an extension in the foil region can only be characterized by variations of this potential along the height of the foils (i.e. along the direction $\mathbf{1}_\beta$, see Figure 3.1) as well as by the component along the foil thickness (i.e. along the direction $\mathbf{1}_\alpha$) of the curl-conforming vector basis functions. In this way, the cut global basis function $\boldsymbol{c}_i$ is also continuously extended, which turns the discrete sum (3.18) into a continuous variation. It is unfortunately impossible to explicitly build a basis for such a space on an arbitrary unstructured mesh $\mathcal{M}(\Omega_{f,i})$ of the foil region, and the orthogonality condition has to be imposed in a weak sense. For example, in the case of first order elements, the magnetic field in $\Omega_{f,i}$ can be expressed by

$$\boldsymbol{h} = \sum_{e \in \mathcal{E}(\Omega_{f,i})} h_e (s_1^{1,e} \cdot \mathbf{1}_\alpha)\mathbf{1}_\alpha + \sum_{n \in \mathcal{N}(\Omega_{f,i})} \phi_n (\mathbf{grad}\, s_1^{0,n} \cdot \mathbf{1}_\beta)\mathbf{1}_\beta + I_i (\boldsymbol{c}_i \cdot \mathbf{1}_\beta)\mathbf{1}_\beta, \quad (3.38)$$

to which the following equations have to be added to express that the curl-conforming field $\boldsymbol{h}^e = \sum_{e \in \mathcal{E}(\Omega_{f,i})} h_e s_1^{1,e}$ in the direction $\mathbf{1}_\beta$ is the gradient of the scalar potential ϕ in this direction:

$$(\boldsymbol{h}^e \cdot \mathbf{1}_\beta, s_1^{1,e} \cdot \mathbf{1}_\beta)_{\Omega_{f,i}} - (\mathbf{grad}\, \phi \cdot \mathbf{1}_\beta, s_1^{1,e} \cdot \mathbf{1}_\beta)_{\Omega_{f,i}} = 0, \quad \forall e \in \mathcal{E}(\Omega_{f,i}). \quad (3.39)$$

3.2.4 Pre-computation of source magnetic fields

A discrete source magnetic field $\boldsymbol{h}_s$ verifying (1.22), i.e. $\mathbf{curl}\, \boldsymbol{h}_s = \boldsymbol{j}_s$ in Ω_s and $\mathbf{curl}\, \boldsymbol{h}_s = 0$ in Ω_s^{C}, belongs to the reduced nullspace of the **curl** operator $\mathcal{NS}_p^1(\Omega, \Omega_s^{\mathrm{C}})$ (see Section 2.6.4.1). It can thus be expressed by (2.70), with the inductor domain Ω_s playing the role of the conductor domain Ω_c and with $\boldsymbol{u} = \boldsymbol{h}_s$, $\boldsymbol{v} = \phi_s$, $\boldsymbol{v}_c = \phi_{s,c}$, $\boldsymbol{v}_l = \phi_{s,l}$ and $\boldsymbol{v}_d = 0$. The potential ϕ_s is a source scalar potential defined in Ω_s^{C}. The support of the source field $\boldsymbol{h}_s$ is thus limited to the inductor Ω_s and to a transition layer associated with the cuts making the complement of the inductor domain topologically simple. Note that the way in which this source field is defined ($\boldsymbol{h}_s$ is equal to zero almost everywhere in non-conducting regions) leads to an elegant manner to reduce the cancellation error in magnetic materials [216]. Indeed, this implicitly defines a total magnetic scalar potential in a formulation that uses a reduced magnetic scalar potential ϕ.

Since $\boldsymbol{j}_s$ must be divergence-free, the source magnetic field $\boldsymbol{h}_s$ also belongs to the reduced orthogonal complement $\mathcal{S}_p^1(\Omega, \Omega_s^{\mathrm{C}})$ to the nullspace of the **curl** operator (see Section 2.6.4.2). It should thus be expressed thanks to (2.75), with $\boldsymbol{u} = \boldsymbol{u}_c = \boldsymbol{h}_s$ and $\boldsymbol{u}_d = 0$. For first order elements, the actual expression of the source field $\boldsymbol{h}_s$ is

thus obtained by restricting the set of edges considered in (2.70) to the edges of a co-tree built in the inductor Ω_s.

Two methods are proposed to actually determine the coefficients of the basis functions of $H_s = \mathcal{NS}^1_p(\Omega, \Omega_s^{\mathrm{C}}) \cap \mathcal{S}^1_p(\Omega, \Omega_s^{\mathrm{C}})$:

1. one method consists in solving an electrokinetic problem with a tensorial conductivity having a principal value along the wires of the inductor, i.e.

$$(\sigma^{-1}\mathbf{curl}\, \boldsymbol{h}_s, \mathbf{curl}\, \boldsymbol{h}'_s)_{\Omega_s} = 0, \quad \forall \boldsymbol{h}'_s \in H_s; \tag{3.40}$$

2. the other one consists in computing $\boldsymbol{h}_s$ through a projection method of a known distribution $\boldsymbol{j}_s$ [86], i.e.

$$(\mathbf{curl}\, \boldsymbol{h}_s, \mathbf{curl}\, \boldsymbol{h}'_s)_{\Omega_s} = (\boldsymbol{j}_s, \mathbf{curl}\, \boldsymbol{h}'_s)_{\Omega_s}, \quad \forall \boldsymbol{h}'_s \in H_s. \tag{3.41}$$

   This approach can also be applied if the source current density $\boldsymbol{j}_s$ is not analytically given, but results from a previous computation [195].

In both cases, the coefficient of the cut basis function is directly given by the magnetomotive force of the fixed current. The degrees of freedom can be fixed to zero on the lateral boundary of the inductor, which implies that the tree of edges has to be complete on this boundary before entering the volume (see Section 2.6.4.2). Both methods are much simpler than the classical inspection procedure (described e.g. in [55]) and far more general (holding for spaces of any order). Of course, when the inspection method is applicable, the cost to solve the linear system resulting from (3.40) or (3.41) must be carefully evaluated.

3.3 Magnetic flux density conforming formulations

3.3.1 Magnetodynamics

3.3.1.1 Generalities

Let us start, as in Section 3.2, from the magnetodynamic problem defined in Section 1.4.2. We want to solve (1.50) together with the constitutive relations (1.8) and (1.12). We start by writing a weak form of Ampère's law (1.50b):

$$(\boldsymbol{h}, \mathbf{curl}\, \boldsymbol{a}')_\Omega + \langle \boldsymbol{n} \times \boldsymbol{h}, \boldsymbol{a}' \rangle_{\Gamma_h} = (\boldsymbol{j}, \boldsymbol{a}')_\Omega, \quad \forall \boldsymbol{a}' \in \boldsymbol{H}^0_e(\mathbf{curl}; \Omega), \tag{3.42}$$

where the field $\boldsymbol{a}'$ is a field of test functions independent of time.

In order to satisfy in a strong sense the lower part of the Tonti diagram (1.55) (i.e. Faraday's and Gauss's law), we first introduce the magnetic and electric constitutive relations (1.8) and (1.12) in the weak form (3.42) to get

$$\begin{aligned}(\mu^{-1}\boldsymbol{b}, \mathbf{curl}\, \boldsymbol{a}')_\Omega + \langle \boldsymbol{n} \times \boldsymbol{h}, \boldsymbol{a}' \rangle_{\Gamma_h} = (\sigma \boldsymbol{e}, \boldsymbol{a}')_{\Omega_c} + (\boldsymbol{j}_s, \boldsymbol{a}')_{\Omega_s}, \\ \forall \boldsymbol{a}' \in \boldsymbol{H}^0_e(\mathbf{curl}; \Omega).\end{aligned} \tag{3.43}$$

We then define the magnetic vector potential $\boldsymbol{a}$ and the electric scalar potential v such that (1.53) and (1.54) hold, i.e. such that $\boldsymbol{b} = \mathbf{curl}\,\boldsymbol{a}$ and $\boldsymbol{e} = -\partial_t \boldsymbol{a} - \mathbf{grad}\, v$. Introducing these two definitions in (3.43), we get

$$(\mu^{-1}\mathbf{curl}\,\boldsymbol{a}, \mathbf{curl}\,\boldsymbol{a}')_\Omega + (\sigma\,\partial_t \boldsymbol{a}, \boldsymbol{a}')_{\Omega_c} + (\sigma\,\mathbf{grad}\, v, \boldsymbol{a}')_{\Omega_c} + \langle \boldsymbol{n}\times\boldsymbol{h}, \boldsymbol{a}'\rangle_{\Gamma_h} = (\boldsymbol{j}_s, \boldsymbol{a}')_{\Omega_s}, \quad \forall \boldsymbol{a}' \in \boldsymbol{H}^0_e(\mathbf{curl};\Omega). \tag{3.44}$$

The vector potential $\boldsymbol{a}$ is uniquely defined in the conducting regions only: we thus have to impose a gauge condition (see Section 3.3.3) everywhere else. The trace of the magnetic field $\boldsymbol{n}\times\boldsymbol{h}$ is subject to a natural boundary condition on the boundaries Γ_h of the domain Ω (or, more precisely, of the domain obtained after the abstraction of the thin regions). This condition can take various forms:

1. the trace of the magnetic field can be locally specified. In particular, this is the case for a homogeneous Neumann boundary condition e.g. imposing a symmetry condition of "zero crossing current" ($\boldsymbol{n}\times\boldsymbol{h}\big|_{\Gamma_h} = 0 \Rightarrow \boldsymbol{n}\cdot\mathbf{curl}\,\boldsymbol{h}\big|_{\Gamma_e} = 0 \Rightarrow \boldsymbol{n}\cdot\boldsymbol{j}\big|_{\Gamma_e} = 0$) or taking a perfect magnetic wall (of infinite magnetic permeability) into account;

2. the trace of the magnetic field can appear in local implicit boundary conditions, such as the conditions established for the treatment of thin structures. This is developed in Section 3.3.1.2;

3. the trace can be a field for which only associated global quantities are known (i.e. functional of $\boldsymbol{n}\times\boldsymbol{h}$). This is developed in Sections 3.3.1.3 and 3.3.1.4 for the treatment of massive, stranded and foil winding inductors;

4. the traces can appear in the definition of an integral operator. In that case they constitute local unknowns of the problem. This is developed in Section 3.3.1.5.

One should also note that the electric scalar potential v is only defined in the conducting regions Ω_c. The weak formulation (3.43) implies, by taking $\boldsymbol{a}' = \mathbf{grad}\, v'$ as a test function, that

$$(\sigma\,\partial_t \boldsymbol{a}, \mathbf{grad}\, v')_{\Omega_c} + (\sigma\,\mathbf{grad}\, v, \mathbf{grad}\, v')_{\Omega_c} = \langle \boldsymbol{n}\cdot\boldsymbol{j}, v'\rangle_{\Gamma_g}, \quad \forall v' \in H^{10}_e(\Omega_c), \tag{3.45}$$

where Γ_g is the part of the boundary of Ω_c which is crossed by a current (Γ_g is the union of all the surfaces $\Gamma_{g,i}$ resulting from the abstraction of the generators $\Omega_{g,i}$: see Section 1.2.2.4). In fact, the formulation (3.45) is the weak form of $\operatorname{div}\boldsymbol{j} = 0$ in Ω_c as well.

3.3.1.2 Thin conducting and magnetic structures

Across conducting and/or magnetic thin structures, the tangential electric field is discontinuous (see Section 1.2.2.1). We thus decompose $\boldsymbol{a}$ as

$$\boldsymbol{a} = \boldsymbol{a}_c + \boldsymbol{a}_d, \tag{3.46}$$

where the tangential components $\boldsymbol{a}_{c,t}$ and $\boldsymbol{a}_{d,t}$ of $\boldsymbol{a}_c$ and $\boldsymbol{a}_d$ are continuous and discontinuous across Ω_t respectively. To simplify further developments, we assume without any loss of generality that the discontinuous part $\boldsymbol{a}_d$ is equal to zero on the side Γ_t^- of the thin structure. Performing the cross product of $\boldsymbol{n}_t$ by (1.21) and developing (1.20), we get, assuming zero initial conditions on $\boldsymbol{a}$:

$$\boldsymbol{n}_t \times \boldsymbol{h}\,\big|_{\Gamma_t^+} + \boldsymbol{n}_t \times \boldsymbol{h}\,\big|_{\Gamma_t^-} = -(\mu\beta)^{-1}\,\boldsymbol{a}_{d,t}\,, \tag{3.47}$$

$$\boldsymbol{n}_t \times \boldsymbol{h}\,\big|_{\Gamma_t^+} - \boldsymbol{n}_t \times \boldsymbol{h}\,\big|_{\Gamma_t^-} = -\sigma\beta\,\partial_t(2\boldsymbol{a}_{c,t} + \boldsymbol{a}_{d,t}), \tag{3.48}$$

which can be solved for $\boldsymbol{n}_t \times \boldsymbol{h}\,\big|_{\Gamma_t^+}$ and $\boldsymbol{n}_t \times \boldsymbol{h}\,\big|_{\Gamma_t^-}$ to give

$$\boldsymbol{n}_t \times \boldsymbol{h}\,\big|_{\Gamma_t^+} = \frac{1}{2}\big[-\sigma\beta\,\partial_t(2\boldsymbol{a}_{c,t} + \boldsymbol{a}_{d,t}) - \frac{1}{\mu\beta}\,\boldsymbol{a}_{d,t}\big], \tag{3.49}$$

$$\boldsymbol{n}_t \times \boldsymbol{h}\,\big|_{\Gamma_t^-} = \frac{1}{2}\big[\sigma\beta\,\partial_t(2\boldsymbol{a}_{c,t} + \boldsymbol{a}_{d,t}) - \frac{1}{\mu\beta}\,\boldsymbol{a}_{d,t}\big]. \tag{3.50}$$

Reducing Ω_t to Γ_t in the same way as for the $\boldsymbol{h}$-conforming formulation (see Section 3.2.1.2), the surface term in (3.44) successively becomes

$$\begin{aligned}\langle \boldsymbol{n}\times\boldsymbol{h}, \boldsymbol{a}'\rangle_{\Gamma_t^+\cup\Gamma_t^-\cup\Gamma_t^=} &= -\langle \boldsymbol{n}_t\times\boldsymbol{h}, \boldsymbol{a}'\rangle_{\Gamma_t^+} + \langle \boldsymbol{n}_t\times\boldsymbol{h}, \boldsymbol{a}'\rangle_{\Gamma_t^-}\\ &= -\langle \frac{1}{2}\big[-\sigma\beta\,\partial_t(2\boldsymbol{a}_{c,t}+\boldsymbol{a}_{d,t}) - \frac{1}{\mu\beta}\,\boldsymbol{a}_{d,t}\big], \boldsymbol{a}'_c + \boldsymbol{a}'_d\rangle_{\Gamma_t}\\ &\quad + \langle \frac{1}{2}\big[\sigma\beta\,\partial_t(2\boldsymbol{a}_{c,t}+\boldsymbol{a}_{d,t}) - \frac{1}{\mu\beta}\,\boldsymbol{a}_{d,t}\big], \boldsymbol{a}'_c\rangle_{\Gamma_t}.\end{aligned} \tag{3.51}$$

The magnetic flux density conforming magnetodynamic formulation (3.44) then becomes

$$\begin{aligned}&(\mu^{-1}\mathbf{curl}\,\boldsymbol{a}, \mathbf{curl}\,\boldsymbol{a}')_\Omega + (\sigma\,\partial_t\boldsymbol{a}, \boldsymbol{a}')_{\Omega_c} + (\sigma\,\mathbf{grad}\,v, \boldsymbol{a}')_{\Omega_c} + \langle \boldsymbol{n}\times\boldsymbol{h}, \boldsymbol{a}'\rangle_{\Gamma_h-\Gamma_t}\\ &\quad +2\langle\sigma\beta\,\partial_t\boldsymbol{a}_{c,t}, \boldsymbol{a}'_c\rangle_{\Gamma_t} + \langle\sigma\beta\,\partial_t\boldsymbol{a}_{d,t}, \boldsymbol{a}'_c\rangle_{\Gamma_t} + \langle\sigma\beta\,\partial_t\boldsymbol{a}_{c,t}, \boldsymbol{a}'_d\rangle_{\Gamma_t}\\ &\quad +\frac{1}{2}\langle\sigma\beta\,\partial_t\boldsymbol{a}_{d,t}, \boldsymbol{a}'_d\rangle_{\Gamma_t} + \frac{1}{2}\langle\frac{1}{\mu\beta}\boldsymbol{a}_{d,t}, \boldsymbol{a}'_d\rangle_{\Gamma_t} = (\boldsymbol{j}_s, \boldsymbol{a}')_{\Omega_s},\\ &\qquad \forall \boldsymbol{a}' \in \boldsymbol{H}^0_e(\mathbf{curl};\Omega).\end{aligned} \tag{3.52}$$

3.3.1.3 Voltages as strong global quantities

The $\boldsymbol{b}$-conforming formulation does not need a source field in the same sense as the $\boldsymbol{h}$-conforming formulation. Nevertheless, a similar approach can be considered to define another kind of source field which will be used to produce circuit relations.

Voltage driven massive inductors can be considered through a unit source electric scalar potential $v_{s,i}$ associated with a unit voltage for each inductor $\Omega_{m,i}$, and leading to

$$v = \sum_i V_i v_{s,i}, \tag{3.53}$$

where V_i is the voltage drop between the electrodes $\Gamma_{g,i}^+$ and $\Gamma_{g,i}^-$ of the ith massive inductor $\Omega_{g,i}$ (see Section 1.2.2.3). The volume part of the formulation (3.44) then becomes

$$(\mu^{-1}\mathbf{curl}\,\boldsymbol{a},\mathbf{curl}\,\boldsymbol{a}')_\Omega + (\sigma\,\partial_t\boldsymbol{a},\boldsymbol{a}')_{\Omega_c} + \sum_i V_i(\sigma\,\mathbf{grad}\,v_{s,i},\boldsymbol{a}')_{\Omega_{m,i}} = (\boldsymbol{j}_s,\boldsymbol{a}')_{\Omega_s},$$
$$\forall \boldsymbol{a}' \in \boldsymbol{H}_e^0(\mathbf{curl};\Omega). \tag{3.54}$$

The voltage associated with a massive inductor then explicitly appears in the equations as a global quantity defined in a strong sense, e.g. as an essential global constraint when prescribed. Formulation (3.54) is a generalization of the modified vector potential formulation given in [63, 12]. These formulations do not need any gauge condition in the conducting regions Ω_c nor on its boundary (since $\operatorname{div}\boldsymbol{j} = 0$ implies $\partial_t \operatorname{div}\sigma\boldsymbol{a} = 0$). The pre-computation of the source scalar potential $v_{s,i}$ can be done by using the electrokinetic formulation

$$(\sigma\,\mathbf{grad}\,v_{s,i},\mathbf{grad}\,v')_{\Omega_{m,i}} = 0, \quad \forall v' \in H_e^{10}(\Omega_{m,i}), \tag{3.55}$$

defined in each massive inductor and with appropriate boundary conditions, in particular $v_{s,i}$ equal to 0 and 1 on its two respective electrodes. Note that (3.55) is a part of (3.45). While the potential $v_{s,i}$ as defined in (3.55) has a clear physical meaning, it can nevertheless be calculated in a more efficient and direct way if it is defined as a kind of generalized source potential, lacking such a meaning: it is sufficient that $v_{s,i}$ is equal to 1 on one electrode, to 0 on the other one and varies continuously in $\Omega_{m,i}$ (which gives the electric field needed in the electromotive force region $\Omega_{g,i}$). The construction of such a generalized source field is made at the discrete level by reducing its support to a transition layer connected to $\Gamma_{g,i}$. It is interesting to notice that the decomposition of the problem into the pre-computation of a source scalar potential and the actual computation of the vector potential is precisely what is done in two-dimensional problems, where the electrokinetic problem (3.55) has a trivial solution: $\mathbf{grad}\,v$ is constant in each conductor and is equal to $V_i\mathbf{1}_z$ [146].

The treatment of foil winding inductors is based on the treatment of massive inductors, with the aim of considering the actual distribution of the current in the foils, while avoiding modeling each foil separately. For this purpose, a continuum will be defined for the foil voltage (see the next section).

The treatment of stranded inductors is somewhat different. What is actually known in the case of a stranded inductor is a current density distribution, and it is not possible to have a priori information available about one kind of unit voltage. This points out a loss of a part of the duality between $\boldsymbol{h}$- and $\boldsymbol{b}$-conforming formulations: the current will be rather a strong quantity for stranded inductors, through $\boldsymbol{j}_s$ in (3.44).

3.3.1.4 Currents as weak global quantities and circuit relations

With the $\boldsymbol{b}$-conforming formulation, the total current flowing in a conductor can only be expressed in a weak sense, e.g. as a natural global constraint, because it

comes from Ampère's law which is itself expressed in a weak form. The current I_i through the section $\Gamma_{g,i}$ of an inductor can be obtained from (3.45) with v' equal to the source scalar potential $v_{s,i}$. Indeed, with $v' = v_{s,i}$, the surface integral term in (3.45) written for the ith inductor $\Omega_{m,i}$ gives

$$\langle \boldsymbol{n} \cdot \boldsymbol{j}, v_{s,i} \rangle_{\Gamma_{g,i}} = \langle \boldsymbol{n} \cdot \boldsymbol{j}, 1 \rangle_{\Gamma_{g,i}} = I_i, \tag{3.56}$$

and thus (3.45) becomes

$$(\sigma\, \partial_t \boldsymbol{a}, \mathbf{grad}\, v_{s,i})_{\Omega_{m,i}} + (\sigma\, \mathbf{grad}\, v, \mathbf{grad}\, v_{s,i})_{\Omega_{m,i}} = I_i, \tag{3.57}$$

or, with $v = V_i v_{s,i}$,

$$(\sigma\, \partial_t \boldsymbol{a}, \mathbf{grad}\, v_{s,i})_{\Omega_{m,i}} + V_i (\sigma\, \mathbf{grad}\, v_{s,i}, \mathbf{grad}\, v_{s,i})_{\Omega_{m,i}} = I_i. \tag{3.58}$$

Equation (3.58) is the circuit relation associated with the inductor $\Omega_{m,i}$, i.e. a relation between its voltage V_i and its current I_i. One should note that the global current is obtained from a volume integration and not from a surface integration of $\boldsymbol{n}\cdot\boldsymbol{j} = \boldsymbol{n}\cdot\sigma\boldsymbol{e}$ on the section of the inductor, which would depend on the choice of the integration surface [20].

The treatment of foil windings is based on the same principle, with the exception that we want to build a continuum for the foil voltage, with the aim of making the definition of all the foils superfluous. Three principal directions are defined in the winding, namely $\mathbf{1}_\alpha$, $\mathbf{1}_\beta$ and $\mathbf{1}_\gamma$, being the directions perpendicular to the foils, along their height and their length respectively. Coordinates α, β and γ are associated with these directions (see Figure 1.5). The winding has N_i turns ("foils") and its total thickness is L_i. Let us apply (3.58) to a given foil of the winding, the middle of which is located at position α. If we make the hypothesis that the vector potential $\boldsymbol{a}$ does not vary along the thickness of the foil, the volume integral can be replaced by a surface integral over the mean surface $\Gamma^\alpha_{f,i}$ of the foil (i.e. the surface described by β and γ for α fixed), leading to the following circuit relation:

$$\frac{L_i}{N_i} \langle \sigma\, \partial_t \boldsymbol{a}, \mathbf{grad}\, v_{s,i} \rangle_{\Gamma^\alpha_{f,i}} + V_i^\alpha \frac{L_i}{N_i} \langle \sigma\, \mathbf{grad}\, v_{s,i}, \mathbf{grad}\, v_{s,i} \rangle_{\Gamma^\alpha_{f,i}} = I_i, \tag{3.59}$$

where V_i^α is the voltage associated with the foil. It is important to note that $\mathbf{grad}\, v_{s,i}$ does not depend on the actual foil being considered. In order to weakly satisfy (3.59) for all the elementary foils, V_i^α is extended to a continuum, i.e. $V_i(\alpha)$, for all the foils and a projection equation is expressed:

$$\begin{aligned} \frac{L_i}{N_i} (\sigma\, \partial_t \boldsymbol{a}, V_i'(\alpha) \mathbf{grad}\, v_{s,i})_{\Omega_{f,i}} + V_i(\alpha) \frac{L_i}{N_i} (\sigma\, \mathbf{grad}\, v_{s,i}, V_i'(\alpha) \mathbf{grad}\, v_{s,i})_{\Omega_{f,i}} \\ = I_i \int_\alpha V_i'(\alpha)\, d\alpha, \quad \forall V_i'(\alpha) \in \mathbb{R}([0, L_i]). \end{aligned} \tag{3.60}$$

The test function for the foil winding circuit relation appears as being $V_i'(\alpha)\mathbf{grad}\, v_{s,i}$, while it was $\mathbf{grad}\, v_{s,i}$ for a single conductor. This formulation generalizes the method

presented in [76] in both two and three dimensions. The total voltage of the foil winding can be determined from $V_i(\alpha)$, i.e.

$$V_i = \frac{N_i}{L_i} \int_\alpha V_i(\alpha)\, d\alpha. \tag{3.61}$$

Note that a strong constraint fixing a constant current in each elementary foil can only be obtained with a $\boldsymbol{h}$-conforming formulation. In case the support of the source scalar potential $v_{s,i}$ is limited to a subset of $\Omega_{f,i}$ (e.g. a transition layer connected to $\Gamma_{g,i}$, see Section 3.3.3.2), it is necessary to define an anisotropic tensor value for the conductivity σ in (3.60), with a zero value in direction $\mathbf{1}_\alpha$. In this way, (3.60) weakly fixes the current in each elementary foil in the support of $v_{s,i}$, while the anisotropic conductivity prevents the current from penetrating the foil interfaces in the whole inductor.

For a stranded inductor, the circuit relation cannot be issued from (3.58). Indeed, to enable this, the gradient of the source scalar potential $v_{s,i}$ should be the electric field in the stranded inductor $\Omega_{s,i}$ associated with a unit voltage. Nevertheless it is generally impossible to determine a priori such an electric field because the distribution of the voltage in the wires is precisely a part of the solution of the magnetodynamic problem. This reveals the impossibility of directly controlling the function space of the current density in the case of the $\boldsymbol{b}$-conforming formulation. One should rather consider the circuit relation obtained from the $\boldsymbol{h}$-conforming formulation, and express it in terms of the vector potential [60]. And so the first term of (3.23) is integrated by parts to get

$$\partial_t(\mu \boldsymbol{h}, \boldsymbol{h}_{s,i})_\Omega = \partial_t(\mathbf{curl}\, \boldsymbol{a}, \boldsymbol{h}_{s,i})_\Omega = \partial_t(\boldsymbol{a}, \mathbf{curl}\, \boldsymbol{h}_{s,i})_\Omega + \partial_t \langle \boldsymbol{n} \times \boldsymbol{a}, \boldsymbol{h}_{s,i} \rangle_{\partial\Omega}. \tag{3.62}$$

If the surface integral vanishes (which is usually the case), (3.62) becomes

$$\partial_t(\mu \boldsymbol{h}, \boldsymbol{h}_{s,i})_\Omega = \partial_t(\boldsymbol{a}, \boldsymbol{j}_{s,i})_\Omega = \partial_t(\boldsymbol{a}, \boldsymbol{j}_{s,i})_{\Omega_{s,i}}, \tag{3.63}$$

where the integration support has been reduced to the inductor (this is not the case with the magnetic field conforming formulation where the entire domain has to be considered). Consequently, (3.23) becomes

$$\partial_t(\boldsymbol{a}, \boldsymbol{j}_{s,i})_{\Omega_{s,i}} + I_i(\sigma^{-1} \boldsymbol{j}_{s,i}, \boldsymbol{j}_{s,i})_{\Omega_{s,i}} = -V_i, \tag{3.64}$$

which is the circuit relation associated with the $\boldsymbol{b}$-conforming formulation, i.e. in which a direct control of the current is possible. This relation is actually the summation of elementary relations of the same kind for all the turns of the winding (this sum would not have been possible with (3.58)). Different expressions of the unit current density $\boldsymbol{j}_{s,i}$ can be considered, which lead to different approximations of the winding distribution. The commonly used form for $\boldsymbol{j}_{s,i}$ is

$$\boldsymbol{j}_{s,i} = \frac{N_i}{S_i} \boldsymbol{t}_i = \boldsymbol{w}_i, \tag{3.65}$$

where $\boldsymbol{t}_i$ is a unit vector tangent to the winding direction, S_i is the surface area of the inductor and $\boldsymbol{w}_i$ is called the wire density vector. With such a form, (3.64) comes down to the classically used circuit relation [142, 94]:

$$\partial_t(\boldsymbol{a}, \boldsymbol{w}_i)_{\Omega_{s,i}} + R_i I_i = -V_i, \tag{3.66}$$

where R_i is the resistance of the inductor. The distribution of $\boldsymbol{j}_{s,i}$ can also be calculated thanks to a source scalar or vector electric potential [60]:

1. $\boldsymbol{j}_{s,i}$ can be calculated as the gradient of the source scalar potential $-\sigma\mathbf{grad}\, v^0$ obtained from the resolution of an electrokinetic problem with a tensorial conductivity:

$$(\sigma\mathbf{grad}\, v^0, \mathbf{grad}\, v')_{\Omega_{s,i}} = \langle \boldsymbol{n} \cdot \boldsymbol{j}_{s,i}, v' \rangle_{\Gamma_{g,i}}, \quad \forall v' \in H_e^{10}(\Omega_{s,i}). \tag{3.67}$$

   The sources for this problem are the uniform current densities (equal to N_i/S_i) on the boundaries $\Gamma_{g,i}$ that are crossed by a current. Note that only the surface areas of the input and output boundaries have to be known. Another way to obtain a similar form for $\boldsymbol{j}_{s,i}$ is to use a projection method [86] of a known distribution $\boldsymbol{j}^0$:

$$(\sigma\mathbf{grad}\, v^0, \mathbf{grad}\, v')_{\Omega_{s,i}} = (-\boldsymbol{j}^0, \mathbf{grad}\, v')_{\Omega_{s,i}}, \quad \forall v' \in H_e^{10}(\Omega_{s,i}). \tag{3.68}$$

   Note that the generalized potential used in the case of massive inductors, as well as a potential obtained using a scalar conductivity, would not be appropriate for a correct consideration of stranded inductors: the winding can only be correctly taken into account through the physical electric potential v^0;

2. $\boldsymbol{j}_{s,i}$ can be calculated as the curl of an electric vector potential having the same definition as the source magnetic field used in the $\boldsymbol{h}$-conforming formulation, i.e. obtained by solving (3.40) or (3.41). Such a potential can be used to enable a good convergence of a non-gauged resolution [183].

The choice of a particular method should not have a significant influence on the distribution of the magnetic flux density in the main parts of the system. Nevertheless, they could influence the expression of the flux linked to the windings, because such expressions precisely make use of $\boldsymbol{b}$ (through $\boldsymbol{a}$) in these windings. It is interesting to remark that the method developed above for foil windings could also be applied to stranded inductors, with the wires taken as the elementary regions. An advantage in three-dimensional problems could be the reduction of the number of non-zero entries in the algebraic system of equations due to the circuit relation in comparison with the method presented here.

3.3.1.5 Integral operators

For open boundary problems, the surface term $\langle \boldsymbol{n} \times \boldsymbol{h}, \boldsymbol{a}' \rangle_{\Gamma_h}$ in (3.44) is not fixed a priori and constitutes an unknown of the problem. Using the exterior hybrid

approach presented in Appendix C, we introduce a boundary operator relating the trace of the magnetic field on the boundary Γ_h and the magnetic vector potential $\boldsymbol{a}$ in the exterior domain $\mathbb{E}^3 - \Omega$, which leads in a natural way to a classical magnetic flux density hybrid finite element and boundary element method [186, 191, 192].

In the presence of a source current $\boldsymbol{j}_e$ in the exterior inductor domain Ω_e, the magnetic flux density in $\mathbb{E}^3 - \Omega$ can be decomposed as

$$\boldsymbol{b} = \boldsymbol{b}_e + \boldsymbol{b}_r = \boldsymbol{b}_e + \mathbf{curl}\, \boldsymbol{a}, \tag{3.69}$$

where $\boldsymbol{b}_e$ is a source magnetic flux density due to the source current (determined by the Biot-Savart law) and $\boldsymbol{b}_r$ is a reduced magnetic flux density deriving from the magnetic vector potential $\boldsymbol{a}$.

Let us define the integral operator $\boldsymbol{\mathcal{A}}^e(0, \boldsymbol{\sigma})$ as

$$\boldsymbol{\mathcal{A}}^e(0, \boldsymbol{\sigma}) = \boldsymbol{x} \mapsto \frac{1}{4\pi} \int_{\Gamma_h} \frac{\boldsymbol{\sigma}(\boldsymbol{y})}{|\boldsymbol{x} - \boldsymbol{y}|}\, d\boldsymbol{y}. \tag{3.70}$$

Its normal derivative at a point $\boldsymbol{x}$ on Γ_h is given by the Fredholm integral of the second kind:

$$\boldsymbol{n} \times \mathbf{curl}\, \boldsymbol{\mathcal{A}}^e(0, \boldsymbol{\sigma}) = \boldsymbol{x} \mapsto \frac{1}{2}\boldsymbol{\sigma}(\boldsymbol{x}) + \frac{1}{4\pi} \int_{\Gamma_h} \frac{\boldsymbol{n}(\boldsymbol{x}) \times ((\boldsymbol{y} - \boldsymbol{x}) \times \boldsymbol{\sigma}(\boldsymbol{y}))}{|\boldsymbol{x} - \boldsymbol{y}|^3}\, d\boldsymbol{y}. \tag{3.71}$$

Thanks to the properties of $\boldsymbol{\mathcal{A}}^e(0, \boldsymbol{\sigma})$, at any point $\boldsymbol{x}$ in the exterior domain $\mathbb{E}^3 - \Omega$, the vector potential can then be expressed as

$$\boldsymbol{a}(\boldsymbol{x}) = \mu\, \boldsymbol{\mathcal{A}}^e(0, \boldsymbol{\sigma}), \tag{3.72}$$

and its derivative at a point $\boldsymbol{x}$ on Γ_h can be expressed as

$$\boldsymbol{n} \times \mathbf{curl}\, \boldsymbol{a}(\boldsymbol{x}) = \mu\, \boldsymbol{n} \times \mathbf{curl}\, \boldsymbol{\mathcal{A}}^e(0, \boldsymbol{\sigma}). \tag{3.73}$$

It is interesting to note that the sources $\boldsymbol{\sigma}$ of the integral operator can, in this case, be interpreted as virtual magnetization currents. The goal of the hybrid formulation is then to establish a relation between $\boldsymbol{n} \times \boldsymbol{h}$ and $\boldsymbol{a}$ on Γ_h, which can be obtained in various ways depending on the scheme chosen to discretize (3.72)–(3.73). Following the strategy presented in Appendix C for the discretization of the sources $\boldsymbol{\sigma}$, the variational formulation becomes: find $\boldsymbol{\sigma} \in \boldsymbol{H}_e^0(\mathrm{div}; \Gamma_h)$ and $\boldsymbol{a} \in \boldsymbol{H}_e^0(\mathbf{curl}; \Gamma_h)$ such that

$$\langle \boldsymbol{a}, \boldsymbol{\sigma}' \rangle_{\Gamma_h} = \langle \mu \boldsymbol{\mathcal{A}}^e(0, \boldsymbol{\sigma}), \boldsymbol{\sigma}' \rangle_{\Gamma_h}, \quad \forall \boldsymbol{\sigma}' \in \boldsymbol{H}_e^0(\mathrm{div}; \Gamma_h), \tag{3.74}$$

and

$$\langle \boldsymbol{n} \times \boldsymbol{h}, \boldsymbol{a}' \rangle_{\Gamma_h} = \langle \boldsymbol{n} \times \mathbf{curl}\, \boldsymbol{\mathcal{A}}^e(0, \boldsymbol{\sigma}), \boldsymbol{a}' \rangle_{\Gamma_h} + \langle \mu^{-1} \boldsymbol{n} \times \boldsymbol{b}_e, \boldsymbol{a}' \rangle_{\Gamma_h}, \quad \forall \boldsymbol{a}' \in \boldsymbol{H}_e^0(\mathbf{curl}; \Gamma_h). \tag{3.75}$$

The generalized collocation technique can be applied in exactly the same way as in Section C.4.2. It is important to note that the source $\boldsymbol{\sigma}$ is not unique, and a gauge condition has to be applied (see Section 3.3.3).

3.3.2 Magnetostatics

Keeping in mind the developments that were made for the magnetodynamic problem in the previous section, we now consider the simplified case of magnetostatics, where all time dependent phenomena are neglected (see Section 1.4.1).

Let us start by writing a weak form of (1.44a), i.e.

$$(\boldsymbol{h}, \mathbf{curl}\, \boldsymbol{a}')_\Omega + \langle \boldsymbol{n} \times \boldsymbol{h}, \boldsymbol{a}' \rangle_{\Gamma_h} = (\boldsymbol{j}_s, \boldsymbol{a}')_{\Omega_s}, \quad \forall \boldsymbol{a}' \in \boldsymbol{H}^0_e(\mathbf{curl}; \Omega). \tag{3.76}$$

In order to satisfy in a strong sense the lower part of the Tonti diagram (1.49), we first introduce (1.12) into (3.76) to get

$$(\mu^{-1}\boldsymbol{b}, \mathbf{curl}\, \boldsymbol{a}')_\Omega + \langle \boldsymbol{n} \times \boldsymbol{h}, \boldsymbol{a}' \rangle_{\Gamma_h} = (\boldsymbol{j}_s, \boldsymbol{a}')_{\Omega_s}, \quad \forall \boldsymbol{a}' \in \boldsymbol{H}^0_e(\mathbf{curl}; \Omega). \tag{3.77}$$

Then, deriving $\boldsymbol{b} \in \boldsymbol{H}(\mathrm{div}; \Omega)$ from a vector potential $\boldsymbol{a}$ such that $\boldsymbol{b} = \mathbf{curl}\, \boldsymbol{a}$ everywhere in Ω, the weak form (3.77) can be written as

$$(\mu^{-1}\mathbf{curl}\, \boldsymbol{a}, \mathbf{curl}\, \boldsymbol{a}')_\Omega + \langle \boldsymbol{n} \times \boldsymbol{h}, \boldsymbol{a}' \rangle_{\Gamma_h} = (\boldsymbol{j}_s, \boldsymbol{a}')_{\Omega_s}, \quad \forall \boldsymbol{a}' \in \boldsymbol{H}^0_e(\mathbf{curl}; \Omega). \tag{3.78}$$

The treatment of thin magnetic structures is similar to the treatment of thin magnetic and conducting structures presented in Section 3.3.1.2. We first decompose the magnetic vector potential as in (3.46). Since in the static limit case (i.e. for $\beta = d/2$), (3.51) becomes

$$\langle \boldsymbol{n} \times \boldsymbol{h}, \boldsymbol{a}' \rangle_{\Gamma_t^+ \cup \Gamma_t^- \cup \Gamma_t^=} = \langle (\mu d)^{-1}\, \boldsymbol{a}_{d,t}, \boldsymbol{a}'_c + \boldsymbol{a}'_d \rangle_{\Gamma_t} - \langle (\mu d)^{-1}\, \boldsymbol{a}_{d,t}, \boldsymbol{a}'_c \rangle_{\Gamma_t}, \tag{3.79}$$

the weak form (3.78) can be rewritten as

$$(\mu^{-1}\mathbf{curl}\, \boldsymbol{a}, \mathbf{curl}\, \boldsymbol{a}')_\Omega + \langle \boldsymbol{n} \times \boldsymbol{h}, \boldsymbol{a}' \rangle_{\Gamma_h - \Gamma_t} + \langle (\mu d)^{-1} \boldsymbol{a}_{d,t}, \boldsymbol{a}'_d \rangle_{\Gamma_t} = (\boldsymbol{j}_s, \boldsymbol{a}')_{\Omega_s}. \tag{3.80}$$

The treatment of global electrical quantities as well as the introduction of integral operators for the treatment of unbounded domains is the same as what has been presented for the magnetodynamic formulation in Sections 3.3.1.3, 3.3.1.4 and 3.3.1.5. As in the magnetodynamic case, it is necessary to define a gauge condition in order to choose one representative of the magnetic vector potential $\boldsymbol{a}$ among the infinity of valid choices. The gauge condition will be introduced at the discrete level in the next section.

3.3.3 Discretization

3.3.3.1 Local quantities

The magnetic vector potential in the magnetic flux density conforming formulations established above is discretized by curl-conforming mixed finite elements. In the magnetodynamic formulation, the vector potential belongs to the reduced orthogonal complement to the nullspace of the **curl** operator ($\mathcal{S}^1_p(\Omega, \Omega^{\mathrm{C}}_c)$) defined in Section 2.6.4.2. Its discrete expression is thus given by (2.75), with $\boldsymbol{u} = \boldsymbol{a}$, $\boldsymbol{u}_c = \boldsymbol{a}_c$

and $\boldsymbol{u}_d = \boldsymbol{a}_d$. In the case of the magnetostatic formulation, the vector potential belongs to $\mathcal{S}_p^1(\Omega)$ and is given by (2.77), with $\boldsymbol{u} = \boldsymbol{a}$, $\boldsymbol{u}_c = \boldsymbol{a}_c$ and $\boldsymbol{u}_d = \boldsymbol{a}_d$.

The source $\boldsymbol{\sigma}$ of the integral operator $\boldsymbol{\mathcal{A}}(0, \boldsymbol{\sigma})$, which belongs to $W_p^2(\Gamma_h)$, is discretized by the trace of the curl-conforming finite elements presented in Chapter 2 (see Sections 2.3.5 and C.4). It should be gauged in the same way as the vector potential in order to generate a non-singular system matrix.

3.3.3.2 Global quantities

The generalized source potential $v_{s,i}$ is equal to 1 on one electrode ($\Gamma_{g,i}^+$), is equal to 0 on the other one ($\Gamma_{g,i}^-$) and varies continuously in $\Omega_{m,i}$. One possibility to construct a discrete field which fulfills these conditions is to reduce the support of $v_{s,i}$ to a transition layer $\text{supp}(v_{s,i})$ connected to the electrode (i.e. to the set of elements connected to the "+" side of the abstracted generator $\Gamma_{g,i}$), exactly in the same way as the discontinuity of the field across the cutting surfaces has been introduced in Section 2.6.4.1:

$$v_{s,i} = \sum_{n \in \mathcal{N}(\Gamma_{g,i})} g_n \quad \text{with} \quad g_n = \begin{cases} s_1^{0,n} & \text{in supp}(v_{s,i}) \\ 0 & \text{otherwise} \end{cases}. \tag{3.81}$$

The reduction of the support of $v_{s,i}$ to a transition layer permits to reduce the number of unknowns involved in the circuit relations (3.22), (3.23), (3.58), (3.60) and (3.64), allowing to reduce the number of non-zero entries of this equation in the system matrix.

In the case of foil windings, the voltage is extended to a continuum $V_i(\alpha)$ (see (3.60) and (3.61) in Section 3.3.1.4). At the discrete level, an approximation of $V_i(\alpha)$, being also used for $V_i'(\alpha)$, has to be defined. Such quantities are called spatially dependent global quantities [49], in contrast with the classical global quantities defined above. One-dimensional complete or piece-wise polynomial variations are examples of possible approximations, with the general interpolation form

$$V_i(\alpha) = \sum_{k=1}^{n} V_{i,k}\, s_k(\alpha). \tag{3.82}$$

On the one hand, complete polynomials in α permit a global interpolation. On the other hand, piece-wise polynomials enable a finite element approximation, with a possible non-uniform discretization of the one-dimensional α domain $\mathbb{R}([0, L_i])$. These approximations are totally independent of the mesh used for the computation of the local quantities (i.e. the vector potential $\boldsymbol{a}$). Compared to the approximation presented in [76] for the two-dimensional case, they do not need an additional regular volume mesh, which particularly facilitates three-dimensional treatments.

Chapter 4

Numerical Tests

4.1 Introduction

In this chapter we present a series of numerical tests undertaken to validate the theoretical developments presented in Chapters 2 and 3. These numerical tests should by no means be considered as practical applications: they are specifically chosen to highlight the originalities of this thesis, and should thus be simple enough for the different aspects of the developments to be examined separately. We consider that the real practical applications of this thesis are the two computer codes described in Appendix D, which have been extensively used for both collaborative research and "real life" engineering problems.

The first numerical test consists in the study of a spherical shell immersed in a spatially uniform magnetic field. The aim of this test is to validate the dual hybrid formulations as well as the thin shell approximation. The second numerical test is derived from an international test problem consisting in an inductor-core-shield system. In addition to the validation of the developments mentioned above in a topologically non-trivial domain, it permits to test the coupling between local and global quantities for the three considered kinds of inductors. It should be noted that all the dynamic cases have been solved in the frequency domain, using the complex formalism (see Section 1.1).

4.2 Hollow sphere

A hollow sphere (of radius $r = 50\,\text{mm}$ and thickness $d = 1\,\text{mm}$), magnetic or not, conducting or not, is immersed in a spatially uniform magnetic field, which may be time dependent (see Figure 4.1, with $b_e = 1\,\text{T}$). Only 1/16th of the structure is modeled[1]. Two families of finite element meshes are considered:

1. the meshes $\mathcal{M}_i^s$, $i = 1, \ldots, 5$, form a sequence of quasi-uniform structured meshes (consisting of hexahedra and prisms) of the domain Ω before abstrac-

[1] One could of course, in a much more efficient way, take the axisymmetry of the problem into account using appropriate two-dimensional formulations, but that is not our goal here.

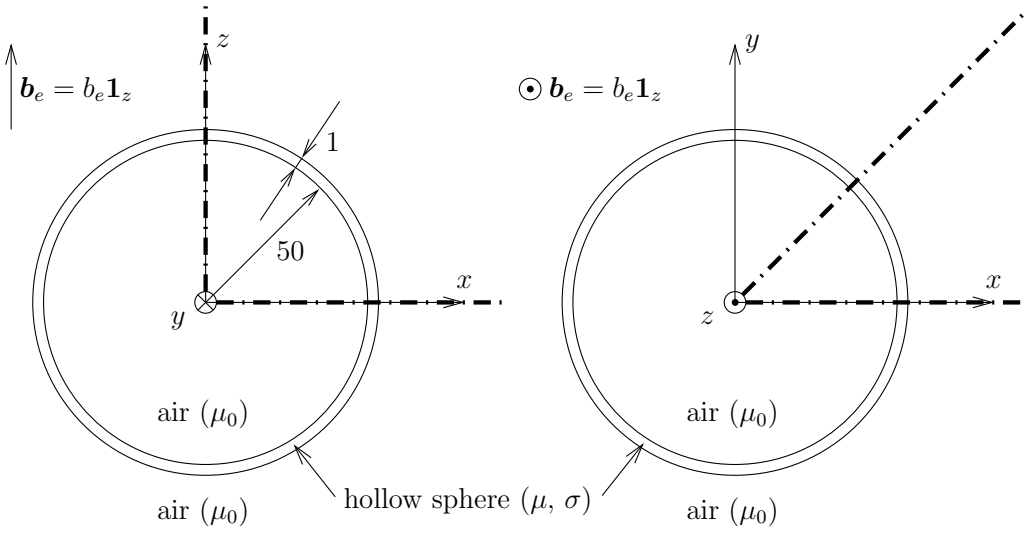

Figure 4.1: Geometry of the hollow sphere problem. All dimensions are in mm.

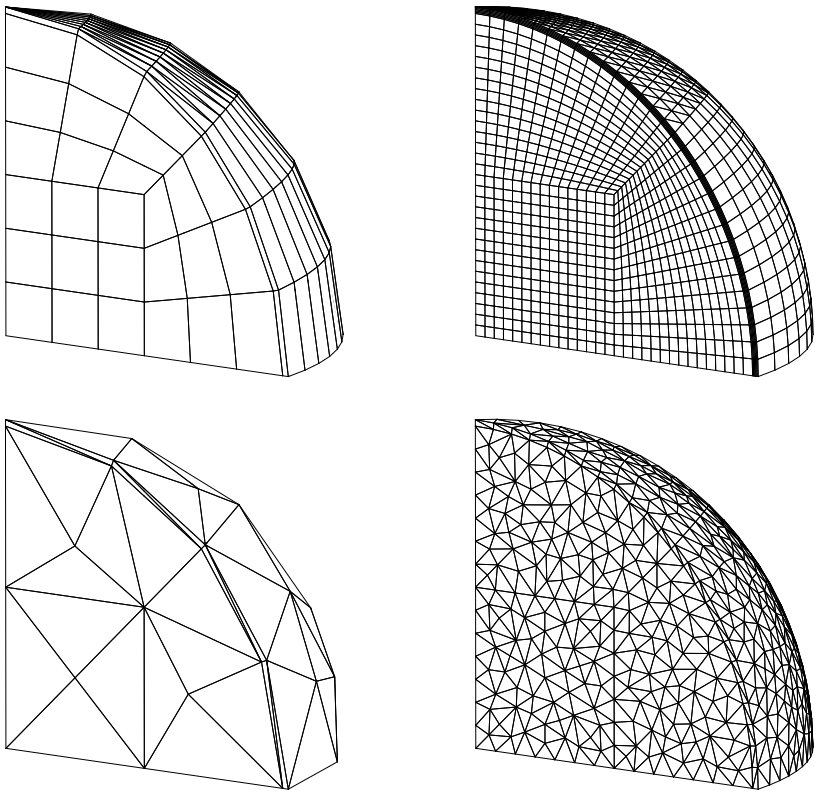

Figure 4.2: Hollow sphere. Detail of the meshes $\mathcal{M}_1^s$ (top left), $\mathcal{M}_5^s$ (top right), $\mathcal{M}_1^u$ (bottom left) and $\mathcal{M}_5^u$ (bottom right).

tion of the thin regions (see Figure 4.2, top). The size of the elements (i.e. the length of their longest edge, see Section 2.7.3) making up the ith mesh is approximately half the size of the elements in the $(i-1)$th mesh. A variant for

Table 4.1: Hollow Sphere. Comparison of the modulus of the magnetic flux density at the center of the sphere with $\boldsymbol{h}$- and $\boldsymbol{b}$-conforming formulations, with ($\mathcal{M}_1^{t\prime}$) or without ($\mathcal{M}_1^{s\prime}$) abstraction of the thin region.

			Relative difference (in %)	
f (Hz)	δ (mm)	d/δ	$\boldsymbol{b}$-conforming	$\boldsymbol{h}$-conforming
0	∞	0	3.05	2.99
1	5.033	0.199	3.32	3.27
50	0.712	1.405	2.59	2.50
1000	0.159	6.283	2.71	0.13

$\mu_r = 1000$, $\sigma = 10^7$ S/m, $d = 1$ mm.

each mesh in the sequence, in which the thin regions are replaced by surfaces (see Section 1.2.2.4), is denoted by $\mathcal{M}_i^t$, $i = 1, \ldots, 5$. An additional mesh, denoted by $\mathcal{M}_1^{s\prime}$, is obtained by manually refining the structured mesh around the hollow sphere. This mesh is considered as the reference mesh for all the numerical tests. A variant for $\mathcal{M}_1^{s\prime}$, in which the thin regions are replaced by surfaces, is denoted by $\mathcal{M}_1^{t\prime}$;

2. the meshes $\mathcal{M}_i^u$, $i = 1, \ldots, 5$, form a sequence of unstructured meshes (consisting of tetrahedra) of the domain Ω, where the thin regions have been abstracted (see Figure 4.2, bottom). In the same way as for the structured meshes, the size of the elements making up the ith mesh is approximately half the size of the elements in the $(i-1)$th mesh. The two variants for the first mesh in the sequence resulting from the *hp*-adaptation scheme presented in Section 2.7.5.4 are denoted by $\mathcal{M}_1^{u\prime}$ and $\mathcal{M}_1^{u\prime\prime}$ respectively.

Let us first compare the solution obtained with the reference meshes, before and after abstraction of the thin region (i.e. with $\mathcal{M}_1^{s\prime}$ and $\mathcal{M}_1^{t\prime}$). The z-component of the magnetic flux density computed along the line $\{y = z = 0\}$ is shown in Figures 4.3 to 4.8, for several variants of the problem. Figures 4.3 and 4.4 permit to compare the magnetic flux density in the static case, where the relative permeability of the sphere is taken equal to 100 and 1000. Figures 4.5 to 4.8 permit to compare the magnetic flux density in the dynamic case, where the frequency and the conductivity are maintained constant ($f = 50$ Hz and $\sigma = 10^7$ S/m), while the permeability is chosen in order to obtain skin depths δ from 22.5 mm ($\mu_r = 1$) to 0.712 mm ($\mu_r = 1000$). In both the static and the dynamic case, the results obtained when the thin region is abstracted from the computational domain are in very good accordance with the results obtained when no abstraction is performed. Table 4.1 compares the results obtained with the two kinds of formulations for increasing frequencies (the permeability and the conductivity are fixed: $\mu_r = 1000$ and $\sigma = 10^7$ S/m). The difference between the two sets of dual formulations appears to be approximately the same (under 4 %) regardless of the ratio between the thickness of the thin region and the skin depths.

Figure 4.9 shows the convergence of the error in the magnetic constitutive relation ε^μ (see section 2.7.4) in function of the number of elements in the meshes. One

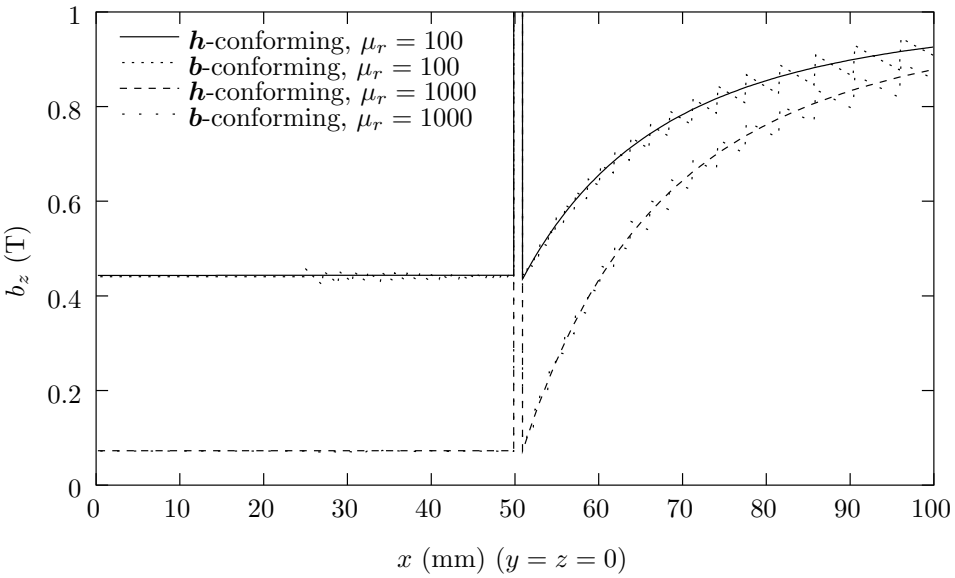

Figure 4.3: Hollow sphere. Static z-component of the magnetic flux density along the line $\{y = z = 0\}$, without abstraction of the thin region ($\mu_r = 100$ and $\mu_r = 1000$; mesh $\mathcal{M}_1^{s\prime}$).

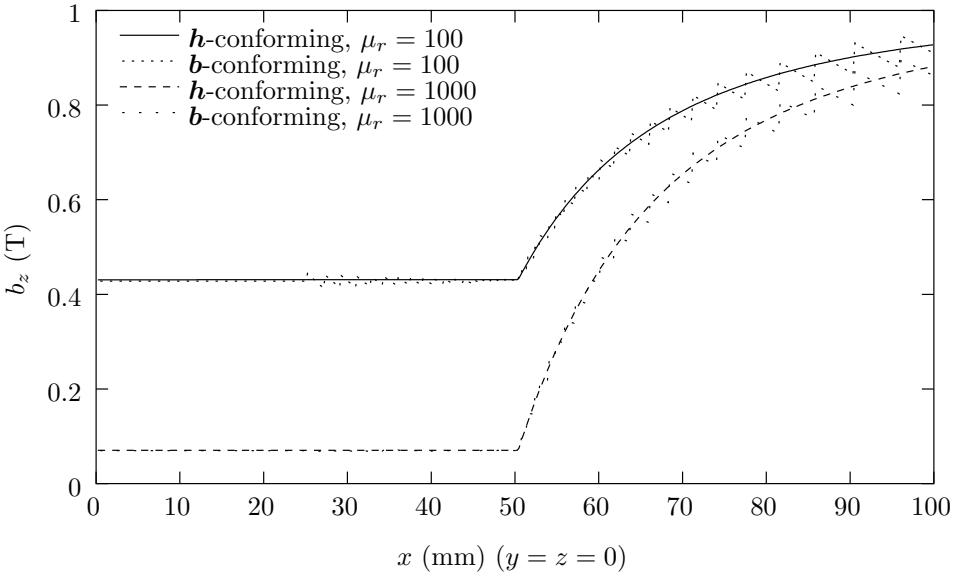

Figure 4.4: Hollow sphere. Static z-component of the magnetic flux density along the line $\{y = z = 0\}$, with abstraction of the thin region ($\mu_r = 100$ and $\mu_r = 1000$; mesh $\mathcal{M}_1^{t\prime}$).

can see that the *hp*-adaptation scheme provides an efficient way to speed up the convergence of the discretization error. Due to the greater richness of the discrete spaces associated with hexahedral and prismatic elements, one can notice that structured meshes behave better than their unstructured counterparts. A detail of the adapted meshes $\mathcal{M}_1^{t\prime}$ and $\mathcal{M}_1^{u\prime}$ is given in Figure 4.10. The *hp*-adapted mesh $\mathcal{M}_1^{u\prime\prime}$

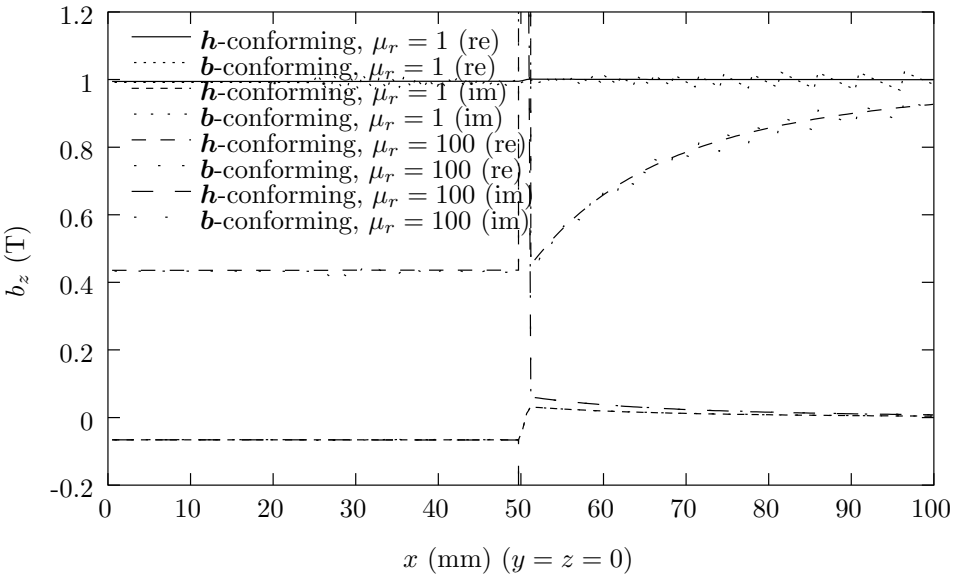

Figure 4.5: Hollow sphere. Real and imaginary parts of the z-component of the magnetic flux density along the line $\{y = z = 0\}$, without abstraction of the thin region ($f = 50\,\mathrm{Hz}$; $\mu_r = 1$ and $\mu_r = 100$; $\sigma = 10^7\,\mathrm{S/m}$; mesh $\mathcal{M}_1^{s\prime}$).

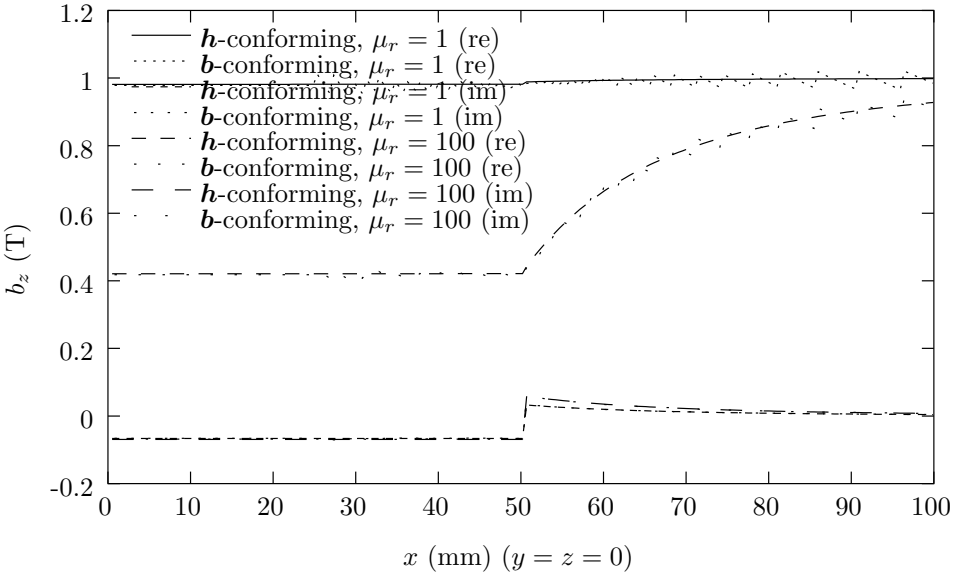

Figure 4.6: Hollow sphere. Real and imaginary parts of the z-component of the magnetic flux density along the line $\{y = z = 0\}$, with abstraction of the thin region ($f = 50\,\mathrm{Hz}$; $\mu_r = 1$ and $\mu_r = 100$; $\sigma = 10^7\,\mathrm{S/m}$; mesh $\mathcal{M}_1^{t\prime}$).

contains 14% of third order elements, 41% of second order elements, and 40% of first order elements. The *hp*-adaptation in the dynamic case leads to similar results, since no magnetic or conducting materials are left after the abstraction of the thin region. It should be pointed out that in this case, even with the coarsest meshes, the complementarity of the dual formulations has always been observed. This may

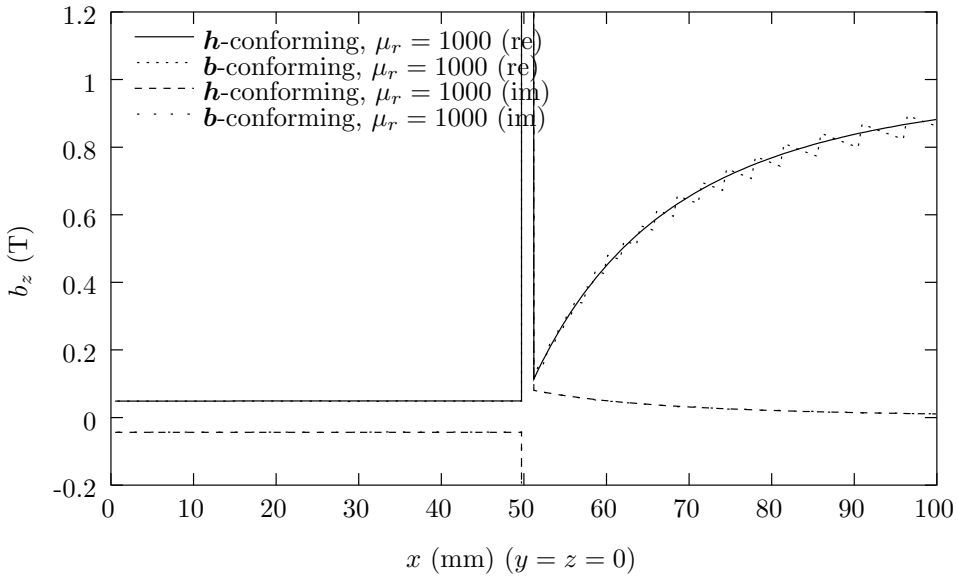

Figure 4.7: Hollow sphere. Real and imaginary parts of the z-component of the magnetic flux density along the line $\{y = z = 0\}$, without abstraction of the thin region ($f = 50\,\mathrm{Hz}$; $\mu_r = 1000$; $\sigma = 10^7\,\mathrm{S/m}$; mesh $\mathcal{M}_1^{s\prime}$).

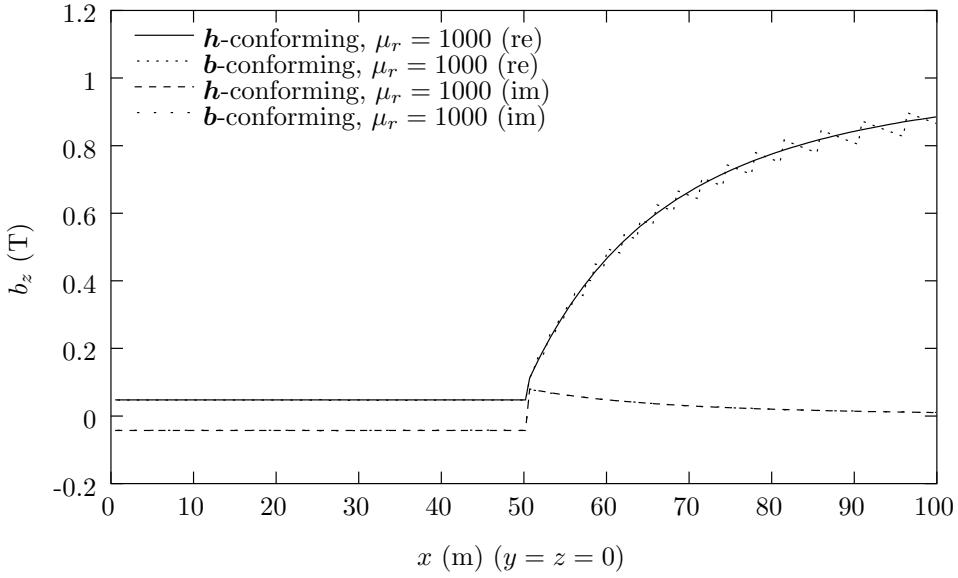

Figure 4.8: Hollow sphere. Real and imaginary parts of the z-component of the magnetic flux density along the line $\{y = z = 0\}$, with abstraction of the thin region ($f = 50\,\mathrm{Hz}$; $\mu_r = 1000$; $\sigma = 10^7\,\mathrm{S/m}$; mesh $\mathcal{M}_1^{t\prime}$).

be explained by the fact that even the coarsest mesh is adapted to the nature of the solution after abstraction of the hollow sphere, since no more regions with skin effect exist in the computational domain.

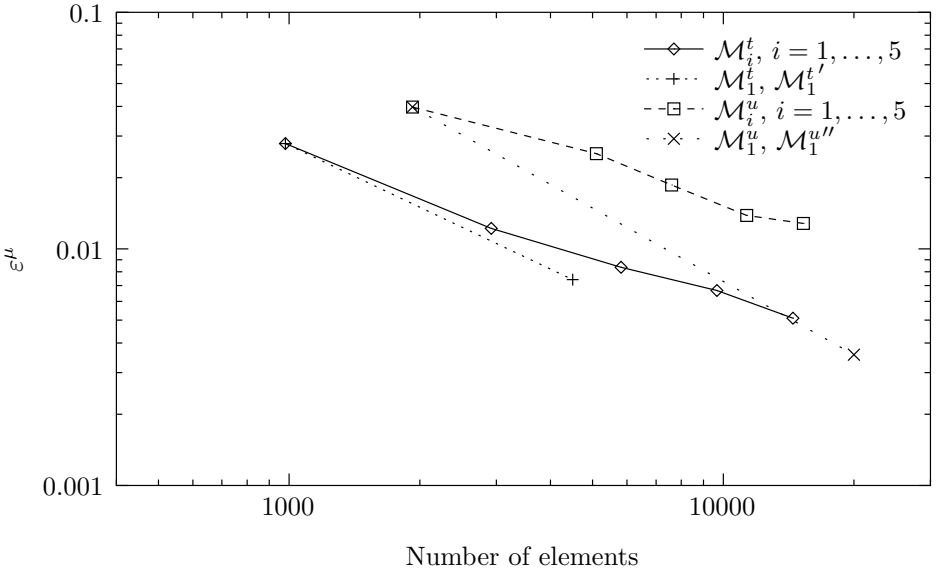

Figure 4.9: Hollow sphere. Convergence of the error in the magnetic constitutive relation ε^μ in the static case ($\mu_r = 100$).

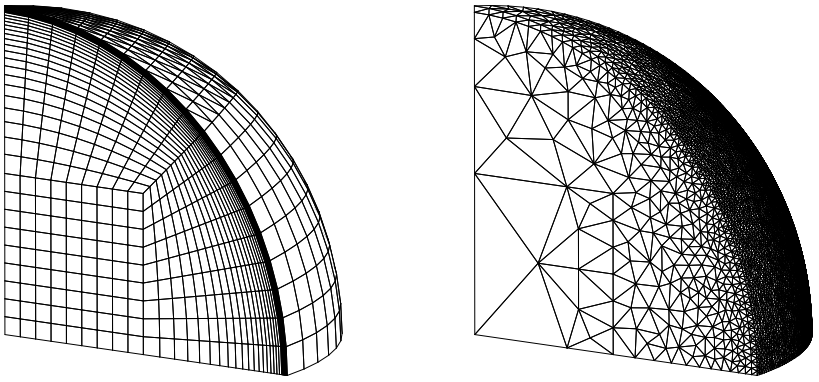

Figure 4.10: Hollow sphere. Detail of the adapted meshes $\mathcal{M}_1^{t\prime}$ (left) and $\mathcal{M}_1^{u\prime}$ (right).

4.3 Inductor-core-shield problem

A parallelepipedic core (of relative magnetic permeability μ_r^c and conductivity σ^c) is surrounded by a coil in which an excitation current flows. A magnetic shield (of relative magnetic permeability $\mu_r = 1000$ and conductivity $\sigma = 2\,10^6\,\mathrm{S/m}$) surrounds the core and the coil (see Figure 4.11). When the excitation current is static ($I = 3000\,\mathrm{A}$) and when the core is highly magnetic ($\mu_r^c = 1000$), this problem is a test-case proposed by the Institute of Electrical Engineers of Japan [158]. In the dynamic case, we will consider several variants of this problem to highlight the behavior of the dual formulations when dealing with stranded, massive and foil winding inductors. In the same way as in Section 4.2, two families of finite element meshes are considered, namely $\mathcal{M}_i^s$ (and its variants $\mathcal{M}_i^t$) and $\mathcal{M}_i^u$, for $i = 1, \ldots, 5$. The size factor between two successive meshes in each sequence is however chosen as approximately 1.5 (instead of 2). The corresponding adapted structured and unstructured meshes are denoted by $\mathcal{M}_1^{s\prime}$, $\mathcal{M}_1^{u\prime}$ and $\mathcal{M}_1^{u\prime\prime}$ (the reference mesh $\mathcal{M}_1^{s\prime}$ is shown in Figure 4.12).

4.3.1 Stranded inductor

We first consider the case of an imposed current density $\boldsymbol{j}_s$. The cutting surface considered in the $\boldsymbol{h}$-conforming formulations is shaded in Figure 4.11, and the source field $\boldsymbol{h}_s$ is calculated by projection as described in Section 3.2.4. Table 4.2 compares experimental results [158] to the results obtained with the dual magnetostatic formulations, with and without abstraction of the thin region (an illustration of the magnetic field $\boldsymbol{h}$ on the section $\{y = 0\}$ is shown in Figure 4.13). The z-component of the magnetic flux density along the lines $\{y = 0, z = 110\,\mathrm{mm}\}$ and $\{y = 0, z = 210\,\mathrm{mm}\}$ is presented in Figures 4.14 and 4.15. The results of similar computations carried out in dynamic regime (with $f = 50\,\mathrm{Hz}$, $\mu_r^c = 1000$ and $\sigma^c = 2\,10^6\,\mathrm{S/m}$) are summarized in Figures 4.16 and 4.17. As in the case of the hollow sphere problem, an excellent agreement is observed between all the formulations.

Table 4.2: Inductor-core-shield problem. Comparison of the computed and measured static magnetic flux density ($\|\boldsymbol{b}\|$, in T).

	Mesh	Position (mm)		
		$(0, 0, 110)$	$(40, 0, 110)$	$(40, 40, 110)$
Measured		0.02400	0.02981	0.03550
$\boldsymbol{b}$-conforming	$\mathcal{M}_1^{s\prime}$	0.0242349	0.0297104	0.0349587
	$\mathcal{M}_1^{t\prime}$	0.0242313	0.0297043	0.0349503
$\boldsymbol{h}$-conforming	$\mathcal{M}_1^{s\prime}$	0.0242716	0.0302545	0.0360349
	$\mathcal{M}_1^{t\prime}$	0.0242673	0.0302478	0.0360257

The convergence of the error in the magnetic constitutive relation is shown in Figure 4.18 for the static case (the results in dynamic regime are similar). A detail of the adapted mesh $\mathcal{M}_1^{u\prime}$ is given in Figure 4.19. The hp-adapted mesh $\mathcal{M}_1^{u\prime\prime}$ contains

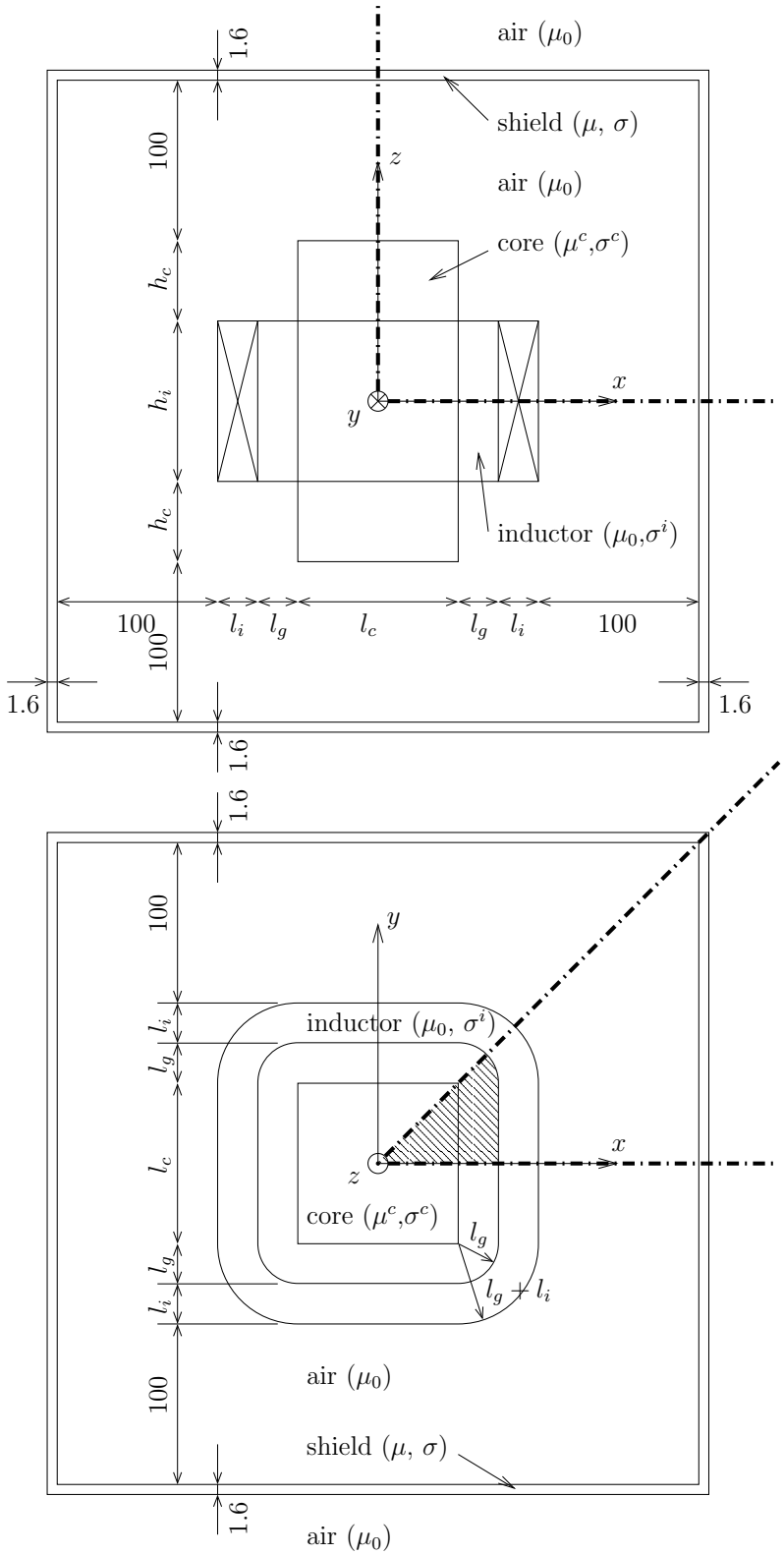

Figure 4.11: Geometry of the inductor-core-shield problem. Original geometry: $l_i = l_g = 25$, $h_c = 50$ and $l_c = h_i = 100$. Modified geometry: $l_i = 25$, $l_g = 8.333$, $h_c = 10$ and $l_c = 33.333$, $h_i = 100$. All dimensions are in mm.

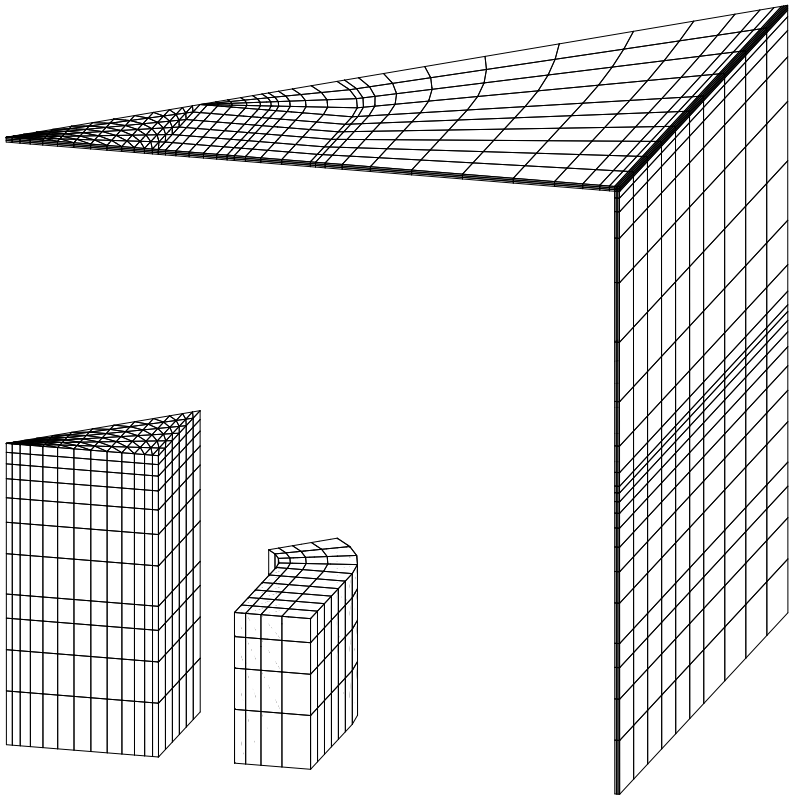

Figure 4.12: Inductor-core-shield problem. Detail of the reference mesh $\mathcal{M}_1^{s\prime}$.

less than 1% of third order elements, 22% of second order elements, and 77% of first order elements.

After these preliminary tests, which confirm the conclusions drawn for the hollow sphere problem, let us now examine the behavior of the system when it is driven by global quantities, i.e. by a global current or voltage. For this purpose we compute the impedance of the inductor for different characteristics of the system. In each case, a magnetomotive force of 1 A is enforced, which corresponds to a current of 0.001 A if we consider a 1000-turn stranded inductor (i.e. with $N_1 = 1000$). The core is considered to be non-conducting ($\sigma^c = 0$) and the electrical conductivity of the inductor is taken as $\sigma^i = 1.475\,10^7$ S/m. In order to highlight the differences between the three kinds of inductors considered, the original geometrical model is slightly changed to consider a proportionally wider inductor, closer to the core: $l_i = 25$, $l_g = 8.333$, $h_c = 10$ and $l_c = 33.333$, $h_i = 100$ (see Figure 4.11).

The inductances computed with the $\boldsymbol{h}$- and $\boldsymbol{b}$-conforming formulations are given in Figure 4.20 for frequencies of 50 Hz and 100 Hz and for a relative magnetic permeability of the core equal to 10. They are independent of the frequency and tend to limit values when the mesh is refined. The value of the resistance, equal to 14.3 $\mu\Omega$ (or 14.3 Ω for a 1000-turn inductor), is independent of the frequency and is accu-

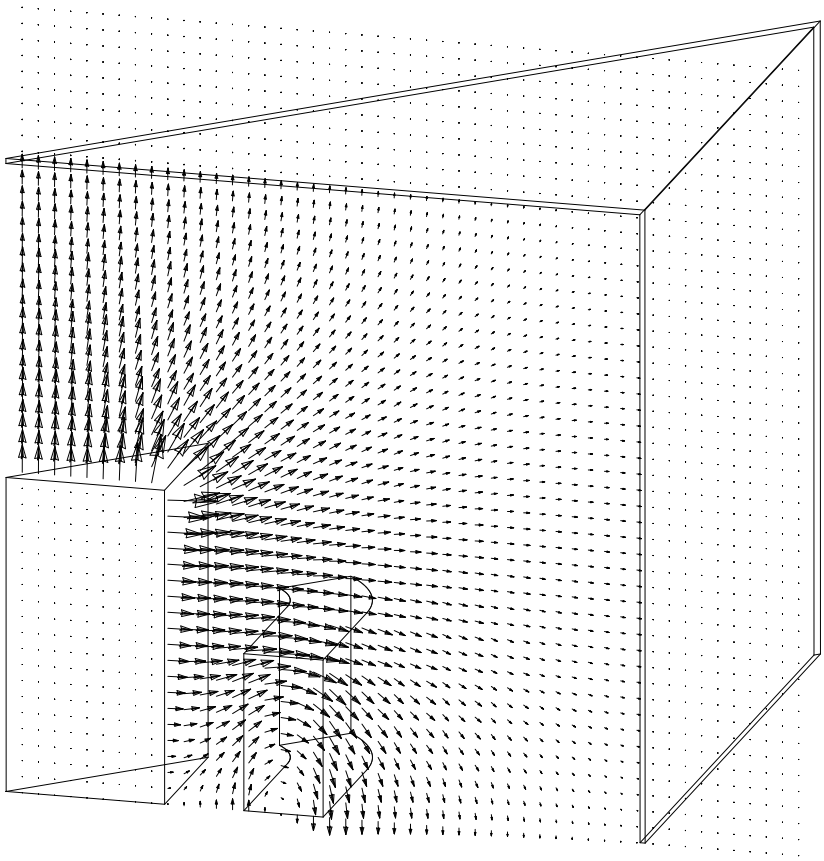

Figure 4.13: Inductor-core-shield problem. Static magnetic field $\boldsymbol{h}$ on the section $\{y = 0\}$ ($\mu_r^c = 1000$; $\max_{\boldsymbol{h}} = 4.86\,10^4$ A/m; mesh $\mathcal{M}_3^{s\prime}$).

rately computed with both formulations and with any mesh in the sequences. The unit source field $\boldsymbol{h}_{s,1}$ involved in the $\boldsymbol{h}$-conforming formulation (see Section 3.2.1.3) is shown in Figure 4.21 (left). Its discontinuous nature in the inductor, due to the tree gauging, as well as the extension of its support to the transition layer associated with the cut is clearly visible. The unit source scalar potential v^0 involved in the magnetic flux density formulation, computed thanks to an electrokinetic formulation (see Section 3.3.1.4), is shown in Figure 4.21 (right). It can be seen that the associated voltage is higher for the wires in the outer part of the coil than for those in the inner part, which is coherent with the difference of length of the turns. The alternative method to compute the source current, by means of an electric vector potential defined in the same way as the source magnetic potential $\boldsymbol{h}_{s,1}$, leads to identical values of the resistance and inductance of the inductor.

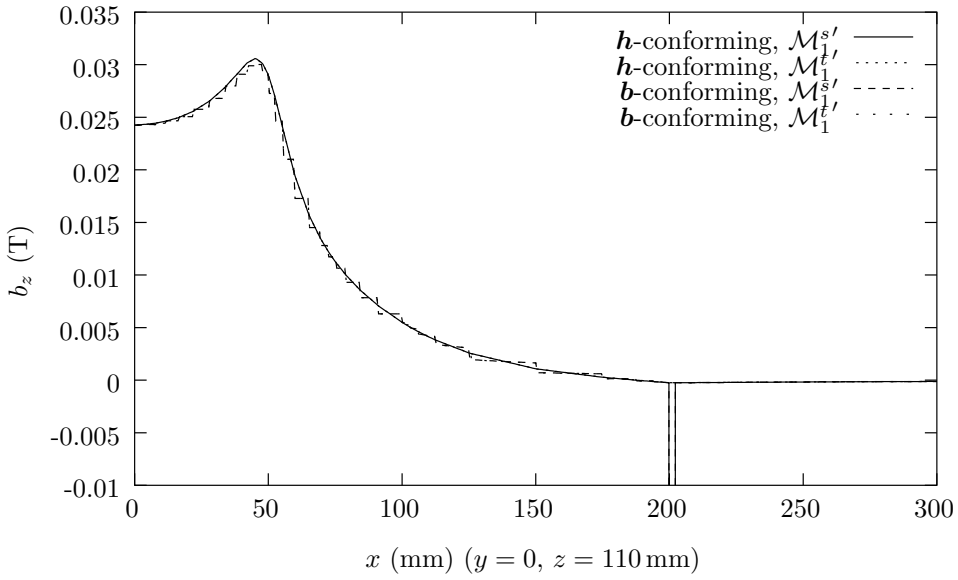

Figure 4.14: Inductor-core-shield problem. Static z-component of the magnetic flux density along the line $\{y = 0, z = 110\,\mathrm{mm}\}$ ($\mu_r^c = 1000$; meshes $\mathcal{M}_1^{s\prime}$ and $\mathcal{M}_1^{t\prime}$).

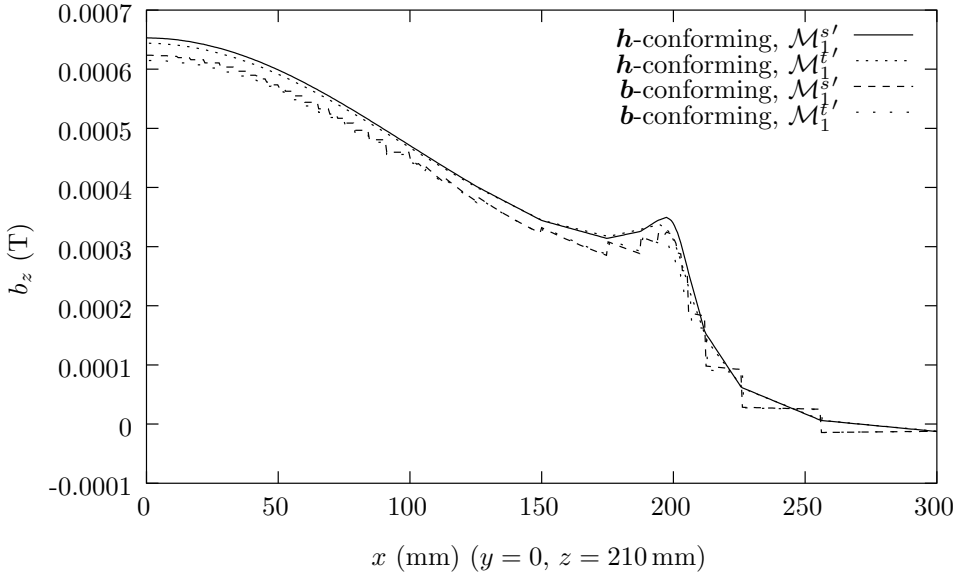

Figure 4.15: Inductor-core-shield problem. Static z-component of the magnetic flux density along the line $\{y = 0, z = 210\,\mathrm{mm}\}$ ($\mu_r^c = 1000$; meshes $\mathcal{M}_1^{s\prime}$ and $\mathcal{M}_1^{t\prime}$).

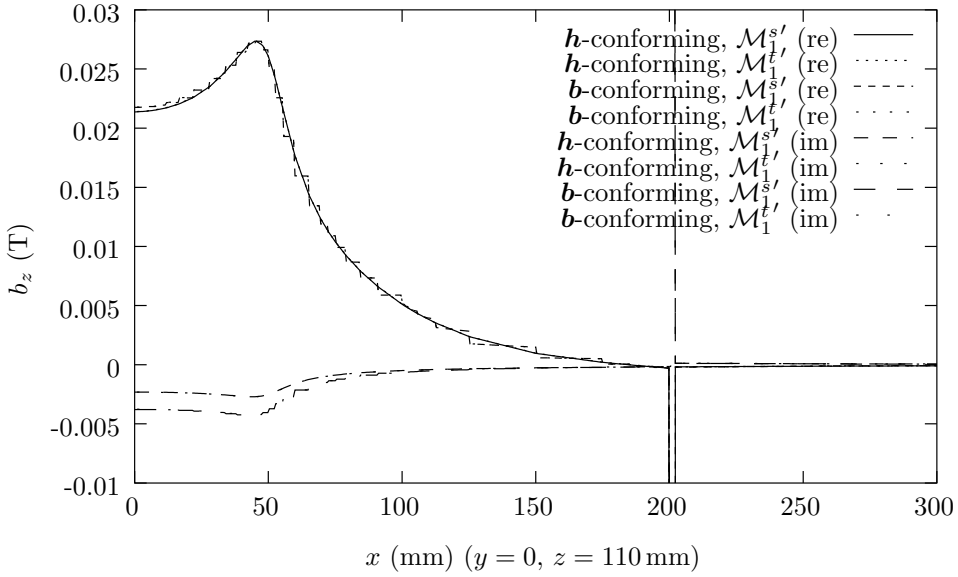

Figure 4.16: Inductor-core-shield problem. Real and imaginary parts of the z-component of the magnetic flux density along the line $\{y = 0, z = 110\,\mathrm{mm}\}$ ($f = 50\,\mathrm{Hz}$; $\mu_r^c = 1000$; $\sigma = 2\,10^6\,\mathrm{S/m}$; meshes $\mathcal{M}_1^{s\prime}$ and $\mathcal{M}_1^{t\prime}$).

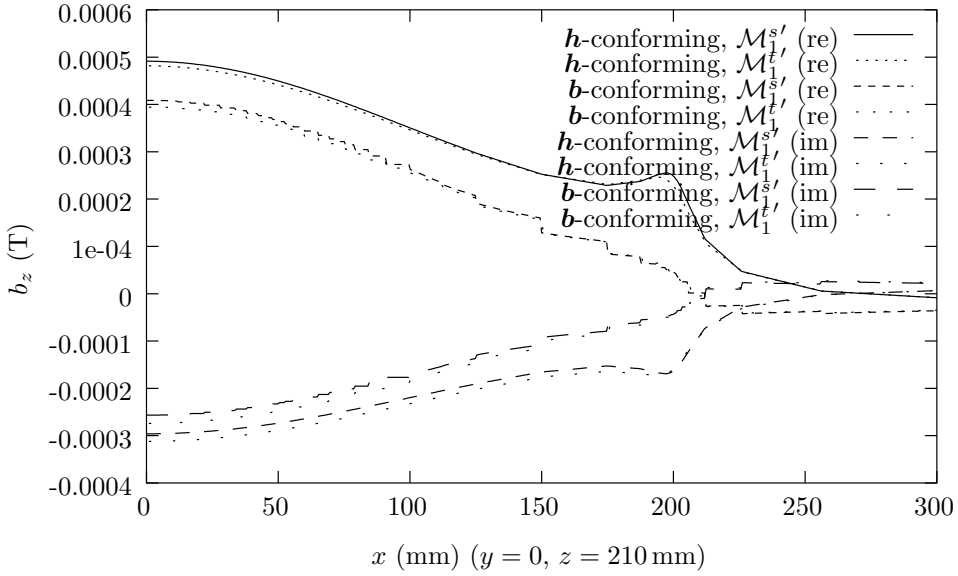

Figure 4.17: Inductor-core-shield problem. Real and imaginary parts of the z-component of the magnetic flux density along the line $\{y = 0, z = 210\,\mathrm{mm}\}$ ($f = 50\,\mathrm{Hz}$; $\mu_r^c = 1000$; $\sigma = 2\,10^6\,\mathrm{S/m}$; meshes $\mathcal{M}_1^{s\prime}$ and $\mathcal{M}_1^{t\prime}$).

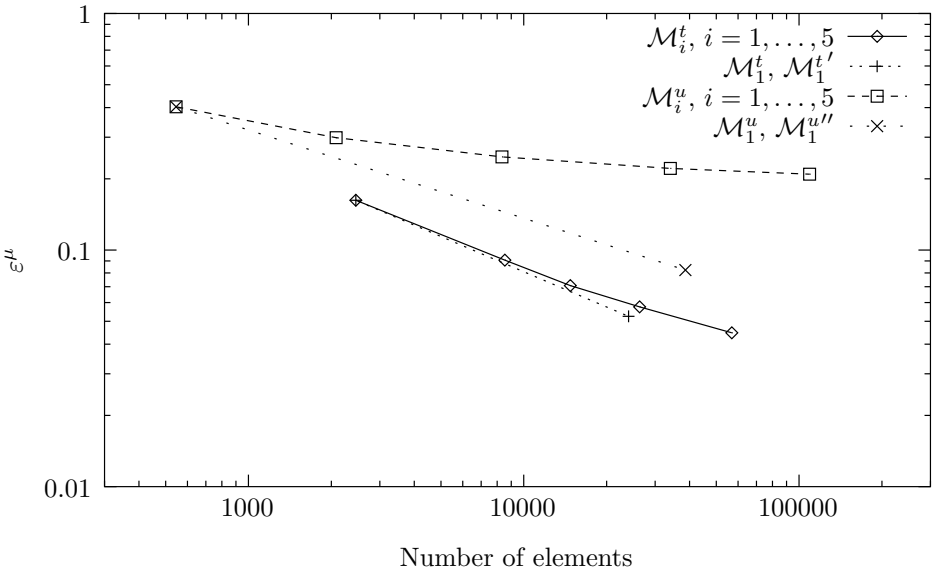

Figure 4.18: Inductor-core-shield problem. Convergence of the error in the magnetic constitutive relation in the static case ($\mu_r^c = 1000$).

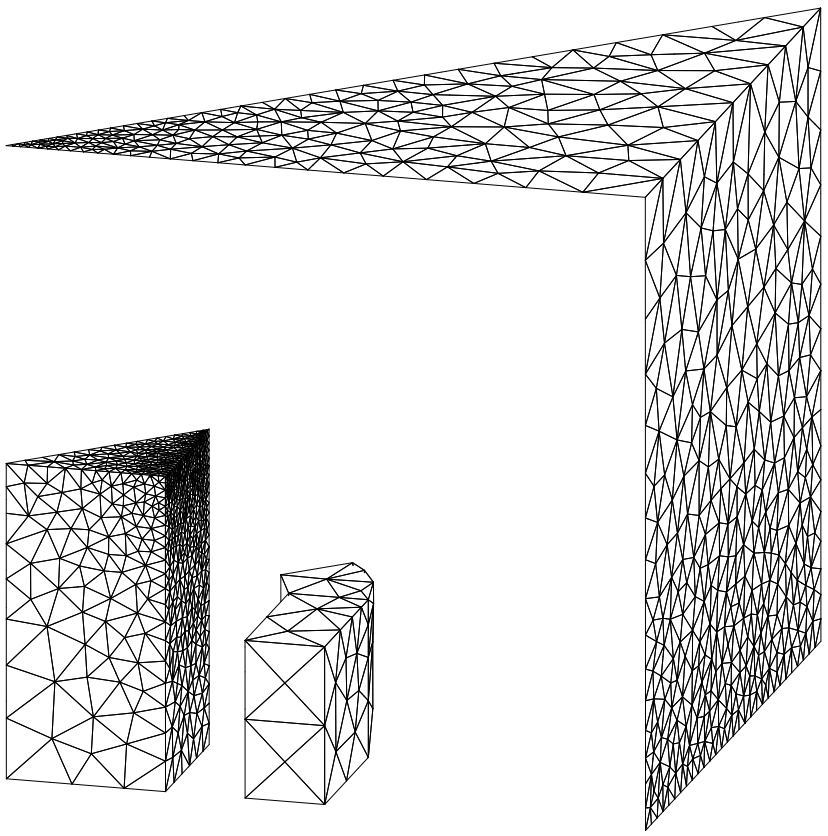

Figure 4.19: Inductor-core-shield problem. Detail of the adapted mesh $\mathcal{M}_1^{u\prime}$.

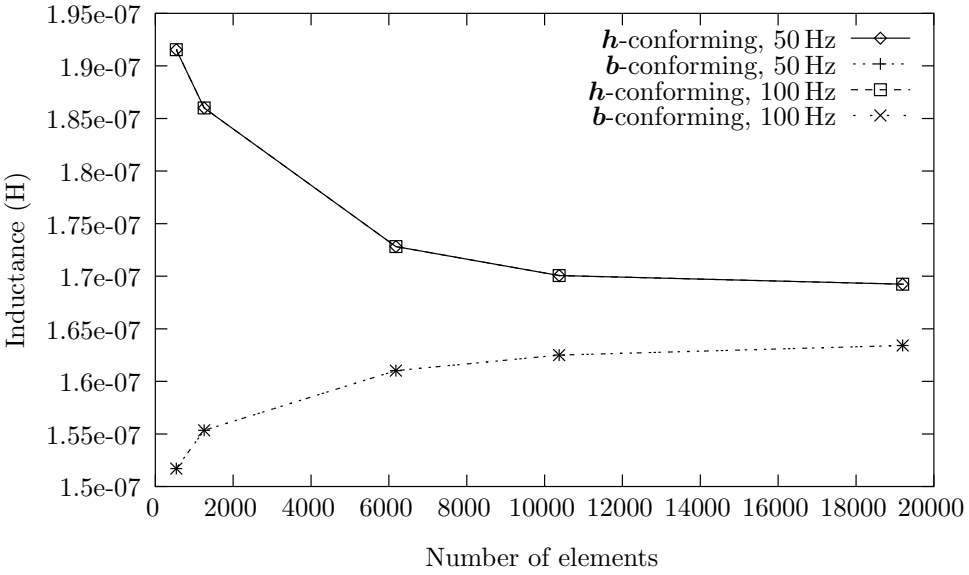

Figure 4.20: Stranded inductor. Convergence of the inductance value at 50 Hz and 100 Hz ($\mu_r^c = 10$; meshes $\mathcal{M}_i^s$, $i = 1, \ldots, 5$).

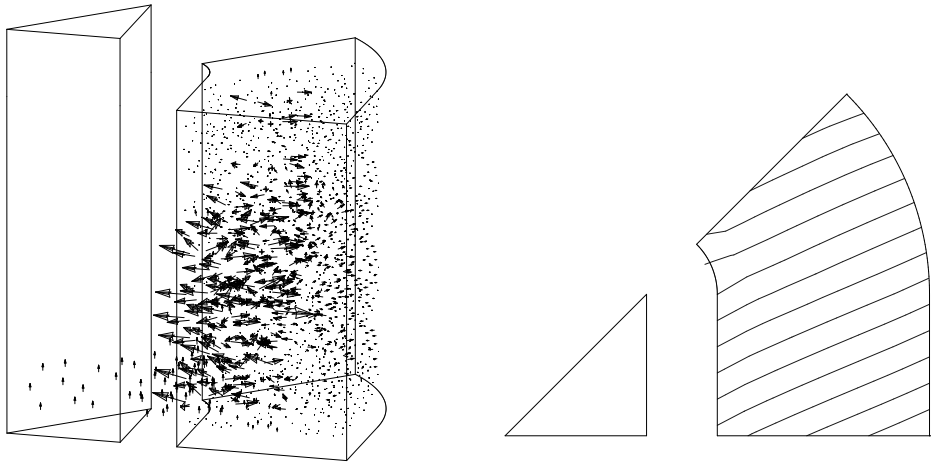

Figure 4.21: Stranded inductor. Source field $\boldsymbol{h}_{s,1}$ (left; mesh $\mathcal{M}_3^u$; $\max_{\boldsymbol{h}_{s,1}} = 5.2\,10^2$ A/m) and equipotential lines of the electrokinetic source scalar electric potential v^0 on the section $\{z = 0\}$ (right; mesh $\mathcal{M}_2^u$).

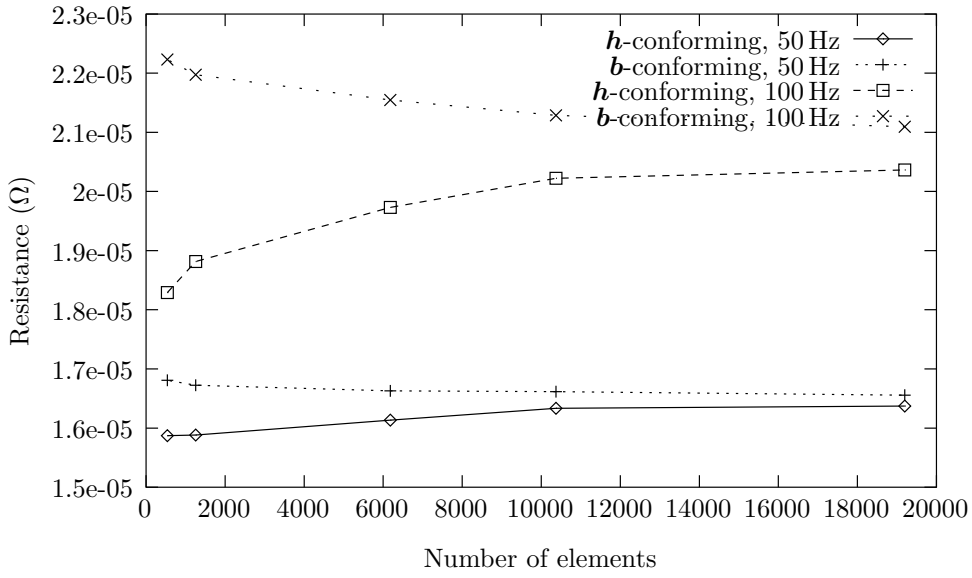

Figure 4.22: Massive inductor. Convergence of the resistance value at 50 Hz and 100 Hz ($\mu_r^c = 10$; meshes $\mathcal{M}_i^s$, $i = 1, \ldots, 5$).

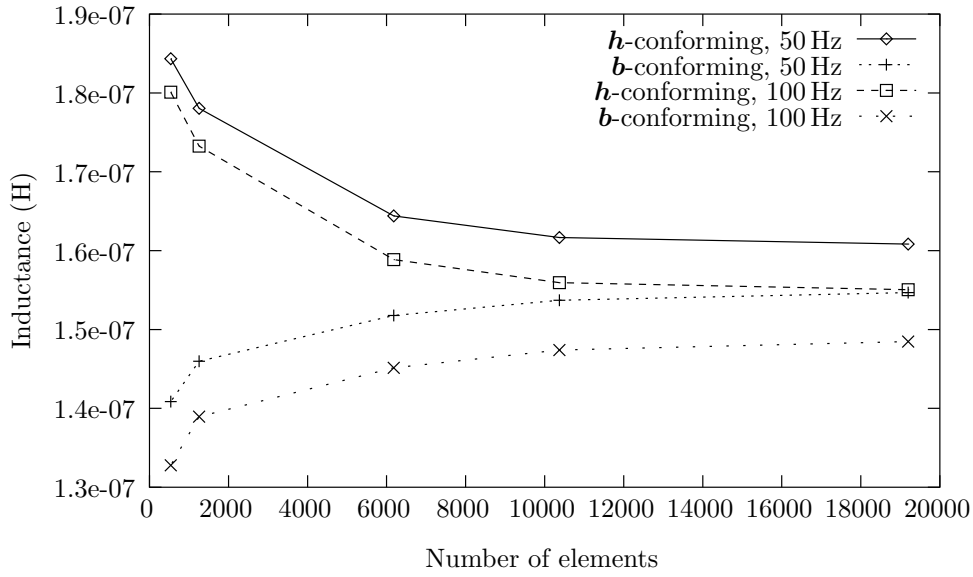

Figure 4.23: Massive inductor. Convergence of the inductance value at 50 Hz and 100 Hz ($\mu_r^c = 10$; meshes $\mathcal{M}_i^s$, $i = 1, \ldots, 5$).

4.3.2 Massive inductor

The resistances and inductances computed with the $\boldsymbol{h}$- and $\boldsymbol{b}$-conforming formulations when the inductor is considered as massive are given in Figures 4.22 and 4.22. The generalized source scalar potential $v_{s,1}$ involved in the magnetic flux density formulation (see Section 3.3.1.3) is shown in Figure 4.24. This figure also shows the equipotential lines on the section $\{z = 0\}$ of the source potential that would have resulted from the resolution of an electrokinetic problem. The general-

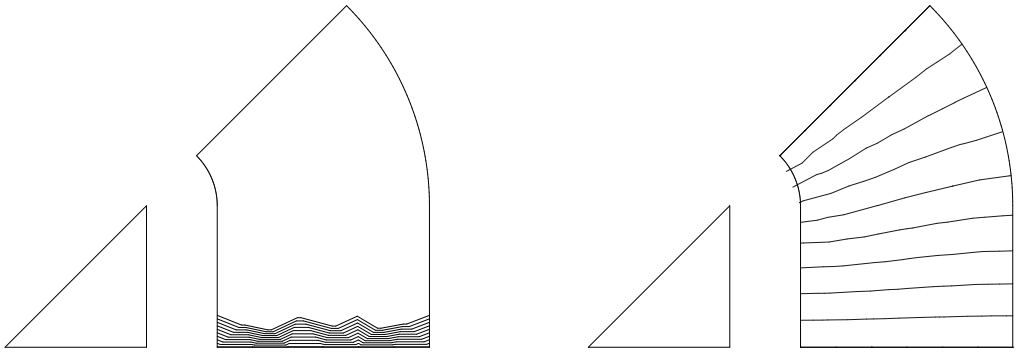

Figure 4.24: Massive inductor. Equipotential lines of the generalized (left) and electrokinetic (right) source scalar electric potential $v_{s,1}$ on the section $\{z = 0\}$ (mesh $\mathcal{M}_2^u$).

ized source potential should be favored since it does not require any finite element pre-computation and leads to a lower bandwidth in the system of equations when voltages are considered as unknowns.

As in the case of stranded inductors, the values of the inductance and resistance converge (in a complementary way) toward limit values when the meshes are refined, which is a good way to validate the coupling of local and global quantities in both $\boldsymbol{h}$- and $\boldsymbol{b}$-conforming formulations.

4.3.3 Foil winding inductor

When the foil windings are considered as a set of massive conductors, the $\boldsymbol{h}$-conforming formulation leads to the computation of a scalar potential along the foil interfaces. Figure 4.25 compares the γ-component of current density in the foils obtained in this case and when the scalar potential is continuously extended in the foil region (see Section 3.3.1.4). Note that, contrary to the stranded and massive cases, we consider a reference source magnetomotive source of 6 A, i.e. a current of 1 A for half of a 6-turn foil inductor. This enables a direct comparison of the thus normalized voltages and current densities for inductors with different numbers of foils. A very good agreement is observed between the two computations, which validates the orthogonal decomposition of the magnetic field described in Section 3.3.1.4.

When the foils are classically treated as individual massive conductors, the $\boldsymbol{b}$-conforming formulation leads to the computation of a constant voltage for each entity. A spatially dependent global quantity has to be considered for the voltage if the foil region is extended to a continuum (see Section 3.3.3.2). Several approximations for the voltage continuum $V_i(\alpha)$ are displayed in Figure 4.26. It can be seen that complete and piece-wise polynomials in α both lead to a good accuracy of the voltage in comparison with the discrete values of the individual massive inductors (for $N_1 = 6$, 12 and 18). The correspondence is valid for different permeabilities of

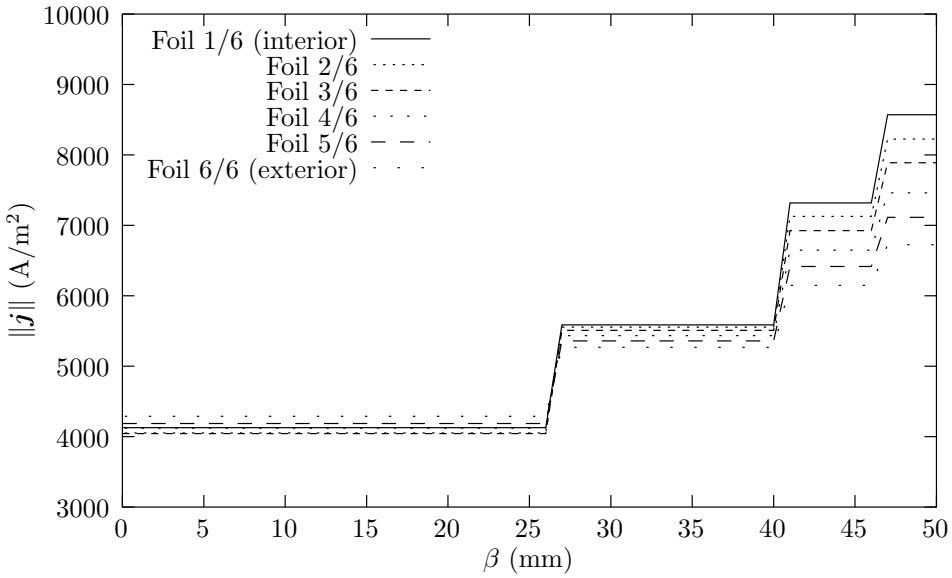

Figure 4.25: Foil winding inductor. γ-component of the current density along the height of the foil region at 6 α positions ($\boldsymbol{h}$-conforming formulation; mesh $\mathcal{M}_1^{s\prime}$).

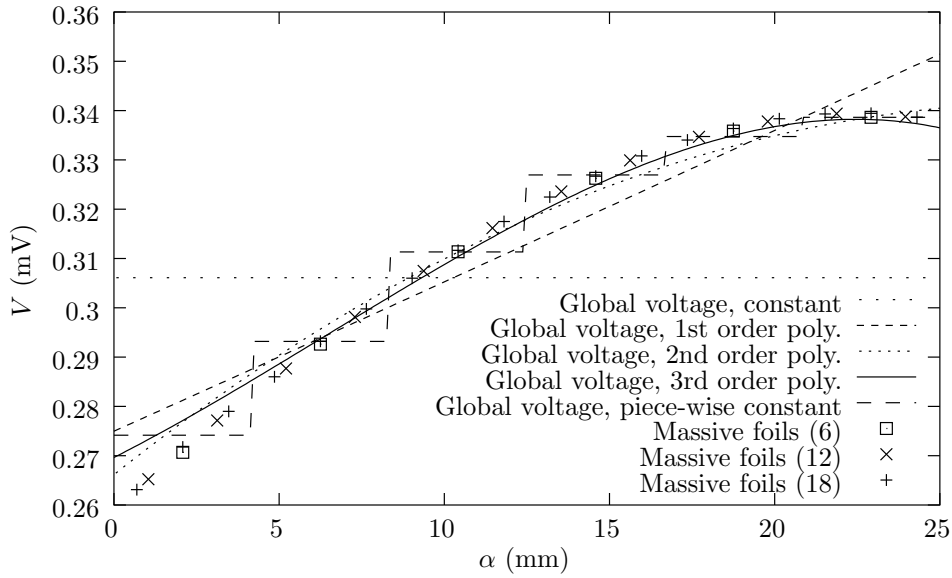

Figure 4.26: Foil winding inductor. Voltage of the foils in an N_1-foil winding ($N_1 = 6,\ 12,\ 18$) and its continuum in the associated foil region approximated by complete and piece-wise polynomials ($\boldsymbol{b}$-conforming formulation; $\mu_r^c = 10$; mesh $\mathcal{M}_1^{s\prime}$).

the core (see Figure 4.27) and the anisotropic tensor form of the electric conductivity of the foil region is essential to correctly describe the behavior of the current in foils (see Figure 4.28).

The current density distribution in the foil region is comparable to the one obtained with individual massive inductors (see Figure 4.29). Its variation along the

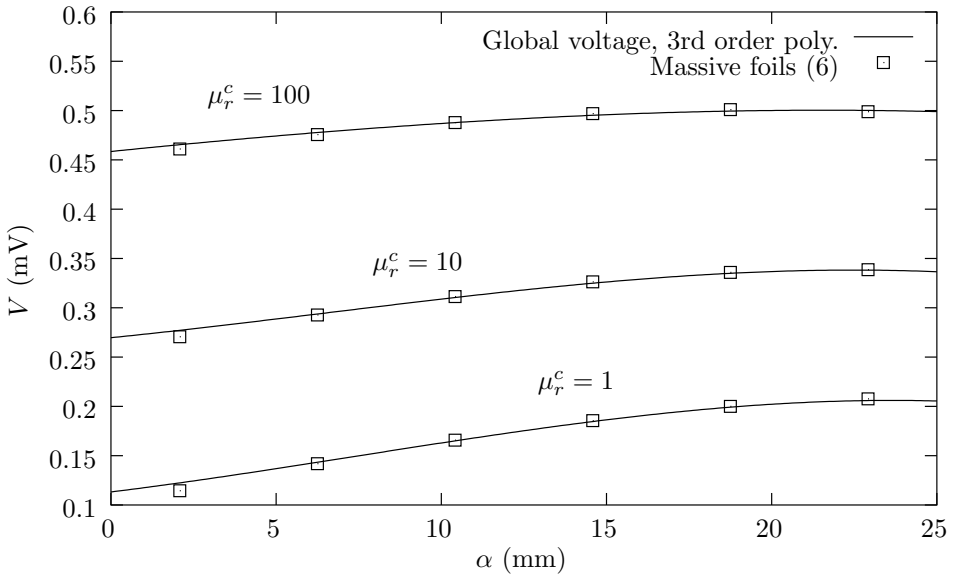

Figure 4.27: Foil winding inductor. Voltage of the foils in a 6-foil winding and its continuum in the associated foil region approximated by complete 3rd order polynomials (***b***-conforming formulation; $\mu_r^c = 1$, 10 and 100; mesh $\mathcal{M}_1^{s\prime}$).

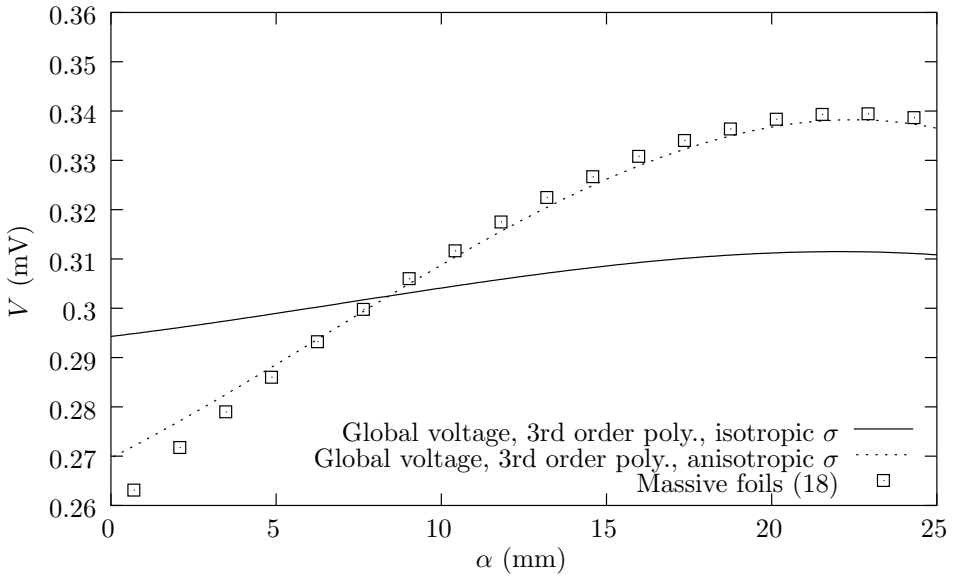

Figure 4.28: Foil winding inductor. Voltage of the foils in an 18-foil winding and its continuum in the associated foil region approximated by complete 3rd order polynomials, with an isotropic or anisotropic electric conductivity for the foil region (***b***-conforming formulation; $\mu_r^c = 10$; mesh $\mathcal{M}_1^{s\prime}$).

height of the foil region is shown in Figure 4.30. For the simulated 6-turn winding, the total currents in the foils are, from the interior to the exterior of the winding, 1.040 A, 0.994 A, 0.996 A, 1.000 A, 0.997 A and 0.972 A. Such a distribution points out the absence of skin effect in the α direction. Without the application of the

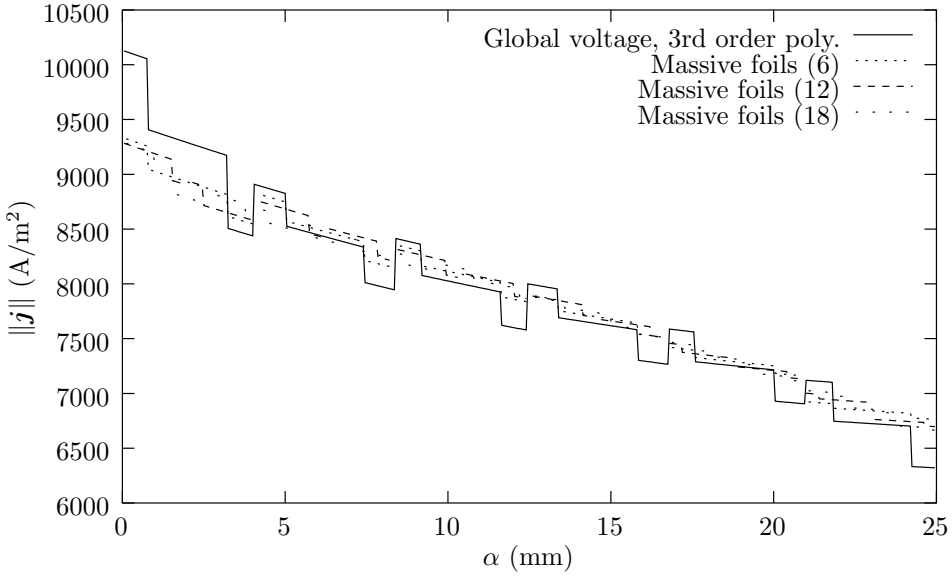

Figure 4.29: Foil winding inductor. γ-component of the current density on the top of the foils along the α direction in an N_1-foil winding ($N_1 = 6$, 12, 18) and in the associated foil region with a complete 3rd order polynomial (***b***-conforming formulation; $\mu_r^c = 10$; mesh $\mathcal{M}_1^{s\prime}$).

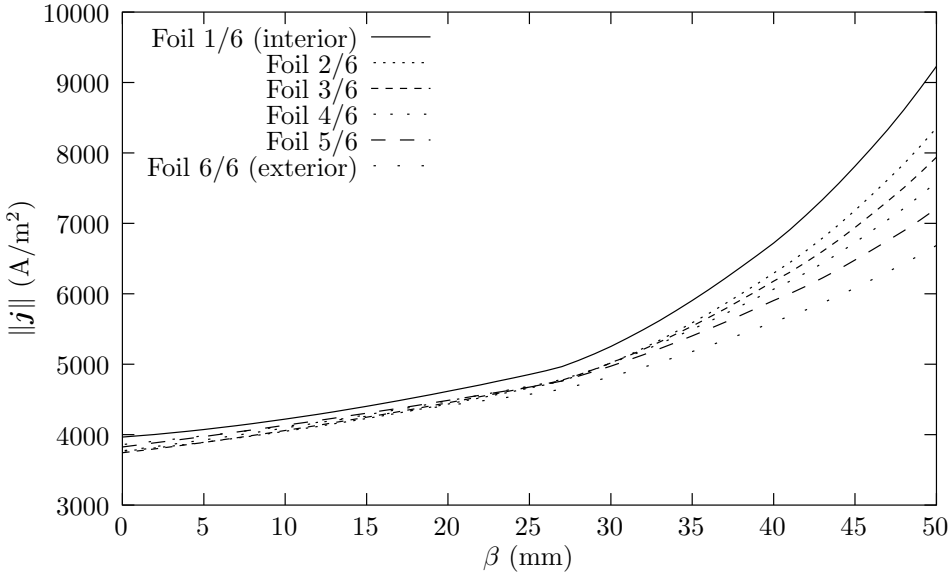

Figure 4.30: Foil winding inductor. γ-component of the current density along the height of the foil region at 6 α positions (***b***-conforming formulation; complete 3rd order polynomial; $\mu_r^c = 10$; mesh $\mathcal{M}_1^{s\prime}$).

proposed method, the total currents would have been 1.260 A, 1.153 A, 0.974 A, 0.916 A, 0.845 A and 0.813 A. It should be pointed out that the mesh of the foil region can be defined independently of the foil interfaces, but that it has nevertheless to be compatible with the variation of the voltage, i.e. fine enough to take these

variations into account.

General conclusions

A solution strategy for computing local and global electromagnetic quantities by finite element-type techniques in three-dimensional structures has been presented. The main achievements of this thesis (concerning mixed finite elements and dual hybrid formulations) are summarized hereafter, as well as conclusions that can be drawn from the numerical tests and some important future prospects. For a succinct summary of the original contributions of the thesis (with the list of associated publications), please refer to the introduction, page 5.

Mixed finite elements

First we have presented a generalized summary of the construction of mixed finite elements built on a collection of tetrahedra, hexahedra and prisms, which can be combined in the same mesh. These elements exhibit three main characteristics:

1. they form a complete sequence for three-dimensional computations, i.e. they are conforming either in $H^1(\Omega)$, $\boldsymbol{H}(\mathbf{curl};\Omega)$, $\boldsymbol{H}(\mathrm{div};\Omega)$ or $L^2(\Omega)$. Finite elements of class $H^1(\Omega)$ interpolate scalar fields that are continuous across any interface (like the scalar magnetic potential and the scalar electric potential). Finite elements of class $\boldsymbol{H}(\mathbf{curl};\Omega)$ or $\boldsymbol{H}(\mathrm{div};\Omega)$ only ensure the continuity of the tangential or normal part of the interpolated fields respectively, and are thus well suited for the discretization of the magnetic field, the electric field and the magnetic vector potential, or for the current density and the electric displacement respectively. Finite elements of class $L^2(\Omega)$ do not impose any inter-element continuity and are thus well adapted to discretize densities (as for example the electric charge density);

2. they extend the classical Whitney elements to higher orders in a hierarchical way, i.e. they span higher order polynomial spaces by ensuring that the basis functions for a given interpolation order are a subset of the basis functions used for the interpolation at any higher order. With a judicious choice of degrees of freedom associated with all the geometrical entities of the elements (i.e. the nodes, the edges, the faces and the volume), this makes it easy to combine elements of different orders and different geometrical shapes in the same mesh;

3. they are built in a recursive way, starting from the classical Whitney ele-

ments (and their generalization to hexahedra and prisms) for the first order, and are extended by respecting the Helmholtz decomposition of the function spaces they span in the construction of their bases. This permits to explicitly characterize the global finite spaces discretizing the nullspace and range of the associated differential operators by extending the fundamental results demonstrated for Whitney elements.

Next we have set out a deterministic procedure for the optimization of the global finite element spaces built with a collection of these mixed tetrahedral, hexahedral and prismatic finite elements. This optimization is based on an *hp*-refinement procedure, where the error estimation is based on the error in the constitutive relations.

Hybrid formulations

In order to compute the error in the constitutive relations in a rigorous way, we have developed two families of hybrid finite element formulations, which generalize existing formulations on three levels:

1. an original treatment of thin conducting and magnetic regions is elaborated: contrary to current approaches, the one-dimensional approximations are not introduced at the discrete level (by defining special finite elements) but directly in the weak form of the formulations, thanks to an appropriate treatment of the surface integral terms. Moreover, all developments are carried out for both magnetic field and magnetic flux density conforming formulations;

2. a natural method for the coupling between local field quantities and global electrical variables is proposed. The treatment of massive, stranded and foil winding inductors in the case of the magnetic field conforming formulation appears to be entirely new. In the case of the magnetic flux density conforming formulation, the treatment of massive and stranded inductors generalizes the existing modified vector potential formulations proposed in the literature, while the treatment of foil windings generalizes the existing method developed for two-dimensional problems. The computation of source fields in the magnetic field conforming formulations being mandatory, an original method to construct such global basis functions of minimal geometrical support (i.e. limited to the inductors and the neighboring of the cutting surfaces) is also presented, based on a projection technique. If this method may appear less efficient than purely algebraic ones (working locally by inspection), it permits to handle high order mixed elements in a straightforward way;

3. a rationale for the choice of the discretization method for the sources of the integral operators is given, stemming from differential geometry concepts and generalizing the widely used collocation techniques. This notably shows that the dualism of electromagnetism is not yet fully exploited and understood when constructing numerical approaches for field computation, especially when it comes to techniques using integral operators. It is for example pointed out

that the use of the dual mesh is mandatory as soon as collocation techniques are sought.

Numerical tests

The numerical experiments have shown that the complementarity of the developed formulations exists both for local and global quantities and that the computed values tend to limit values when the mesh is refined, which is a way to validate the methods at a global level. In all cases, a very good agreement has been found between the dual formulations, discretized with all developed kinds of mixed finite elements up to the order three. The abstraction of the thin regions has turned out to provide excellent results in comparison with the classical formulations, and the *hp*-adaptation procedure has proved to greatly accelerate the convergence of the discretization error. As for the coupling between finite element and boundary element methods, the numerical tests tend to show that the de Rham approach performs slightly better (in terms of convergence) than the Galerkin method. We deliberately have not pursued a thorough comparison of the actual relative efficiency of these methods, since we do not consider our current implementation as optimal. Nevertheless, the algorithmic complexity is similar.

If we had to favor one of the dual approaches, we would undoubtedly choose the magnetic field conforming formulations. Although they require the (sometimes complex) construction of cuts, the direct use of a scalar potential in the non-conducting regions permits, as far as performance is concerned, to avoid the costly use of a vector potential in the whole domain of study. Moreover, we have had some difficulties to achieve reasonable convergence of the iterative solvers for the gauged magnetic flux density conforming formulations in the complex formalism. In the same way, the choice of de Rham- or Galerkin-type formulations is, in practice, difficult to make on the basis of efficiency considerations. At this point of our understanding of the methods, we would only recommend the de Rham approach for the discretization of the integral equation part of the hybrid formulations, since it avoids some of the tedious double integrations encountered with the Galerkin approach and seems to converge better. From the classical finite element method point of view, it nevertheless requires some unusual handling of dual meshes. In any case, all the developed software tools are freely available on the Internet for further tests (see Appendix D).

Future prospects

Several suggestions for future research are given below:

1. the actual choice of the degrees of freedom (and thus the choice of the basis functions) of the high order mixed elements should be made with the aim to achieve an optimal conditioning of the discretized operator [207]. A better comprehension of the associated high order basis functions as high order

Whitney maps should also permit to extend the de Rham map to high order elements (see [22] in the case of non-hierarchical elements);

2. the treatment of the thin conducting and magnetic regions could be enhanced in the time domain, using an approach similar to the one used in finite difference methods in the case of high frequency problems (see e.g. [199, 66]). The extension to nonlinear cases could also be performed (see e.g. [130, 129]);

3. the investigation of iterative algorithms better suited for the resolution of systems of equations with populated lines (due to the presence of global quantities in the formulations) should be carried on;

4. the current implementation of the integral part of the hybrid formulations remains costly at the computational level. Besides a thorough comparison with transformation techniques for low frequency problems (see e.g. [181, 107]) and with perfectly matched layers for propagation phenomena (see e.g. [10, 156]), a fast multipole expansion should be introduced in order to accelerate the BEM (see e.g. [198, 46]). The acceleration of the FEM could be achieved thanks to the implementation of a hierarchical multigrid solver based on the proposed high order mixed elements [112];

5. in order to efficiently apply the solving strategies developed in this thesis to high frequency problems, a comparison between the implicit and explicit time integration should be undertaken. In particular, the critical time step size governed by a Courant-Friedrichs-Levy condition as well as the loss of accuracy due to the lumping of the system matrix, regarding the size and distortion of the elements, should be analyzed in the case of explicit schemes (see e.g. [102, 45, 140, 65, 225, 85, 24, 9]). A better quality enforcement of the three-dimensional unstructured meshes is likely to be mandatory [122].

Appendix A

Mathematical framework

A.1 Formalism

We consider the oriented Euclidean space $\mathbb{E}^3$ as the framework for all developments. Together with an absolute time variable, this is a good approximation of the Minkowsky space-time (we consider only non-moving systems, and we ignore both special relativity and quantum effects [68, 115, 200]).

But it is worth noticing that the structure presented in the Section 1.3 is not limited to open sets of the oriented Euclidean space. It could be extended to n-dimensional manifolds, and the scalar and vector fields appearing in all developments could be considered as the representation, in three dimensions, of other geometric elements: differential forms [69, 201, 220, 17]. The difficulty in keeping the formalism straightforwardly understandable (particularly when dealing with integral operators: see for example [214] for an analysis of this question) has refrained us from using differential forms in the text.

Nevertheless, since differential forms have influenced the way in which this work is structured, it is worth highlighting some of the most fundamental concepts of this formalism so that a deeper understanding of the concepts can be achieved. Roughly stated, in a three-dimensional space, to vector fields like the magnetic field $\boldsymbol{h}$ or the electric field $\boldsymbol{e}$ belonging to $\boldsymbol{H}(\mathbf{curl}; \Omega)$, for which it makes sense to compute the circulation on a contour, correspond differential forms of degree one (called 1-forms), whereas to vector fields like the magnetic flux density $\boldsymbol{b}$ or the current density $\boldsymbol{j}$ belonging to $\boldsymbol{H}(\mathrm{div}; \Omega)$, and for which it makes sense to compute the flux across a surface, correspond differential forms of degree two (2-forms) (for the definition of $\boldsymbol{H}(\mathbf{curl}; \Omega)$ and $\boldsymbol{H}(\mathrm{div}; \Omega)$, see section A.2.5). In a similar way, to scalar fields like the electric potential v or the charge density q, belonging respectively to $H^1(\Omega)$ and $L^2(\Omega)$, which are evaluated locally or integrated over a volume, correspond differential forms of degree zero and three (0-forms and 3-forms). Differential geometry defines a single derivation operator (the exterior derivative d), transforming $(p-1)$-forms into p-forms, of which the **grad**, **curl** and div operator are the representatives in three dimensions. Another important operator is the Hodge operator, which transforms p-forms into $(n-p)$-forms. Whereas the exterior derivative (and

thus the **grad**, **curl** and div operators) is a purely topological operator, one can show that the Hodge operator involves the metric of the space where the forms are defined. The interpretation of the Galerkin and de Rham methods presented in Appendix C can be greatly simplified if one keeps these two aspects in mind.

A.2 Function spaces

The following section is only given as a short reminder (see e.g. [37] for an extensive coverage of the subject), so that all the essential building blocks for the numerical approaches are explicitly defined. Scalar and vector fields[1] are defined at any point $\boldsymbol{x} = (x, y, z) \in \mathbb{E}^3$ and at any time instant $t \in \mathbb{R}$. Please note that the space-time dependence of the fields will be generally omitted: the scalar field $f(\boldsymbol{x}, t) = f(x, y, z, t)$ and the vector field $\boldsymbol{f}(\boldsymbol{x}, t) = \boldsymbol{f}(x, y, z, t)$ will thus be often simply denoted by f and $\boldsymbol{f}$. In Cartesian coordinates, the three components of the vector field $\boldsymbol{f}$ are denoted by f_x, f_y and f_z respectively, and the vector field can then be denoted by $\boldsymbol{f} = (f_x, f_y, f_z)^T$.

We consider an open set Ω of $\mathbb{E}^3$, whose boundary is a closed surface Γ of exterior unit normal $\boldsymbol{n}$.

A.2.1 Vector spaces and function spaces

Let E be a set and x, y, z, elements of E. Let the scalars α, β, γ be elements of a field K (i.e. a commutative division algebra, or a *corps commutatif* in French). The set E is a vector space on the field K if

1. to each pair of elements x and y of E corresponds an element $x + y$ belonging to E and if this addition rule satisfies the following conditions ($\forall x, y, z \in E$):
   (a) $x + y = y + x$;
   (b) $x + (y + z) = (x + y) + z$;
   (c) there exists an element 0 such that $x + 0 = 0 + x = x$;
   (d) for every element $x \in E$ there exists an element $(-x)$ such that $x+(-x) = (-x) + x = 0$;
2. to each pair of elements $\alpha \in K$ and $x \in E$ corresponds an element $\alpha x \in E$ and if this multiplication by a scalar rule satisfies the following conditions ($\forall \alpha, \beta \in K$ and $\forall x, y \in E$):
   (a) $\alpha(\beta x) = (\alpha\beta)x$;
   (b) there exists an element 1 such that $1x = x$;
   (c) $\alpha(x + y) = \alpha x + \alpha y$;

[1] We use the terms "scalar field" and "function" equally and we do so for the terms "vector field" and "vector valued function" as well.

(d) $(\alpha + \beta)x = \alpha x + \beta x$.

If the elements of a vector space are functions, the vector space is called a function space.

A vector space E is normed if to each element $x \in E$ corresponds a non-negative number $\|x\|$ such that

1. $\|x\| = 0$ if and only if $x = 0$;
2. $\|\alpha x\| = |\alpha|\|x\|, \ \forall \alpha \in K$;
3. $\|x + y\| \leq \|x\| + \|y\|, \ \forall y \in E$.

If a space is normed, the distance between two elements x and y is defined as

$$d(x, y) = \|x - y\|. \tag{A.1}$$

A.2.2 Hilbert spaces

Let E be a normed vector space. A sequence $\{x_n\}$ is called a Cauchy sequence if

$$\forall \epsilon > 0, \ \exists N(\epsilon) : \ n > N(\epsilon) \text{ and } m > N(\epsilon) \Rightarrow d(x_m, x_n) < \epsilon. \tag{A.2}$$

E is complete if every Cauchy sequence converges toward an element of E. A vector space that is normed and complete is called a Banach space.

If E is a vector space equipped with a scalar product and if E is complete for the norm derived from this scalar product, then E is a Hilbert space.

A.2.3 Square integrable field spaces

The space $L^2(\Omega)$ of square integrable scalar fields on Ω and the space $\boldsymbol{L}^2(\Omega)$ of square integrable vector fields on Ω are defined by

$$L^2(\Omega) = \Big\{ u : \int_\Omega u^2(\boldsymbol{x}) \, d\boldsymbol{x} < \infty \Big\}, \tag{A.3}$$

$$\boldsymbol{L}^2(\Omega) = \Big\{ \boldsymbol{u} : \int_\Omega \|\boldsymbol{u}(\boldsymbol{x})\|^2 \, d\boldsymbol{x} < \infty \Big\}, \tag{A.4}$$

where $\boldsymbol{x}$ is a point of space, $d\boldsymbol{x}$ a volume element and $\|\boldsymbol{u}(\boldsymbol{x})\|$ represents the Euclidean norm of $\boldsymbol{u}(\boldsymbol{x})$. These spaces are Hilbert spaces and can welcome physical fields, characterized by a finite energy. The scalar product of two elements of $L^2(\Omega)$ and $\boldsymbol{L}^2(\Omega)$ is defined by

$$(u, v)_\Omega = \int_\Omega u(\boldsymbol{x}) \, v(\boldsymbol{x}) \, d\boldsymbol{x} \quad \text{and} \quad (\boldsymbol{u}, \boldsymbol{v})_\Omega = \int_\Omega \boldsymbol{u}(\boldsymbol{x}) \cdot \boldsymbol{v}(\boldsymbol{x}) \, d\boldsymbol{x}. \tag{A.5}$$

The norm of an element $u \in L^2(\Omega)$ and $\boldsymbol{u} \in \boldsymbol{L}^2(\Omega)$ is defined by

$$\|u\|_{L^2(\Omega)} = (u, u)_\Omega^{1/2} = \Big[\int_\Omega u^2(\boldsymbol{x}) \, d\boldsymbol{x} \Big]^{1/2}, \tag{A.6}$$

$$\|\boldsymbol{u}\|_{\boldsymbol{L}^2(\Omega)} = (\boldsymbol{u},\boldsymbol{u})_\Omega^{1/2} = \Big[\int_\Omega \|\boldsymbol{u}(\boldsymbol{x})\|^2\, d\boldsymbol{x}\Big]^{1/2}. \tag{A.7}$$

The following notation is also introduced for integrals over a surface Γ:

$$\langle u, v\rangle_\Gamma = \int_\Gamma u(\boldsymbol{x})\, v(\boldsymbol{x})\, d\boldsymbol{x} \quad \text{and} \quad \langle \boldsymbol{u}, \boldsymbol{v}\rangle_\Gamma = \int_\Gamma \boldsymbol{u}(\boldsymbol{x}) \cdot \boldsymbol{v}(\boldsymbol{x})\, d\boldsymbol{x}. \tag{A.8}$$

The notations introduced in this section are used throughout this work. The parenthesis notation will thus always denote a scalar product of its arguments.

A.2.4 Sobolev spaces

The Sobolev spaces of scalar fields $H^1(\Omega)$ and vector fields $\boldsymbol{H}^1(\Omega)$ are defined by

$$H^1(\Omega) = \Big\{u \in L^2(\Omega) : \partial_x u, \partial_y u, \partial_z u \in L^2(\Omega)\Big\}, \tag{A.9}$$

$$\boldsymbol{H}^1(\Omega) = \Big\{\boldsymbol{u} \in \boldsymbol{L}^2(\Omega) : \partial_x \boldsymbol{u}, \partial_y \boldsymbol{u}, \partial_z \boldsymbol{u} \in \boldsymbol{L}^2(\Omega)\Big\}, \tag{A.10}$$

where the space derivatives have to be understood in the sense of distributions [37]. These two spaces are thus respectively subspaces of $L^2(\Omega)$ and $\boldsymbol{L}^2(\Omega)$, for which all first order partial derivatives are also square integrable.

In the same way, one can define the Sobolev spaces $H^p(\Omega)$ and $\boldsymbol{H}^p(\Omega)$, $\forall p > 1$:

$$H^p(\Omega) = \Big\{u \in H^{p-1}(\Omega) : \partial_x u, \partial_y u, \partial_z u \in H^{p-1}(\Omega)\Big\}, \tag{A.11}$$

$$\boldsymbol{H}^p(\Omega) = \Big\{\boldsymbol{u} \in \boldsymbol{H}^{p-1}(\Omega) : \partial_x \boldsymbol{u}, \partial_y \boldsymbol{u}, \partial_z \boldsymbol{u} \in \boldsymbol{H}^{p-1}(\Omega)\Big\}. \tag{A.12}$$

Note that if we define the **grad** operator in Cartesian coordinates for scalar fields f in $C^1(\Omega)$ as

$$\mathbf{grad}\, f = (\partial_x f, \partial_y f, \partial_z f)^T, \tag{A.13}$$

it follows that $H^1(\Omega) = H(\mathbf{grad}; \Omega)$:

$$H(\mathbf{grad}; \Omega) = \big\{u \in L^2(\Omega) : \mathbf{grad}\, u \in \boldsymbol{L}^2(\Omega)\big\}. \tag{A.14}$$

A.2.5 Stream function spaces and flux spaces

Much effort has been spent on devising finite element schemes for variational problems in the Sobolev spaces $H^1(\Omega)$ and $H^2(\Omega)$. Yet, other spaces of vector valued functions, based on the "incomplete" differential operators from vector analysis **curl** and div, are of importance in many physical problems, and in particular for Maxwell's equations.

To begin with, we recall the classical definition of the **curl** and div operators for vector fields $\boldsymbol{f} = (f_x, f_y, f_z)^T$ in $\boldsymbol{C}^1(\Omega)$:

$$\mathbf{curl}\, \boldsymbol{f} = (\partial_y f_z - \partial_z f_y, \partial_z f_x - \partial_x f_z, \partial_x f_y - \partial_y f_x)^T, \tag{A.15}$$

$$\operatorname{div} \boldsymbol{f} = \partial_x f_x + \partial_y f_y + \partial_z f_z. \tag{A.16}$$

Note that these operators have also to be understood in the sense of distributions, as the formal adjoints of the **grad** and **curl** operators respectively (see section A.3). Based on these concepts of weak **curl** and div, we define the Hilbert spaces of stream functions and fluxes:

$$\boldsymbol{H}(\mathbf{curl};\Omega) = \left\{\boldsymbol{u} \in \boldsymbol{L}^2(\Omega) : \mathbf{curl}\,\boldsymbol{u} \in \boldsymbol{L}^2(\Omega)\right\}, \tag{A.17}$$

$$\boldsymbol{H}(\operatorname{div};\Omega) = \left\{\boldsymbol{u} \in \boldsymbol{L}^2(\Omega) : \operatorname{div}\boldsymbol{u} \in L^2(\Omega)\right\}. \tag{A.18}$$

A.2.6 de Rham complexes

Since we have $\mathbf{grad}\, H^1(\Omega) \subset \boldsymbol{H}(\mathbf{curl};\Omega)$, $\mathbf{curl}\,\boldsymbol{H}(\mathbf{curl};\Omega) \subset \boldsymbol{H}(\operatorname{div};\Omega)$ and $\operatorname{div}\boldsymbol{H}(\operatorname{div};\Omega) \subset L^2(\Omega)$, or, equivalently, $\mathcal{R}(\mathbf{grad}) \subset \mathcal{D}(\mathbf{curl})$, $\mathcal{R}(\mathbf{curl}) \subset \mathcal{D}(\operatorname{div})$, and $\mathcal{R}(\operatorname{div}) \subset L^2(\Omega)$, the spaces $H^1(\Omega)$, $\boldsymbol{H}(\mathbf{curl};\Omega)$, $\boldsymbol{H}(\operatorname{div};\Omega)$ and $L^2(\Omega)$ form a complex:

$$H^1(\Omega) \xrightarrow{\mathbf{grad}} \boldsymbol{H}(\mathbf{curl};\Omega) \xrightarrow{\mathbf{curl}} \boldsymbol{H}(\operatorname{div};\Omega) \xrightarrow{\operatorname{div}} L^2(\Omega) \tag{A.19}$$

If $\Omega = \mathbb{E}^3$, one has $\mathcal{R}(\mathbf{grad}) = \mathcal{NS}(\mathbf{curl})$ and $\mathcal{R}(\mathbf{curl}) = \mathcal{NS}(\operatorname{div})$, and the sequence (A.19) is said to be exact. In this case, the image of $H^1(\mathbb{E}^3)$ in $\boldsymbol{H}(\mathbf{curl};\mathbb{E}^3)$ by the **grad** operator is exactly the kernel of the **curl** operator, which means that all curl-free fields are gradients. In the same way, the image of $\boldsymbol{H}(\mathbf{curl};\mathbb{E}^3)$ in $\boldsymbol{H}(\operatorname{div};\mathbb{E}^3)$ by the **curl** operator is exactly the kernel of the div operator, which means that all divergence-free fields can be expressed as the **curl** of some other field.

If Ω is a bounded set of $\mathbb{E}^3$, as it is the case in this work, the sequence is not exact any more, except for trivial topologies (for example if Ω is simply connected). The study of the "defects of exactness" is the basis of the theory of cohomology, closely related to the theory of homology by de Rham's theorem [149,131]. The only (simple) results of homology and cohomology that will be exploited in this work are presented in sections 1.2.1 and 1.3.1 respectively.

A.2.7 Affine spaces

Let E be a vector space on a field K, and let A be a nonempty set. For any $p \in A$ and $x \in E$ we define an addition $p + x \in A$. If the addition fulfills the following properties (for $p, q \in A$ and $x, y \in E$):

1. $p + 0 = p$,
2. $(p + x) + y = p + (x + y)$,
3. for any q in A, there exists a unique vector x in E such that $q = p + x$,

then A is an affine space. The dimension of A is the same as the dimension of E.

A.3 Strong and weak solutions

Let L be a differential operator of order n defined on Ω. The operator L^* (of order n) is the adjoint of L if one can write, $\forall u \in \mathcal{D}(L)$ and $\forall v \in \mathcal{D}(L^*)$:

$$(Lu, v)_\Omega - (u, L^* v)_\Omega = \int_\Gamma Q(u, v) ds, \tag{A.20}$$

where Q is a bilinear function of u and v and in their derivatives up to the order $n-1$. This expression is the generalized Green relation. Note that an operator is called self-adjoint if $L = L^*$.

Let us now consider two differential operators L and B, and let f and g be two functions defined on Ω and Γ respectively. If u is an unknown function defined on $\bar{\Omega}$, the partial derivative problem

$$Lu = f \text{ in } \Omega \tag{A.21}$$

$$Bu = g \text{ in } \Gamma \tag{A.22}$$

constitutes what is called a strong formulation. A function u that verifies this problem is called a strong solution. A weak formulation of the same problem is defined as being of the form

$$(u, L^* v)_\Omega - (f, v)_\Omega + \int_\Gamma Q_g(v)\, ds = 0, \quad \forall v \in V(\Omega), \tag{A.23}$$

where L^* is defined by (A.20), where Q_g is a linear form in v which depends on g and where the space $V(\Omega)$ is a space of test functions (which we have to define in accordance with L^*). A function u that satisfies (A.23) for all test functions $v \in V(\Omega)$ is called a weak solution. The generalized Green formula (A.20) can be applied to (A.23) in order to switch from L^* to L, which is in general equivalent to performing an integration by parts.

Two particular cases of the generalized Green relation (A.20) are extensively used in this work: the **grad**-div and **curl-curl** Green formulas. Let u be a function of $\Omega \mapsto \mathbb{R}$ and $\boldsymbol{v}$ a function of $\Omega \mapsto \mathbb{E}^3$. Integrating the following vector analysis formula

$$\boldsymbol{v} \cdot \mathbf{grad}\, u + u \operatorname{div} \boldsymbol{v} = \operatorname{div}(u\boldsymbol{v}) \tag{A.24}$$

over Ω, and applying the divergence theorem, we obtain the Green formula of type **grad**-div, $\forall \boldsymbol{v} \in \boldsymbol{H}^1(\Omega)$ and $\forall u \in H^1(\Omega)$:

$$(\boldsymbol{v}, \mathbf{grad}\, u)_\Omega + (\operatorname{div} \boldsymbol{v}, u)_\Omega = \langle u, \boldsymbol{n} \cdot \boldsymbol{v} \rangle_\Gamma. \tag{A.25}$$

Let $\boldsymbol{w}$ be a function of $\Omega \mapsto \mathbb{E}^3$. Proceeding in the same way as for the Green formula of type **grad**-div, but with the formula

$$\boldsymbol{v} \cdot \mathbf{curl}\, \boldsymbol{w} - \boldsymbol{w} \cdot \mathbf{curl}\, \boldsymbol{v} = \operatorname{div}(\boldsymbol{w} \times \boldsymbol{v}), \tag{A.26}$$

we obtain the Green formula of type **curl-curl**, $\forall \boldsymbol{v}, \boldsymbol{w} \in \boldsymbol{H}^1(\Omega)$:

$$(\boldsymbol{v}, \mathbf{curl}\, \boldsymbol{w})_\Omega - (\mathbf{curl}\, \boldsymbol{v}, \boldsymbol{w})_\Omega = \langle \boldsymbol{v} \times \boldsymbol{n}, \boldsymbol{w} \rangle_\Gamma. \tag{A.27}$$

Appendix B

Analytic integration

B.1 Thin shells

Let us consider an infinitely wide structure Ω_t, with thickness d, permeability μ and conductivity σ, immersed in a time-harmonic magnetic field of angular frequency ω (see Figure B.1). The permeability and conductivity of the material are assumed to be independent of the value of the local electromagnetic fields. It is also assumed that displacement currents can be neglected compared to conduction currents (see Section 1.4.2). Under these hypotheses, Maxwell's equations (1.16) and (1.17) can be rewritten, in harmonic regime, as

$$\mathbf{curl}\,\mathbf{curl}\,\boldsymbol{h} = -i\omega\sigma\mu\,\boldsymbol{h} \quad \text{and} \quad \mathbf{curl}\,\mathbf{curl}\,\boldsymbol{e} = -i\omega\sigma\mu\,\boldsymbol{e}. \tag{B.1a,b}$$

Let us for example consider the equation involving the magnetic field, written in Cartesian coordinates (see Figure B.1). Due to the symmetry of the problem, all derivatives with respect to x and y vanish, as well as the z-component of the field. Equation (B.1a) thus simply amounts to two one-dimensional equations (the components of the magnetic field being completely uncoupled):

$$\frac{\partial^2 h_x}{\partial z^2} = i\omega\sigma\mu\,h_x \quad \text{and} \quad \frac{\partial^2 h_y}{\partial z^2} = i\omega\sigma\mu\,h_y. \tag{B.2a,b}$$

Posing $\gamma^2 = i\omega\sigma\mu$, (B.2a) can be rewritten as

$$\frac{\partial^2 h_x}{\partial z^2} = \gamma^2 h_x, \tag{B.3}$$

with

$$\gamma = \frac{1+i}{\delta} \quad \text{and} \quad \delta = \sqrt{\frac{2}{\omega\sigma\mu}}. \tag{B.4}$$

The general solution of (B.3) is

$$h_x(z) = A\exp^{-\gamma z} + B\exp^{\gamma z}, \tag{B.5}$$

where the two constants A and B are determined thanks to the boundary conditions

$$h_x(d/2) = h_x^+ \quad \text{and} \quad h_x(-d/2) = h_x^-. \tag{B.6}$$

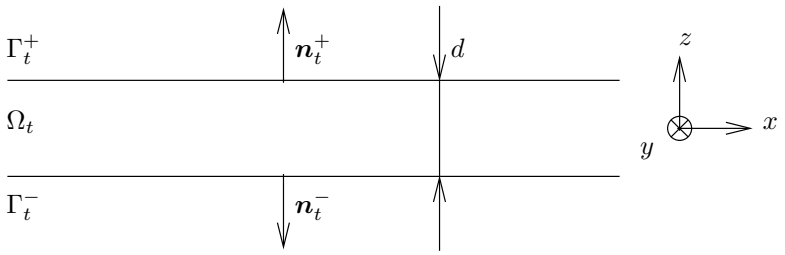

Figure B.1: Infinitely wide region Ω_t of finite thickness d

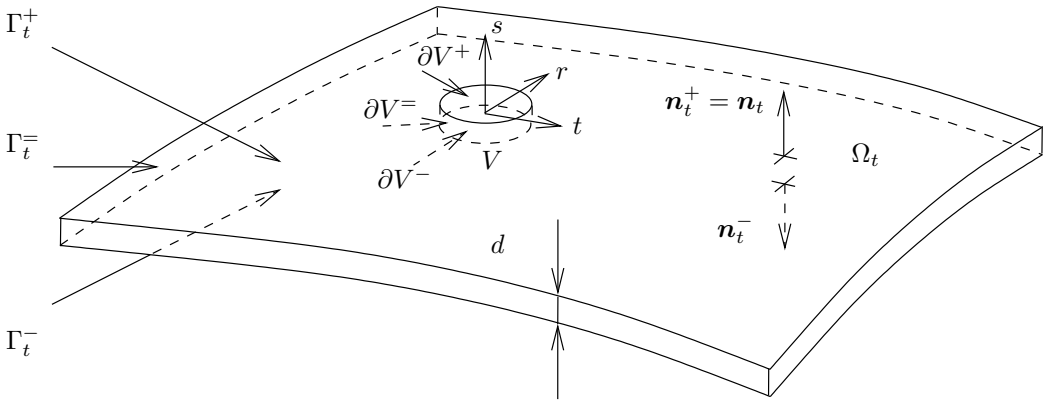

Figure B.2: Thin shell Ω_t

After some elementary calculations, (B.5) becomes

$$h_x(z) = \frac{1}{\sinh(\gamma d)}\Big[h_x^- \sinh\big(\gamma(d/2 - z)\big) + h_x^+ \sinh\big(\gamma(d/2 + z)\big)\Big]. \tag{B.7}$$

The solution of (B.2b) is, of course, similar.

Let us now consider the actual case of a finite width thin shell. The thin shell hypothesis is as follows: if $\Omega_{t,i}$ is sufficiently thin and locally sufficiently flat, the magnetic field still has no component along the thickness of the shell, and the other components fulfill relations similar to (B.7). If we denote the tangential component $\boldsymbol{n} \times (\boldsymbol{f} \times \boldsymbol{n})$ of a field $\boldsymbol{f}$ on a surface of normal $\boldsymbol{n}$ by $\boldsymbol{f}_t$, we can define a local coordinate system (r, s, t) whose t coordinate is chosen in the same direction as the tangential component $\boldsymbol{f}_t$, and whose s component is directed along the thickness of the shell (see Figure B.2). If we assume the thin shell hypothesis to hold, the

component t of the magnetic field $\boldsymbol{h}$ can then be written inside the shell as

$$\boldsymbol{h}_t(s) = \frac{1}{\sinh(\gamma d)}\Big[\boldsymbol{h}_t\big|_{\Gamma_t^-}\sinh\big(\gamma(d/2-s)\big) + \boldsymbol{h}_t\big|_{\Gamma_t^+}\sinh\big(\gamma(d/2+s)\big)\Big]. \tag{B.8}$$

Since the electric field fulfills the same equation as the magnetic field (see (B.1)), one also has

$$\boldsymbol{e}_t(s) = \frac{1}{\sinh(\gamma d)}\Big[\boldsymbol{e}_t\big|_{\Gamma_t^-}\sinh\big(\gamma(d/2-s)\big) + \boldsymbol{e}_t\big|_{\Gamma_t^+}\sinh\big(\gamma(d/2+s)\big)\Big]. \tag{B.9}$$

We should now look for a relation linking the traces $\boldsymbol{n}\times\boldsymbol{h}$ and $\boldsymbol{n}\times\boldsymbol{e}$ of the magnetic and electric fields on both sides of Ω_t.

Let us consider a magnetic field $\boldsymbol{h}$ whose only non-zero component is directed along t. Integrating (1.17) over the elementary volume V of boundary $\partial V = \partial V^+ \cup \partial V^- \cup \partial V^=$ (see Figure B.2), we get, assuming that the area of ∂V^+ and ∂V^- is equal to a:

$$\int_V \mathbf{curl}\,\boldsymbol{h}\,dV = \int_V \boldsymbol{j}\,dV = \sigma a\int_{-d/2}^{d/2}\boldsymbol{e}_t(s)\,ds = \sigma a\frac{1}{\gamma}\tanh\big(\frac{\gamma d}{2}\big)(\boldsymbol{e}_t\big|_{\Gamma_t^-} + \boldsymbol{e}_t\big|_{\Gamma_t^+}). \tag{B.10}$$

Since $\int_V \mathbf{curl}\,\boldsymbol{h} = \int_{\partial V^+}\boldsymbol{n}_t^+\times\boldsymbol{h} + \int_{\partial V^-}\boldsymbol{n}_t^-\times\boldsymbol{h}$, we thus locally have

$$\boldsymbol{n}_t^+\times\boldsymbol{h}\big|_{\Gamma_t^+} + \boldsymbol{n}_t^-\times\boldsymbol{h}\big|_{\Gamma_t^-} = \sigma\frac{1}{\gamma}\tanh\big(\frac{\gamma d}{2}\big)(\boldsymbol{e}_t\big|_{\Gamma_t^-} + \boldsymbol{e}_t\big|_{\Gamma_t^+}). \tag{B.11}$$

Analogously, considering an electric field $\boldsymbol{e}$ whose only non-zero component is directed along t and integrating (1.16) over the elementary volume V, we get

$$\boldsymbol{n}_t^+\times\boldsymbol{e}\big|_{\Gamma_t^+} + \boldsymbol{n}_t^-\times\boldsymbol{e}\big|_{\Gamma_t^-} = -i\omega\mu\frac{1}{\gamma}\tanh\big(\frac{\gamma d}{2}\big)(\boldsymbol{h}_t\big|_{\Gamma_t^-} + \boldsymbol{h}_t\big|_{\Gamma_t^+}). \tag{B.12}$$

If we define a single field of normals $\boldsymbol{n}_t = \boldsymbol{n}_t^+ = -\boldsymbol{n}_t^-$ for the thin shell Ω_t and if we define

$$\beta = \frac{1}{\gamma}\tanh\big(\frac{\gamma d}{2}\big), \tag{B.13}$$

(B.11) and (B.12) can finally be written as

$$\boldsymbol{n}_t\times\boldsymbol{h}\,\big|_{\Gamma_t^+} - \boldsymbol{n}_t\times\boldsymbol{h}\,\big|_{\Gamma_t^-} = \sigma\beta\,(\boldsymbol{e}_t\big|_{\Gamma_t^+} + \boldsymbol{e}_t\big|_{\Gamma_t^-}), \tag{B.14}$$

$$\boldsymbol{n}_t\times\boldsymbol{e}\,\big|_{\Gamma_t^+} - \boldsymbol{n}_t\times\boldsymbol{e}\,\big|_{\Gamma_t^-} = -\partial_t\big[\mu\beta\,(\boldsymbol{h}_t\big|_{\Gamma_t^+} + \boldsymbol{h}_t\big|_{\Gamma_t^-})\big]. \tag{B.15}$$

Equations (1.20) and (1.21) are the relations we are looking for. They are often called the impedance boundary conditions for the thin shell Ω_t [152, 11, 114]. It is interesting to notice that if γd is small, (B.13) simplifies to

$$\beta = \frac{d}{2}, \tag{B.16}$$

and the magnetic and electric fields vary linearly along the thickness of the shell.

B.2 Singular kernels

The integration of the volume and surface terms encountered in all the formulations of Chapter 3 is an important aspect in the practical implementation of the computer code (see Appendix D). When the integrands are regular (when they contain no Green functions, they are polynomials of relatively low orders), the integration can be handled efficiently by a Gauss formula, with a number of evaluation points depending on the polynomial order of the integrand [64]. However, integrals with singular or quasi-singular kernels appear in all hybrid formulations. The approach we follow is classical: the exterior integral (which arises with all the Galerkin formulations as well as some de Rham formulations—see Appendix C) is treated with a Gauss formula, while the interior integration is performed either analytically for constant shape functions (see e.g. [184]), or numerically for higher order shape functions (see [96, 46]). For the two-dimensional case presented in Appendix C, the analytic developments are given in [80].

Appendix C

Discretization of sources of integral operators

C.1 Introduction

The discrete form of the hybrid formulations established in Chapter 3 is commonly obtained thanks to the Galerkin or the collocation technique, sometimes leading to numerical difficulties like slow convergence or oscillations in particular coupling configurations [104]. We have shown in [209,88] that the dualism of electromagnetism is not yet fully exploited and understood in constructing numerical approaches for field computation, especially when it concerns techniques using integral operators, and that significant improvements can be obtained by expressing the integral equations in terms of equivalent sources and by paying extra attention to the discretization of these sources. This chapter presents a summary of the observations made in [209,88], and justifies the choice of the schemes applied in Chapter 3 for the discretization of the integral parts of the hybrid finite element formulations. For details about the special case of purely integral (i.e. non-hybrid) formulations, not studied in this thesis, and for the comparison of these integral schemes with and without the introduction of equivalent sources, please refer to [209].

To avoid the topological problems introduced by three-dimensional analyzes, we consider a simple magnetostatic problem in the two-dimensional Euclidean space $\mathbb{E}^2$. The magnetostatic field, described with the flux density $\boldsymbol{b}$ and the field strength $\boldsymbol{h}$, fulfills

$$\mathbf{curl}\,\boldsymbol{h} = \boldsymbol{j}, \quad \operatorname{div}\boldsymbol{b} = 0 \quad \text{and} \quad \boldsymbol{b} = \mu\boldsymbol{h}, \tag{C.1}$$

where $\boldsymbol{j}$ is the source current density and $\mu = \mu_0\mu_r = \mu_0(1+\chi)$ is the magnetic permeability (see Section 1.4.1). Furthermore, both field quantities $\boldsymbol{b}$ and $\boldsymbol{h}$ should vanish to infinity.

An equivalent way to express problem (C.1) is to introduce the potential a such that $\boldsymbol{b} = \mathbf{1}_z \times \mathbf{grad}\,a$ and to impose

$$\Delta a = -\mu_0 j_z + \operatorname{div}\frac{\chi}{\mu_r}\,\mathbf{grad}\,a. \tag{C.2}$$

As $\operatorname{div}\chi/\mu_r\,\mathbf{grad}\,a$ can be identified with a magnetic current generating the same

magnetic field as magnetization, (C.2) can be recognized as a standard Poisson equation where the right hand side represents the source terms. Here, the sources are the current density j_z and the equivalent magnetization current. This observation will be a key point when developing hybrid schemes using integral operators for the solution of problem (C.1).

At the discrete level the main question will be: how should the source terms be discretized? Traditionally, not much attention is paid to this issue. We will show that, by exploiting the dualism in electromagnetism, more robust numerical approaches can be found.

C.2 Interior Hybrid Formulation (FEM-IEM)

Let $\Omega \subset \mathbb{E}^2$ be a bounded domain whose boundary is denoted by Γ. Domain Ω is considered to be open and to contain all the magnetic materials as well as the source currents. The boundary Γ is assumed to be smooth and the outward pointing normal is named $\boldsymbol{n}$.

Let τ be a smooth curve drawn perpendicularly through Γ from the interior of Ω onto the exterior space, and which is parametrized by $t \in [-1, 1]$ such that $\tau(t)$ is the boundary point and $\|\partial_t \tau\big|_{t=0}\| = 1$. We shall denote by

$$\partial_{\boldsymbol{n}}^{-} a = \lim_{t \to 0^-} \frac{\partial a(\tau(t))}{\partial t}, \tag{C.3}$$

$$\partial_{\boldsymbol{n}}^{+} a = \lim_{t \to 0^+} \frac{\partial a(\tau(t))}{\partial t} \tag{C.4}$$

the interior and exterior normal derivatives on the boundary Γ respectively. The field defined by the bilinear integral operator

$$\mathcal{A}^i(\rho, \sigma) = \boldsymbol{x} \mapsto \int_\Omega \rho \, \ln |\boldsymbol{x} - \boldsymbol{y}| \, d\boldsymbol{y} + \int_\Gamma \sigma \, \ln |\boldsymbol{x} - \boldsymbol{y}| \, d\boldsymbol{y} \tag{C.5}$$

fulfills the following conditions [205]:

$$\Delta \mathcal{A}^i = \rho \quad \text{in} \quad \Omega, \tag{C.6}$$

$$\partial_{\boldsymbol{n}}^{-} \mathcal{A}^i = \partial_{\boldsymbol{n}} \mathcal{A}^i + \frac{1}{2}\sigma, \quad \partial_{\boldsymbol{n}}^{+} \mathcal{A}^i = \partial_{\boldsymbol{n}} \mathcal{A}^i - \frac{1}{2}\sigma \quad \text{in} \quad \Gamma. \tag{C.7}$$

One should notice that the integrals in (C.5) are singular, but due to the weak singularity it is still possible to define $\Delta \mathcal{A}^i$ within Ω and $\partial_{\boldsymbol{n}} \mathcal{A}^i$ on the boundary Γ. Equations (C.7) imply that the normal derivative is not continuous over the boundary. However, $\partial_{\boldsymbol{n}} \mathcal{A}^i$ has a definite value on the boundary Γ although it does not coincide with the limits from inside to outside and from outside to inside.

The idea is now to search for the solution of the magnetostatic problem in the form

$$a = \mathcal{A}^i(\rho_s + \rho, \sigma), \tag{C.8}$$

by requiring the proper boundary conditions to hold on Γ. We know that within Ω

$$\operatorname{div} \frac{1}{\mu} \mathbf{grad}\, a = -j_z \tag{C.9}$$

has to hold, and on Γ the continuity conditions of the magnetic field imply

$$\frac{1}{\mu^-} \partial_{\boldsymbol{n}}^- a - \frac{1}{\mu^+} \partial_{\boldsymbol{n}}^+ a = 0. \tag{C.10}$$

What remains to do is to set the right conditions for the source terms. From (C.2), we have

$$\rho_s = -\mu_0 j_z, \quad \text{and} \quad \rho = \operatorname{div} \frac{\chi}{\mu_r} \mathbf{grad}\, a. \tag{C.11}$$

From (C.7) and (C.10) we have

$$(1+\mu_r)\sigma = 2\chi \partial_{\boldsymbol{n}} \mathcal{A}^i(\rho_s + \rho, \sigma), \tag{C.12}$$

assuming that $\mu^+ = \mu_0$.

The magnetostatic field given in (C.1) can thus be characterized by

$$a = \mathcal{A}^i(\rho_s + \rho, \sigma), \tag{C.13}$$

$$\rho_s = -\mu_0 j_z, \quad \rho = \operatorname{div} \frac{\chi}{\mu_r} \mathbf{grad}\, a, \quad \sigma = \frac{2\chi}{1+\mu_r} \partial_{\boldsymbol{n}} a. \tag{C.14}$$

In order to express the boundary conditions of the finite element method implicitly, we will take advantage of the fact that the potential on Γ can be expressed with the aid of the integral operator given in (C.13). This integral operator depends only on what happens inside Ω and on Γ. With this consideration in mind, we can build the interior hybrid formulations, which will lead to the FEM-IEM formulations after discretization.

C.2.1 Dirichlet

Let t denote the trace operator on Γ. Applying the following bijective operator (where $\bar{\Omega}$ represents the closure of Ω)

$$\mathrm{t} \times \Delta : H^1(\bar{\Omega}) \to H^1(\Gamma) \times L^2(\Omega) \tag{C.15}$$

to (C.13), and using (C.6), we get

$$\mathrm{t}a = \mathrm{t}\mathcal{A}^i(\rho - \mu_0 j_z, \sigma), \tag{C.16}$$

$$\Delta a = -\mu_0 j_z + \operatorname{div} \frac{\chi}{\mu_r} \mathbf{grad}\, a. \tag{C.17}$$

Equations (C.16) and (C.17), together with source equations (C.14), constitute the interior Dirichlet hybrid formulation with equivalent sources. For the establishment of the standard hybrid Dirichlet formulation (without equivalent sources), see e.g. [127].

C.2.2 Neumann

The interior Neumann hybrid formulation with equivalent sources is obtained by applying the bijective operator (where $\boldsymbol{x}_0$ is a point on Γ)

$$\mathrm{t} \times \partial_{\boldsymbol{n}} \times \Delta : H^1(\bar{\Omega}) \to H^1(\boldsymbol{x}_0) \times \boldsymbol{H}(\mathbf{curl}; \Gamma) \times L^2(\Omega) \tag{C.18}$$

to (C.13). The part $\mathrm{t} : H^1(\bar{\Omega}) \to H^1(\boldsymbol{x}_0)$ of this operator is needed to keep it bijective (it is the ordinary gauge condition required to impose a unique solution for a). Using (C.6), we get

$$a(\boldsymbol{x}_0) = 0, \quad \partial_{\boldsymbol{n}} a = \partial_{\boldsymbol{n}} \mathcal{A}^i(\rho - \mu_0 j_z, \sigma), \tag{C.19}$$

$$\Delta a = -\mu_0 j_z + \operatorname{div} \frac{\chi}{\mu_r} \mathbf{grad}\, a. \tag{C.20}$$

The source terms given in (C.14), (C.19) and (C.20) together form the interior Neumann problem. The corresponding formulation without equivalent sources can, for example, be found in [72, 127].

C.3 Exterior Hybrid Formulation (FEM-BEM)

Instead of working from inside Ω toward the boundary as in Section C.2, one can also work from outside Ω toward the boundary. Therefore, let us now denote by Γ the boundary of $\mathbb{E}^2 - \Omega$. The exterior normal n is now pointing outside from $\mathbb{E}^2 - \Omega$, i.e. into Ω. The field defined by the integral operator

$$\mathcal{A}^e(0, \sigma) = \boldsymbol{x} \mapsto \int_\Gamma \sigma \, \ln |\boldsymbol{x} - \boldsymbol{y}| \, d\boldsymbol{y} \tag{C.21}$$

fulfills the following conditions:

$$\Delta \mathcal{A}^e = 0 \quad \text{in} \quad \mathbb{E}^2 - \Omega, \tag{C.22}$$

$$\partial_{\boldsymbol{n}}^+ \mathcal{A}^e = \partial_{\boldsymbol{n}} \mathcal{A}^e + \frac{1}{2}\sigma, \;\; \partial_{\boldsymbol{n}}^- \mathcal{A}^e = \partial_{\boldsymbol{n}} \mathcal{A}^e - \frac{1}{2}\sigma \quad \text{in} \quad \Gamma. \tag{C.23}$$

If the solution in the exterior domain is given by

$$a = \mathcal{A}^e(0, \sigma) \quad \text{in} \quad \mathbb{E}^2 - \Omega, \tag{C.24}$$

then one can show [15, 19] that on boundary Γ and within Ω hold

$$\partial_{\boldsymbol{n}} a = \partial_{\boldsymbol{n}} \mathcal{A}^e(0, \sigma), \tag{C.25}$$

$$\operatorname{div} \frac{1}{\mu} \mathbf{grad}\, a = -j_z. \tag{C.26}$$

Equations (C.24), (C.25) and (C.26) constitute the exterior hybrid formulation, which results in a FEM-BEM formulation after discretization. Note that, since a is the solution of the exterior Dirichlet problem, (C.25) is an application of the so-called Dirichlet-to-Neumann map (or Poincaré-Steklov operator [15, 19]). We do not look for a symmetric discrete approximation of this operator (see e.g. [184, 19, 113]).

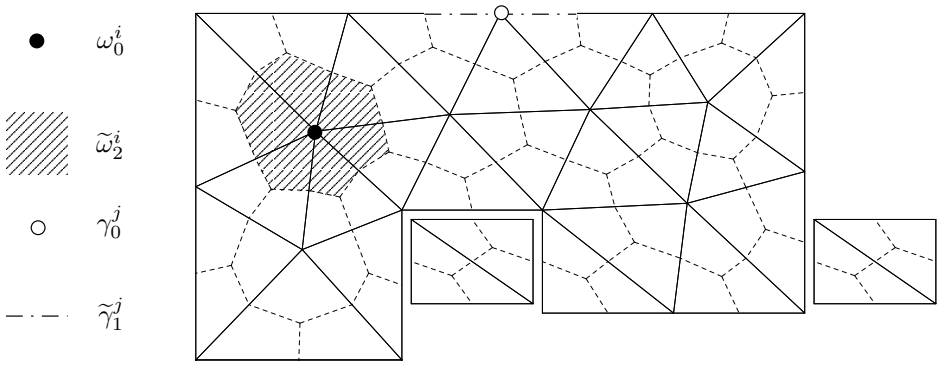

Figure C.1: A two-dimensional example of primal and dual meshes.

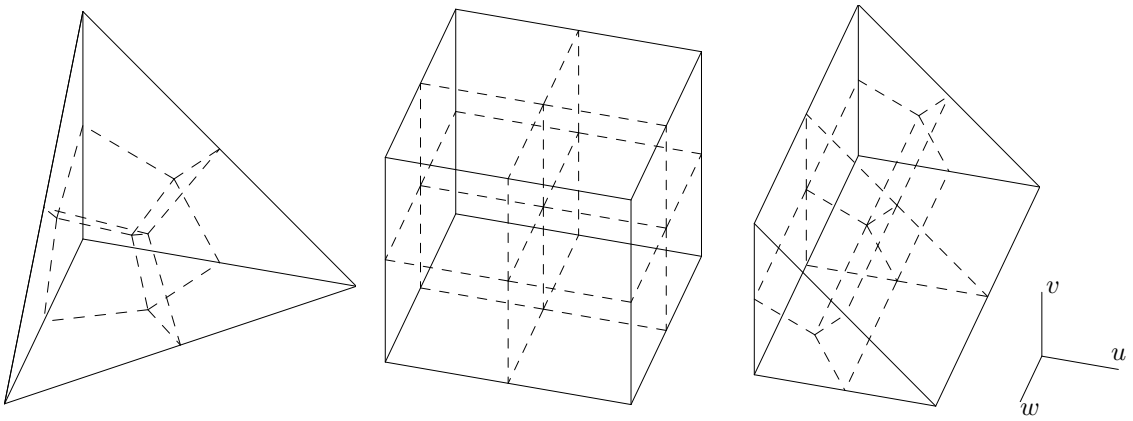

Figure C.2: Dual entities in the reference three-dimensional elements.

C.4 Discretization

We consider a triangulation of Ω (called the primal mesh) and its dual counterpart obtained by barycentric subdivision (see Figure C.1) [20]. The discretization of the hybrid formulations is based on the following principle: if we choose to associate the field (here the potential a) with the primal mesh, then the sources (ρ and σ) should be assigned to the dual mesh [209]. To show this, we should rewrite (C.2) in terms of differential forms [69], i.e.

$$\mathrm{d} * \mathrm{d}a = \mu_0 j_z + \mu_0 \mathrm{d}(\chi/\mu) * \mathrm{d}a,$$

where d represents the exterior derivative, and $*$ is the Hodge operator mapping p-forms to $(n-p)$-forms (where n is the dimension; here $n = 2$). At the discrete level the Hodge operator can be interpreted as a mapping between the primal and dual sides of the mesh, whereas the exterior derivative maps within the same side [208,20]. As a result, if a is a 0-form on the primal side, then $\rho = \mathrm{d} * \mathrm{d}a$ is a 2-form that should be on the dual side.

C.4.1 The Galerkin Method

The very idea of the Galerkin technique is to represent the potential a in a finite dimensional space and to impose the basic equations in the weak sense by exploiting the basis functions also as test functions. Obviously, the source terms ρ and σ need to be approximated in discrete spaces as well.

Here, as usual, the potential is expressed as $a = \sum_{i\in\mathcal{N}(\cdot)} a_i\lambda_i$, where $\mathcal{N}(\cdot)$ represents the set of nodes of its argument and λ_i is the conforming mixed element of degree 1 associated with the node i. The space spanned by the nodal elements is named W_1^0.

Since we do not have at our disposal mixed finite elements for the dual mesh, the sources need to be given with the aid of the primal side functions:

$$\rho = \sum_{i\in\mathcal{N}(\Omega)} \rho_i\,\lambda_i \quad \text{and} \quad \sigma = \sum_{i\in\mathcal{N}(\Gamma)} \sigma_i\,\mathrm{t}\lambda_i, \tag{C.27}$$

where $\mathrm{t}\lambda_i$ is the trace of λ_i on Γ. This choice differs from the classical approach followed e.g. in [192], and is guided by the expression of ρ and σ in terms of differential forms: $\rho = \sum_{i\in\mathcal{N}(\Omega)} \rho_i * \lambda_i$ and $\sigma = \sum_{i\in\mathcal{N}(\Gamma)} \sigma_i * \mathrm{t}\lambda_i$ (where the Hodge operator is associated with the inner product in Ω and Γ respectively) [209].

Equations (C.16) and (C.17) may now be imposed in the weak sense resulting in the following problem: find a such that $\forall a' \in W_1^0$

$$\int_\Gamma a\,a'\,d\boldsymbol{x} = \int_\Gamma \mathrm{t}\mathcal{A}(\rho - \mu_0 j_z, \sigma)\,a'\,d\boldsymbol{x}, \tag{C.28}$$

$$\int_\Omega \mu^{-1}\mathbf{grad}\,a\cdot\mathbf{grad}\,a'\,d\boldsymbol{x} = -\int_\Omega j_z\,a'\,d\boldsymbol{x} \tag{C.29}$$

hold.

In the same manner (C.19) and (C.20) result in the weak problem: find a such that $\forall a' \in W_1^0$

$$\int_\Gamma \partial_{\boldsymbol{n}} a\,a'\,d\boldsymbol{x} = \int_\Gamma \partial_{\boldsymbol{n}}\mathcal{A}^i(\rho - \mu_0 j_z, \sigma)\,a'\,d\boldsymbol{x}, \tag{C.30}$$

$$\int_\Omega \mu^{-1}\mathbf{grad}\,a\cdot\mathbf{grad}\,a'\,d\boldsymbol{x} = -\int_\Omega j_z\,a'\,d\boldsymbol{x} + \int_\Gamma \mu^{-1}\partial_{\boldsymbol{n}} a\,a'\,d\boldsymbol{x} \tag{C.31}$$

hold. Likewise, (C.25) and (C.26) result in finding a such that

$$\int_\Gamma \partial_{\boldsymbol{n}} a\,a'\,d\boldsymbol{x} = -\int_\Gamma \partial_{\boldsymbol{n}}\mathcal{A}^e(0,\sigma)\,a'\,d\boldsymbol{x} \tag{C.32}$$

and (C.31) hold for all $a' \in W_1^0$.

The next step is to discretize the source equations (C.14). By projecting the volume source term into W_1^0 and after integration by parts, we get

$$\int_\Omega \rho\,\rho'\,d\boldsymbol{x} = \int_\Omega \frac{\chi}{\mu_r}\mathbf{grad}\,a\cdot\mathbf{grad}\,\rho'\,d\boldsymbol{x} - \int_\Gamma \frac{\chi}{\mu_r}\partial_{\boldsymbol{n}} a\,\rho'\,d\boldsymbol{x}, \tag{C.33}$$

which should hold for all $\rho' \in W_1^0$. Discrete boundary sources are obtained in the same way. That is, for all $\sigma' \in W_1^0$ should hold

$$\int_\Gamma \sigma\, \sigma'\, d\boldsymbol{x} = \int_\Gamma \frac{2\chi}{1+\mu_r} \partial_{\boldsymbol{n}} a\, \sigma'\, d\boldsymbol{x} \tag{C.34}$$

in the case of the interior formulations, or

$$\int_\Gamma a\, \sigma'\, d\boldsymbol{x} = \int_\Gamma \mathcal{A}^e(0,\sigma)\, \sigma'\, d\boldsymbol{x} \tag{C.35}$$

in the case of the exterior formulation.

C.4.2 The de Rham Map

Another possibility to discretize the hybrid formulations is to employ the de Rham map [208, 209], which is a generalization of the collocation technique (see [208, 20] for the relation between Galerkin and dual mesh de Rham approaches in the case of partial differential finite element methods). We define the primal (respectively dual) de Rham map as an integration operator that, when applied to a p-form f, returns a real number for each p-cell (i.e. node, edge and face for $p = 0, 1, 2$) of the primal (respectively dual) mesh:

$$(\mathcal{C}f)_i = \int_{\omega_p^i} f\, d\boldsymbol{x} \quad \text{and} \quad (\widetilde{\mathcal{C}}f)_i = \int_{\widetilde{\omega}_p^i} f\, d\boldsymbol{x}, \tag{C.36}$$

where ω_p^i is the ith p-cell of the mesh of Ω and where $\widetilde{\omega}_p^i$ is the dual counterpart of ω_{n-p}^i. To be concise, we denote by γ_p^i and $\widetilde{\gamma}_p^i$ the primal and dual cells paving Γ (now with $p = 0, 1$). See Figure C.1 for a graphical illustration of these definitions.

Equations (C.16) and (C.17) are imposed by applying the de Rham map (and the Stokes theorem: ∂ denotes the boundary operator and $\boldsymbol{n}'$ the exterior normal to this boundary): find a such that for all nodes and all 2-cells of the mesh hold

$$\int_{\gamma_0^i} a\, d\boldsymbol{x} = \int_{\gamma_0^i} \mathrm{t}\mathcal{A}(\rho - \mu_0 j_z, \sigma)\, d\boldsymbol{x}, \tag{C.37}$$

$$\int_{\partial\widetilde{\omega}_2^i} \boldsymbol{n}' \cdot \mu^{-1} \mathbf{grad}\, a\, d\boldsymbol{x} = -\int_{\widetilde{\omega}_2^i} j_z\, d\boldsymbol{x}. \tag{C.38}$$

In the same manner (C.19) and (C.20) lead to the following problem: find a such that for all 1- and 2-cells of the mesh hold

$$\int_{\widetilde{\gamma}_1^i} \partial_{\boldsymbol{n}} a\, d\boldsymbol{x} = \int_{\widetilde{\gamma}_1^i} \partial_{\boldsymbol{n}} \mathcal{A}^i(\rho - \mu_0 j_z, \sigma)\, d\boldsymbol{x}, \tag{C.39}$$

$$\int_{\partial\widetilde{\omega}_2^i} \boldsymbol{n}' \cdot \mu^{-1} \mathbf{grad}\, a\, d\boldsymbol{x} = -\int_{\widetilde{\omega}_2^i} j_z\, d\boldsymbol{x} + \int_{\widetilde{\gamma}_1^i} \mu^{-1} \partial_{\boldsymbol{n}} a\, d\boldsymbol{x}. \tag{C.40}$$

Likewise, (C.25) and (C.26) result in finding a such that for all 1- and 2-cells of the mesh hold [208]

$$\int_{\widetilde{\gamma}_1^i} \partial_{\boldsymbol{n}} a \, d\boldsymbol{x} = - \int_{\widetilde{\gamma}_1^i} \partial_{\boldsymbol{n}} \mathcal{A}^e(0, \sigma) \, d\boldsymbol{x} \tag{C.41}$$

and (C.40).

The final step is to discretize the source equations by applying the dual de Rham map to (C.14). For all 2-cells should hold

$$\int_{\widetilde{\omega}_2^i} \rho \, d\boldsymbol{x} = \int_{\partial\widetilde{\omega}_2^i} \boldsymbol{n}' \cdot \frac{\chi}{\mu_r} \mathbf{grad}\, a \, d\boldsymbol{x} - \int_{\widetilde{\gamma}_1^i} \frac{\chi}{\mu_r} \partial_{\boldsymbol{n}} a \, d\boldsymbol{x}, \tag{C.42}$$

while for all boundary 1-cells or boundary nodes should hold

$$\int_{\widetilde{\gamma}_1^i} \sigma \, d\boldsymbol{x} = \int_{\widetilde{\gamma}_1^i} \frac{2\chi}{1+\mu_r} \partial_{\boldsymbol{n}} a \, d\boldsymbol{x} \quad \text{or} \quad \int_{\gamma_0^i} a \, d\boldsymbol{x} = \int_{\gamma_0^i} \mathcal{A}^e(0, \sigma) \, d\boldsymbol{x}. \tag{C.43}$$

C.5 Numerical Tests

We consider a simple two-dimensional magnetostatic problem: the so-called C-dipole magnet [72]. Figure C.3 illustrates one of the numerical problems mentioned in the introduction, as well as the advantage of locating sources on the dual mesh. It is interesting to notice that the ordinary solution to the problem encountered when locating the sources on the primal mesh in exterior hybrid formulations is to perform the FEM-BEM coupling not directly on the boundary of magnetic materials, but by locating Γ in the air, at a distance from any magnetic materials [104, 192].

Figure C.4 displays the convergence of different discretization schemes when the mesh is refined. All schemes are applied with two variations: first with the sources discretized in the classical way, then with the sources discretized by taking the duality into account. From this figure it can be seen that the classical exterior hybrid formulation (the exterior Galerkin formulation with primal mesh located sources) does not converge, whereas the interior Neumann formulations seem to converge only very slowly. Furthermore, for this two-dimensional problem, the de Rham-based schemes globally seem to behave better than their Galerkin counterparts. Be aware that, from Figure C.4, one should not conclude that interior formulations are preferable to exterior ones: the discretized operator in the FEM-IEM coupling is less sparse than in the FEM-BEM coupling, so that the overall computing time (for the same number of elements) is significantly higher. One should also keep in mind that the number of elements in the finite element reference computation totalizes the elements necessary to mesh a portion of air around the magnet and a geometrically transformed region (which is needed to take into account the extension of the fields toward infinity [164]).

These considerations permit to select the discretization schemes for the family of hybrid formulations presented in Chapter 3. Other combinations of the proposed discretization schemes could also be studied, since each scheme could be applied to the field and the source equations separately. For example, an approach combining

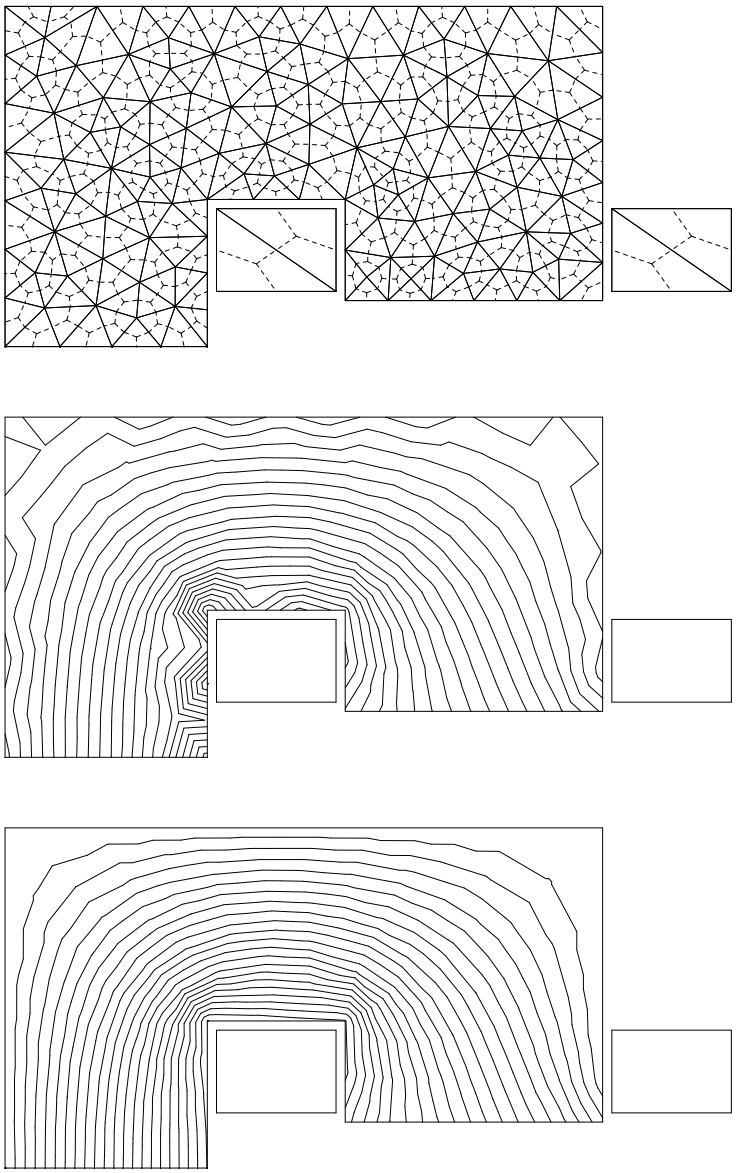

Figure C.3: Field lines obtained with the exterior hybrid formulation, with sources located on primal (middle) and dual (bottom) meshes.

the Galerkin technique for the partial differential equation part and a de Rham map for the integral equation would lead to a generalization of the well-known FEM-BEM approach with collocation.

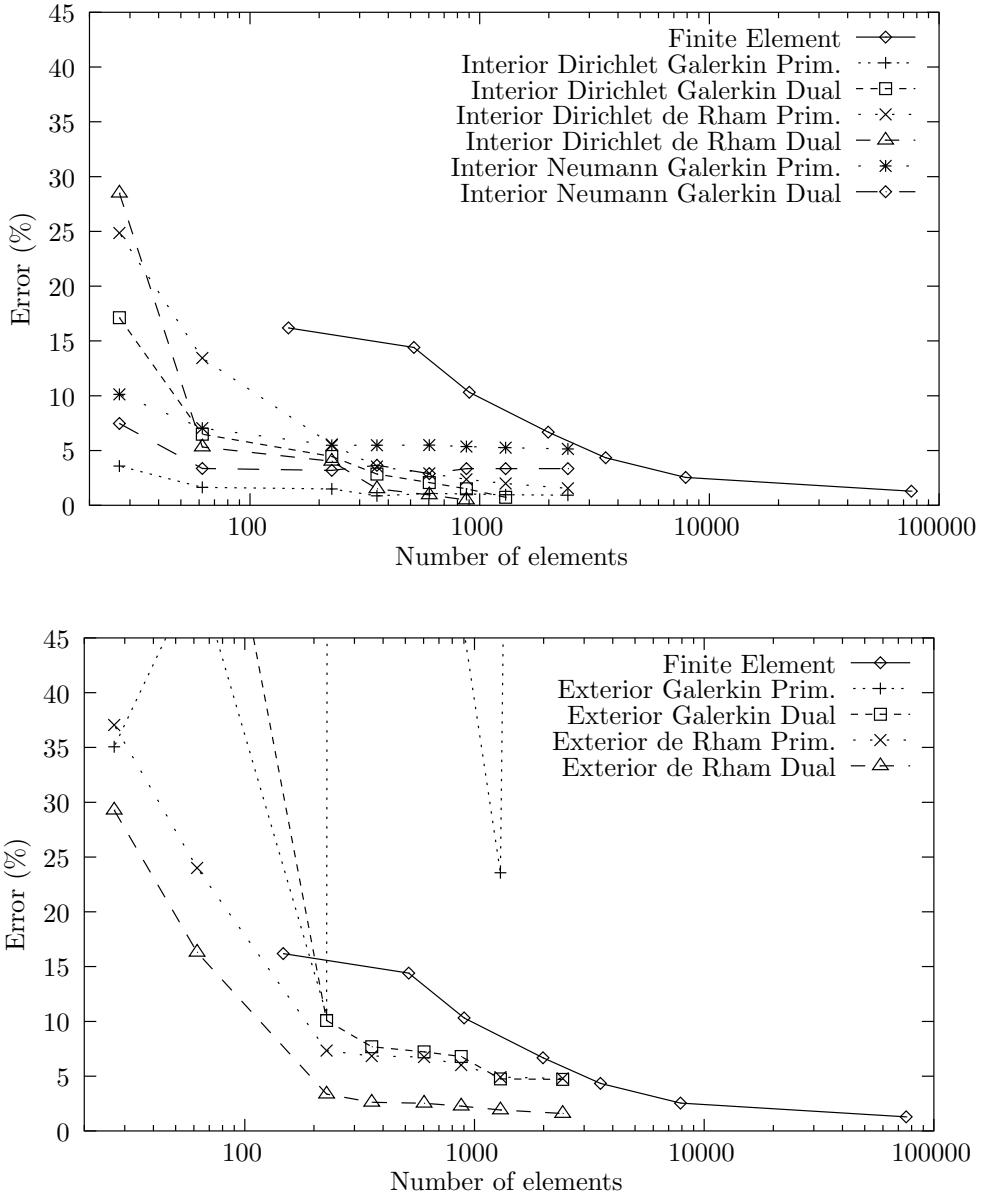

Figure C.4: Global error on the energy versus number of elements in the mesh for a selection of interior (top) and exterior (bottom) hybrid formulations. "Prim." and "Dual" indicate whether the sources are located on the primal or on the dual mesh.

Appendix D

Practical implementation

Two original computer codes have been developed, which implement the methods described in this thesis. The purpose of this appendix is to present the philosophy behind these software tools. They have both been designed with an overall aim of generality, to provide versatile tools for the solution of coupled discrete problems arising in multi-physic simulations without compromising performance or accuracy.

Both environments are available on the Internet [77, 91] in order to give a free alternative to commercial software for collaborative research. They aim at this goal by providing transparent access to all implemented methods through dedicated languages.

D.1 GetDP

D.1.1 Introduction

The first software project, called GetDP (a General environment for the treatment of Discrete Problems [53, 59, 51, 50, 81, 78]) and realized in collaboration with P. Dular, benefits from the experience gathered in the Department of Electrical Engineering of the University of Liège for the last decade, and provides an original approach to the implementation of weighted residual methods. GetDP is open to the coupling of physical problems (electromagnetic, thermal, mechanical, acoustic, etc.) as well as of numerical methods (finite element method, integral methods, etc.) and can deal with such problems of various dimensions (1D, 2D or 3D) and time states (static, transient or harmonic). Its main feature is the closeness between its internal structure, the organization of data defining discrete problems (written by the user in ASCII text data files) and the symbolic mathematical expressions of these problems. Its aim is to be welcoming and of easy use at both development and application levels: it consists of a general working environment in which the definition of any problem makes use of a limited number of elements (ten objects, briefly described in the next section), which makes the environment structured and concise.

Besides the high order hybrid finite element formulations presented in this work [209, 88, 87, 178, 180], their application to the modeling of thin structures [82, 83]

and their coupling with global quantities [86, 52, 54, 57, 49], GetDP has been successfully used for both research collaborations and industrial projects. A non-exhaustive list of research subjects includes: inductive heating processes [59] (and in particular the optimization of the thixoforming of steels [174]), electromagnetic wave propagation around antennas [85], eigenvalue problems in non-homogeneous waveguides [98], rotating machines [48, 67], multi-harmonic simulations [100], piezoelectric devices, etc. Many practical engineering problems have also been solved in the same environment by researchers in several countries: for the computation of electromagnetic fields in low and high frequency shielding problems, in the vicinity of high voltage towers or underground cables, in breakers and cable junctions; for magnet optimization in magnetrons; for the computation of thermal effects in breakers; for the computation of acoustic waves in the vicinity of inductors; etc.

This generality could only be achieved thanks to the tight closeness ensured between the mathematical formulation of the problem, its description by means of the dedicated language (analyzed by Lex and Yacc [143]) and the corresponding internal data structure, which forms a reduced-size kernel written in ANSI C [124]. This kernel contains neither a geometrical pre-processor (and a fortiori no graphical interface), nor linear algebra routines: the mesh generation and the visualization of the results are relegated to other software tools (like Gmsh, described in Section D.2), and the computationally intensive linear algebra code (all matrix and vector operations, as well as all linear solvers) is transparently interfaced with dedicated toolkits (GetDP does not specify any vector or matrix formats, but relies on dedicated functions in the linear algebra toolkits to particularize its generic access methods). For example, GetDP can be linked with SPARSKIT [203] or with PETSc [167] in order to achieve high computational efficiency either sequentially or in distributed computing environments (in this case with the help of appropriate partitioning tools, like e.g. Metis [123]). There is thus no particular multi-processor version of GetDP: the sequential version of the software is simply a special case of the more general parallel implementation.

The next section briefly defines the objects that have to be constructed by the users in ASCII text files in order to set up the definition of discrete problems. We intentionally do not present any syntax (see [78] for this, or [51, 81] for a concise summary): the goal is to show how all the techniques involved in modern finite element-type methods prove advantageous when defined as interdependent general objects with evolutionary possibilities.

D.1.2 Working philosophy

The resolution of a discrete problem with GetDP requires the definition, in a text data file, of the GetDP objects listed (together with their dependences) in Table D.1 and Figure D.1. The gathering of all these objects constitutes the problem definition structure, which is a copy of the formal mathematical formulation of the problem. Reading the first column of the table from top to bottom pictures the working philosophy and the linking of operations peculiar to GetDP, from the definition of groups to the visualization of results.

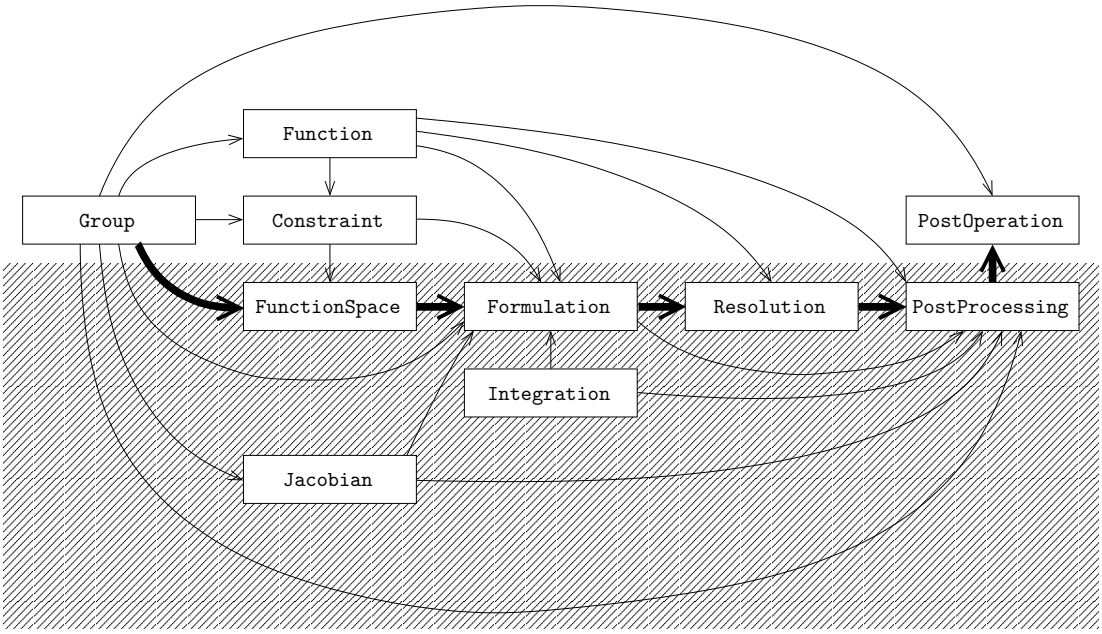

Figure D.1: Objects and dependences. The decomposition points out the separation between the objects defining the method of resolution, which may be isolated in a "black box" (bottom) and those defining the data peculiar to a given problem (top).

Table D.1: Objects and dependences.

`Group`	—
`Function`	`Group`
`Constraint`	`Group`, `Function`, (`Resolution`)
`FunctionSpace`	`Group`, `Constraint`, (`Formulation`), (`Resolution`)
`Jacobian`	`Group`
`Integration`	—
`Formulation`	`Group`, `Function`, (`Constraint`), `FunctionSpace`, `Jacobian`, `Integration`
`Resolution`	`Function`, `Formulation`
`PostProcessing`	`Group`, `Function`, `Jacobian`, `Integration`, `Formulation`, `Resolution`
`PostOperation`	`Group`, `PostProcessing`

The computational tools which are at the center of a problem definition structure are formulations (`Formulation`) and function spaces (`FunctionSpace`). Formulations define the equations that have to be solved, while function spaces contain the discrete approximations of all the quantities involved in formulations, i.e. fields of vectors or co-vectors, as well as the associated constraints.

Each object of a problem definition structure must be defined before being referred to by others. A linking which always respects this property is

the following: it first contains the objects defining particular data of a problem, such as geometry, physical characteristics and boundary conditions (i.e. `Group`, `Function` and `Constraint`) followed by those defining a resolution method, such as unknowns, equations and related objects (i.e. `Jacobian`, `Integration`, `FunctionSpace`, `Formulation`, `Resolution` and `PostProcessing`). The processing cycle ends with the presentation of the results (i.e. lists of numbers in various formats), defined in `PostOperation` fields. Note that this decomposition points out the possibility of building black boxes, containing objects of the second group, adapted to treatments of defined problems (see Figure D.1).

Each of these objects makes an abundant use of the basic tool of GetDP: expressions. These cover a wide range of functional expressions, from constants to formal expressions containing functions (built-in or user-defined, depending on space coordinates and on time, etc.), arguments, discrete quantities and their associated differential operators, etc. A brief description of the ten objects is given hereafter.

`Group`: defining topological entities

> Besides the file containing the definition of the problem structure, a file containing a mesh must be specified. This mesh file contains a list of nodes (with their coordinates) and a list of geometrical elements with, for each one, a number characterizing its geometrical type (i.e. line, triangle, quadrangle, tetrahedron, hexahedron, prism, etc.), a number indicating the physical region to which it belongs and the list of its nodes.
>
> Groups of geometrical entities of various types can be defined, based on this mesh, and are used in many objects. There are region groups, of which the entities are regions (and used for example as the support for piece-wise defined functions, or as domains of integration), and function groups which define lists of geometrical entities (e.g. nodes for nodal elements, edges for edge elements, edges of tree for gauge conditions, groups of nodes for floating potentials, elements on one side of a surface for cuts, etc.).

`Function`: defining global and piece-wise expressions

> A function can be global in space or piece-wise defined in region groups. A physical characteristic is an example of a piece-wise defined function (e.g. magnetic permeability, electric conductivity, etc.) and can be simply a constant, for linear materials, or a function of one or several arguments for nonlinear materials. Such functions can of course depend on space coordinates or time, which can be necessary to express complex constraints.

`Constraint`: specifying constraints on function spaces and formulations

> Constraints can be referred to in `FunctionSpace` objects to be used for boundary or initial conditions, to impose global quantities, etc. These constraints can be expressed with functions or be imposed by the resolution of another discrete problem. Other types of constraints can be defined as well, e.g. constraints of network type for the definition of circuit connections, to be used in `Formulation` objects.

`FunctionSpace`: building function spaces

A `FunctionSpace` is characterized by the type of its interpolated fields, by one or several basis functions and by optional constraints (in space and time). Subspaces of a function space can be defined (e.g. for the use with hierarchical elements), as well as direct associations of global quantities (e.g. floating potential, electric charge, current, voltage, magnetomotive force, etc.).

A key point is that basis functions are defined by any number of subsets of functions, being added. Each subset is characterized by associated built-in functions for evaluation, a support of definition and a set of associated supporting geometrical entities (e.g. nodes, edges, faces, volumes, groups of nodes, edges incident to a node, etc.). The freedom in defining various kinds of basis functions, associated with different geometrical entities permits to build made-to-measure function spaces adapted to a wide variety of field approximations.

`Jacobian`: defining Jacobian methods

Jacobian methods can be referred to in `Formulation` and `PostProcessing` objects to be used in the computation of integral terms and for changes of coordinates. They are based on `Group` objects and define the geometrical transformations applied to the reference elements (i.e. lines, triangles, quadrangles, tetrahedra, prisms, hexahedra, etc.). Besides the classical line, surface and volume Jacobians, the `Jacobian` object allows the construction of various transformation methods (e.g. axisymmetric transformation or infinite transformations for unbounded domains) thanks to dedicated Jacobian methods.

`Integration`: defining integration methods

Various numerical or analytical integration methods (see Section B.2) can be referred to in `Formulation` and `PostProcessing` objects to be used in the computation of integral terms, each with a set of particular options (number of integration points for quadrature methods, definition of transformations for singular integrations, etc.). The choice between several integration methods can be made according to user-defined criteria (e.g. on the interpolation order, on an error estimation, on the proximity between the source and computation points in integral formulations, etc.).

`Formulation`: building equations

The `Formulation` tool permits to deal with volume, surface and line integrals as well as with the punctual evaluation of many kinds of densities, written in a form that is similar to their symbolic expression (it uses the same expression syntax as elsewhere in GetDP). This permits to take various kinds of elementary matrices directly into account (e.g. with scalar or cross products, anisotropies, nonlinearities, time derivatives, various test functions, etc.). In case nonlinear physical characteristics are considered, arguments are simply used for associated functions. In that way many formulations can be directly written in the data file, just as they are written symbolically. Fields involved

in each formulation are declared as belonging to beforehand defined function spaces. The uncoupling between formulations and function spaces allows to maintain a generality in both their definitions.

A `Formulation` is characterized by its type (for example a finite element method), the involved quantities (of local, global or integral type) and a list of local or global equation terms.

`Resolution`: solving systems of equations

The `Resolution` object defines all the operations to be performed on the equations specified in a set of formulations, in order to obtain a solution to the discrete problem. These operations may comprise: the generation of a linear system and its solving with a given linear solver (which is independent of GetDP, see Section D.1), the saving of the solution or its transfer to another resolution, the definition of a time stepping method (e.g. a theta scheme or the Newmark algorithm), the construction of iterative loops for nonlinear problems (e.g. Newton-Raphson or fixed point methods), the computation of a Fourier transform, etc. Multi-harmonic resolutions, coupled problems (e.g. magneto-thermal-mechanical) or chained problems (e.g. pre-computations of source fields) are thus easily defined in GetDP.

`PostProcessing`: exploiting computational results

The `PostProcessing` object is based on the quantities defined in a `Formulation` and permits the construction, with the same expression mechanism as elsewhere in GetDP, of any piece-wise defined quantity of interest.

`PostOperation`: exporting results

The `PostOperation` is the bridge between results obtained with GetDP and the external world. It defines several elementary operations on `PostProcessing` quantities (e.g. evaluation on a region, cut on a user-defined plane, etc.), and outputs the results in several file formats.

For a complete definition of all these objects and examples showing how to define the formulations developed in this work, see [81, 78, 77].

D.2 Gmsh

D.2.1 Introduction

As mentioned in the previous section, GetDP can be considered as a non-graphical kernel for the solving of weighted residual type problems. In order to perform mesh generation and adaptation, a side project has been developed in collaboration with J.-F. Remacle, which goal is to provide a simple three-dimensional mesh generator with parametric input and up-to-date visualization capabilities required

for fully three-dimensional analyzes. The resulting effort, called Gmsh, is an automatic three-dimensional mesh generator, primarily Delaunay, with built-in pre- and post-processing facilities. One of the strengths of Gmsh is its ability to respect a characteristic length field for the generation of adapted meshes on lines, surfaces and volumes. These adapted meshes can be mixed with simple structured meshes (extruded, transfinite, elliptic, hyperbolic) in order to augment the flexibility in the testing of methods for solving problems involving thin structures. All the meshes produced by Gmsh are conforming in the sense of finite element meshes (see Section 2.6.1).

As for GetDP, all geometrical, mesh, solver and post-processing instructions are prescribed in a language analyzed by Lex and Yacc [143]. The code itself is written in C++ [206], while the graphics are rendered with OpenGL [202, 166] and the user interface is based on the FLTK widget set [70].

D.2.2 Working philosophy

Gmsh is structured around four modules: geometry, mesh, solver and post-processing. The specification of any input to these modules is done either interactively, or in text data files (interactive specifications generate language bits in the input file, and vice versa). The accessibility of most features in the ASCII text file makes it possible to automate all treatments (loops, tests and external access methods permit advanced scripting capabilities). The internal kernel of Gmsh reflects this structure: it is built around a geometry, mesh, solver and post-processing database. It is interesting to notice that the data can be provided to these databases either in the native format or thanks to dynamically loadable modules (plug-ins). This is most interesting to convert CAD data from other description languages (e.g. DXF or STEP), to launch external applications from inside Gmsh (e.g. GetDP or other solvers) or to apply complex user-defined treatments to geometry, mesh or post-processing data. A brief description of the four modules is given hereafter.

`Geometry`: geometrical entity definition

> Geometries are created in a bottom-up flow by successively defining points, oriented curves (segments, circles, ellipses, splines, etc.), oriented surfaces (plane surfaces, ruled surfaces, etc.) and volumes. Compound groups of geometrical entities can be defined, based on these elementary parametrized geometric entities. The scripting possibilities (with loops, tests, arrays of variables, etc.) allow fully parametrized definitions of all geometrical entities.

`Mesh`: mesh generation

> The mesh generation is performed in the same order as the geometry creation: curves are discretized first; the mesh of the curves is then used to mesh the surfaces; then the mesh of the surfaces is used to mesh the volumes. This automatically assures the continuity of the mesh when, for example, two surfaces share a curve. Every meshing step is constrained by the characteristic

length field, which can be uniform, specified by a characteristic length associated with elementary geometrical entities, or associated with another mesh (the background mesh, which can for example be created with the elementary sizes resulting from the optimization procedures presented in Section 2.7).

For each meshing step (i.e. the discretization of lines, surfaces and volumes), all structured mesh directives are executed first, and serve as additional constraints for the unstructured parts. The implemented transfinite, elliptic and hyperbolic structured algorithms are e.g. described in [116], and can be combined with the extrusion of curve and surface meshes. The implemented Delaunay algorithm [75] is subdivided in the following five steps for surface/volume discretization:

1. trivial meshing of a box including the convex polygon/polyhedron defined by the boundary nodes resulting from the discretization of the curves/surfaces;
2. creation of the initial mesh by insertion of all the nodes on the curves/surfaces thanks to the Bowyer algorithm;
3. boundary restoration to force all the edges/faces of the curves/surfaces to be present in the initial mesh;
4. suppression of all the unwanted triangles/tetrahedra (in particular those containing the nodes of the initial box);
5. insertion of new nodes by the Bowyer algorithm until the characteristic size of each simplex is lower or equal to the characteristic length field evaluated at the center of its circumscribed circle/sphere.

Additional steps involve mesh smoothing and mesh quality enforcement. General considerations on the implementation can be found in [176, chapter 4].

`Solver`: external solver interface

External solvers can be interfaced with Gmsh through a socket mechanism, which permits to easily launch computations either locally or on remote computers, and to collect and exploit the simulation results within Gmsh. A common file format makes it possible to combine the output from the different solvers in order to perform various couplings (of physical problems and numerical methods) and opens the way to the implementation of various optimization procedures (which may depend on the geometrical or mesh parameters of the model through the integrated scripting language).

`Post-processing`: field visualization

Multiple post-processing scalar or vector maps can be loaded and manipulated (globally or individually) along with the geometry and the mesh. Scalar fields are represented by iso-value curves/surfaces or color maps and vector fields by three-dimensional arrows or displacement maps. Post-processing functions include arbitrary section computation, offset, elevation, boundary extraction,

color map and range modification, animation, vector graphic output [90], etc. All post-processing options can be accessed either interactively or through the input ASCII text files. Scripting permits to automate all the post-processing operations (e.g. for the creation of complex animations).

For a complete description of Gmsh as well as for examples, see [91].

Bibliography

[1] A. Ahagon, K. Fujiwara, and T. Nakata, *Comparison of various kinds of edge elements for electromagnetic field analysis*, IEEE Transactions on Magnetics **32** (1996), no. 3, 898–901.

[2] R. Albanese and R. Fresa, *Upper and lower bounds for local electromagnetic quantities*, International Journal for Numerical Methods in Engineering **42** (1998), 499–515.

[3] R. Albanese, R. Fresa, and G. Rubinacci, *Local error bounds for static and stationary fields*, IEEE Transactions on Magnetics **36** (2000), no. 4, 1615–1618.

[4] R. Albanese and G. Rubinacci, *Integral formulation for 3D eddy-current computation using edge elements*, IEE Proceedings **135, Pt. A** (1988), no. 7, 457–462.

[5] ———, *Magnetostatic field computations in terms of two-component vector potentials*, International Journal for Numerical Methods in Engineering **29** (1990), 515–532.

[6] I. Babuska and B. Guo, *Direct and inverse approximation theorems for the p-version of the finite element method in the framework of weighted Besov spaces, Part II: Optimal rate of convergence of the p-version finite element solutions*, Technical report TICAM 99-32, Texas Institute for Computational and Applied Mathematics, University of Texas at Austin, September 1999.

[7] I. Babuska and W. C. Rheinboldt, *Adaptative approaches and reliability estimators in finite element analysis*, Journal of Computational Methods in Applied Mechanics and Engineering **17/18** (1979), 519–540.

[8] I. Babuska and M. Suri, *The p and hp versions of the finite element method, an overview*, Journal of Computational Methods in Applied Mechanics and Engineering **80** (1990), 5–26.

[9] S. Benhassine, W. P. Carpes, Jr., and L. Pichon, *Comparison of mass lumping techniques for solving the 3D Maxwell's equations in the time domain*, IEEE Transactions on Magnetics **36** (2000), no. 4, 1548–1552.

[10] J. Berenger, *A perfectly matched layer for the absorption of electromagnetic waves*, Journal of Computational Physics **114** (1994), no. 1, 185–200.

[11] O. Biró, I. Bárdi, K. Preis, W. Renhart, and K. R. Richter, *A finite element formulation for eddy current carrying ferromagnetic thin sheets*, IEEE Transactions on Magnetics **33** (1997), no. 2, 1173–1178.

[12] A. Bossavit, *Two dual formulations of the 3D eddy currents problem*, International Journal for Computation and Mathematics in Electrical and Electronic Engineering, COMPEL **4** (1984), 103–116.

[13] ———, *Magnetostatic problems in multiply connected regions: some properties of the curl operator*, IEE Proceedings **135, Pt. A** (1988), no. 3, 179–187.

[14] ———, *Whitney forms: a class of finite elements for three-dimensional computations in electromagnetism*, IEE Proceedings **135, Pt. A** (1988), no. 8, 493–499.

[15] ———, *Modèles et modélisation en électrotechnique*, Techniques de l'Ingénieur, Traité Généralité **A 1 207** (1989), 1–25.

[16] ———, *Un nouveau point de vue sur les éléments mixtes*, Bulletin de la Société de Mathématiques Appliquées et Industrielles **20** (1989), 23–35.

[17] ———, *Differential geometry for the student of numerical methods in electromagnetism*, Lecture notes, 1991.

[18] ———, *Électromagnétisme, en vue de la modélisation*, Springer-Verlag, 1993.

[19] ———, *Computational electromagnetism. Variational formulations, edge elements, complementarity*, Academic Press, 1998.

[20] ———, *How weak is the weak solution in finite element methods?*, IEEE Transactions on Magnetics **34** (1998), no. 5, 2429–2432.

[21] ———, *A rationale for "edge-elements" in 3-D fields computations*, IEEE Transactions on Magnetics **24** (1998), no. 1, 74–79.

[22] ———, *Generating Whitney forms of polynomial degree one and higher*, To appear in IEEE Transactions on Magnetics **38** (2002), no. 2.

[23] A. Bossavit, C. R. I. Emson, and I. D. Mayergoyz, *Méthodes numériques en électromagnétisme : Géométrie différentielle, éléments finis, modèles d'hystérésis*, Collection de la Direction des Études et Recherches d'Électricité de France, no. 76, Eyrolles, 1991.

[24] A. Bossavit and L. Kettunen, *Yee-like schemes on a tetrahedral mesh, with diagonal lumping*, International Journal of Numerical Modelling **12** (1999), 129–142.

[25] A. Bossavit and J.-C. Vérité, *A mixed FEM-BIEM method to solve 3D eddy current problems*, IEEE Transactions on Magnetics **18** (1982), no. 2, 431–435.

[26] _____, *The "TRIFOU" code: Solving the 3-D eddy-currents problem by using H as state variable*, IEEE Transactions on Magnetics **19** (1983), no. 6, 2465–2471.

[27] A. Bossavit, A. Vourdas, and K. J. Binns, *Correspondence on "magnetostatics with scalar potentials in multiply connected regions"*, IEE Proceedings **136, Pt. A** (1989), no. 5, 260–261.

[28] C. A. Brebbia and S. Walker, *Boundary element techniques in engineering*, Newnes-Butterworth, 1980.

[29] F. Brezzi and M. Fortin, *Mixed and hybrid finite element methods*, Springer-Verlag, 1991.

[30] X. Brunotte and G. Meunier, *Line element for efficient computation of the magnetic field created by thin iron plates*, IEEE Transactions on Magnetics **26** (1990), no. 5, 2196–2198.

[31] P. Carnevali, B. Morris, Y. Tsuji, and G. Taylor, *New basis functions and computational procedures for p-version finite element analysis*, International Journal for Numerical Methods in Engineering **36** (1993), 3759–3779.

[32] Z. J. Cendes, *Vector finite elements for electromagnetic field computation*, IEEE Transactions on Magnetics **27** (1991), no. 5, 3958–3966.

[33] K. C. Chellamuthu and N. Ida, *A posteriori element by element local error estimation technique and 2D & 3D adaptative finite element mesh refinement*, IEEE Transactions on Magnetics **30** (1994), no. 5, 3527–3530.

[34] M. Clemens and T. Weiland, *Transient eddy-current calculation with the FI-method*, IEEE Transactions on Magnetics **35** (1999), no. 3, 1163–1166.

[35] J.-L. Coulomb, F.-X. Zgainski, and Y. Maréchal, *A pyramidal element to link hexahedral, prismatic and tetrahedral edge finite elements*, IEEE Transactions on Magnetics **33** (1997), no. 2, 1362–1365.

[36] G. Dahlquist, A. Björck, and N. Anderson, *Numerical methods*, Prentice-Hall, 1974.

[37] R. Dautray and J.-L. Lions, *Analyse mathématique et calcul numérique pour les sciences et les techniques*, vol. 3, Transformations, Sobolev, Opérateurs, Masson, 1987.

[38] _____, *Analyse mathématique et calcul numérique pour les sciences et les techniques*, vol. 5, Spectres des Opérateurs, Masson, 1988.

[39] ———, *Analyse mathématique et calcul numérique pour les sciences et les techniques*, vol. 6, Méthodes intégrales et numériques, Masson, 1988.

[40] ———, *Mathematical analysis and numerical methods for science and technology*, Springer-Verlag, 1990.

[41] F. Delincé, *Modélisation des régimes transitoires dans les systèmes comportant des matériaux magnétiques non linéaires et hystérétiques*, Ph.D. thesis, University of Liège, Belgium, Faculty of Applied Sciences, December 1994.

[42] A. Demenko and J. K. Sykulski, *Network equivalents of nodal and edge elements in electromagnetics*, To appear in IEEE Transactions on Magnetics **38** (2002), no. 2.

[43] L. Demkowicz, P. Monk, L. Vardapetyan, and W. Rachowicz, *De Rham diagram for hp finite element spaces*, Technical report TICAM 99-06, Texas Institute for Computational and Applied Mathematics, University of Texas at Austin, March 1999.

[44] G. Dhatt and G. Touzot, *Une présentation de la méthode des éléments finis*, Maloine, 1981.

[45] D. Dibben and A. C. Metaxas, *Finite element time domain analysis of multimode applicators using edge elements*, Journal of Microwave Power and Electromagnetic Energy **29** (1994), no. 4, 242–251.

[46] K. C. Donepudi, J.-M. Jin, S. Velamparambil, J. Song, and W. C. Chew, *A higher order parallelized multilevel fast multipole algorithm for 3-D scattering*, IEEE Transactions on Antennas and Propagation **49** (2001), no. 7, 1069–1078.

[47] P. Dular, *Modélisation du champ magnétique et des courants induits dans des systèmes tridimensionnels non linéaires*, Ph.D. thesis 152, University of Liège, Belgium, Faculty of Applied Sciences, November 1994.

[48] P. Dular, M. V. Ferreira da Luz, C. Geuzaine, N. Sadowski, and J. P. A. Bastos, *Connection boundary conditions associated with different types of mixed finite elements with dual formulations*, COMPEL **20** (2001), no. 1, 109–119.

[49] P. Dular and C. Geuzaine, *Spatially dependent global quantities associated with 2D and 3D magnetic vector potential formulations for foil winding modeling*, To appear in IEEE Transactions on Magnetics **38** (2002), no. 2.

[50] P. Dular, C. Geuzaine, A. Genon, and W. Legros, *An evolutive software environment for teaching finite element methods in electromagnetism*, IEEE Transactions on Magnetics **35** (1999), no. 3, 1682–1685.

[51] P. Dular, C. Geuzaine, F. Henrotte, and W. Legros, *A general environment for the treatment of discrete problems and its application to the finite element method*, IEEE Transactions on Magnetics **34** (1998), no. 5, 3395–3398.

[52] P. Dular, C. Geuzaine, and W. Legros, *A natural method for coupling magnetodynamic h-formulations and circuit equations*, IEEE Transactions on Magnetics **35** (1999), no. 3, 1626–1629.

[53] P. Dular, F. Henrotte, C. Geuzaine, and W. Legros, *An open software environment for testing electromagnetic analysis methods*, Proceedings of the Sixth International TEAM Workshop (Rio de Janeiro, Brazil) (R. C. Mesquita, ed.), November 1997, pp. 55–57.

[54] P. Dular, F. Henrotte, and W. Legros, *A general and natural method to define circuit relations associated with magnetic vector potential formulations*, IEEE Transactions on Magnetics **35** (1999), no. 3, 1630–1633.

[55] P. Dular, F. Henrotte, F. Robert, A. Genon, and W. Legros, *A generalized source magnetic field calculation method for inductors of any shape*, IEEE Transactions on Magnetics **33** (1997), no. 2, 1398–1401.

[56] P. Dular, J.-Y. Hody, A. Nicolet, A. Genon, and W. Legros, *Mixed finite elements associated with a collection of tetrahedra, hexahedra and prisms*, IEEE Transactions on Magnetics **30** (1994), no. 5, 2980–2983.

[57] P. Dular, P. Kuo-Peng, C. Geuzaine, N. Sadowski, and J. P. A. Bastos, *Dual magnetodynamic formulations and their source fields associated with massive and stranded inductors*, IEEE Transactions on Magnetics **36** (2000), no. 4, 1293–1299.

[58] P. Dular, A. Nicolet, A. Genon, and W. Legros, *A discrete sequence associated with mixed finite elements and its gauge condition for vector potentials*, IEEE Transactions on Magnetics **31** (1995), no. 3, 1356–1359.

[59] P. Dular, A. Rassili, B. Meys, F. Henrotte, H. Hedia, A. Genon, and W. Legros, *A software environment for the treatment of discrete coupled problems and its application to magneto-thermal coupling*, Proceedings of the 4th International Workshop on Electric and Magnetic Fields, EMF'98 (Marseille, France), May 1998, pp. 547–552.

[60] P. Dular, N. Sadowski, and J. P. A. Bastos, *Dual complete procedures to take stranded inductors into account in magnetic vector potential formulations*, IEEE Transactions on Magnetics **36** (2000), no. 4, 1600–1605.

[61] E. Durand, *Magnétostatique*, Masson, 1968.

[62] *Electromagnetic compatibility panel session,* 13th Conference on the Computation of Electromagnetic Fields, COMPUMAG'2001 (Evian, France), July 2001.

[63] C. R. I. Emson and J. Simkin, *An optimal method for 3-D eddy currents*, IEEE Transactions on Magnetics **19** (1983), no. 6, 2450–2452.

[64] G. Evans, *Practical numerical integration*, John Wiley & Sons, 1993.

[65] M. Feliziani and F. Maradei, *Hybrid finite element solutions of time dependent Maxwell's curl equations*, IEEE Transactions on Magnetics **31** (1995), no. 3, 1330–1335.

[66] ———, *Edge element analysis of complex configurations in presence of shields*, IEEE Transactions on Magnetics **33** (1997), no. 2, 1548–1551.

[67] M. V. Ferreira da Luz, P. Dular, N. Sadowski, C. Geuzaine, and J. P. A. Bastos, *Analysis of a permanent magnet generator with dual formulations using periodicity conditions and moving band*, To appear in IEEE Transactions on Magnetics **38** (2002), no. 2.

[68] R. Feynman, R. Leighton, and M. Sands, *The Feynman lectures on physics*, Addison-Wesley, 1965.

[69] H. Flanders, *Differential forms with applications to the physical sciences*, Dover Publications, 1989.

[70] *FLTK, the fast light tool kit*, http://www.fltk.org.

[71] K. Forsman and L. Kettunen, *Hybrid and integral formulations for 3D eddy current problems*, IEEE Transactions on Magnetics **33** (1997), no. 2, 1255–1258.

[72] K. Forsman, L. Kettunen, and J.-P. Nuutinen, *Properties of b and h-type integral equation formulations*, IEEE Transactions on Magnetics **32** (1996), no. 3, 1421–1424.

[73] F. Gardiol, *Traité d'électricité*, Électromagnétisme Vol. III, Éditions Georgi, 1979.

[74] C. Garing, *Milieux magnétiques*, Ellipses, 1995.

[75] P. L. Georges and H. Borouchaki, *Triangulation de Delaunay et maillage*, Hermes, 1997.

[76] H. De Gersem and K. Hamayer, *A finite element model for foil winding simulation*, IEEE Transactions on Magnetics **37** (2001), no. 5, 3427–3432.

[77] *GetDP, a general environment for the treatment of discrete problems*, http://www.geuz.org/getdp/.

[78] *GetDP manual: the documentation for GetDP, a general environment for the treatment of discrete problems*, http://www.geuz.org/getdp/doc/texinfo/.

[79] C. Geuzaine, *Développement d'éléments finis nodaux et d'arête hiérarchiques 2D et 3D appliqués au problème des courants induits*, Graduate thesis, University of Liège, Belgium, Faculty of Applied Sciences, May 1996.

[80] ———, *Modélisation mathématique et numérique des blindages électromagnétiques*, Rapport de thèse F.R.I.A., 1ère bourse, 1ère année, University of Liège, Belgium, September 1997.

[81] C. Geuzaine, P. Dular, and W. Legros, *A general environment for coupled finite element and boundary integral methods*, Proceedings of the 8th International IGTE Symposium on Numerical Field Calculation in Electrical Engineering (Graz, Austria), September 1998, pp. 106–111.

[82] ———, *Dual formulations for the modeling of thin conducting magnetic shells*, COMPEL **18** (1999), no. 3, 385–397.

[83] C. Geuzaine, P. Dular, B. Meys, and W. Legros, *Dual formulations for the modeling of thin electromagnetic shells using edge elements*, IEEE Transactions on Magnetics **36** (2000), no. 4, 799–803.

[84] C. Geuzaine, P. Dular, B. Meys, W. Legros, J.-F. Remacle, and G. Deliége, *Error convergence of some classical high order curl-conforming finite elements*, Proceedings of the 4th International Workshop on Electric and Magnetic Fields, EMF'98 (Marseille, France), May 1998, pp. 373–378.

[85] C. Geuzaine, B. Meys, V. Beauvois, and W. Legros, *A FETD approach for the modeling of antennas*, IEEE Transactions on Magnetics **36** (2000), no. 4, 892–896.

[86] C. Geuzaine, B. Meys, P. Dular, F. Henrotte, and W. Legros, *A Galerkin projection method for mixed finite elements*, IEEE Transactions on Magnetics **35** (1999), no. 3, 1438–1441.

[87] C. Geuzaine, B. Meys, P. Dular, and W. Legros, *Convergence of high order curl-conforming finite elements*, IEEE Transactions on Magnetics **35** (1999), no. 3, 1442–1445.

[88] C. Geuzaine, T. Tarhasaari, L. Kettunen, and P. Dular, *Discretization schemes for hybrid methods*, IEEE Transactions on Magnetics **37** (2001), no. 5, 3112–3115.

[89] V. Girault and P. A. Raviart, *Finite element methods for Navier-Stokes equations*, Springer-Verlag, 1986.

[90] *Gl2ps: an OpenGL to PostScript printing library*, http://www.geuz.org/gl2ps/.

[91] *Gmsh, a three-dimensional mesh generator with built-in pre- and post-processing facilities*, http://www.geuz.org/gmsh/.

[92] N. A. Golias and T. D. Tsiboukis, *3D eddy-current computation with a self-adaptive refinement technique*, IEEE Transactions on Magnetics **31** (1995), no. 3, 2261–2268.

[93] N. A. Golias, T. D. Tsiboukis, and A. Bossavit, *Constitutive inconsistency: Rigorous solution of Maxwell equations based on a dual approach*, IEEE Transactions on Magnetics **30** (1994), no. 5, 3586–3589.

[94] C. Golovanov, Y. Maréchal, and G. Meunier, *3D edge element based formulation coupled to electric circuits*, IEEE Transactions on Magnetics **34** (1998), no. 5, 3162–3165.

[95] V. Gradinaru and R. Hiptmair, *Whitney elements on pyramids*, Electronic Transactions on Numerical Analysis **8** (1999), 154–168.

[96] R. Graglia, *On the numerical integration of the linear shape functions times the 3-D Green's function or its gradient on a plane triangle*, IEEE Transactions on Antennas and Propagation **41** (1993), no. 10, 1448–1455.

[97] H. J. Greenberg, *The determination of upper and lower bounds for the solution of the Dirichlet problem*, Journal of Mathematics and Physics **27** (1948), no. 3, 161–182.

[98] S. Guenneau, A. Nicolet, F. Zolla, C. Geuzaine, and B. Meys, *A finite element formulation for spectral problems in optical fibers*, COMPEL **20** (2001), no. 1, 120–131.

[99] C. Guérin, G. Tanneau, G. Meunier, P. Labie, T. Ngnegueu, and M. Sacotte, *A shell element for computing 3D eddy currents — application to transformers*, IEEE Transactions on Magnetics **31** (1995), no. 3, 1360–1363.

[100] J. Gyselinck, P. Dular, C. Geuzaine, and W. Legros, *Harmonic balance finite element modelling of electromagnetic devices: a novel approach*, To appear in IEEE Transactions on Magnetics **38** (2002), no. 2.

[101] R. F. Harrington, *Time-harmonic electromagnetic fields*, McGraw-Hill, 1961.

[102] Y. Haugazeau and P. Lacoste, *Condensation de la matrice masse pour les éléments finis mixtes de type H(rot)*, Comptes Rendus de l'Académie des Sciences Série I **316** (1993), no. 5, 509–512.

[103] H. Hedia, *Modélisation non linéaire des effets thermiques dans les systèmes magnétodynamiques*, Ph.D. thesis 176, University of Liège, Belgium, Faculty of Applied Sciences, February 1997.

[104] F. Henrotte, *Modélisation des efforts électromagnétiques et de leurs effets dans des structures quelconques*, Ph.D. thesis 201, University of Liège, Belgium, Faculty of Applied Sciences, February 2000.

[105] F. Henrotte, P. Dular, C. Geuzaine, H. Hedia, and W. Legros, *A general method to compute source fields without defining cuts nor using Biot-Savart*, Proceedings of the 4th International Workshop on Electric and Magnetic Fields, EMF'98 (Marseille, France), May 1998, pp. 361–366.

[106] ———, *An overall magnetic t-ω formulation without cuts*, Proceedings of the 8th Conference on Electromagnetic Field Computation, CEFC'98 (Tucson, USA), June 1998, p. 326.

[107] F. Henrotte, B. Meys, H. Hedia, P. Dular, and W. Legros, *Finite element modelling with transformation techniques*, IEEE Transactions on Magnetics **35** (1999), no. 3, 1434–1437.

[108] F. Hillion, *Remark on Maxwell's divergence equations*, International Journal for Computation and Mathematics in Electrical and Electronic Engineering, COMPEL **18** (1999), no. 1, 77–83.

[109] R. Hiptmair, *Multilevel preconditioning for mixed problems in three dimensions*, Ph.D. thesis, Universität Augsburg, Germany, 1996.

[110] ———, *Canonical construction of finite elements*, Mathematics of Computation **68** (1999), 1325–1346.

[111] ———, *Discrete hodge operators*, Technical report 126, SFB 382, Universität Tübingen, Germany, October 1999.

[112] ———, *Multigrid method for Maxwell's equations*, SIAM J. Numer. Anal. **36** (1999), 204–225.

[113] ———, *Symmetric coupling for eddy current problems*, Technical report 148, SFB 382, Universität Tübingen, Germany, March 2000.

[114] H. Igarashi, A. Kost, and T. Honma, *A three dimensional analysis of magnetic fields around a thin magnetic conductive layer using vector potential*, IEEE Transactions on Magnetics **34** (1998), no. 5, 2539–2542.

[115] J. D. Jackson, *Classical electrodynamics*, third ed., John Wiley & Sons, 1998.

[116] O.-P. Jacquotte, *Structured grid generation: Algebraic method, optimization and adaptation*, Lectures Series 1994-02, Von Karman Institute for Fluid Dynamics, 1994.

[117] R. Janssen, *Industrial requirements for electromagnetic field computation software*, International Compumag Society Newsletter **7** (2000), no. 2, 8–12.

[118] A. J. Jerri, *Introduction to integral equations with applications*, Pure and Applied Mathematics, Marcel Dekker, 1985.

[119] D. Jiles, *Magnetism and magnetic materials*, Chapman and Hall, 1991.

[120] C. Johnson, *Numerical solution of partial differential equations by the finite element method*, Cambridge University Press, 1987.

[121] A. Kameari, *Calculation of transient 3D eddy current using edge-elements*, IEEE Transactions on Magnetics **26** (1990), no. 2, 466–469.

[122] J. Kangas, A. Ahola, J. Keränen, and L. Kettunen, *Partial diagonalization of mass matrix*, To appear in IEEE Transactions on Magnetics **38** (2002), no. 2.

[123] G. Karypis, K. Schloegel, and V. Kumar, *PARMETIS: Parallel graph partitioning and sparse matrix ordering, version 2.0*, Tech. report, University of Minnesota / Army HPC Research Center Minneapolis, 1998.

[124] B. W. Kernighan and D. Ritchie, *The C programming language: ANSI C version*, Prentice-Hall, 1988.

[125] L. Kettunen, K. Forsman, and A. Bossavit, *Discrete spaces for div and curl-free fields*, IEEE Transactions on Magnetics **34** (1998), no. 5, 2551–2554.

[126] ———, *Gauging in Whitney spaces*, IEEE Transactions on Magnetics **35** (1999), no. 3, 1466–1469.

[127] L. Kettunen, K. Forsman, A. Koski, and T. Tarhasaari, *Integral operators in computational electromagnetics*, Proceedings of the 4th International Workshop on Electric and Magnetic Fields, EMF'98 (Marseille, France), May 1998, pp. 7–16.

[128] A. G. Kladas and J. A. Tegopoulos, *A new scalar potential formulation for 3-D magnetostatics necessitating no source field calculation*, IEEE Transactions on Magnetics **28** (1992), no. 2, 1103–1106.

[129] A. Kost, J. P. A. Bastos, K. Miethner, and L. Jänicke, *Improvement of nonlinear impedance boundary conditions*, To appear in IEEE Transactions on Magnetics **38** (2002), no. 2.

[130] A. Kost, L. Jänicke, K. Miethner, J. P. A. Bastos, N. Sadowski, and P. I. Koltermann, *Impedance boundary conditions for thin nonlinear shielding material*, Proceedings of the 9th Conference on Electromagnetic Field Computation, CEFC'2000 (Milwaukee, USA), June 2000, p. 367.

[131] P. R. Kotiuga, *Hodge decomposition and computational electromagnetics*, Ph.D. thesis, Mc Gill University, Montreal, 1984.

[132] ———, *On making cuts for magnetic scalar potentials in multiply connected regions*, Journal of Applied Physics **63** (1987), no. 8, 3916–3918.

[133] ———, *An algorithm to make cuts for magnetic scalar potentials in tetrahedral meshes based on the finite element method*, IEEE Transactions on Magnetics **25** (1989), no. 5, 4129–4131.

[134] ———, *Topological considerations in coupling magnetic scalar potentials to stream functions describing surface currents*, IEEE Transactions on Magnetics **25** (1989), no. 4, 2925–2927.

[135] ———, *Magnetostatics with scalar potentials in multiply connected regions*, IEE Proceedings **137, Pt. A** (1990), no. 4, 231–232.

[136] L. Krähenbühl and D. Muller, *Thin layers in electrical engineering. Example of shell models in analyzing eddy-currents by boundary and finite element methods*, IEEE Transactions on Magnetics **29** (1993), no. 2, 1450–1455.

[137] G. Lacroux, *Les aimants permanents*, Lavoisier, 1989.

[138] P. Ladevèze, J.-P. Pelle, and P. Rougeot, *Error estimation and mesh optimization for classical finite elements*, Engineering Computations **8** (1990), 69–80.

[139] M. H. Lean, *Application of boundary integral methods to electromagnetics*, IEEE Transactions on Magnetics **21** (1985), no. 5, 1823–1828.

[140] J. F. Lee and Z. Sacks, *Whitney elements time domain (WETD) methods*, IEEE Transactions on Magnetics **31** (1995), no. 3, 1325–1329.

[141] J. F. Lee, D. K. Sun, and Z. J. Cendes, *Tangential vector finite elements for electromagnetic field computation*, IEEE Transactions on Magnetics **27** (1991), no. 5, 4032–4035.

[142] P. J. Leonard and D. Rodger, *Voltage forced coils for 3D finite element method electromagnetic model*, IEEE Transactions on Magnetics **24** (1988), no. 5, 2579–2581.

[143] J. R. Levine, T. Mason, and D. Brown, *Lex & yacc*, O'Reilly, 1992.

[144] C. Li, *Modélisation tridimensionnelle des systèmes électromagnétiques à l'aide de formulations duales/complémentaires. Application au maillage auto-adaptatif*, Ph.D. thesis, Université de Paris-Sud, France, 1993.

[145] F. Liorzou, B. Phelps, and D. L. Atherton, *Macroscopic models of magnetization*, IEEE Transactions on Magnetics **36** (2000), no. 2, 418–428.

[146] P. Lombard and G. Meunier, *A general purpose method for electric and magnetic combined problems for 2D, axisymmetric and transient problems*, IEEE Transactions on Magnetics **29** (1993), no. 2, 1737–1740.

[147] J. B. Manges and Z. J. Cendes, *Tree-cotree decomposition for first order complete tangential vector finite elements*, International Journal for Numerical Methods in Engineering **40** (1997), 1667–1685.

[148] F. Marmin, S. Clénet, F. Bouillault, and F. Piriou, *Calculation of complementary solutions in 2D finite element method application to error estimation*, IEEE Transactions on Magnetics **36** (2000), 1583–1587.

[149] W. S. Massey, *Homology and cohomology theory*, Marcel Dekker, 1978.

[150] C. Mattiussi, *An analysis of finite volume, finite element, and finite difference methods using some concepts from algebraic topology*, Journal of Computational Physics **9** (1997), 295–319.

[151] J. C. Maxwell, *A treatise on electricity and magnetism*, third ed., Clarendon Press, 1891.

[152] I. D. Mayergoyz and G. Bedrosian, *On calculation of 3-D eddy currents in conducting and magnetic shells*, IEEE Transactions on Magnetics **31** (1995), no. 3, 1319–1324.

[153] G. Meunier, H. T. Luong, and Y. Maréchal, *Computation of coupled problem of 3D eddy current and electric circuit using t_0-t-ϕ formulation*, IEEE Transactions on Magnetics **34** (1998), no. 5, 3074–3077.

[154] B. Meys, *Modélisation des champs électromagnétiques aux hyperfréquences par la méthode des éléments finis. Application aux problème du chauffage diélectrique*, Ph.D. thesis, University of Liège, Belgium, Faculty of Applied Sciences, December 1999.

[155] B. Meys, C. Geuzaine, F. Henrotte, P. Dular, and W. Legros, *Dual harmonic and time approaches for the design of microwave devices*, IEEE Transactions on Magnetics **35** (1999), no. 3, 1829–1832.

[156] B. Meys, F. Henrotte, C. Geuzaine, H. Hedia, and W. Legros, *An optimization method for the design of physical and Maxwellian absorbers*, IEEE Transactions on Magnetics **35** (1999), no. 3, 1430–1433.

[157] G. Mur and A. T. de Hoop, *A finite-element method for computing three-dimensional electromagnetic fields in inhomogeneous media*, IEEE Transactions on Magnetics **MAG-21** (1985), no. 6, 2188–2191.

[158] T. Nakata, N. Takahashi, K. Fujiwara, and T. Imai, *Effects of permeability of magnetic materials on errors of the T-Ω method*, IEEE Transactions on Magnetics **26** (1990), no. 2, 698–701.

[159] T. Nakata, N. Takahashi, K. Fujiwara, and Y. Okada, *Improvements of the T-Ω method for 3-D eddy current analysis*, IEEE Transactions on Magnetics **24** (1988), no. 1, 94–97.

[160] M. H. Nayfeh and M. K. Brussel, *Electricity and magnetism*, John Wiley & Sons, 1985.

[161] J.-C. Nédélec, *Mixed finite elements in R^3*, Numerische Mathematik **35** (1980), 315–341.

[162] ———, *A new family of mixed finite elements in R^3*, Numerische Mathematik **50** (1986), 57–81.

[163] ———, *Notions sur les techniques d'éléments finis*, Ellipses, 1991.

[164] A. Nicolet, J.-F. Remacle, B. Meys, A. Genon, and W. Legros, *Transformation methods in computational electromagnetics*, Journal of Applied Physics **75** (1994), no. 10, 6036–6038.

[165] J. T. Oden and A. Patra, *A parallel adaptive strategy for hp finite element computations*, Technical report TICAM 94-01, Texas Institute for Computational and Applied Mathematics, University of Texas at Austin, May 1994.

[166] *OpenGL*, http://www.opengl.org.

[167] *PETSc, the portable, extensible toolkit for scientific computation*, http://www.mcs.anl.gov/petsc.

[168] F. Piriou and A. Razek, *Finite element analysis in electromagnetic systems accounting for electric circuits*, IEEE Transactions on Magnetics **29** (1993), no. 2, 1669–1675.

[169] K. Preis, I. Bárdi, O. Biró, C. Magele, G. Vrisk, and K. R. Richter, *Different finite element formulations of 3D magnetostatic fields*, IEEE Transactions on Magnetics **28** (1992), no. 2, 1056–1059.

[170] W. H. Press, S. A. Teukolsky, W. T. Vetterling, and B. P. Flannery, *Numerical recipes in C*, second ed., Cambridge University Press, 1992.

[171] T. W. Preston and A. B. J. Reece, *Solution of 3-dimensional eddy current problems: the $T - \Omega$ method*, IEEE Transactions on Magnetics **18** (1982), no. 2, 486–491.

[172] A. Raizer, G. Meunier, and J.-L. Coulomb, *An approach for automatic adaptative mesh refinement in finite element computation of magnetic fields*, IEEE Transactions on Magnetics **25** (1989), no. 4, 2965–2967.

[173] S. Ramo, J. R. Whinnery, and T. Van Duzer, *Fields and waves in communication electronics*, John Wiley & Sons, 1984.

[174] A. Rassili, C. Geuzaine, W. Legros, M. Bobadilla, A. Cucatto, M. Robelet, S. Abdelfattah, J. Dohmann, and C. Hornradt, *Simulation of adequate inductive heating parameters and the magneto-thermal coupling involved in the SSM processing of steels*, Proceedings of the 6th International Conference on Semi-Solid Processing of Alloys and Composites, SSM'2000 (Turin, Italy), September 2000, pp. 559–564.

[175] P. A. Raviart and J. M. Thomas, *A mixed finite element method for second order elliptic problems*, Springer Lecture Notes in Mathematics **606** (1977), 292–315.

[176] J.-F. Remacle, *Estimation d'erreur dans la modélisation par éléments finis des champs électromagnétiques : Application à l'optimisation de maillages*, Ph.D. thesis, University of Liège, Belgium, Faculty of Applied Sciences, June 1997.

[177] J.-F. Remacle, P. Dular, A. Genon, and W. Legros, *A posteriori error estimation and adaptive meshing using error in constitutive relation*, IEEE Transactions on Magnetics **32** (1996), no. 3, 1369–1372.

[178] J.-F. Remacle, P. Dular, C. Geuzaine, A. Genon, and W. Legros, *Adaptive hp-refinement for finite element computations using nodal and edge elements*, Electromagnetic Field Problems and Applications, ICEF'96 (Z. Keding, ed.), International Academic Publisher, May 1997, pp. 66–69.

[179] J.-F. Remacle, P. Dular, F. Henrotte, A. Genon, and W. Legros, *Error estimation and mesh optimisation using error in constitutive relation for electromagnetic field computation*, IEEE Transactions on Magnetics **31** (1995), no. 6, 3587–3589.

[180] J.-F. Remacle, C. Geuzaine, P. Dular, H. Hedia, and W. Legros, *Error estimation based on a new principle of projection and reconstruction*, IEEE Transactions on Magnetics **34** (1998), no. 5, 3264–3267.

[181] J.-F. Remacle, A. Nicolet, A. Genon, and W. Legros, *Comparison of boundary elements and transformed finite elements for open magnetic problems*, Boundary Elements XVI (C. A. Brebbia, ed.), Computational Mechanics Publications, Elsevier Applied Science, July 1994, pp. 109–116.

[182] Z. Ren, *Auto-gauging of vector potential by iterative solver: Numerical evidence*, Proceedings of the 3rd International Workshop on Electric and Magnetic Fields, EMF'96 (Liège, Belgium), May 1996, pp. 119–124.

[183] ———, *Influence of the R.H.S. on the convergence behaviour of the curl-curl equation*, IEEE Transactions on Magnetics **32** (1996), no. 3, 655–658.

[184] ———, *Contribution à la modélisation des systèmes électromagnétiques tridimensionnels: étude des formulations duales, modélisation des systèmes électromagnétique-mécanique couplés*, Rapport de synthèse pour l'obtention de l'habilitation à diriger des recherches, Université Paris Sud, France, 1997.

[185] ———, *Degenerated Whitney prism elements: General nodal and edge elements for field computation in thin structures*, IEEE Transactions on Magnetics **34** (1998), no. 5, 2547–2550.

[186] Z. Ren, F. Bouillault, A. Razek, A. Bossavit, and J.-C. Vérité, *A new hybrid model using electric field formulation for 3D eddy current problems*, IEEE Transactions on Magnetics **26** (1990), no. 2, 470–473.

[187] Z. Ren, F. Bouillault, A. Razek, and J.-C. Vérité, *Comparison of different boundary integral formulations when coupled with finite elements in three dimensions*, IEE Proceedings **135, Pt. A** (1988), no. 8, 501–507.

[188] Z. Ren and N. Ida, *Computation of magnetostatic field using second order edge elements in 3D*, Proceedings of the 8th International IGTE Symposium on Numerical Field Calculation in Electrical Engineering (Graz, Austria), September 1998.

[189] ———, *High order differential form based elements for the computation of electromagnetic field*, Proceedings of the 12th Conference on the Computation of Electromagnetic Fields, COMPUMAG'99 (Sapporo, Japan), 1999, pp. 764–765.

[190] ———, *High-order elements of complete and incomplete bases in electromagnetic field computation*, IEEE Transactions on Magnetics **36** (2000), no. 4, 1472–1478.

[191] Z. Ren, C. Li, and A. Razek, *Hybrid FEM-BIM formulation using electric and magnetic variables*, IEEE Transactions on Magnetics **28** (1992), no. 2, 1647–1650.

[192] Z. Ren and A. Razek, *Coupling of boundary integral methods with dual finite element methods for electromagnetic field computation*, Boundary Element Technology X, Computational Mechanics Publications, Elsevier Applied Science, September 1995, pp. 89–98.

[193] J. Rikabi, C. F. Bryant, and E. F. Freeman, *Error based derivation of complementary formulations for eddy current problems*, International Journal for Numerical Methods in Engineering **26** (1988), 1963–1987.

[194] ———, *Error based derivation of complementary formulations for eddy current problems*, IEE Proceedings **135, Pt. A** (1988), no. 4, 208–216.

[195] F. Robert, P. Dular, J.-F. Remacle, M. Umé, and W. Legros, *A mixed formulation to compute the source current density in inductors of any shape*, Proceedings of the 12th Annual Review of Progress in Applied Computational Electromagnetics, ACES'96 (Monterey, USA), March 1996, pp. 456–463.

[196] D. Rodger and N. Atkinson, *3D eddy currents in multiply connected thin sheet conductors*, IEEE Transactions on Magnetics **23** (1987), no. 5, 3047–3049.

[197] ———, *Finite element method for 3D eddy current flow in thin conducting sheets*, IEE Proceedings **135, Pt. A** (1988), no. 6, 369–374.

[198] V. Rokhlin, *Rapid solution of integral equations of classical potential theory*, Journal of Computational Physics **60** (1985), 187–207.

[199] M. S. Sarto, *A new model for the FDTD analysis of the shielding performances of thin composite structures*, IEEE Transactions on Electromagnetic Compatibility **41** (1999), no. 4, 298–306.

[200] G. Scharf, *From electrostatics to optics*, Springer-Verlag, 1994.

[201] B. Schutz, *Geometrical methods of mathematical physics*, Cambridge University Press, 1980.

[202] M. Segal and K. Akeley, *The OpenGL graphics system: A specification*, Technical report, Silicon Graphics Computer Systems, 1992.

[203] *SPARSKIT: a basic tool-kit for sparse matrix computations*, http://www.cs.umn.edu/Research/arpa/SPARSKIT/sparskit.html.

[204] J. Stoer and R. Bulirsch, *Introduction to numerical analysis*, Springer-Verlag, 1980.

[205] J. A. Stratton, *Electromagnetic theory*, McGraw-Hill, 1941.

[206] B. Stroustrup, *The C++ programming language*, Addison-Wesley, 1997.

[207] D. K. Sun, J. F. Lee, and Z. J. Cendes, *Rapid multilevel preconditioned convergence with nearly orthogonal nedelec bases*, To appear in IEEE Transactions on Magnetics **38** (2002), no. 2.

[208] T. Tarhasaari, L. Kettunen, and A. Bossavit, *Some realizations of a discrete Hodge operator: a reinterpretation of finite element techniques*, IEEE Transactions on Magnetics **35** (1999), no. 3, 1494–1497.

[209] T. Tarhasaari, L. Kettunen, and C. Geuzaine, *Discretization of sources of integral operators*, IEEE Transactions on Magnetics **36** (2000), no. 4, 659–662.

[210] E. Tonti, *On the geometrical structure of electromagnetism*, Gravitation, Electromagnetism and Geometrical Structures (Pitagora, Bologna, Italy) (G. Ferrarese, ed.), 1996, pp. 281–308.

[211] I. Tsukerman and A. Plaks, *Hierarchical basis multilevel preconditioners for 3D magnetostatic problems*, IEEE Transactions on Magnetics **35** (1999), no. 3, 1143–1146.

[212] C. Vassallo, *Électromagnetisme classique dans la matière*, Dunod, 1980.

[213] J.-S. Wang, *Hierarchic "edge" elements for high-frequency problems*, IEEE Transactions on Magnetics **33** (1997), no. 2, 1536–1539.

[214] K. F. Warnick and D. V. Arnold, *Electromagnetic Green functions using differential forms*, Journal of Electromagnetic Waves and Applications **10** (1996), no. 3, 427–438.

[215] J. P. Webb, *Edge elements and what they can do for you*, IEEE Transactions on Magnetics **29** (1993), no. 2, 1460–1465.

[216] J. P. Webb and B. Forghani, *A single scalar potential method for 3D magnetostatics using edge elements*, IEEE Transactions on Magnetics **25** (1989), no. 5, 4126–4128.

[217] ———, *A scalar-vector method for 3D eddy current problems using edge elements*, IEEE Transactions on Magnetics **26** (1990), no. 5, 2367–2369.

[218] ———, *Hierarchal scalar and vector tetrahedra*, IEEE Transactions on Magnetics **29** (1993), no. 2, 1495–1498.

[219] T. Weiland, *Time domain electromagnetic field computation with finite difference methods*, International Journal of Numerical Modelling **9** (1996), 295–319.

[220] S. H. Weintraub, *Differential forms. A complement to vector calculus*, Academic Press, 1997.

[221] J. S. Welij, *Calculation of eddy currents in terms of h on hexahedra*, IEEE Transactions on Magnetics **21** (1985), no. 6, 2239–2241.

[222] H. Whitney, *Geometric integration theory*, Princeton University Press, 1957.

[223] T. V. Yioultsis and T. D. Tsiboukis, *Multiparametric vector finite elements: a systematic approach to the construction of three-dimensional, higher order, tangential vector shape functions*, IEEE Transactions on Magnetics **32** (1996), no. 3, 1389–1392.

[224] ———, *Development and implementation of second and third order vector finite elements in various 3-D electromagnetic field problems*, IEEE Transactions on Magnetics **33** (1997), no. 2, 1812–1815.

[225] ———, *A fully explicit Whitney element-time domain scheme with higher order vector finite elements for three-dimensional high frequency problems*, IEEE Transactions on Magnetics **34** (1998), no. 5, 3288–3291.

[226] F.-X. Zgainski, J.-L. Coulomb, Y. Maréchal, F. Claeyssen, and X. Brunotte, *A new family of finite elements: the pyramidal elements*, IEEE Transactions on Magnetics **32** (1996), no. 3, 1393–1396.

[227] O. C. Zienkiewicz, D. W. Kelly, and P. Bettess, *The coupling of the finite element method and boundary solution procedures*, International Journal for Numerical Methods in Engineering **11** (1977), 355–375.

[228] O. C. Zienkiewicz and R. L. Taylor, *The finite element method*, fourth ed., McGraw-Hill, 1994.

Author Index

Contents

List of Figures

List of Tables

Version history

December 19, 2001	:	original revision
September 18, 2005	:	small corrections in sections 1.3.2, 2.6.2, 3.2.1.3 and 3.2.3.2 + new A.2.7

Generated on September 18, 2005